

京 都 大 学  
エ ネ ル ギ ー 科 学 研 究

第 3 集

自 平成10年4月  
至 平成11年3月

*Research Activities*  
*in Graduate School of Energy Science*  
*Kyoto University*

*1998/4~1999/3*

*Vol. 3*

*Graduate School of Energy Science*  
*Kyoto University*

*1999.12*

平成 11 年 12 月  
京都大学エネルギー科学研究科

This issue is edited with the aim to introduce our research activities from April 1998 to March 1999, under the four categories.

- A. Current Research Fields
- B. Original Articles
- C. Review Articles
- D. Books

本誌はエネルギー科学研究科における研究活動の紹介をおもな目的とし、次のA、B、CおよびDに分けて編集されたものである。

- A. 研究現況(テーマ)
- B. 研究発表
- C. 総説
- D. 著書(学術図書)

# *Contents*

目次

# Contents

<b>1</b>	<b>Current Research Fields</b>	<b>1</b>
I	Department of Socio-Environmental Energy Science . . . . .	1
II	Department of Fundamental Energy Science . . . . .	4
III	Department of Energy Conversion Science . . . . .	9
IV	Department of Energy Science and Technology . . . . .	12
<b>2</b>	<b>Original Articles</b>	<b>17</b>
I	Department of Socio-Environmental Energy Science . . . . .	17
1:	* Bulk nano-scale multilayers prepared by repeated pressing-rolling . . . . .	17
2:	* Magnetoresistance of Nanoscale Fe/Ag Multilayer Produced by Repeated Press-rolling . . . . .	17
3:	Market Penetration and Cost-Effectiveness Analysis of Thermal Storage System Using Integrated Resource Planning Model with Endogenized Technological Learning . . . . .	18
4:	Mechanism of Cellulose Pyrolysis -Reactivity of an Intermediate, Levoglucosan . . . . .	18
5:	Removal of Toxic Substances of Chloroform and Benzen by Carbonized Woody Materials . . . . .	19
6:	* SiO <sub>2</sub> -P <sub>2</sub> O <sub>5</sub> -B <sub>2</sub> O <sub>3</sub> Wood-Inorganic Composites Prepared by Metal Alkoxide Oligomers and their Fire-resisting Properties . . . . .	19
7:	Antimicrobial TMSAH-added wood-inorganic composites prepared by the sol-gel process . . . . .	20
8:	* Recent Progress in Topochemistry of Wood-Inorganic Composites as Prepared by the Sol-Gel Process . . . . .	20
9:	* Fire-resisting Wood-Inorganic Composites as Prepared by the Sol-Gel Process . . . . .	21
10:	Chemical Conversion of Various Cellulose in Supercritical Water to Glucose . . . . .	21
11:	* Longevity of Wood by Inorganic co-modification . . . . .	22
12:	Interaction of pyrylium dye with self-complementary DNA oligomer as studied by <sup>1</sup> H NMR spectroscopy . . . . .	22
13:	Redox behavior of DMPO and its derivatives as studied by electrochemical measurements . . . . .	23
14:	Reaction mechanism for formation of 2'-deoxyoxanosine from 2'-deoxyguanosine, a new DNA lesion by NO and HNO <sub>2</sub> . . . . .	23
15:	Inhibition of human T-cell leukemia virus type 1 replication by antisense <i>env</i> oligodeoxynucleotide . . . . .	23

16:	Neuroprotective effects of pterin-6-aldehyde in gerbil global brain ischemia: comparison with those of $\alpha$ -phenyl- <i>N</i> - <i>tert</i> -butyl nitron	23
17:	Oxypurinol, a xanthine oxidase inhibitor and a superoxide scavenger, did not attenuate ischemic neuronal damage in gerbils	24
18:	Misincorporation of 2'-deoxyoxanosine 5'-triphosphate by DNA polymerases and its implication to mutagenesis	24
19:	<sup>1</sup> H nuclear magnetic resonance study on equilibrium between two four-stranded solution conformations of short d(CnT)	24
20:	Preparation of stereoregulated antisense oligodeoxyribonucleoside phosphorothioate and interaction with its complementary DNA and RNA	24
21:	Two four-stranded structures of d(CnT) in solution by <sup>1</sup> H-NMR	25
22:	Formation of porphyrin-metal complex catalyzed by single-strand DNA	25
23:	Products in the reaction of 2'-deoxyguanosine with NO in the presence and absence of O <sub>2</sub>	25
24:	Intermediate in the reaction of 2'-deoxycytidine with nitrous acid and nitric oxide	25
25:	Characterization of ultrahigh molecular weight polyethylene irradiated with $\gamma$ -rays and electron beams to high doses	26
26:	Stability of the Dimerization Domains Effects the Cooperative DNA Binding of Short Peptides	26
27:	Isolation and characterization of diazoate intermediate upon nitrous acid and nitric oxide treatment of 2'-deoxycytidine	26
28:	Kinetic Studies of Sequence-Specific Binding of GCN4-bZIP Peptides to DNA Strands Immobilized on a 27-MHz Quartz-Crystal Microbalance	26
29:	Cooperative DNA Binding by Short Peptides	27
30:	Comparison of the Sequence-Selective DNA Binding by Peptide Dimers with Covalent and Noncovalent Dimerization Domains	27
31:	Intermediate upon nitrous acid- or nitric oxide-treatment of 2'-deoxycytidine	27
32:	Analysis of Operator's Diagnostic Behavior and its Application to the Human Modeling	27
33:	Simulation based Evaluation of Man-Machine Interface in Power Plants	28
34:	A New VR-based CSCW Environment for Conceptual Design of A Space Power Reactor	28
35:	A Basic Study on Real-time Method of Human Cognitive Process Estimation by Using Speech Recognition	29
36:	Construction and Evaluation of a WWW-based CAI system based on Cognitive Design Guideline	29
37:	A Study on Pupillary Response to Depth Cue of Linear Perspective	29
38:	An Experimental Study on Pupillary Response under Binocular Parallax by Using Eye-Sensing Head Mounted Display	30
39:	Teleoperation Environment based on Virtual Reality, - Application of Two-Planes Method for Position Measurement -	30
40:	A Computer-aided Sensing and Design Methodology for the Simulation of Natural Human Body Motion and Facial Expression	31

41:	Study on Developing a Computerized Model of Human Cognitive Behaviors in Monitoring and Diagnosing Plant Transients . . . . .	31
42:	Application of Machine Speech Recognition for Real-time Estimation of Human Cognitive Process at Man-Machine Interface . . . . .	32
43:	Development of Head-attached Interface Device (HIDE) and its Application Experiments . . . . .	32
44:	An Experimental Study on Distributed Virtual Environment for Integrated Training System on Machine Maintenance . . . . .	33
45:	A Study on Design Support System for Constructing Machine-Maintenance Training Environment Based on Virtual Reality Technology . . . . .	33
46:	Basic Experiments for Evaluating Peculiar Ocular Characteristics Caused by Artificial Binocular Vision . . . . .	33
47:	Development of Head-attached Interface Device (HIDE) and its Functional Evaluation . . . . .	34
48:	A Study on Design Support for Constructing Machine-maintenance Training System by using Virtual Reality Technology . . . . .	34
49:	Construction of a WWW-based CAI System Based on Cognitive Design Guideline	35
50:	Usage of Computer Simulation of Human-Machine Interaction for the Human Reliability Enhancement in Human Machine System . . . . .	35
51:	Application of Human Model Simulation to Deduce Human Error Probability Parameter for PSA/HRA Practice . . . . .	35
52:	A Basic Study of Virtual Collaborator - The First Prototype System Integration	36
53:	Simulation-based Evaluation System for Man-Machine Interfaces in Nuclear Power Plants . . . . .	36
54:	* Identification of mixing state of sulfate and nitrate ions in individual aerosol particles using a mixing thin film created by dual simultaneous vacuum deposition	37
55:	* Characterization of Atmospheric Aerosols Applying PIXE Method . . . . .	37
56:	* Application of X-Ray Absorption Fine Structure (XAFS) Spectrometry to Identify the Chemical States of Atmospheric Aerosols . . . . .	38
57:	Life Cycle Analysis of Automobiles with Regard to Air Pollutants Emissions in Japan . . . . .	38
58:	Bayesian Analysis of Public Views on the Safety of Nuclear Developments . . . .	39
59:	The Strengthened Nuclear Non-proliferation Export Control Regime and Possible Future Improvements . . . . .	39
60:	Nuclear Development in the "Knowledge Society" . . . . .	40
61:	The Demise of National COCOM and the Establishment of the Wassenaar Arrangement . . . . .	40
62:	A Ripple of the "Atomausstieg" Policy of the New German Government . . . . .	41
63:	* Multiplicity and Energy of Neutrons from $^{235}\text{U}(\text{nth},\text{f})$ Fission Fragments . . . .	41
64:	* Multi-parametric Measurement of Prompt Neutrons and Fission Fragments for $^{233}\text{U}(\text{nth},\text{f})$ . . . . .	42
65:	Fission Fragment Configurations at the Scission Point of $^{233}\text{U}$ , $^{235}\text{U}$ and $^{239}\text{Pu}(\text{nth},\text{f})$	

66:	MOX Fuel Core Physics Experiments and Analysis -Aiming for Plutonium Effective Use- . . . . .	43
67:	Neutron activation analysis of ivory of Africa elephants . . . . .	43
II	Department of Fundamental Energy Science . . . . .	44
68:	Effect of Aging on Yttria-Stabilized Zirconia I. A Study of Its Electrochemical Properties . . . . .	44
69:	Effect of Aging on Yttria-Stabilized Zirconia II. A study of Effect of the Microstructure on Conductivity . . . . .	45
70:	Effect of Aging on Yttria-Stabilized Zirconia III. A study of Effect of the Local Structures on Conductivity . . . . .	45
71:	* Protonic and Native Conduction in Sr-Substituted LaPO <sub>4</sub> Studied by Thermo- electric Power Measurements . . . . .	46
72:	* Intermittent Heat Transport Using Hydrogen Absorbing Alloys . . . . .	47
73:	* Long-Distance Heat Transport System Using a Hydrogen Compressor . . . . .	47
74:	Relaxation of Internal Stress Generated in Hydrogen Absorbing Alloy Vessels . . . . .	48
75:	Stability of LiAlO <sub>2</sub> as electrolyte matrix for molten carbonate fuel cells . . . . .	48
76:	Formation of Fine Nickel Particles by Discharge Electrolysis in Molten Chloride System . . . . .	49
77:	* Electrochemical reduction of nitrogen gas in a molten chloride system . . . . .	49
78:	* Thermodynamic and Kinetic Properties of the N <sub>2</sub> Gas Electrode in a Molten LiCl-KCl-Li <sub>3</sub> N System . . . . .	50
79:	* Discharge electrolysis in molten chloride: formation of fine silver particles . . . . .	50
80:	First-nearest-neighbour interatomic potentials for light-actinide metals . . . . .	50
81:	Molecular dynamics simulations of the self-diffusion phenomena in Ni <sub>2</sub> Y inter- metallic phase . . . . .	51
82:	Clustering Process of the Cuprate Phase in Ag-Added BPSCCO Composites . . . . .	51
83:	Behavior of Percolative Transport Paths in Pr-Doped Y <sub>1</sub> Ba <sub>2</sub> Cu <sub>3</sub> O <sub>y</sub> . . . . .	52
84:	Synthesis of Functional Ceramic Materials from Aqueous Solutions . . . . .	52
85:	Hydrothermal Synthesis and Crystal Structure of Barium Hewettite: BaV <sub>6</sub> O <sub>16</sub> · nH <sub>2</sub> O . . . . .	53
86:	Crystal Structure and Metal Distribution of α-CoV <sub>3</sub> O <sub>8</sub> . . . . .	53
87:	Crystal Structures and Transition Mechanism of VO <sub>2</sub> (A) . . . . .	54
88:	Metal-Insulator Transition and Crystal Structure of La <sub>1-x</sub> Sr <sub>x</sub> CoO <sub>3</sub> as Functions of Sr-Content, Temperature, and Oxygen Partial Pressure . . . . .	54
89:	Superstructure of Strontium Vanadium Oxide, Sr <sub>0.5</sub> V <sub>2</sub> O <sub>5</sub> : Their Twinning, Groupoid Symmetry and Interpretation as OD Structure . . . . .	55
90:	Structure of Strontium Vanadium Oxyhydrates, SrV <sub>12</sub> O <sub>27</sub> ·3H <sub>2</sub> O: A Vanadium Oxide Bronze with New Vanadate Framework . . . . .	55
91:	Optimization of Preparation Conditions of Spinel Li <sub>4/3</sub> Mn <sub>5/3</sub> O <sub>4</sub> as a Cathode Material for Rechargeable Lithium Battery . . . . .	56
92:	Novel Method for Zirconium Oxide and Rare Earth-Transition Metal Perovskite Oxides Synthesis from Aqueous Solutions . . . . .	56
93:	Effect of Doping Strontium to LaMnO <sub>3</sub> on the Electrode Properties . . . . .	57

94:	Kinetics of Vapor-Phase Electrolytic Deposition of Yttria-Stabilized Zirconia Thin Films . . . . .	57
95:	Preparation of Perovskite-Type $\text{La}_{1-x}\text{Sr}_x\text{MnO}_3$ Films by Vapor-Phase Processes and Their Electrochemical Properties. Part 2. Effects of Doping Strontium to $\text{LaMnO}_3$ on the Electrode Properties . . . . .	58
96:	Preparation of Macroporous Titania Films by a Sol-Gel Dip-Coating Method from the System Containing Poly(ethylene glycol) . . . . .	58
97:	Macroporous Morphology of the Titania Films Prepared by a Sol-Gel Dip-Coating Method from the System Containing Poly(ethylene glycol). I. Effect of Humidity . . . . .	59
98:	Macroporous Morphology of the Titania Films Prepared by a Sol-Gel Dip-Coating Method from the System Containing Poly(ethylene glycol). II. Effect of Solution Composition . . . . .	59
99:	Internal Disruptions in Heliotron E . . . . .	59
100:	Damping of Surface Alfvén Wave in a Slab Plasma . . . . .	60
101:	Stabilization of Resistive Wall Mode Due to Shear Alfvén Resonance in a Cylindrical Plasma with a Uniform Longitudinal Flow . . . . .	60
102:	Gyrokinetic Particle Simulation Using the Orbit Average Electron Drift-Kinetic Equation . . . . .	61
103:	Integral Suppression of Pfirsch-Schlüter Current in the Inward Shifted Stellarator Plasma in Heliotron E . . . . .	61
104:	* Physical Property of Plasmas in the L=1 Heliotron . . . . .	62
105:	* Local Stability of High Beta Low Aspect Ratio Tokamak with Negative Shear . . . . .	62
106:	* Formation and Termination of High Ion Temperature Mode in Heliotron/Torsatron Plasmas . . . . .	63
107:	* Experiments on Li Pellet Injection into Heliotron E . . . . .	63
108:	Sawtooth Control by On-Axis Electron Cyclotron Current Drive on the WT-3 Tokamak . . . . .	64
109:	* Formation and Confinement of Non-neutral Electron Plasmas in a Multi-Ring Electrodes Trap Using with a Field Emitter Array Cathode . . . . .	64
110:	* Experiments on Non-Neutral Long Spheroidal Electron Plasmas in a Multi-Ring-Electrode Trap . . . . .	64
111:	Profile Control Studies on Heliotron E . . . . .	65
112:	Structure of the Edge Magnetic Field of the $\ell = 1$ Helical Axis Heliotron . . . . .	65
113:	ECH Launching Conditions in Helical System . . . . .	66
114:	In-Situ Surface Modification by ECH Plasma in Heliotron E . . . . .	66
115:	The New Helical Plasma Device at IAE, Kyoto University . . . . .	66
116:	Numerical analysis of small movable ICRF antenna loading resistance in Heliotron-E . . . . .	67
117:	Integral Suppression of Pfirsch-Schlüter Current in the Inward Shifted Stellarator Plasma in Heliotron E . . . . .	67
118:	Studies of Magnetic Surface Control and Electron Orbit Loss in Heliotron DR . . . . .	68
119:	Influence of Magnetic Configuration and Heating Methods on Distribution of Diverted Plasmas in Heliotron E . . . . .	68

120:	Dependence of Plasma Profiles on ECH Power Absorption in Heliotron-E . . . . .	68
121:	Effects of Magnetic Shear on Electron Cyclotron Resonance Heating in Heliotron/Torsatron Configurations . . . . .	69
122:	Oblique Launching Experiment for ECH and ECCD in Heliotron-E . . . . .	69
123:	Divertor Studies in Heliotron/torsatrons . . . . .	70
124:	Experiments on Li pellet injection into Heliotron E . . . . .	71
125:	Complete integral suppression of Pfirsch-Schluter current in a Stellarator plasma in Heliotron E . . . . .	71
126:	The new helical plasma device at IAE, Kyoto University . . . . .	72
127:	Heliotron J experimental program . . . . .	72
128:	Stellarator transport simulation using $\delta f$ Monte Carlo algorithms . . . . .	72
129:	Numerical analysis of small movable ICRF antenna loading resistance in Heliotron-E . . . . .	73
130:	Experiments on Li pellet injection into Heliotron E . . . . .	73
131:	Metal deposition into a porous silicon layer by immersion plating: Influence of halogen ions . . . . .	74
132:	* Dopant and fluence effects on the ablation of silicon surfaces under pulsed CO <sub>2</sub> laser irradiation . . . . .	74
133:	* Characteristics of the species ablated from silicon surface by pulsed CO <sub>2</sub> laser irradiation . . . . .	75
134:	Magnetic shielding tensor calculations of cluster models and comparison with nuclear magnetic resonance spectra of porous silicon . . . . .	75
135:	Diffusivity and Solubility of Hydrogen in Ti-Al Alloys . . . . .	76
136:	* Changes in the environment of hydrogen in porous silicon with thermal annealing . . . . .	76
137:	* Absorption of pulsed CO <sub>2</sub> laser in silicon and resulting laser ablation and surface damage formation . . . . .	77
138:	* Structural study of porous silicon and its oxidized states by solid-state high-resolution <sup>29</sup> Si NMR spectroscopy . . . . .	77
139:	* Structure of as-prepared and annealed porous silicon surface studied by nuclear magnetic resonance spectroscopy . . . . .	78
140:	* Chemical etching of porous silicon in diluted hydrofluoric acid . . . . .	78
141:	Long-Range Attractive Interaction between Macroparticles in a Binary Fluid Mixture . . . . .	78
142:	Calculation of Solvation Free Energy Using RISM Theory for Peptide in Salt Solution . . . . .	79
143:	Singular Behavior of the RISM Theory Observed for Peptide in Salt Solution . . . . .	79
144:	* Interaction between Macroparticles in a Binary Fluid Mixture: Anomalous Effects Due to the Bulk Composition . . . . .	80
145:	Analysis on Conformational Stability of C-Peptide of Ribonuclease A in Water Using the Reference Interaction Site Model Theory and Monte Carlo Simulated Annealing . . . . .	80
146:	First-Principles Calculations of Light Elements/Metal Surface and Liquid/Metal Interface Systems . . . . .	81

147:	* Solvation Structure of Solutes in Supercritical Fluids Analyzed by the HNC Theory . . . . .	81
148:	* Selective Separation of Trypsin from Pancreatin Using Bioaffinity in Reverse Micellar System Composed of a Nonionic Surfactant . . . . .	82
149:	* Structure and Properties of Fluids Composed of Polyelectrolyte and Ionic Surfactant in Organic Phase: Poly(acrylic acid) and Didodecyldimethyl Ammonium Bromide . . . . .	82
150:	* Structure and Properties of Fluids Composed of Polyelectrolyte and Ionic Surfactant in Organic Phase: Poly(allylamine) and Sodium Bis(2-ethylhexyl) Sulfosuccinate . . . . .	83
151:	* Formation Processes of Silica-Microstructures in Micellar and Reverse-Micellar Solutions . . . . .	83
152:	* Preparation of Cadmium Sulfide Ultrafine Particles with Sharp Size-Distribution Using Cadmium Dioleoylphosphate Microemulsion . . . . .	84
153:	* A Molecular Dynamics Study of the Stereoselective Interaction between an Enantiomeric Amino Acid Ester and an L-Histidine-containing Catalyst in the Bilayer Membrane . . . . .	84
154:	* Identification of Lipid Inhibitor of Mammalian Phospholipase D . . . . .	85
155:	* Enhanced Levels of Oleate-dependent and Arf-dependent Phospholipase D Isoforms in Experimental Colon Cancer . . . . .	85
156:	Time-spatial neutron measurement by using position-sensitive $^3\text{He}$ proportional counter . . . . .	86
157:	Modified Explicit Higher Order Perturbation Method with Two Energy Groups . . . . .	86
158:	* Formulation of Data Synthesis Technique for Feynman- $\alpha$ Method . . . . .	87
159:	Variance-to-Mean Method Generalized by Linear Difference Filter Technique . . . . .	87
160:	Analysis of KUCA Critical Experiments Using MVP Code and JENDL-3.2 . . . . .	88
161:	Research Needed for Core Design of Thorium Cycle Reactors Including Accelerator Driven Subcritical Reactors . . . . .	88
162:	Time-spatial neutron measurement by using position-sensitive $^3\text{He}$ proportional counter . . . . .	88
163:	Study on Conceptual Neutronics Design of "Neutron Factory" as a Future Facility in Kyoto University Research Reactor Institute (KURRI) . . . . .	89
164:	Burnup Study of Reactor Grade Plutonium in Molten Salt Reactor . . . . .	89
165:	* Experimental Study on Thorium Fuel Cycle by Using the Kyoto University Critical Assembly (KUCA) . . . . .	90
166:	* Verification of Neutron Radiographic Measurement of Void Fraction by Monte Carlo Simulation . . . . .	90
167:	* Evaluation of Scattered Neutron Component in Thermal Neutron Radiography Image: Influence of Scattered Neutrons and Unparallelness of Incident Neutron Beam . . . . .	91
168:	Local Measurements of Interfacial Area, Interfacial Velocity and Liquid Turbulence in Two-Phase Flow . . . . .	91
169:	Scaling Parameter of CHF under Oscillatory Flow Condition . . . . .	92

170:	Effect of Flow-Induced Vibration on Local Flow Parameters of Two-Phase Flow . . . . .	92
171:	Development of High-Frame-Rate Neutron Radiography and Quantitative Measurement Method for Multiphase Flow Research . . . . .	93
172:	* The Review of the Application of Neutron Radiography to Thermal Hydraulic Research . . . . .	93
173:	* Application of High-Frame-Rate Neutron Radiography to Steam Explosion Research . . . . .	94
174:	* Visualization and Measurement of Gas-Liquid Metal Two-Phase Flow with Large Density Difference Using Thermal Neutrons as Microscopic Probes . . . . .	94
175:	Local Flow Measurements of Vertical Upward Air-Water Flow in a Round Tube . . . . .	95
176:	Flow Regime Transition Criteria for Vertical Upward Two-Phase Flow in Narrow Rectangular Ducts . . . . .	95
177:	Axial Development of Liquid Turbulence and Interfacial Area in Bubbly Two-Phase Flows . . . . .	96
178:	* Study on Flow Characteristics in Gas-Molten Metal Mixture Pool Simulating Core Disruptive Accident of FBR . . . . .	96
179:	Mechanism of Periodical Dryout under Oscillatory Flow Condition . . . . .	97
180:	Visualization of Molten-Metal/Water Interaction Using High-Frame-Rate Neutron Radiography . . . . .	97
181:	* Experimental Study on Interfacial Area Transport in Bubbly Two-Phase Flows . . . . .	98
182:	Experimental Study on Two-Phase Natural Circulation and Flow Termination in a Loop . . . . .	98
183:	* Visualization Study of Molten Metal-Water Interaction by Using Neutron Radiography . . . . .	99
184:	* Application of Photocatalytic Reactions Caused by TiO <sub>2</sub> Film to Improve the Maintenance Factor of Lighting Systems . . . . .	99
185:	* Electrochemical Behavior of Highly Conductive Boron-Doped Diamond Electrodes for Oxygen Reduction in Alkaline Solution . . . . .	100
186:	* Metal Black Pattern Formation on Photofunctional ZnO Thin Films by Electroless Deposition . . . . .	100
187:	* AFM Observation of Surface Reconstruction of C <sub>60</sub> Single Crystals . . . . .	101
188:	* Photoelectrochemical Reduction of CO <sub>2</sub> at High Current Densities at p-InP Electrodes . . . . .	101
189:	* Adhesion Mechanism of Electroless Copper Film Formed on Ceramic Substrates Using ZnO Thin Film as an Intermediate Layer . . . . .	101
190:	* Observation of Electrochemical C <sub>60</sub> Reduction of a Diamond Thin Film Electrode at Room Temperature . . . . .	102
191:	* Examination of the Photoreaction of <i>p</i> -Nitrobenzoic Acid on Electrochemically Roughened Silver Using Surface-Enhanced Raman Imaging (SERRS) . . . . .	102
192:	* External Magnetic Field Effect on the Photoinduced Magnetization in a Cobalt Iron Cyanide . . . . .	103
193:	* Electrochemical Reduction of CO <sub>2</sub> in Micropores . . . . .	103
194:	* AFM Study of Surface Phenomena Based on C <sub>60</sub> Film Growth . . . . .	104

195:	* Soliton Superlattices on the (0001) Surface of C <sub>70</sub> Single Crystals . . . . .	104
196:	* Effect of Adsorbed Water on the Photoelectrorheology of TiO <sub>2</sub> Particle Suspensions . . . . .	105
197:	* Bactericidal and Detoxification Effects of TiO <sub>2</sub> Thin Film Photocatalysts . . . . .	105
198:	* Photoinduced Dislocation Lines on the (111) Face of C <sub>60</sub> Single Crystals . . . . .	106
199:	* Surface-Enhanced Raman Imaging (SERI) as a Technique for Imaging Molecular Monolayers with Chemical Selectivity Under Ambient Conditions . . . . .	106
200:	* Surface Functionalization of Doped CVD Diamond <i>via</i> Covalent Bond. An XPS Study on the Formation of Surface-bound Quaternary Pyridinium Salt . . . . .	106
201:	* Normally Aligned $\pi$ -conjugated Langmuir-Blodgett Films of Oligo-acene Amphiphiles . . . . .	107
202:	* Effect of Ultrasonic Treatment on Highly Hydrophilic TiO <sub>2</sub> Surfaces . . . . .	107
203:	* Preparation of Electrolessly Plated Au Films with High Adhesive Strength Using a TiO <sub>2</sub> -ZnO Composite Film as an Adhesive Layer . . . . .	108
204:	* Titanium Oxide-Coated Glass: Self-Cleaning and Anti-Fogging Properties and Applications . . . . .	108
205:	* New Mesostuctured Porous TiO <sub>2</sub> Surface Prepared Using a Two-Dimensional Array-Based Template of Silica Particles . . . . .	109
206:	* Formation of Catalytic Pd on ZnO Thin Films for Electroless Metal Deposition . . . . .	109
207:	* Photocatalytic Degradation of Gaseous Formaldehyde Using TiO <sub>2</sub> Film . . . . .	110
208:	* Photoelectrochemical Reduction of CO <sub>2</sub> in a High-Pressure CO <sub>2</sub> +Methanol Medium at p-Type Semiconductor Electrodes . . . . .	110
209:	* Grain Size of a Hard Molecule-Based-Magnet of Manganese Porphyrin-Tetracyanoethylene Charge Transfer Salt . . . . .	111
210:	* Mosbauer Study on Characterization of Co[Fe(CN) <sub>5</sub> NH <sub>3</sub> ] $\cdot$ xH <sub>2</sub> O . . . . .	111
211:	* Continuous-Flow Photoreactor Packed with Titanium Dioxide Immobilized on Large Silica Gel Beads to Decompose Oxalic Acid in Excess Water . . . . .	111
212:	* Influence of the Rotation Rate of a Rotary Viscometer on the Photoelectrorheological Properties of TiO <sub>2</sub> Particle Suspensions . . . . .	112
213:	* Effect of ZnO Film Thicknesses on the Adhesive Strength of Electroless Cu Deposits . . . . .	112
214:	* ZnO Thin Film-Based New Electroless Metal Deposition . . . . .	113
215:	* Electrochemical Reduction of Cu <sup>2+</sup> without Surface Trapping on Synthetic Conductive Diamond Electrodes . . . . .	113
216:	* Band-Edge Movements of Semiconducting Diamond in Aqueous Electrolyte Induced by Anodic Surface Treatment . . . . .	113
217:	* Photoelectrodeposition of Copper on Boron-Doped Diamond Films: Application to Conductive Pattern Formation on Diamond. The Photographic Diamond Surface Phenomenon . . . . .	114
218:	* Selective Electrochemical Detection of Dopamine in the Presence of Ascorbic Acid at Anodized Diamond Thin Film Electrodes . . . . .	114
219:	* Electrochemical Behavior of Highly Conductive Boron-Doped Diamond Electrodes for Oxygen Reduction in Acid Solution . . . . .	115

220:	* Studies of Surface Wettability Conversion on TiO <sub>2</sub> Single-Crystal Surfaces . . . . .	115
III	Department of Energy Conversion Science . . . . .	117
221:	Effect of Exhaust Gas Recirculation and Injection Pressure on Exhaust Emissions from a Diesel Engine . . . . .	117
222:	Spatial Distribution of Initial Droplets of a Diesel Spray . . . . .	117
223:	Reduction of Nitrogen Oxides of Diesel Engines by Exhaust-Gas-Selective Recir- culation . . . . .	118
224:	* Flame Stability and NO <sub>x</sub> Formation in a High-Intensity Swirl Burner . . . . .	118
225:	* CFD Simulation for Predicting Combustion and Pollutant Formation in a Homogeneous- Charge Spark-Ignition Engine . . . . .	119
226:	Discussion on Accuracy of PIV Measurement . . . . .	119
227:	Performance and NO <sub>x</sub> Formation in a Hydrogen Premixed-Charge Engine . . . . .	119
228:	Gas-Flow Measurements in a Jet Flame Using Cross-Correlation of High-Speed Particle-Images . . . . .	120
229:	* A Laminar Flamelet Model for Turbulent Pre-mixed Combustion . . . . .	120
230:	* Performance and NO <sub>x</sub> Formation in a Hydrogen Premixed-Charge Engine . . . . .	121
231:	* Deformation of Spherical Living Tissue Cells by Using Shock Waves . . . . .	121
232:	* Macro- and Microscopic Simulation of Materio-Thermo-Mechanical Fields . . . . .	121
233:	* Computer Simulation of Residual Stresses/distorsion and Structural Change in the course of Scanning Induction Hardening . . . . .	122
234:	Residual Stress and Distortion — Metallo-thermo-mechanics Simulation of Engi- neering Processes incorporating Phase Transformation . . . . .	122
235:	Stress-strain Relation of CuAlNi SMA Single Crystal under Biaxial Loading - Constitutive Model and Experiments . . . . .	122
236:	* Simulation of Dual Frequency Induction Hardening Process of a Gear Wheel . . . . .	123
237:	* Progress of Phase Boundaries and Walls in Thermo-deformable Solids: A Canon- ical Approach . . . . .	123
238:	* Molecular Dynamics Simulation of Change in Surface Shape and Microstructure of Thin Film during Melting and Solidification Process . . . . .	124
239:	* Molecular Dynamics Simulation of Melting/Solidification and Induced Stresses . . . . .	124
240:	* Phase Transformation and Related Thermo-Mechanical Behavior — A Molecular Dynamics Approach . . . . .	125
241:	* Simulation of Materio-Thermo-Mechanical Fields — Macro- and Microscopic Ap- proach . . . . .	125
242:	* Experiment and Simulation for Thick-Plate Bending by High Frequency Inductor . . . . .	126
243:	* Stress Analysis of Quenching Process Following Draw Forming . . . . .	126
244:	Measurement of Static Strain Distribution Using Piezoelectric Polymer Film (Prin- ciple and Application to a Holed Plate) . . . . .	127
245:	Stress Magnetization Properties of Low Carbon Steel (SM490A) and Ni . . . . .	127
246:	Magnetic Impedance of Fe-28% Mn-Si-Cr Shape Memory Alloy . . . . .	127
247:	Effects of Stress on Magnetostriction and Magnetization Curve of Ferromagnetic Materials . . . . .	128
248:	Effect of Specimen Geometry on Strength in Engineering Ceramics . . . . .	128

249:	* Bending Strength of Borosilicate Glass Coated with Alumina and Silicon Carbide by RF Magnetron Sputtering . . . . .	129
250:	Interrelation Analyses of Mechanical Properties in Commercial Ceramics Using Cataloged Data . . . . .	129
251:	* Estimation of Residual Stress with Non-Uniform Distribution by Indentation-Fracture Method in Ceramics . . . . .	130
252:	Public Acceptance of Fusion Energy and Scientific Feasibility of a Fusion Reactor III Summary . . . . .	130
253:	Design of a Steady-State Tokamak Device with Superconducting Coils for a Volumetric Neutron Source . . . . .	131
254:	Inertial Electrostatic Confinement Fusion Simulation . . . . .	131
255:	Experimental Results of Inertial- Electrostatic Confinement Fusion . . . . .	132
256:	Decay Rate Measurements in a Negative Ion Rich Plasma . . . . .	132
257:	Study of the Performance Characteristics of a Travelling-Wave RF-Gun . . . . .	133
258:	Improvements of a Staggered-Array Undulator by Tapered Iron Disks . . . . .	133
259:	Numerical Study on Improvements of Beijing FEL Lasing Performances through Modifications of the Beam-Duct Geometry . . . . .	134
260:	Study on Inertial Electrostatic Confinement Fusion as a Portable Neutron Source	134
261:	Accelerator Plasma-Target-Based Fusion Neutron Source . . . . .	134
262:	* Studies of Inertial Electrostatic Confinement Fusion Neutron Source . . . . .	135
263:	Evolution of Field Reversed Configuration Plasma with Rotating Magnetic Field	135
264:	Development of an Improved Two-Dimensional Finite-Element Code for Cylindrically Symmetric Eigenmodes . . . . .	136
265:	Experimental Studies of Inertial Electrostatic Confinement Fusion at Institute of Advanced Energy . . . . .	136
266:	* Numerical Studies of Inertial Electrostatic Confinement Fusion Taking Account of Atomic Processes . . . . .	136
267:	Perspective of Inertial-Electrostatic Confinement Fusion . . . . .	137
268:	Dependence of Ductile-Brittle Transition Behavior on the Specimen Size and Location of Notch in the HAZ of Welded A533B PVS . . . . .	137
269:	Dependence of Impact Properties on Irradiation temperature in Reduced Activation Martensitic steels . . . . .	138
270:	* Enhancement of Irradiation Hardening by Nickel Addition in the Reduced-Activation 9Cr-2W Martensitic Steel . . . . .	138
271:	Swelling Behavior of V-Fe Binary and V-Fe-Ti Ternary Alloys . . . . .	139
272:	Production of Low Activation Steel; JLF-1, Large Heats-Current Status and Future Plan . . . . .	139
273:	* Assessment of Helium Embrittlement of Reduced-Activation 9Cr Martensitic Steels . . . . .	140
274:	Factors Controlling Kinetics of Hydrogen Embrittlement of Intermetallic Compounds . . . . .	140
275:	Advanced Experimental Techniques for Material Engineering Workability Evaluation Technique – Evaluation of High Temperature Dynamic Fracture Toughness .	141

276:	Magnetic Nondestructive Evaluation of Fatigue Damage of Ferromagnetic Steels for Nuclear Fusion Energy Systems . . . . .	141
277:	Round-robin Test for Nondestructive Evaluation of Steel Components in Nuclear Power Plants . . . . .	142
278:	* Magnetic Nondestructive Evaluation of Accumulated Fatigue Damage in Ferromagnetic Steels for Nuclear Plant Component . . . . .	142
279:	Intelligent Beam Transforming Earthquake Force into Vibration Control Force and Its Optimal Design . . . . .	143
280:	Method for Reducing Sound Radiated From Structures Using Vibration Absorbers Optimized with a Neural Network . . . . .	143
281:	Piezoelectric Sensor and Electromagnetic Linear Actuator System and Its Application to Vibration Control of a Motor on a Flexible Structure . . . . .	144
282:	* Nonlinear Vibration Control for a High-Tc Superconducting Levitation System	144
283:	Vibration Control of Spindles of Machine Tools by Using Piezoelectric Actuators Under the Disturbance Cancellation and H-Infinity Control . . . . .	145
284:	Vortex Shedding Resonance From a Rotationally Oscillating Cylinder . . . . .	145
285:	Active Control of Vortex Shedding from Circular Cylinder by Rotary Oscillations (Optimized with Neural Network) . . . . .	146
286:	Micro-Vibration Suppression Mechanism and Adaptive Control for a Milling Machine Spindle . . . . .	146
287:	Control for Passing Through Critical Speeds of a Superconducting Radial Bearing by Using Electromagnetic Actuators . . . . .	147
IV	Department of Energy Science and Technology . . . . .	148
288:	Design of a Bit-Serial Word-Parallel Functional Memory with Ferroelectric Capacitor . . . . .	148
289:	Simulation on Thermionic Electron Emission Rate Considering Local Field in Ferroelectric Thin Film . . . . .	148
290:	Crystal growth of layered perovskite $Sr_2Nb_2O_7$ and $Sr_2Ta_2O_7$ film by sol-gel technique . . . . .	149
291:	* Importance of Metal-Metal Bondings at the Interface of MgO and 3 <i>d</i> -Transition Metals . . . . .	149
292:	* Electronic Mechanism of Ag-Cluster Formation in AgBr and AgI . . . . .	150
293:	* Chemical Bonding at the Fe/TiX(X=C, N or O) Interfaces . . . . .	150
294:	* Electronic Structures and Chemical Bonding of $TiX_2$ (X=S, Se, and Te) . . . . .	151
295:	* Chemical Bondings around Intercalated Li Atoms in $LiTiX_2$ (X=S, Se, and Te)	151
296:	* Electronic Structure and Chemical Bondings of $TiS_2$ by Cluster Calculation . .	152
297:	* Analysis of Covalent Effects on the Multiplet Structure of Ruby Based on First-Principles Cluster Calculations . . . . .	152
298:	* Electronic States of Solid State Materials Using Model Clusters (in Japanese)	153
299:	* Chemical bonding of 3d transition-metal disilicides . . . . .	153
300:	* Madelung energy of metal-metalloid compounds . . . . .	153
301:	* Interaction between Oxygen and 3d Transition-metal Impurities on ZnO(10-10) Surface . . . . .	154

302:	* Calculation of Grain-Boundary Bonding in Rare-Earth-Doped $\beta$ -Si <sub>3</sub> N <sub>4</sub> . . . . .	154
303:	* Cluster Calculation of oxygen K-edge electron-energy-loss near-edge structure of NiO . . . . .	154
304:	Steady and Unsteady Heat Transfer from a Flat Plate in Subcooled He II . . . . .	154
305:	Electrical Resistivity of a High-T <sub>c</sub> Superconductor for Electric Current Higher Than $I_c$ . . . . .	155
306:	Incipient Boiling Superheat in Liquid Sodium . . . . .	156
307:	Mechanisms of Subcooled Flow Boiling Critical Heat Fluxes on Vertical Cylinder Surface and on Short Tube Inner Surface in Water Flowing Upward at Various Pressures . . . . .	156
308:	Transient Heat Transfer Caused by a Stepwise Heat Input to a Flat Plate in Pressurized He II . . . . .	157
309:	Critical Heat Flux on Various Sized Flat Plates in Pressurized He II . . . . .	157
310:	A Model for the CHF of One-wall Heated Rectangular He II Channel Critical Heat Flux on Various Sized Flat Plates in Pressurized He II. . . . .	158
311:	Critical Heat Fluxes in Subcooled Boiling of Water Flowing Upward in a Vertical Tube for Wide Ranges of Liquid Velocity, Subcooling and Pressure . . . . .	158
312:	* Experimental Study on Superconducting Fault Current Limiter with Adjustable Trigger Current Level . . . . .	159
313:	Thermoelectric Power Generation: Converting Low-Grade Heat into Electricity . . . . .	159
314:	Experimental Phase Diagram in the Ag-Cu <sub>2</sub> O-CuO System . . . . .	160
315:	Thermodynamic description of the Pb-O System . . . . .	160
316:	Experimental Phase Equilibria in the PbO <sub>x</sub> -CaO System . . . . .	160
317:	Thermoelectric Properties of the Fe-Al and Fe-Al-Si Alloys for Thermoelectric Generation Utilizing Low-Temperature Heat Sources . . . . .	161
318:	Titanium Powder Production by TiCl <sub>4</sub> Gas Injection into Magnesium through Molten Salts . . . . .	161
319:	New Iron-Based Thermoelectric Junctions and Thermoelectric Generation Concept	162
320:	Solid State Deoxidation of Niobium by Vacuum Deposited Titanium . . . . .	162
321:	Evaporation Process in Vacuum Metallurgy . . . . .	162
322:	Thermodynamic considerations of zirconia electrochemical sensors . . . . .	163
323:	A thermodynamic study of Calcium cyanamide . . . . .	163
324:	Activities of phosphorous in Cu-Co-P alloys at 1573 K . . . . .	164
325:	Equilibrium between aluminum and oxygen in Fe-36 . . . . .	164
326:	Trends and Short-Term Prospects for Energy Consumption from a Statistical Point of View . . . . .	164
327:	Instabilities in the Consumption and Production for Cobalt . . . . .	165
328:	* Fluorescent Approach to Visualize Grout Injected into rock Masses . . . . .	165
329:	Topographic Survey in Open-cut Mines by Using RTK-GPS . . . . .	166
330:	Use of GPS for Generating Topographic Maps and Production Schedules of Open Pit Mines . . . . .	166
331:	Numerical Model for Gas-Liquid Two-Phase Mixture Flow in a Vertical Pipe with a Sudden Enlargement in Diameter . . . . .	167

332:	* A Simple Approach to Plane Strain Extrusion with Dead Metal Zone Using Upper-Bound Theorem . . . . .	168
333:	* Modelling on Flow Stress of Mg-Al-Zn Alloys at Elevated Temperatures . . . . .	168
334:	* Finite Element Analysis of Forming Limit in Bore Expanding of Aluminium Alloy Sheets . . . . .	168
335:	Collision Dynamics of a Water Droplet Impinging on a Hot Solid Surface . . . . .	169
336:	* Numerical Analysis of the Formability of an Aluminium 2024 Alloy Sheet and Its Laminates with Steel Sheets . . . . .	169
337:	* Formability of a Commercially Pure Zirconium Sheet . . . . .	170
338:	Theoretical Analysis of Flow Characteristics of Multiphase Mixtures in a Vertical Pipe . . . . .	170
339:	* Reduction of Noise Radiated from Supersonic Jet by Interaction between the Screech and Cavity Tones . . . . .	171
340:	* Acoustic Characteristics of the Noise Radiated from Supersonic Multi-Jets . . . . .	171
341:	Numerical Simulation of Unsteady Supersonic Circular Jet . . . . .	171
342:	* Effect of Hydrolysed Metal Cations on the Liquid-Liquid Extraction of Silica Fines with Cetyltrimethylammonium Chloride . . . . .	172
343:	Recycling of Disposal Consumer Electronics Goods – Recovery of Copper Components from Disposed Print Wiring Boards by Hydrocyclone . . . . .	172
344:	* Two-Liquid Flotation of Fine Oxide Particles with 8-Hydroxyquinoline . . . . .	173
345:	* Measurements of Concentration Profiles of Cu <sup>2+</sup> and H <sup>+</sup> Ion near a Plane Vertical Anode by Two-Wavelength Holographic Interferometry . . . . .	173
346:	* Physical Modelling of Top Injection Smelting . . . . .	174
347:	* Electrodeposition of Copper under Microgravity Conditions . . . . .	174
348:	Electrochemical Interfacial Phenomena under Microgravity Part 1 Electrochemical Dissolution of Copper in Drop Shaft . . . . .	175
349:	Characteristics of the NIJI-IV FEL at the electron-beam energy of 263 MeV . . . . .	175
350:	Positron annihilation induced Auger electron spectroscopy with an intense slow-positron beam . . . . .	176
351:	The Development of Ferritic Steels for DEMO Blanket . . . . .	176
352:	Progress in the Development of SiC/SiC Composites for Advanced Energy Systems:CREST-ACE Program . . . . .	177
353:	Roles of Interfacial Microstructure on Interfacial Shear Strength of SiC/SiC . . . . .	177
354:	Microstructural Evolution of SiC/SiC Composite under Irradiation . . . . .	177
355:	Effect of Fiber Coating on Initiation and Growth Characteristics in SiC/SiC under Indentation Test . . . . .	178
356:	Evaluation of Low-Temperature Swelling in Austenitic Stainless Steels . . . . .	178
357:	* The HFIR 14J SiC/SiC Composite and SiC Fiber Collaboration . . . . .	179
358:	Analysis of Interfacial Shear Process of CMCs . . . . .	179
359:	Weld Cracking Behavior of Neutron Irradiated Austenitic Stainless Steel . . . . .	179
360:	Development of High Performance Composites for Environment-Conscious Energy Applications . . . . .	180

361:	Multiple Beams-Material Interface Research Facility at Kyoto University and Prospective Application to Advanced Energy Materials Study . . . . .	180
362:	Interfacial Fracture Behavior of SiC/SiC Composites for Fusion Application . . . . .	181
363:	Fatigue Property of Low Activation Ferritic Steel and Its Weld Joint . . . . .	181
364:	Dislocation Evolution in an Austenitic Alloy Induced by Post-irradiation Micro-Indentation . . . . .	182
365:	Effect of Fiber Coatings on Crack Behaviors in SiC/SiC . . . . .	182
366:	Fabrication of High Performance SiC/SiC Composite by Polymer Impregnation and Pyrolysis Method . . . . .	183
367:	CREST-ACE(R & D of Advanced Material Systems for Conversion of Energy) Program and Materials R & D Strategy for Nuclear Fusion Applications . . . . .	183
368:	Current Status and Future R&D for Reduced-Activation Ferritic/Martensitic Steels	184
369:	* Effect of Fiber Coating on Interfacial Shear Strength of SiC/SiC by Nano-indentation Technique . . . . .	184
370:	Crack Initiation and Growth Characteristics in SiC/SiC under Indentation Test . . . . .	184
371:	Current Status of SiC/SiC Composite R&D . . . . .	185
372:	Influence of Tantalum and Nitrogen Contents, Normalizing Condition and TMCP Process on Mechanical Properties of Low Activation 9Cr-2W-0.2V-Ta Steels for Fusion Application . . . . .	185
373:	Dependence of Post - Irradiation Impact Properties on the Irradiation Temperature in Reduced Activation 9Cr-2W Martensitic Steels . . . . .	186
374:	Glass-ceramic Joining and Coating of SiC/SiC for Fusion Applications . . . . .	186
375:	Radiation Response of SiC-based Fibers . . . . .	187
376:	Neutron Irradiation Experiments for Fusion Reactor Materials through JUPITER Program . . . . .	187
377:	Materials Design and Relating R&D Issues for the Force-Free Helical Reactor(FFHR)	188
378:	Coherent soft X-ray generation with femtosecond high-intensity lasers . . . . .	188
379:	Strong-field interaction for high-order harmonic generation . . . . .	189
380:	The white light supercontinuum is indeed an ultrafast white light laser . . . . .	189
381:	Coherent control of photoabsorption: Application to real atoms . . . . .	189
382:	* Collisional relaxation of the 5d6p J=1 states of laser-ablated Ba in He gas at room temperature . . . . .	190
383:	* Temperature-dependent depolarization cross sections of the 5d6p $^3P_1$ and $^3D_1$ states of laser-ablated Ba in He gas in the range of 10-300K . . . . .	190
384:	* Population transfer in N-level systems assisted by dressing fields . . . . .	190
385:	Radiative lifetimes and collisional deactivation cross sections of the 5d6p states of laser-ablated Ba in He gas . . . . .	191
386:	Origin of the phase lag in the modulation of photoabsorption products under two-color excitation . . . . .	191
387:	Critical Heat Fluxes in Subcooled Boiling of Water Flowing Upward in a Vertical Tube for Wide Ranges of Liquid Velocity, Subcooling and Pressure . . . . .	192

388:	Critical Heat Flux on Various Sized Flat Plates in Pressurized He III. . . . .	192
389:	Transient Heat Transfer Caused by Stepwise Heat Input to a Flat Plate in Pressurized He II . . . . .	193
390:	A Model for the CHF of One-wall Rectangular He II Cannel . . . . .	193
391:	Mechanisms of Subcooled Flow Boiling Critical Heat Fluxes on Vertical Cylinder Surface and on Short Tube Inner Surface in Water Flowing Upward at Various Pressures . . . . .	194
392:	Incipient Boiling Superheat in Liquid Sodium . . . . .	194
393:	Effect of Surface Conditions on Pool Boiling Critical Heat Fluxes in Saturated and Subcooled Liquid Nitrogen at Various Pressures . . . . .	195
394:	Steady and Unsteady Heat Transfer from a Flat Plate in Subcooled Helium II . . .	195
395:	Electrical Resistivity of a High-Tc Superconductor for Electric Current Higher than $I_c$ . . . . .	196
<b>3</b>	<b>Review Articles</b>	<b>197</b>
I	Department of Socio-Environmental Energy Science . . . . .	197
1:	Supercritical Fluids to Biomass Research . . . . .	197
2:	Topochemistry of Wood-Inorganic Composites as Prepared by the Sol-Gel Process	197
3:	Biomass for Clean Energy Sources . . . . .	198
4:	Environmental Life Science of NO . . . . .	198
5:	Review on Present State of Human Model Researches in Nuclear Engineering and the Prospect for their Industrial Applications . . . . .	198
6:	Nuclear Energy Demand in Asia . . . . .	199
7:	Constraint of CO <sub>2</sub> Emission Right and Estimation of Nuclear Generation in Asia	199
II	Department of Fundamental Energy Science . . . . .	200
8:	Surface Modification by Molten Salt Electrochemical Process . . . . .	200
9:	New Trends in Molten Salt Technology . . . . .	200
10:	Crystal Chemistry of Novel Complex Vanadium Oxides with Layered Structures	200
11:	Characterization of Mixed Conducting Fluorite Oxides and Their Application to Electrodes for High Temperature Steam Electrolysis . . . . .	201
12:	Electronic Structure of Cathode Materials for 5V Lithium Ion Batteries . . . . .	201
13:	Structural Phase Transition of Metastable A-type Vanadium Dioxide VO <sub>2</sub> (A) . . .	201
14:	Progress of Plasma Physics . . . . .	202
15:	Long-range Attractive Interaction between Macroparticles in Solvents . . . . .	202
16:	Theoretical Analysis on Structure of the Metal-Aqueous Electrolyte Solution Interface . . . . .	202
17:	The Present Active Status of Domestic Critical Assemblies and the Perspective for Their Future - Thire Role Explored in National Nuclear Power Utilization - . . . .	203
18:	Visualization and Measurement Technique Using Neutron Radiography . . . . .	203
19:	The Proposal to Evaluate Activation of Protect Pollution by Photocatalysis . . . .	203
20:	TiO <sub>2</sub> Photocatalyst for Water Treatment . . . . .	203
21:	Be the Real Active Core of Research Exchange . . . . .	204
22:	Possibility to apply Photocatalyst for Hypersensitivity of Chemical Substances .	204
23:	Photocatalyst-Applied Expension for the Field of Illumination . . . . .	204

24:	"Light Cleaning" Learn a Plant . . . . .	204
25:	BUKKATENPOU . . . . .	204
26:	TiO <sub>2</sub> Photocatalyst build Next Generation of Civilization . . . . .	205
27:	The Light Start a Revolution of the Environment . . . . .	205
28:	Related Topics and Future View of the Research of Photocatalyst . . . . .	205
29:	Antibacteria and Protect Pollution by TiO <sub>2</sub> Photocatalyst . . . . .	205
30:	Photocatalyst-The Light Clean the Environment . . . . .	205
31:	TiO <sub>2</sub> Photocatalyst can Clean the Environment . . . . .	206
32:	Antibacteria by TiO <sub>2</sub> Photocatalyst Reaction . . . . .	206
33:	Active Species Behavior of TiO <sub>2</sub> Photocatalyst Reaction . . . . .	206
34:	The Photocatalyst of Today and Future . . . . .	206
III	Department of Energy Conversion Science . . . . .	207
35:	Engineering Approach for Mitigation of Greenhouse-Effect Gases . . . . .	207
36:	Development of Combustion Diagnostics . . . . .	207
37:	Development of Combustion Diagnostics 2 Gas-Flow Measurement using Particle Image Velocimetry . . . . .	207
38:	Combustion in Hydrogen Engines . . . . .	208
39:	Technology for Emission Control in Internal Combustion Engines . . . . .	208
40:	Fuel-Air Turbulence Mixing and It's Effects . . . . .	208
41:	Solid Mechanics under Magnetic Field . . . . .	209
42:	Fracture and Probabilistic Models in Advanced Materials — (2) Ceramics, Part 1 Properties of Static Fracture Strength . . . . .	209
43:	Fracture and Probabilistic Models in Advanced Materials — (2) Ceramics, Part 2 Properties of Static and Cyclic Fatigue . . . . .	210
44:	Fracture and Probabilistic Models in Advanced Materials — (2) Ceramics, Part 3 Proof Testing . . . . .	211
45:	Fracture and Probabilistic Models in Advanced Materials — (2) Ceramics, Part 4 Evaluation of Scatter in Strength and Fatigue Life . . . . .	211
46:	Method for Reducing Noise of a DC-Motor with Constant Current Control . . . . .	212
47:	On the Electromagnetic Vibration of Rotating Machine . . . . .	212
IV	Department of Energy Science and Technology . . . . .	213
48:	Integrated Circuit . . . . .	213
49:	Phase Control of photoabsorption processes . . . . .	213
<b>4</b>	<b>Books</b>	<b>215</b>
1:	Persuit of Happiness . . . . .	215
2:	The Encyclopedia of Wood Industry . . . . .	215
3:	Human Interface . . . . .	215
4:	Cognitive Systems Engineering in Process Control '96 . . . . .	216
5:	Tomorrow Energy and Environment, Suggestion from Kyoto, Japan . . . . .	216
6:	Stellarator and Heliotron Devices . . . . .	216
7:	Modeling and simulation methods for plasma processing . . . . .	217
8:	Gas-Flow Measurement of Micro-Structure in a Jet Flame by PIV(Innovative Mea- surements in Thermo-Fluids) . . . . .	217

9:	Hydrogen Engine (Exergy Engineering) . . . . .	217
10:	Fundamentals of Strength Analyses . . . . .	218
11:	Handbook of Cryogenic Engineering, Chapter 3 Cryogenic Heat Transfer, 3-3-2 Predicting the Critical Heat Flux for a Horizontal Cylinder in Saturated Liquid He I	218
<b>5</b>	<b>List of Academic Staff</b>	<b>221</b>

## *A. Current Research Fields*

A. 研究現況

# Chapter 1

## Current Research Fields

### I Department of Socio-Environmental Energy Science

a1-1	Pursuit of happiness	幸福論
a1-2	New material for energy saving	低環境負荷材料の開発
a1-3	Recycle process	リサイクルプロセス
a2-1	Analysis of Energy Supply and Demand in Japan	日本のエネルギー需給分析
a2-2	Quantitative Analysis of the Moratorium on the Development of Nuclear Power	原子力開発の停滞による影響の定量的評価
a2-3	Life Cycle Analysis of Electric Vehicle	電気自動車のライフサイクル分析
a2-4	Economic Analysis of Energy Efficient Technologies	省エネルギー技術の経済性分析
a2-5	Measures for Economic Penetration of the Photovoltaic Power System for Residential Use	住宅用太陽光発電の経済的普及方策
a2-6	Measures for Economic Support of the Construction of Power Plants	発電所の立地に関する経済的支援方策
a3-1	Chemical conversions of biomass and plastics wastes to their liquified fuels by the supercritical fluids	超臨界流体によるバイオマスおよび廃プラスチックの液体燃料化に関する研究
a3-2	Bioconversion of lignocellulosics to ethanol by the supercritical water	超臨界水によるリグノセルロースのエタノールへの酵素変換に関する研究

a3-3	Pyrolysis of lignocellulosics to value-added chemicals	リグノセルロースの熱分解による有用物質への変換
a3-4	Topochemistry of biocarbon-inorganic composites for their property-enhancement	無機質複合化バイオカーボンの諸機能発現に関するトポ化学
a3-5	Long-living of wood enhanced by antimicrobial treatments	防菌・防黴性付与による木材のロングライフ化に関する研究
a3-6	Forest soil and carbon cycling in earth ecology	地球生態系での炭素循環と森林土壌に関する研究
a4-1	Environmentally clean renewable energy production by biological systems	生化学システムによるクリーンエネルギー生産
a4-2	Exploration of bioremediation systems for environmental toxic molecules	生化学システムによる除去
a4-3	Biochemical and chemical studies on the interaction of nitric oxide with gene and its regulation in the transcription process	一酸化窒素による遺伝子損傷とその制御
a4-4	Structural studies on nucleic acids by magnetic resonance spectroscopy	核酸の構造化学
a4-5	Electrical and thermodynamic phenomena on the metal/metal and metal/semiconductor diamond interfaces	金属/金属、金属/半導体界面の電氣的・熱力学的性質
a5-1	Development of Mutual Adaptive Interface with Eye-Sensing HMD	アイセンシングHMDによる相互協調型インタフェースの開発
a5-2	A Study on a Human Model based on Artificial Intelligence	AIによるヒューマンモデルの構築
a5-3	Adaptive Interface based on Recognition of Facial Expression and Verbal Protocol	顔表情・発話認識を用いた適応型インタフェース
a5-4	A Study on Integrated CAI system	統合型教育支援システムの構築
a5-5	Development of Maintenance Training System based on Networked Virtual Environment	共有仮想空間を用いた保修訓練システムの構築
a5-6	Optimal Planning of Autonomous Decentralized Energy System	自律分散型エネルギーシステムの計画
a6-1	Characterization of Physical and Chemical Properties of Atmospheric Aerosols	大気エアロゾルの物理・化学的性状の特性化

a6-2	Application of PIXE Analysis to Atmospheric Sciences	PIXE 分析法の大気環境科学への応用
a6-3	Analysis and Modelling of Deposition of Air Pollutants	大気汚染物質の沈着機構の解析とモデル化
a6-4	Long-Range Transport of Gaseous and Particulate Air Pollutants Combined with Chemical Transformation and Removal	沈着、変質を伴う大気汚染物質の長距離輸送モデルの開発
a6-5	Evaluation of Radiative Forcing by Atmospheric Aerosols	大気エアロゾル粒子の放射収支への影響評価
a6-6	Analysis of Environmental Loads in Energy Systems	エネルギーシステムにおける環境負荷評価
a7-1	Conceptual Study on Symbiotic Energy Plants in Local Regions	地域共生プラントの概念検討
a7-2	Study on the Social Acceptance of Energy	エネルギーの社会受容に関する研究
a7-3	Rating of the Degree of Sensationality of Media Expression	メディア表現のセンセーショナル度評価
a7-4	Study of the Lifestyle Taking into Account the Environmental Condition	環境問題を考慮したライフスタイルの研究
a7-5	Research on Social Communication by the Use of Homepage	ホームページの活用によるコミュニケーション
a7-6	Study on the Virtual Environment of Dispersed Type	分散型仮想環境の研究
a8-1	Scientific consideration about best mixture of electricity sources in future	将来における電力源のベストミックス（最適組合せ）に関する科学的考察
a8-2	Investigation on nuclear subjects including non-proliferation, safeguards, physical protection, transportation, criticality safety, radioactive waste management, etc.	核不拡散、保障措置、核物質防護、核燃料輸送、臨界安全、放射性廃棄物管理などの核問題に関する研究
a8-3	Study on application of reactor neutrons to medicine	原子炉中性子の医学への利用に関する研究
a8-4	Neutron radiography	中性子ラジオグラフィ
a8-5	Experimental study on neutron-induced fission	中性子核分裂に関する実験的研究

a8-6	Evaluation of fluence and absorbed dose for neutrons and gamma-rays	中性子、ガンマ線のフルエンス及び吸収線量の評価
a9-1	Formation and evolution of nuclear-safety culture	原子力安全文化の醸成
a9-2	Transmission of information and public relations on energy problems	エネルギー問題に関する情報伝達と公報
a9-3	Formation of public attitudes on nuclear energy or radioactivity issues	原子力・放射線/放射能問題に関する社会の態度形成
a9-4	Neutron Activation Analysis of Ivory of African Elephants	アフリカ象の象牙の中性子放射化分析
a9-5	Physical Interpretation of Adjoint Flux in Reactor Physics	原子炉物理における随伴中性子束の物理的意味
a10-1	Japanese Strategy for Mitigating Global Environmental Issues (Global Warming)	地球環境問題、地球温暖化に対する日本の政策
a10-2	Analysis on Heat Cascading among Industrial Customers	産業需要家間のヒートカスケード化の分析
a10-3	Analysis on Wheeling in Electric Power Network	電力における託送の分析
a10-4	Effective Utilization of Uranium by Using High Burn-up Fuel Technology in Light Water Reactors	軽水炉用高燃焼度燃料によるウラン資源有効活用利用
a10-5	Plutonium Utilization in Light Water Reactors	軽水炉でのプルトニウム有効利用

## II Department of Fundamental Energy Science

b1-1	Electrochemical Energy Conversion by Fuel Cells and Hydrogen Systems	燃料電池、水素エネルギーシステムによる電気化学的エネルギー変換
b1-2	Physical Chemistry of Molten Salts and Applications to Energy Conversion Processes	熔融塩の物性・化学とエネルギー変換プロセスへの応用
b1-3	New Functional Materials and Their Applications	マテリアル・テーラリングによる新規な機能材料の創製と応用
b1-4	Development of Interdisciplinary Fields of Electrochemistry and Plasmas/Ion Beams	プラズマ、イオンビームなどと電気化学の境界領域の開拓

b1-5	Determination of Molecular and Solid Structures by Vibrational Spectroscopies and Diffractions	ラマン分光、中性子回折などによる物質構造の解明
b1-6	Inorganic Halogen Chemistry and Applications to Energy Processes	フッ化物、塩化物の化学とエネルギープロセスへの応用
b2-1	Dynamics of the conduction electrons in chalcogenide semiconductors and the related optical properties	カルコゲン化合物半導体における伝導電子の動的挙動と分光特性
b2-2	The transport processes and the percolative critical phenomena in structurally complicated media	複雑系における伝導プロセスとパーコレーション臨界現象
b2-3	Superconductivity in nano-metrically disordered high- $T_c$ cuprates	乱れたナノ構造を持つ高温超伝導体における超伝導
b2-4	Thermoelectric and galvanomagnetic effects in semimetals and semiconductors	半金属と半導体における熱電効果と低温強磁場電流磁気効果
b2-5	Synthesis of High Performance Materials by DC Arc Plasma	DC アークプラズマによる高機能材料の合成
b2-6	Micro-Characterization at the Interface of High Performance Materials	高機能材料界面のマイクロキャラクタリゼーション
b3-1	Analysis and Design of Ceramic Energy Materials	セラミックスエネルギー材料の解析と設計
b3-2	Studies on Rechargeable Lithium Battery Materials	リチウム2次電池の材料開発
b3-3	Development of Solid Oxide Fuel Cell Systems	固体酸化物型燃料電池の開発
b3-4	Synthesis of Functional Ceramic Thin Film from Aqueous Solution	水溶液からの機能性セラミックス薄膜の合成
b3-5	Design and Analysis of Novel Optical Energy Materials	新規光エネルギー材料の設計と解析
b3-6	Development of Hydrogen Energy System Materials	水素エネルギーシステム材料の開発
b4-1	fusion plasma	核融合プラズマ
b4-2	MHD theory	MHD理論
b4-3	plasma transport theory	プラズマ輸送理論

b4-4	optimization of stellarator field	ステラレータ磁場の最適化
b4-5	study of process plasma	プロセスプラズマの研究
b5-1	Studies on multiply-ionized impurity ions in high temperature plasmas.	高温プラズマ中の多価電離不純物イオンの研究
b5-2	Theoretical studies on equilibrium and stability in the 3-dimensional non-axis symmetric torus plasmas.	3次元非軸対称トーラスプラズマの平衡と安定性の理論的研究
b5-3	Studies on magnetohydrodynamic(MHD) equilibrium and plasma current in non-uniform magnetic field.	磁場測定による不均一磁場中の超高温プラズマの平衡および内部電流の研究
b5-4	Studies on radiation by bolometric and spectroscopic diagnostics from high temperature plasmas.	ボロメーターおよび分光による高温プラズマからの輻射の研究
b5-5	Studies on neutron energy spectrum by D-D reaction.	高温プラズマ中の D-D 反応による中性子のエネルギースペクトルの研究
b6-1	Electron cyclotron heating and current drive	プラズマの電子サイクロトロン加熱・電流駆動
b6-2	Control of MHD instabilities by LHCD	低域混成電流駆動による磁気流体不安定性の制御
b6-3	Control of MHD instabilities by ECH	電子サイクロトロン加熱による磁気流体不安定性の制御
b6-4	Plasma diagnostics (soft X-ray CT and ECE)	プラズマ診断法の開発(軟 X 線トモグラフィと電子サイクロトロン輻射計測)
b6-5	Confinement and nonlinear waves in non-neutral plasmas	非中性プラズマの閉じ込めと非線形波動
b7-1	Confinement Study of High Temperature Plasma in Helical System	ヘリオトロン装置による高温プラズマの閉じ込め制御
b7-2	Study of Helical Magnetic Configuration	ヘリカル磁場構造の研究
b7-3	Control of Edge Plasma	プラズマ閉じ込め領域周辺部におけるプラズマ制御
b7-4	Divertor Study	ダイバータ基礎研究

b7-5	Study of Plasma Production and Heating by Electron Cyclotron Wave	電子サイクロトロン波によるプラズマ生成・加熱の研究
b7-6	Study of Plasma Heating by Neutral Beam Injection	高速中性粒子によるプラズマ加熱の研究
b8-1	Study on High Temperature Plasma Heating and Confinement	超高温プラズマの加熱・閉じ込めに関する研究
b8-2	Experimental Analysis of Vacuum Magnetic Field Structure	真空磁場配位の実験構造解析
b8-3	Development of Monte Carlo Calculation Scheme for the Simulation of Plasma Transport and Heating	プラズマの輸送と加熱のシミュレーションのための新しいモンテカルロ計算スキームの開発
b8-4	Theoretic Analysis on Charged Particle Orbit in the None-axisymmetrical Torus with Adiabatic Constants	非軸対称トーラスにおける荷電粒子軌道の断熱不変量をもちいた理論解析
b8-5	Study on the Advanced Heliotron Magnetic Field with the Control of Chaotic and Statistic Characteristics	磁力線のカオスや統計的性質の制御に基づいたヘリオトロン磁場の高性能化に関する研究
b8-6	Study on the Optimization of Ion Cyclotron Heating Antenna for Various Heating Modes	イオンサイクロトロン加熱の加熱モードによるアンテナ最適化の研究
b9-1	Infrared Photochemical Reaction of Haloalkanes.	ハロアルカン類の赤外光化学反応
b9-2	Hydrogen in and on Inorganic Solid Materials.	無機固体材料中の水素の挙動
b9-3	Photo Excitation, Relaxation, and Reactions on a Semiconductor Electrode.	半導体電極における光励起, 緩和, および反応機構
b9-4	Microstructure of Porous Materials and Their Physicochemical Properties.	多孔質材料の微細構造と物理化学特性
b9-5	Laser Ablation of Inorganic Solid Surfaces.	固体材料表面のレーザーアブレーション
b10-1	Design of Functional Supramolecules Based on Amphiphilic Molecular Assembly and their Utilization for Chemical Reaction and Separation of Substances	両親媒性分子集合体を用いた超分子集合体の構造設計とその反応分離場への応用
b10-2	Construction of Advanced Materials with Nano-Meso Sized Structure Using Amphiphilic Molecular Assemblies as Template	両親媒性分子集合体を鋳型として用いたナノ・メゾ材料の構築

b10-3	Method to Integrate the Processes for Obtaining Materials with Hierarchical Structures	階層構造を持つ材料作成プロセスのインテグレート手法
b10-4	Interaction between Solutes in Aqueous and Nonaqueous Solvents	水溶液中及び非水溶媒中における溶質間相互作用
b10-5	Prediction of Ternary Structures of Proteins in Aqueous Solutions	水溶液中におけるタンパク質の3次構造予測
b11-1	Molecular design of plastic enzyme	プラスチック酵素の分子設計
b11-2	Molecular design of asymmetric photocatalyst	不斉光触媒の分子設計
b11-3	Photo-induced enzyme reaction	酵素による光触媒反応
b11-4	Creation of high quality enzyme by artificial evolution	人工進化高機能酵素の創製
b12-1	Research on high-temperature batteries for energy storage	エネルギー貯蔵用高温二次電池の研究
b12-2	Elucidation of electrochemical behavior of sulfur dioxide and nitrogen oxides as the environmental pollutants	二酸化硫黄や窒素酸化物などの環境汚染物質の電気化学的挙動の解明
b12-3	Electrodeposition of refractory metals in molten salts	熔融塩電解によるリフラクトリーメタルの析出
b12-4	Analysis of current and potential distributions in electrochemical cells	電気化学セルにおける電流・電位分布の解析
b13-1	Study on nuclear characteristics of high performance reactors in next-generation	次世代の高性能新型原子炉の核特性研究
b13-2	Development of high performance advanced research reactor as neutron source	高性能研究用中性子源炉の開発
b13-3	Nuclear reactors utilizing thorium-uranium fuel cycle	トリウム・ウラン燃料サイクル原子炉
b13-4	Hybrid reactor system of accelerator driven fission reactor	加速器と核分裂炉のハイブリッド炉
b13-5	Transmutation and incineration of high level nuclear waste	高レベル放射性廃棄物の消滅処理
b13-6	Criticality safety study of nuclear fuel facility	核燃料施設の臨界安全性研究

b14-1	Study on target cooling of a spallation neutron source	スプレーション中性子源のターゲット冷却に関する研究
b14-2	Flow and heat transfer characteristics of gas-liquid two-phase flow in narrow channels	狭小流路における気液二相流の流動と伝熱
b14-3	Characteristics of two-phase flow with a large liquid/gas density ratio	高密度比気液二相流の特性
b14-4	Study on Thermal-Hydraulic Phenomena under Severe Accident Conditions	シビアアクシデント時の熱流動現象に関する研究
b14-5	Study on basic phenomena in post-CHF heat transfer	ポスト限界熱流束熱伝達の基礎的現象に関する研究
b14-6	Visualization and measurement of multiphase phenomena by neutron radiography	中性子ラジオグラフィによる混相流現象の可視化と計測
b15-1	Studies on TiO <sub>2</sub> thin film photocatalysts under weak UV light illumination.	酸化チタン光触媒反応の研究
b15-2	Applications and coating of fine particles	微粒子で構成される薄膜の作成と応用
b15-3	Studies on conductive diamond electrodes	導電性ダイヤモンド薄膜電極の研究

### III Department of Energy Conversion Science

c1-1	Mitigation of Pollutants in Thermal Energy Conversion Systems	熱エネルギー変換システムにおける汚染物質低減
c1-2	Mixture Formation and Combustion in Diesel and Spark-Ignition Engines	ディーゼル機関および火花点火機関の混合気形成と燃焼
c1-3	Spray Characteristics and Their Effects on Combustion	噴霧特性ならびにその燃焼への作用
c1-4	Prediction of Combustion Processes in Internal Combustion Engines	内燃機関内燃焼過程の予測
c1-5	Alternative Fuels in Combustion Systems	燃焼システムにおける代替燃料
c1-6	Optimum Design of Power Plants	動力プラントの最適設計
c2-1	Ignition and Combustion of Homogeneous and Heterogeneous Mixtures	均一および不均一混合気の着火と燃焼

c2-2	Chemical Reaction Kinetics of Pollutant Formation	汚染物質生成の化学反応動力学
c2-3	Structure of Turbulent Diffusion Flames	乱流拡散火炎の構造
c2-4	Laser Diagnosis and Image Analysis for Combustion Research	レーザ計測および画像解析による燃焼診断
c2-5	Numerical Simulation of Turbulent Flows and Combustion	乱流および燃焼の数値シミュレーション
c2-6	Mechanical Effects of Fluid Energy on Bio-Tissues and Cells	生体組織および細胞に及ぼす流体エネルギーの力学的作用
c3-1	Inelastic Constitutive Equation of High Temperature Materials and Construction of the Data Base	高温における非弾性構成式とそのデータベース化
c3-2	Foundation of Materio-Thermo-Mechanics and Computer Simulation of Some Processes Incorporating Phase Transformation	変態・熱・力学の基礎と相変態を伴う工学過程のコンピューターシミュレーション
c3-3	Analysis of Plastic Forming Process under Large Deformation Depending on Microstructural Evolution	大変形を伴う塑性加工過程の解析とそれに及ぼす組織の効果
c3-4	Development of Sheet Metal Bending Process by Line Heating Technology	線状加熱による板材の曲げ加工機の試作開発
c3-5	Molecular Dynamics Simulation of Thermo-Mechanical Fields under Phase Transformation	分子動力学による相変態過程とそれに伴う熱・力学場のシミュレーション
c4-1	Mechanics of Electromagnetic Materials	電磁気材料の力学
c4-2	Mechanics and Application of Functional Materials	機能材料の力学と応用
c4-3	Nondestructive Evaluation of Stress, Damage and Inhomogeneity by Ultrasonic Waves and Electromagnetic Phenomena	超音波と電磁気現象による応力, 損傷, 非均質の非破壊評価
c4-4	Processing of Ceramic-Coated Materials and Analysis of Their Structure and Deformation	セラミックス・コーティング材料の創成とその構造および変形の解析
c4-5	Strength Evaluation of Advanced Ceramics and Its Numerical Simulation	先進セラミックスの強度評価とその数値シミュレーション

c4-6	Computer Simulation of Fatigue Strength in Metallic Materials	金属材料の疲労強度コンピュータ・シミュレーション
c5-1	Assessment of Fusion Reactor	核融合炉のアセスメント
c5-2	Study of the Compact Neutron Source using Inertial Electrostatic Confinement Fusion	慣性静電閉じ込め方式核融合を用いたコンパクト中性子源の研究
c5-3	Study of the Radiation Divertor using Impurity Pellet Injection	不純物ペレット入射による放射ダイバータの研究
c5-4	Study of the Production Mechanism of Negative Hydrogen Ion in Plasmas	プラズマ中での負イオン生成メカニズムの解明
c6-1	Free Electron Laser	自由電子レーザーの研究
c6-2	Particle Simulation for Advanced Klystron Tube and RF Guns	クライストン及びRFガンの高性能化のための粒子シミュレーション研究
c6-3	D- <sup>3</sup> He Advanced Fuel Fusion	D- <sup>3</sup> He 先進燃料核融合炉の研究
c6-4	Beam-Beam Colliding Fusion (IECF)	ビーム衝突型核融合の研究 (慣性静電閉じ込め方式核融合)
c6-5	Spherical Plasma Generation and Application	球状プラズマの生成及び応用の研究
c7-1	Radiation Effects on Fusion Materials	核融合炉材料の照射効果
c7-2	Evaluation of Performance of Nuclear Reactor Structural Materials	原子炉構造材料の特性評価
c7-3	Environmental Effects on Advanced Intermetallic Compounds	先進金属間化合物の環境効果
c7-4	A Computational Study of Radiation Damage Processes	放射線照射損傷過程の計算機シミュレーション
c7-5	Magnetic Nondestructive Evaluation Techniques for the Integrity of Nuclear Power Plants	原子力プラント保全のための磁気的非破壊評価法
c8-1	Nonlinear Continuum Mechanics	非線形連続体力学
c8-2	Nonlinear Wave Propagation in Solids	固体における非線形波動
c8-3	Free/Moving/Growing Boundary Problem	自由/移動/成長 A

## IV Department of Energy Science and Technology

d1-1	Study on structure and process of VLSI	超L S I のデバイスプロセスに関する研究
d1-2	Study on electrical characteristics of scaled-down MOS devices	サブミクロンM O S デバイスに関する研究
d1-3	Study on reliability physics and modeling on carrier transport in insulating films	M O S 界面の信頼性物理とモデリングに関する研究
d1-4	Investigation of local chemical bondings of ceramics by EELS	高空間分解能 EELS 法による局所化学結合状態の解明
d1-5	Material design of new functional ceramics through electronic calculations	新しい機能性セラミックス材料の量子設計
d1-6	Electronic states of ceramic interfaces	セラミックス界面の機能と電子状態
d2-1	Heat transfer characteristics of cryogenic liquids (LN <sub>2</sub> , LHe, HeII) in relation to the cooling of superconducting magnets.	超伝導マグネット冷却に関連した極低温流体 (LN <sub>2</sub> , LHe, 超流動 He) の熱伝達特性
d2-2	High density heat removal from plasma facing devices in nuclear fusion systems.	核融合装置プラズマ対向壁からの高密度除熱
d2-3	Non-boiling and boiling heat transfer in liquid metals.	液体金属の非沸騰及び沸騰熱伝達
d2-4	Superconducting magnet energy storage system in electrical power system.	超伝導エネルギー貯蔵装置の電力系統特性に関する研究
d2-5	Power system characteristics of superconducting fault current limiter.	超伝導故障電流限流器の電力系統特性に関する研究
d2-6	Energy transfer between superconducting magnets.	超伝導マグネット間のエネルギー転送に関する研究
d3-1	Iron-Based Devices for Low Temperature Thermoelectric Generator.	低温用鉄基熱電素子の開発
d3-2	New Continuous Process for Production of Titanium Metal.	金属チタンの新しい連続精錬プロセスの開発
d3-3	Ammonium Gas Steel-Making.	アンモニアガス製鋼法
d3-4	Production of Functional Materials by Ozone Gas.	オゾンガスによる機能材料創製
d3-5	Thermodynamics of Superconductive Oxides.	酸化物超伝導材料の熱力学

d3-6	Refining of Refractory Metals.	高融点金属の精錬
d4-1	Physical Chemistry of Radioactive Nuclear Waste Management	放射性廃棄物処理の物理化学
d4-2	Thermochemistry of steelmaking	製鋼プロセスの熱化学
d4-3	Chemical sensors for metallurgical processes	材料プロセス用化学センサ
d4-4	Oxidation-reduction equilibrium in molten slags, fluxes and salts.	溶融スラグ、フラックス、ソルト中の酸化還元平衡
d4-5	Recovery of iron unit from waste generated at steel works	製鉄所起源の廃棄物からの鉄資源回収
d5-1	The Earth Energy and Mineral Resources	地球エネルギーと鉱物資源
d5-2	Trends and Forecasts for the Supply and Demand of Resources and Energy	資源エネルギーの需給動向と予測
d5-3	Geological Studies of Radioactive Waste Disposal	放射性廃棄物の地層処分
d5-4	Resources Development and Environmental Protection	資源開発と環境保全
d6-1	Theoretical Analysis of Air-Lift Pump System for Conveying Marine Mineral Resources from Deep-Sea Bed	深海底鉱物資源の揚鉱理論
d6-2	Analysis of Heat Transfer by Impinging Jet	衝突噴流による熱伝達解析
d6-3	Numerical Simulation of Working Processes	数値加工プロセス
d6-4	Behaviour of Liquid Droplets on Super-High Temperature Metal Surface	超高温金属表面における液滴の挙動
d6-5	Combined Simulation of Fluid Flow and Heat Transfer	流動・伝熱複合シミュレーション
d6-6	Prediction of Forming Limit in Sheet Metal Forming Processes	板材成形における成形限界予測
d7-1	Characteristics of supersonic pulse jet	超音速パルスジェットの特性的研究
d7-2	Numerical simulation of multi-phase flows	混相流の数値解析

d7-3	Electrochemical processing for compound semiconductor solar cell	化合物半導体太陽電池の電気化学プロセッシング
d7-4	Non-equilibrium electrochemical interfacial phenomena in space station	宇宙ステーションにおける非平衡電気化学界面現象に関する基礎的研究
d7-5	Fundamental studies on the liquid-liquid extraction of fine metal-oxide particles using chelating reagent as collector	キレート試薬を用いた液-液抽出による金属酸化物微粒子の分離に関する基礎的研究
d7-6	Development of the environmentally benign separation processes for ultrafine particles	地球環境調和型微粒子分離プロセスの開発
d8-1	NMR study of quantum spin-gap in low dimensional spin system	低次元スピン系における量子スピンギャップの核磁気共鳴
d8-2	NMR Study of Magnetic Frustration	フラストレートするスピン系における核磁気共鳴
d8-3	Generation of high-brightness electron beam	高輝度電子ビームの発生
d8-4	Generation of free-electron lasers	自由電子レーザーの発生
d8-5	Application of free-electron lasers	自由電子レーザーの応用
d8-6	Generation of novel high-brightness radiation	次世代の高輝度放射の発生
d9-1	R&D of Advanced Reduced-Activation Materials	先進低放射化材料の開発及び基礎研究
d9-2	Ceramic Composite Materials for Advanced Energy Systems	セラミクス系複合材料の開発と先進エネルギーシステムへの応用
d9-3	Physics and Irradiation Effects in Energy Conversion Materials	エネルギー変換材料の照射効果と物理
d9-4	Small Specimen Testing Technologies for Energy Materials Research	微小試験片による材料強度特性評価法の研究
d9-5	Joining of Materials for Nuclear Energy Systems	先進核融合・原子力材料等の接合の科学
d9-6	Fundamental Processes of Irradiation Creep	粒子線場における静的塑性変形挙動基礎過程の研究
d10-1	Development of advanced lasers	高機能レーザー開発
d10-2	Coherent interaction of lasers with atoms, molecules and solids	レーザーと原子・分子・固体とのコヒーレント相互作用

- |       |  |                          |
|-------|--|--------------------------|
| d10-3 | Strong-field phenomena and their applications                        | 高強度レーザー誘起現象とその応用         |
| d10-4 | Advanced energy transportation processes                             | 先端エネルギー輸送プロセス            |
| d10-5 | Heat transfer in normal liquids, liquid sodium and cryogenic liquids | 通常流体、液体ナトリウム及び低温液体中での熱伝達 |

## ***B. Original Articles***

*The mark (\*) indicates that the work was financially supported by Grant-in-Aid for Scientific Research, Ministry of Education, Science, Sports and Culture, Japan.*

## **B. 研究発表**

題目左肩の\*印は、文部省科学研究費補助金による研究であることを示す。

## Chapter 2

# Original Articles

### I Department of Socio-Environmental Energy Science

(エネルギー社会・環境科学専攻)

#### 1: \* Bulk nano-scale multilayers prepared by repeated pressing-rolling

Huang Bin Ishihara, K.N. Shingu, H.P.

Acta Metall. Sin., vol.34, no.5, 455-8, (1998)

Bulk nano-scale multilayers have been prepared by repeated pressing-rolling the initially macroscopically thick layered sample. The SEM and TEM observations revealed that the final layer thickness in the regular laminates is about 10 nm. The Fe/Cu multilayers exhibited a clear magnetoresistance (MR) ratio at 77 K. The tensile strength is over 1500 MPa and its elongation is about 0.8% at room temperature.

#### 2: \* Magnetoresistance of Nanoscale Fe/Ag Multilayer Produced by Repeated Press-rolling

金属粉末を繰り返し圧縮・圧延することにより作製した Fe/Ag ナノスケール人工格子の磁気抵抗効果の評価

Masaru Hashimoto, Akira Otsuki, Keiichi N.Ishihara and Hideo P.Shingu

Reprinted from Journal of the Japan Society of Powder and Powder Metallurgy 45 (1998), 962

粉体および粉末冶金第 45 巻第 10 号

Starting from the mixture of elemental powder mixtures, we produced bulk nanoscale Fe/Ag multilayers by the repeated press-rolling method. The average thickness of this sample was 5nm for Fe and 8nm for Ag. This sample exhibited the CIP-MR of 8.5

### 3: Market Penetration and Cost-Effectiveness Analysis of Thermal Storage System Using Integrated Resource Planning Model with Endogenized Technological Learning

生産習熟効果を考慮した統合型資源計画モデルによる蓄熱式空調機器の普及規模と費用対効果の分析

Masahito Takahashi\*, Hiroshi Asano\*, Yutaka Nagata  
\*(CRIEPI)

Trans. IEE Japan, Vol.119-B, No.2, pp.268-275, 1999

電気学会論文集B, 119巻2号, pp. 268-275, 1999年

Demand-Side Management (DSM) gives the utility flexible load management measures of electric power system and, to promote it to the power system, it is necessary to study the long-term cost-effectiveness of DSM programs as well as the short-term one. We have developed a prototype model of Integrated Resource Planning (IRP) to optimize dynamically the promotion of the DSM programs in the planning period in comparison with supply-side resources. The DSM program promotion costs the utility direct payment to program participants and lost revenue caused by change of load shape. Technological learning of DSM equipment is also incorporated endogeneously into the model to analyze dynamical penetration of the new technology. We show the importance of technology learning in the cost-effectiveness analysis through a case study for commercial thermal storage system that are the most promising DSM program in Japan. We evaluated market penetration, cost-effectiveness of the program and the resulting effect in the power system until the year 2014.

### 4: Mechanism of Cellulose Pyrolysis -Reactivity of an Intermediate, Levoglucosan

Haruo Kawamoto, Masaru Murayama, Shiro Saka

Proceedings of XIXth International Carbohydrate Symposium, DP59 (1998)

Levoglucosan, an important intermediate of cellulose pyrolysis, was heated at 250~400°C for 30~120 sec under nitrogen, and change in the products composition was carefully studied by the following four fractions, that is, gaseous, MeOH-soluble, water-soluble, and insoluble fractions. MeOH-soluble fraction was characterized to be a mixture of unreacted levoglucosan, lower molecular weight (MW) products, and di- and trisaccharides. Water-soluble and insoluble fractions were also characterized to be polysaccharides and char, respectively. As the pyrolysis proceeded, products composition was changed in the direction of MeOH-soluble water-soluble insoluble fractions. Interestingly, insoluble fraction (char) was formed only with a decrease in the water-soluble fraction (polysaccharides). A mechanism of cellulose pyrolysis is proposed, in which two competitive reactions, e.g., ring-opening polymerization into polysaccharides and fragmentation into lower MW products, take place simultaneously for levoglucosan intermediate, and then, char is formed from the polysaccharides. This mechanism also suggests that blocking the polymerization of levoglucosan could be effective in order to prevent the char formation. This idea was supported by the results of the cellulose pyrolysis in sulfolane which is a good solvent for levoglucosan.

**5: Removal of Toxic Substances of Chloroform and Benzen by Carbonized Woody Materials****Shiro Saka, Makoto Doi**

Materials Sci. Res. International, 4, No.4, 249-253, 1998

In a global expansion of environmental pollutions, trihalomethanes in water and aromatic toxic substances in air are both increasing. In this study, therefore, an effort has been made to develop carbonized woody materials to remove specifically these polluting materials and explore a potential of developing more functionalized new woody carbonized materials. It was found by elemental analysis that carbonized woody material prepared under hydrogen gas was more reduced, compared with that under nitrogen gas, particularly over 550 °C. Both carbonized woody materials were decreased in vapor adsorption of water with increasing the temperature, whereas adsorption of chloroform and benzene was instead improved and over 550 °C, carbonized woody materials under hydrogen gas was superior to that from nitrogen gas in their adsorption. Carbonized woody materials with these characteristics were found to adsorb chloroform in water and benzene in atmosphere effectively. These lines of evidence would support a concept that hydrogenative reduction of woody materials would be effective to enhance its adsorptivity against chloroform in water and benzene in atmosphere.

**6: \* SiO<sub>2</sub>-P<sub>2</sub>O<sub>5</sub>-B<sub>2</sub>O<sub>3</sub> Wood-Inorganic Composites Prepared by Metal Alkoxide Oligomers and their Fire-resisting Properties****Hisashi Miyafuji, Shiro Saka, Akira Ymamoto\***

\* Shin-Etsu Chemical Co.,Ltd

Holzforschung, 52, No.4, 410-416, 1998

SiO<sub>2</sub>-P<sub>2</sub>O<sub>5</sub>-B<sub>2</sub>O<sub>3</sub> wood-inorganic composites from metal alkoxide monomers revealed a high fire-resistance, whereas these composites have some problems in the stabilities of P<sub>2</sub>O<sub>5</sub> and B<sub>2</sub>O<sub>3</sub> gels as well as environmental safety for their preparation. Therefore, some silicon alkoxide oligomers with ethylphosphite residue and/or boric hydroxide residue were prepared and applied for SiO<sub>2</sub>-P<sub>2</sub>O<sub>5</sub>-B<sub>2</sub>O<sub>3</sub> wood-inorganic composites preparation. The obtained composites could have high fire-resistance and prevent these gels from leaching. Additionally, the prepared oligomers are non-toxic so that the environmental safety for their preparation was achieved. By adding 2-heptadecafluorooctylethyltrimethoxysilane (HFOETMOS) to the oligomer reaction system, the obtained composites could improve further the anti-leachability of P<sub>2</sub>O<sub>5</sub> and B<sub>2</sub>O<sub>3</sub> gels.

**7: Antimicrobial TMSAH-added wood-inorganic composites prepared by the sol-gel process**

**Fumie Tanno, Shiro Saka, Akira Yamamoto\*, Keiji Takabe\*\***

**\*Shin-Etsu Chemical Co.,Ltd, \*\*Grad. School of Agr. Kyoto Univ.**

Holzforschung, 52, No.4, 410-416, 1998

To add stable antimicrobial properties to woods, an amphoteric sterilant, 3- (trimethoxysilyl) propyl (carboxymethyl) decylmethyl ammonium hydroxide inner salt (TMSAH) was applied to the sol-gel process, as SiO<sub>2</sub> wood- inorganic composites were prepared. The obtained TMSAH-added SiO<sub>2</sub> composites could reveal the high antimicrobial activities against a fungal attack by brown-rot fungi, but their activities against white-rot fungi were somewhat less. This results would be, therefore, due to the amphoteric nature of the TMSAH sterilant, which was stable under acidic conditions. However, the addition of property-enhancer, 2- heptadecafluorooctylethyltrimethoxysilane (HFOETMOS) to the above reaction system could provide HFOETMOS-(TMSAH-SiO<sub>2</sub>) composites with water- repellency and its water-repellent property has improved antimicrobial in the composites, against both brown-rot and white-rot fungi.

**8: \* Recent Progress in Topochemistry of Wood-Inorganic Composites as Prepared by the Sol-Gel Process**

**Shiro Saka**

Proceedings of The Fourth Pacific Rim Bio-Based Composites Symposium, Bogor, Indonesia, pp.386-404, 1998

Wood has been the most intimate materials with mankind since the ancient time. However, it has some defects due to natural materials such as combustibility, dimensional instability and biodeterioration. To remove such defects and add the value on to woody materials, wood-inorganic composites prepared with metal alkoxides by the sol-gel process have been studied for the property enhancement of wood. Therefore, in this paper, a recent progress in topochemistry of the wood-inorganic composites as prepared by the sol-gel process will be presented on enhancing the properties of wood such as dimensional stability, termite-resistance, fire-retardance, water-repellency, anti-leachability and anti- microbial activity. Throughout the studies, it has been elucidated that the topochemical effects exist for enhancing these properties of wood in wood- inorganic composites.

**9: \* Fire-resisting Wood-Inorganic Composites as Prepared by the Sol-Gel Process****Hisashi Miyafuji Shiro Saka**

Proceedings of The Fourth Pacific Rim Bio-Based Composites Symposium, Bogor, Indonesia, pp.405-421, 1998

A study on the wood-inorganic composites prepared by the sol-gel process with a metal alkoxide indicated that an inorganic modification of wood with SiO<sub>2</sub> gels from tetraethoxysilane (TEOS) can improve its properties in dimensional stability, combustibility, and biodeterioration. However, the SiO<sub>2</sub> composites still have the potential to be improved further for such properties. The binary and ternary systems to prepare the SiO<sub>2</sub> wood-inorganic composites were thus studied in this work by adding trimethylphosphite (TMP) or/and trimethylborate (TMB) to a reaction system of TEOS/EtOH/acetic acid (1:1:0.01 in molar ratio). The obtained SiO<sub>2</sub>-P<sub>2</sub>O<sub>5</sub>, SiO<sub>2</sub>-B<sub>2</sub>O<sub>3</sub>, and SiO<sub>2</sub>-P<sub>2</sub>O<sub>5</sub>-B<sub>2</sub>O<sub>3</sub> wood-inorganic composites from metal alkoxide monomers were then studied regarding their enhanced thermal properties of wood. The results clearly indicated that compared with the SiO<sub>2</sub> composites, such binary and ternary systems of the sol-gel process could improve greatly the properties of wood in fire-resistance in their composites, keeping the porous structure of the wood. However, these composites have some problems in the stability of P<sub>2</sub>O<sub>5</sub> and B<sub>2</sub>O<sub>3</sub> gels as well as environmental safety for their preparation. Therefore, some silicon alkoxide oligomers with ethylphosphite residue and/or boric hydroxide residue were prepared and applied for preparation of SiO<sub>2</sub>-P<sub>2</sub>O<sub>5</sub>-B<sub>2</sub>O<sub>3</sub> wood-inorganic composites from metal alkoxide oligomers. The obtained composites could have high fire-resistance and prevent these gels from leaching. Additionally, the prepared oligomers are non-toxic so that the environmental safety for their preparation was achieved. By adding a property-enhancer, 2-heptadecafluorooctylethyltrimethoxysilane (HFOETMOS) to the oligomer reaction system, the obtained composites could improve further the anti-leachability of P<sub>2</sub>O<sub>5</sub> and B<sub>2</sub>O<sub>3</sub> gels. Furthermore, it can be revealed by SEM-EDXA analysis on these composites that the topochemical effect of the inorganic gels and property-enhancer exists for enhancing the properties of wood in wood-inorganic composites.

**10: Chemical Conversion of Various Cellulose in Supercritical Water to Glucose****Shiro Saka, Tomonori Ueno**

Biomass for Energy and Industry, 10th European Conference and Technology Exhibition, Proceedings of the Conference, Wurzburg, Germany, pp.1815-1818, 1998

The supercritical water biomass conversion system was designed and devised in our laboratory to cover a range of up to 500kgf/cm<sup>2</sup> in pressure and up to 550 °C in temperature. The reaction vessel with cellulose sample was treated with this system at supercritical state of water for designated period (20~120 sec) under the conditions of the tin bath temperature of 500 °C and pressure of 350kgf/cm<sup>2</sup>. The recovered products of hydrolysates were then analyzed by high performance liquid chromatography. The obtained results indicated that a high amount of glucose can be achieved for 25sec treatment which indicates 15sec

preheating up to critical temperature of 374 °C and 10sec in supercritical treatment of water. Furthermore, with the longer treatment than 25sec, pyrolyzed products were found to be increased. Therefore, 10sec of supercritical treatment would be appropriate for getting a high yield of glucose in supercritical conditions. In such conditions, the glucose yield from cellulose I and cellulose II were almost the same as that of corn starch. Therefore, it may be concluded that cellulose must be hydrolyzed to the same degree as in corn starch under supercritical state. This finding suggests that the supercritical treatment can overcome the difficulties in hydrolyzing cellulose to glucose and that glucose can be achieved from cellulose readily as in the case of starch.

**11: \* Longevity of Wood by Inorganic co-modification**

無機・有機共複合による木材のロングライフ化

**Shiro Saka**

Proceedings of the 28th Symposium of Wood Chemical Modification, pp.37-44, 1998

第 28 回木材の化学加工研究会シンポジウム講演集

Wood has been the most intimate materials with mankind since the ancient time. However, it has some defects due to natural materials such as combustibility, dimensional instability and biodeterioration. To remove such defects and add the value on to woody materials, wood-inorganic composites prepared with metal alkoxides by the sol-gel process have been studied for the property enhancement of wood. Therefore, in this paper, a recent progress in topochemistry of the wood-inorganic composites as prepared by the sol-gel process will be presented on enhancing the properties of wood such as dimensional stability, termite-resistance, fire-retardance, water-repellency, anti-leachability and anti- microbial activity. Throughout the studies, it has been elucidated that the topochemical effects exist for enhancing these properties of wood in wood- inorganic composites.

**12: Interaction of pyrylium dye with self-complementary DNA oligomer as studied by <sup>1</sup>H NMR spectroscopy**

**K. Kanaori, K. Yokoyama, K. Tajima, N. Yamamoto, T. Okamoto, and K. Makino**

Nucleosides & Nucleotides, 17, 603-611 (1998)

- 13: Redox behavior of DMPO and its derivatives as studied by electrochemical measurements

N. Endoh, K. Kanaori, K. Tajima, and K. Makino

Magn. Reson. Med., 9, 52-55 (1998)

- 14: Reaction mechanism for formation of 2'-deoxyoxanosine from 2'-deoxyguanosine, a new DNA lesion by NO and HNO<sub>2</sub>

T. Suzuki, M. Yamada, T. Nakamura, K. Kanaori, K. Tajima, and K. Makino

Magn. Reson. Med., 9, 99-101 (1998)

- 15: Inhibition of human T-cell leukemia virus type 1 replication by antisense *env* oligodeoxynucleotide

N. Maeda, T. Kawamura, H. Hoshino, N. Yamada, J. Blackard, S. Kushida, N. Miyano-Kurosaki, N. Yamamoto, K. Makino, T. Yokota, K. Uchida, and M. Miwa

Biochem. Biophys. Res. Commun., 243, 109-112 (1998)

- 16: Neuroprotective effects of pterin-6-aldehyde in gerbil global brain ischemia: comparison with those of  $\alpha$ -phenyl-*N*-tert-butyl nitron

H. Mori, T. Arai, H. Ishii, T. Adachi, N. Endo, K. Makino, and K. Mori

Neuroscience lett., 241, 99-102 (1998)

- 17: **Oxypurinol, a xanthine oxidase inhibitor and a superoxide scavenger, did not attenuate ischemic neuronal damage in gerbils**

T. Arai, H. Mori, H. Ishii, T. Adachi, N. Endo, K. Makino, and K. Mori

Life Sci., 63, 107-112 (1998)

- 18: **Misincorporation of 2'-deoxyoxanosine 5'-triphosphate by DNA polymerases and its implication to mutagenesis**

T. Suzuki, M. Yoshida, M. Yamada, H. Ide, M. Kobayashi, K. Kanaori, K. Tajima, and K. Makino

Biochemistry, 37, 11592-11598 (1998)

- 19:  **$^1\text{H}$  nuclear magnetic resonance study on equilibrium between two four-stranded solution conformations of short d(CnT)**

K. Kanaori<sup>1</sup>, A. Maeda<sup>1</sup>, H. Kanehara, K. Tajima<sup>1</sup>, and K. Makino

Biochemistry, 37, 12979-12986 (1998)

- 20: **Preparation of stereoregulated antisense oligodeoxyribonucleoside phosphorothioate and interaction with its complementary DNA and RNA**

Y. Tamura, H. Miyoshi, T. Yokota, K. Makino, and A. Murakami

Nucleosides & Nucleotides, 17, 269-282 (1998)

**21: Two four-stranded structures of d(CnT) in solution by  $^1\text{H-NMR}$**

**K. Kanaori, K. Tajima, and K. Makino**

Nucl. Acids Chem. Symp. Ser., 39, 127-128 (1998)

**22: Formation of porphyrin-metal complex catalyzed by single-strand DNA**

**K. Tajima, K. Kanaori, and K. Makino**

Nucl. Acids Chem. Symp. Ser., 39, 169-170 (1998)

**23: Products in the reaction of 2'-deoxyguanosine with NO in the presence and absence of  $\text{O}_2$**

**T. Suzuki, M. Yamada, K. Kanaori, K. Tajima, and K. Makino**

Nucl. Acids Chem. Symp. Ser., 39, 177-178 (1998)

**24: Intermediate in the reaction of 2'-deoxycytidine with nitrous acid and nitric oxide**

**T. Suzuki, T. Nakamura, K. Kanaori, K. Tajima, and K. Makino**

Nucl. Acids Chem. Symp. Ser., 39, 235-236 (1998)

- 25: Characterization of ultrahigh molecular weight polyethylene irradiated with  $\gamma$ -rays and electron beams to high doses**

Y. Ikada, K. Nakamura, S. Ogata, K. Makino, K. Tajima, N. Endoh, T. Hayashi, S. Fujita, A. Fujisawa, S. Masuda, and H. Oonishi

J. Polym. Sci., 37, 159-168 (1999)

- 26: Stability of the Dimerization Domains Effects the Cooperative DNA Binding of Short Peptides**

Y. Aizawa, Y. Sugiura, M. Ueno, Y. Mori, K. Imoto, K. Makino and T. Morii

Biochemistry 38, 4008-4017 (1999)

- 27: Isolation and characterization of diazoate intermediate upon nitrous acid and nitric oxide treatment of 2'-deoxycytidine**

T. Suzuki, T. Nakamura, M. Yamada, H. Ide, K. Kanaori, K. Tajima, T. Morii, and K. Makino

Biochemistry, accepted (1999)

- 28: Kinetic Studies of Sequence-Specific Binding of GCN4-bZIP Peptides to DNA Strands Immobilized on a 27-MHz Quartz-Crystal Microbalance**

Y. Okahata, K. Niikura, Y. Sugiura, M. Sawada and T. Morii

Biochemistry 37, 5666-5672 (1998)

**29: Cooperative DNA Binding by Short Peptides**

**Y. Aizawa, T. Morii and Y. Sugiura**

Nucleic Acids Symp. Series 39, 67-68 (1998)

**30: Comparison of the Sequence-Selective DNA Binding by Peptide Dimers with Covalent and Noncovalent Dimerization Domains**

**Y. Aizawa, Y. Sugiura and T. Morii**

Biochemistry 38, 1626-1632 (1999)

**31: Intermediate upon nitrous acid- or nitric oxide-treatment of 2'-deoxycytidine**

**T. Suzuki, T. Nakamura, H. Ide, K. Kanaori, K. Tajima, and K. Makino**

Biological Chemistry and Cellular Targets of Nitric Oxide, pp.61 (1998)

**32: Anlysis of Operator's Diagnostic Behavior and its Application to the Human Modeling**

**Takahashi,M., Wu,W., Yasuta,A., Yoshikawa,H., Nakatani,Y.(Mitsubishi Electric), Nakagawa,T.**

In.Cognitive Systems Engineering in Process Control '96 (Eds. E. Hollnagel & H. Yoshikawa), ESSCS, Groningen, The Netherlands, pp.39-47, 1998.

Cognitive behavior analysis is quite important to evaluate the effectiveness of the man-machine interface for huge, complex engineering systems. This paper presents a cognitive behavior analysis method based on a laboratory experiment using nuclear power plant simulator and experienced subjects and it's application to the human modeling. The analysis is focused on the diagnosis process for plant anomaly. The cognitive behavior analysis was performed based on the Questionnaire Answers(QA) and operational sequence history(OSH) recorded during simulator runs. The results of cognitive behavior analysis of three subjects utilizing QAs and OSHs showed that diagnosis processes are successfully represented by the proposed

analysis technique. The knowledge obtained from the analysis was then utilized to construct human model for each subject on the computer. The results of numerical simulation demonstrated that the developed models are capable of representing individual diagnosis behavior properly.

### **33: Simulation based Evaluation of Man-Machine Interface in Power Plants**

**Nakagawa,T., Nakatani,Y.(Mitsubishi Electric), Yoshikawa,H., Takahashi,M., Furuta,T.(Tokyo Univ.)**

In.Cognitive Systems Engineering in Process Control '96 (Eds. E. Hollnagel & H. Yoshikawa), ESSCS, Groningen, The Netherlands, pp.115-121, 1998.

An integrated software system has been under development which aims at analyzing and evaluating the effectiveness of man-machine system design from the viewpoints of various human factors, by simulating plant, man-machine interface and operator. In this paper, the configuration of this software system which is named SEAMAID is first introduced, followed by an explanation of how the operator simulator model is constructed. Also presented is an example of the operator simulator using Petri net model. We developed a prototype of the SEAMAID system, and the possibility of constructing a total system was confirmed by a simulation using prototype system. A model of human error analysis is also described.

### **34: A New VR-based CSCW Environment for Conceptual Design of A Space Power Reactor**

**Shimoda,H., Yoshikawa,H., Takahashi,M., Nagamatsu,T., Takeoka,S.**

In.Cognitive Systems Engineering in Process Control '96 (Eds. E. Hollnagel & H. Yoshikawa), ESSCS, Groningen, The Netherlands, pp.138-147, 1998.

The conceptual design of a space power reactor core requires cooperative work by a group of experts from various fields. It is necessary to implement mechanisms to realize an effective computerized support system for group activity by different engineers. We aimed at incorporating tasks into a workable human interface system based on virtual reality technology with the full usage of advanced information technology on 3D graphics, numerical calculation and AI processing. We also aimed at developing a WWW-based design support system for the same work domain for higher levels of flexibility in cooperative work using distributed computer systems.

**35: A Basic Study on Real-time Method of Human Cognitive Process Estimation by Using Speech Recognition**

音声認識を用いた動的認知過程推定手法の基礎研究

Ozawa,T., Umeda,N., Shimoda,H., Yoshikawa,H.

The transactions of Human Interface Society, Vol.1, No.1, pp.19-28, 1999.

ヒューマンインタフェース学会論文誌, Vol.1, No.1, pp.19-28, 1999.

A real-time analysis method is proposed to trace cognitive process in diagnosing plant anomalies. The method under development is to apply for a real-time cognitive process estimator, with the aim of realizing adaptive interface for training the skill of plant anomaly diagnosis. The major point of the real-time estimator is that it is equipped with the Causal Relation Diagram (CRD) which represents the causal relationship between the major nuclear power plant (NPP) parameters. By using CRD and two types of information, one from data of operational sequence to user interface, and the other from verbal information taken by speech recognition machine, this estimator computes degree of operators' confidence in judging primary cause of plant anomaly for each major NPP parameters in CRD. The method, function of the estimator and the result of experimental evaluation are described in this paper. (in Japanese)

**36: Construction and Evaluation of a WWW-based CAI system based on Cognitive Design Guideline**

インターネットを用いた知的教育システムの認知心理学に基づく設計と実験評価

Obayashi,F., Shimoda,H., Yoshikawa,H.

The transactions of Human Interface Society, Vol.1, No.1, pp.9-18, 1999.

ヒューマンインタフェース学会論文誌, Vol.1, No.1, pp.9-18, 1999.

Firstly, a "Cognitive Design Guideline" was derived for designing an effective WWW

**37: A Study on Pupillary Response to Depth Cue of Linear Perspective**

線遠近法による心理的な単眼立体視要因に対する瞳孔反応

Fukushima,S., Morikawa,D., Yoshikawa,H.

Transactions of the Society of Instrument and Control Engineers, Vol.35, No.1, pp.38-45, 1999.

計測自動制御学会論文集, Vol.35, No.1, pp.38-45, 1999.

Accommodation, convergence and pupil constriction, which are called near triad, will usually respond simultaneously at near reflex in natural view condition. It has been reported that accommodation will happen to respond not only to visual distance of a real object but also by psychological factor in relation to perspective, but no research has been made on pupil behavior as another element of near reflex which

would be correlated to psychological perspective. Laboratory experiments were conducted on several subjects, to examine pupillary response by psychological factor to an image with linear perspective on the display, by using Eye-Sensing Head Mounted Display (ES-HMD). The ES-HMD can monitor the user's both eyes and obtain ocular information such as pupil size, eyeblink or eye movement, while presenting visual stimulus to his both eyes. It was found that for some subjects pupil would respond by psychological factor for the perspective image, which is similar to near reflex of pupil, and its response is correlated with psychological distance given by the image. (in Japanese)

**38: An Experimental Study on Pupillary Response under Binocular Parallax by Using Eye-Sensing Head Mounted Display**

両眼視差による瞳孔反応の Eye-Sensing HMD による実験研究

**Fukushima,S., Morikawa,D., Yoshikawa,H.**

Transactions of the Society of Instrument and Control Engineers, Vol.35, No.2, pp.191-199, 1999.

計測自動制御学会論文集, Vol.35, No.2, pp.191-199, 1999.

Accommodation, convergence and pupil constriction, which are called near triad, usually respond simultaneously at near reflex in natural view condition, but no research has been made on how pupil behaves following artificial near vision generated by binocular parallax. Laboratory experiments were conducted on several subjects, to examine eye movement and pupillary response under artificial binocular parallax, by using Eye-Sensing Head Mounted Display (ES-HMD). The ES-HMD can monitor the user's both eyes and calculate ocular information such as pupil size, eyeblink or eye movement, while presenting visual stimulus to his both eyes. It was found that pupil constricts according to the increase of binocular parallax and vice versa, for the case of vergence normal subjects who have an ability of adaptation to binocular parallax, while conjugate eye movement instead of vergent eye movement appeared for the case of vergence anomaly subjects who would not succeed in binocular fusion. It was also found for a vergence normal subject that continuous periodic pupillary movement of constriction and dilation has tendency of hysteresis, which is caused by different muscle organ between constriction and dilation. Another results also suggest that the direction of smooth pursuit eye movement in a vergence anomaly under binocular parallax depends on the dominant eye. (in Japanese)

**39: Teleoperation Environment based on Virtual Reality, - Application of Two-Planes Method for Position Measurement -**

人工現実感を用いたテレオペレーション環境－ 2 平面法に基づく位置計測の応用－

**Yoshikawa,H., Tezuka,T., Inoue,R.**

Transactions of IWW of Japan, Vol.1 118-C, No.9, pp.1329-1336 (1998)

電気学会論文誌 C, Vol.1 118-C, No.9, pp.1329-1336 (1998)

A teleoperation system based on virtual environment (VE) is an emergent technology for operating a robot in remote or hazardous environment. We have developed a VE-based teleoperation system for

robot-arm manipulation in a simplified real world. The VE for manipulating the robot arm is constructed by measuring the 3D positions of the objects around the robot arm by motion-stereo method. The 3D position is estimated by using two-(calibration) planes method based on images captured by the CCD camera on the robot-arm, since the two-planes method does not need pin-hole-model assumption to the camera system. The precision of this 3D-measurement is evaluated through experiments and the derived is the theoretical model to the error in the measurement. This measurement system is applied to VE-based teleoperation experiment for Peg-in-hole practice by the robot arm.

**40: A Computer-aided Sensing and Design Methodology for the Simulation of Natural Human Body Motion and Facial Expression**

**Shimoda,H., Ando,H., Yang,D., Kunihiro,T., Wu,W., Yoshikawa,H.**

Proc. of EDA(Engineering Design and Analysis)'98 (CD-ROM), 1998.

Development of sensing and composing methodology has been made for real-time simulation of natural human body motion and facial expression as one of the key technology for realizing a new human interface to communicate between human and agent in virtual reality space. In order to realize the simulation methods, we have thus far developed two systems separately: one is to simulate human body motion and the other is for facial expression. Both systems are based on actual measurement of human behavior. Details of the two systems are described with respect to measurement methods for human behavior and how to construct computer graphics in concern.

**41: Study on Developing a Computerized Model of Human Cognitive Behaviors in Monitoring and Diagnosing Plant Transients**

**Wu,W., Yoshikawa,H.**

Proc. of IEEE-SMC'98, pp.1121-1126, 1998.

A computerized model of human cognitive behavior in monitoring and diagnosing plant transient has been developed as a part of integrated simulation system of human-machine-interaction (HCI) in nuclear power plant. The employed general framework of human modeling is first described, followed by the description of detailed modeling of both the monitoring and diagnosing phases. For the usability validation of the developed human modeling, computer simulation experiments have been conducted to deduce human cognitive reliability curves, by connecting the computerized model of human cognitive information processing with the dynamic simulator of nuclear power plant through man-machine interface simulator. The results of computer simulation were well agreed with those of laboratory experiments.

**42: Application of Machine Speech Recognition for Real-time Estimation of Human Cognitive Process at Man-Machine Interface**

**Ozawa,T., Shimoda,H., Yoshikawa,H.**

Proc. of IEEE-SMC'98, pp.4127-4132, 1998.

A real-time cognitive process estimation system has been developed, by employing machine speech recognition to estimate operators' thinking processes. The developed system consists of four components; (1) user-interface, (2) speech recognition subsystem, (3) real-time cognitive process estimator and (4) nuclear power plant (NPP) simulator. The major point of the real-time estimator is that it equipped with the Causal Relation Diagram (CRD) which presents the physical relations between the NPP parameters on MMI. By using CRD and two types of information, one from data of operational sequence to MMI, and the other from verbal information taken by speech recognition subsystem, this estimator computes degree of operators' confidence in judging primary cause of plant anomaly for each plant parameters of CRD. By a laboratory experiment, it was confirmed that the developed system would be usable for real-time monitoring operators' thinking process in diagnosing the plant anomaly at MMI.

**43: Development of Head-attached Interface Device (HIDE) and its Application Experiments**

**Shimoda,H., Hayashi,N., Nikaido,Y., Yoshikawa,H.**

Proc. of IEEE-SMC'98, pp.1145-1150, 1998.

Head-attached interface device (HIDE) has been developed as a new type of human interface device in an actual work environment. The HIDE has flexible integrated functions which consist of speech recognition and view direction detection as hand-free input channels, direct presentation of audio/visual information as output channels, and mobile system configuration. In this paper, the design concept of the HIDE was first introduced, and individual functions to configure the design concept were developed by their separate testing. An integrated prototype system HIDE was then produced, and its functional evaluation test was made to examine the individual functions. According to the evaluation result, we proposed a design guideline of application software, and developed an example software.

**44: An Experimental Study on Distributed Virtual Environment for Integrated Training System on Machine Maintenance**

**Yamamoto,M., Mitani,T., Ichiguchi,N., Tezuka,T., Yoshikawa,H.**

Proc. of IEEE-SMC'98, pp.1479-1484, 1998.

Distributed Virtual Environment (DVE) has been applied to the development of an integrated training on machine maintenance work by multiple users. The training system gives two types of training: (i) simultaneous training of an instructor and trainees with multi-modal communication through computer network (synchronous system), and (ii) monitoring and recording system both for the purpose of pre-training rehearsal and post-training analysis (asynchronous system). It has been experimentally confirmed that the training in the DVE system with multi-modal communication would provide a new type of the effective training environment.

**45: A Study on Design Support System for Constructing Machine-Maintenance Training Environment Based on Virtual Reality Technology**

**Ishii,H., Tezuka,T., Yoshikawa, H.**

Proc. of IEEE-SMC'98, pp.2635-2640, 1998.

A design support system has been developed for constructing VR-based training environment for machine maintenance work. The features of the developed design support system are : 1) users can construct various training environments under GUI (Graphical User Interface) environment, 2) the users need not any expert knowledge about computer programming, 3) Petri net model is utilized for representing the state transition of objects in virtual environment, and 4) the constructed environment can be easily changed and reused. In this report, the system configuration, how to model the state transition of objects with Petri net and the results of system validation experiments are described.

**46: Basic Experiments for Evaluating Peculiar Ocular Characteristics Caused by Artificial Binocular Vision**

**Fukushima,S., Morikawa,D., Fujiyama,H., Yoshikawa,H.**

Proc. of IFAC-MMS'98, pp.407-412, 1998.

By using Eye-Sensing Head Mounted Display (ES-HMD), basic laboratory experiments were conducted

to evaluate convergent eye movement and pupil size under some specific visual conditions induced by artificial binocular vision; one experimental condition was that asymmetric luminous intensity for both eyes was illuminated. The result shows that each pupil size of both eyes in asymmetric condition is different from in symmetric condition, even if each eye is illuminated by the same luminous intensity for the both conditions. Since the experimental condition would never usually happen in real world, longtime exposure to light in asymmetric luminous condition may lead to visual fatigue. The other experimental condition was binocular vision generated by binocular parallax. It was found that (i) some subjects, who are called vergence normal, can adjust convergence according to the moving target with binocular parallax, but the other called vergence an

**47: Development of Head-attached Interface Device (HIDE) and its Functional Evaluation**

**Shimoda,H., Hayashi,N., Nikaido,Y., Umeda,N., Yoshikawa,H.**

Proc. of IFAC-MMS'98, pp.573-578, 1998.

Head-attached interface device (HIDE) has been developed as a new type of human interface device in an actual work environment. The HIDE has flexible integrated functions which consist of speech recognition and view direction detection as hand-free input channels, direct presentation of audio/visual information as output channels, and mobile system configuration. In this paper, the design concept of the HIDE was first introduced, and individual functions to configure the design concept were developed by their separate testing. An integrated prototype system HIDE was then produced, and its functional evaluation test was made to examine the individual functions as the whole system. It was confirmed that the HIDE would be feasible enough to introduce in practical use.

**48: A Study on Design Support for Constructing Machine-maintenance Training System by using Virtual Reality Technology**

**Ishii,H., Tezuka,T., Yoshikawa,H.**

Proc. of IFAC-MMS'98, pp.389-394, 1998.

A design support system has been developed for constructing VR-based training environments for machine maintenance work without any expertise knowledge and programming effort on VR. Using the developed system, the users can easily construct various training environments under GUI environment. It was verified through some experiments that the developed system can reduce the working hours remarkably and that novice users who have no prior knowledge on the system could construct a training environment successfully after a few hours of tutorial on the system. In this paper, the system configuration and experimental results are described.

**49: Construction of a WWW-based CAI System Based on Cognitive Design Guideline**

**Obayashi,F., Shimoda,H. Yoshikawa,H.**

Proc. of IFAC-MMS'98, pp.155-160, 1998.

Firstly, a "Cognitive Design Guideline" is proposed for designing WWW-based CAI system by applying effective concepts and models in education, which have been proposed in cognitive psychology. A new CAI system was developed as an augmented material of lecturing "Human Interface Science" by Internet. This was designed based on the proposed cognitive guideline and the field experiment was conducted to compare this new CAI system with the conventional CAI system. It was confirmed that the new CAI system be better to promote learning process than the conventional one.

**50: Usage of Computer Simulation of Human-Machine Interaction for the Human Reliability Enhancement in Human Machine System**

**Nakagawa,T., Wu W., Yoshikawa,H., Nakatani,Y.(Mitsubishi Electric)**

International Seminar on Human with Technology(POST-IFAC'98), pp.49-54, 1998.

The usefulness of computer simulation on human-machine interaction is emphasized by introducing the authors' two systems development, SEAMAID for operational problem while DIAS for maintenance, with the purpose of utilizing the computer simulation for the design improvement of Man-Machine Interface issues. Some cases of example evaluation practice by the both systems are presented in order to highlight the usefulness of the computer simulation.

**51: Application of Human Model Simulation to Deduce Human Error Probability Parameter for PSA/HRA Practice**

**Wu,W., Nakagawa,T., Yoshikawa,H.**

Proc. of International Topical Meeting on Safety of Operating Reactors, pp.79-86, 1998.

Human model for simulating the cognitive behaviors of Nuclear Power Plant (NPP) operators is constructed and applied for deducing the Human Error Probability (HEP) parameters required for Human Reliability Analysis (HRA) in conjunction with Probabilistic Safety Assessment (PSA) of NPP. Firstly, a framework for describing the basic HEP parameters is proposed. Then, Human Cognitive Reliability (HCR) curves were deduced by analyzing data of a laboratory experiment in which subjects were asked

to monitor and diagnose certain abnormal transients in NPP. A human model of NPP operator was constructed for both monitoring and diagnosing the NPP anomaly, based on the experimental observation with applying Reason's memory model. By comparing two HCR curves, one deduced by human model simulation and the other from experimental data, it was confirmed that the human model simulation could well explain the probabilistic nature of human response in detecting plant anomaly.

## **52: A Basic Study of Virtual Collaborator - The First Prototype System Integration**

**Ishii,H., Wu,W., Li,D., Ando,H., Shimoda,H., Yoshikawa,H.**

Proc. of AROB 4th '99, pp.682-685, 1999.

The goal of this study is to develop a "virtual collaborator" as a new type of human interface environment. The virtual collaborator is an intelligent agent realized in VR space, who can communicate naturally with human like humans do with each other. As the first step of this study, the authors have constructed a prototype virtual collaborator who can behave just like plant operator in the control room of nuclear power plant, although the present prototype has no communication functions with humans. At the present stage, the virtual collaborator can detect an anomaly, diagnose the root cause and operate the control panel in accordance to the operation manual in the virtual space, where the control room of the nuclear power plant is visualized. The prototype system is constructed as a distributed simulation system, which consists of four subsystems: (1) nuclear power plant simulator, (2) man-machine interface simulator, (3) human model simulator, and (4) human body motion simulator. These subsystems have been separately developed and have been combined afterwards.

## **53: Simulation-based Evaluation System for Man-Machine Interfaces in Nuclear Power Plants**

**Nakagawa,T., Nakatani,Y., Wu,W., Yoshikawa,H., Nakagawa,T., Furuta,T.**

Proc. of IEEE-SMC'98, pp.1278-1283, 1998

The authors have developed SEAMAID system which is a Simulation-based Evaluation and Analysis support system for m-machine Interface Design in the domain of nuclear power plants. The SEAMAID system simulates the interaction between an operator and man machine interfaces (MMI), and supports to evaluate the MMI by using the simulation results. The operator simulator in the SEAMAID copes with a single abnormal event, according to the operation manuals. The Interaction Analyzer (IA) evaluates the simulation results executed by integrating the operator simulator, the Man-Machine-Interface (MMI) simulator, and the Plant simulator. The authors expanded SEAMAID in two features: (1) Realization of flexible modification/addition/deletion of evaluation items and consideration of various kinds of guidelines of Human Interface by representing the items as "frames", and (2) human model of detecting and

diagnosing plant anomaly followed by a sequence of reactions. In this paper, MMI evaluation using the integrated simulation of plant, MMI and operator are discussed. Especially focusing on MMI evaluation process of SEAMAID, "frame" structure is proposed for handling various guidelines and evaluation indices, and providing appropriate guideline to an analyst or a designer.

**54: \* Identification of mixing state of sulfate and nitrate ions in individual aerosol particles using a mixing thin film created by dual simultaneous vacuum deposition**

二元同時蒸着混合薄膜を用いた個別エアロゾル粒子中の硫酸塩および硝酸塩混合状態の同定

**Susumu Tohno, Satoru Chatani\* and Mikio Kasahara**

**\* (Graduate School of Engineering)**

Journal of Aerosol Research, Japan, Volume 13, No.3, pp.230-236, 1998

エアロゾル研究, 第13巻, 第3号, pp.230-236, 1998

Mixing thin film was prepared on a Nuclepore filter by dual vacuum deposition of barium chloride and nitron in order to detect the mixing states of sulfate and nitrate in individual aerosol particles. The mixing states were identified by the characteristic spots of Liesegang ring and/or needle crystals from SEM (scanning electron microscope) observation of the samples. Applicability was examined using sulfate and/or nitrate particles generated by a nebulizer. It was found that the reactions of sulfate with barium chloride and of nitrate with nitron were promoted and reproducible in ethanol and 2-propanol mixing solvent vapor. The mixing thin film method was applied to detect the mixing states of atmospheric aerosols collected by Andersen samplers at Uji in summer and winter seasons. In winter, internally mixed sulfate- nitrate particles were not detected, while internally mixed particles were found to be a few percent in number concentration to the total particles collected on each stages of the sampler in summer (in Japanese).

**55: \* Characterization of Atmospheric Aerosols Applying PIXE Method**

PIXE法を応用した大気エアロゾル粒子の特性化

**Satoru Chatani\*, Mikio Kasahara, Kouhei Yamamoto and Susumu Tohno**

**\* (Graduate School of Engineering)**

Journal of Aerosol Research, Japan, Volume13, No.4, pp.354-360, 1998

エアロゾル研究, 第13巻, 第4号, pp.354-360, 1998

To investigate the physical and chemical characteristics of atmospheric aerosols, three factors of size distribution, concentration and chemical composition are usually most important. Atmospheric aerosols were sampled by using a 12 stages Andersen sampler. Sampling was carried out once a month from July 1995 to June 1996. sampled aerosols were separated into the soluble and insoluble components. The concentrations of 15 elements in both components were determined by a PIXE analysis. The mass size distribution of particulate matter (PM) was described by a bimodal distribution having one peak each in the fine and coarse fractions. The mass distribution of each element was illustrated in three types: mono-modal distribution having only one-peak in the fine or coarse fraction and the bimodal

distribution. The size distribution type of each element was estimated by the mass median diameter. The concentration ratio of the each element to PM in the coarse fraction was higher than that in the fine fraction. Enrichment factor of each element was calculated. and it is suggested that K, Ca, Ti, Mn, Fe in the coarse particles are originated from soil dusts (in Japanese).

**56: \* Application of X-Ray Absorption Fine Structure (XAFS) Spectrometry to Identify the Chemical States of Atmospheric Aerosols**

**Susumu Tohno, Jun Kawai\*, Satoru Chatani\*, Michiharu Ohta\*, Yoshinori Kitajima\*\*, Kouhei Yamamoto, Yasuyuki Kitamura and Mikio Kasahara**

**\* (Graduate School of Engineering)**

**\*\* (Institute of Materials Structure Science, High Energy Accelerator Research Organization)**

Journal of Aerosol Science, Volume29, No.S1, pp.S235-S236, 1998

The depth selective XAFS spectrometry was applied to determine the chemical states of sulfur and silicon in atmospheric aerosols. Atmospheric aerosols were collected on aluminum foils and polyethylene films using a 4-stage cascade impactor and a 12-stage low pressure Andersen sampler, respectively. Sampling were performed at Uji (urban area), and Sakurajima where an active volcano locates. We measured X-ray fluorescence yield (XFY) and total electron yield (sample current) simultaneously to obtain the X-ray absorption near edge structure (XANES) spectra of S and Si in the atmospheric aerosols. Most of aerosol samples showed only  $S^{6+}$  peak and no other peaks were detected except one sample collected at Sakurajima. In case of the Sakurajima samples, both the  $S^{2-}$  and  $S^{6+}$  peaks were observed for sample current measurement, while only the  $S^{6+}$  peak was observed for XFY method. Those results indicate that the particles consist of  $S^{6+}$  sulfur atoms (sulfate) and their surfaces contain both  $S^{6+}$  and  $S^{2-}$  chemical species. Atmospheric aerosols sampled at Sakurajima showed extremely unique Si K-edge XANES spectra. XFY method indicates the particles contain  $Si^{4+}$  silicon atoms whose compounds are considered to be  $SiO_2$ . The sample current spectrum consists of two peaks. One is for  $Si^{4+}$  and the other lies between  $Si^{4+}$  and  $Si^0$ . The peak is considered to be attributable to chemical shift in the Si K-edge of silicate minerals.

**57: Life Cycle Analysis of Automobiles with Regard to Air Pollutants Emissions in Japan**

**Keisuke Nansai, Susumu Tohno, Mikio Kasahara and Yuich Moriguchi\***

**\* (National Institute for Environmental Studies)**

Proceedings of the Third International Conference on EcoBalance, pp.299-302, 1998

Air pollutants ( $NO_x$ ,  $SO_x$ , CO) emissions inventories were created based on the Japan input-output tables. We newly estimated emissions by each sector from self-transport using private motor cars accord-

ing to car and fuel types after allocating self-transport activity to other sectors. Those inventories were used to calculate the amounts of life cycle air pollutants emissions for a gasoline vehicle (GV), a diesel vehicle (DV) and an electric vehicle

#### **58: Bayesian Analysis of Public Views on the Safety of Nuclear Developments**

**H. Yamagata and K. Kanda**

Ann. Nucl. Energy, Vol.25, No.10, pp.709-720, 1998.

The sodium leak accident at Monju, a prototype fast breeder reactor that the Power Reactor and Nuclear Fuel Development Corporation (PNC) has operated since 1995 in Japan, in combination with the PNC's management of the accident, has created public distrust not only in the safety of Monju, but also in the nuclear development policy of Japan. In order to learn a lesson from these events and to assess how a relationship of mutual trust can be established with the public, this paper simulates the processes of establishing public confidence in reliability of a nuclear plant in cases of accidents, no accident, a cover-up, and so on. In this paper, public confidence is defined as the public evaluation of cumulative probability under a certain level of accident rate, conditional on the information available to the public. The conditional probability is estimated by use of Bayes' Theorem. The simulation shows that (1) public confidence is lost by only one accident in an early stage of operation, and can then be recovered only by many subsequent years of accident-free operation, but never by a cover-up, and (2) the more information that is provided to the public, the better the relationship of mutual trust that will be established, especially at an early stage of plant operations.

#### **59: The Strengthened Nuclear Non-proliferation Export Control Regime and Possible Future Improvements**

核不拡散輸出管理体制の強化と将来の課題

**H. Kuniyoshi and K. Kanda**

J. Atom. Energy Soc. of Japan, Vol.40, No.10, pp.767-775, 1998.

日本原子力学会誌、第40巻、第10号、頁767-775、1998年

The Iraqi attempt to develop nuclear weapons which was detected in 1991 made the world recognize the need to strengthen the nuclear non-proliferation regime. In the field of export control, the Nuclear Suppliers Group had implemented export controls on nuclear materials and equipments since 1977. In addition to this, the group introduced, in 1992, the control of nuclear-related 'dual-use' items such as machine tools and carbon fiber, which are usually used for non-nuclear products but can possibly be used for nuclear activities. Also, the control guidelines of nuclear export, which had already been under control (such as the transfer of nuclear materials), were made stronger by introducing the full-scope safeguards by IAEA as a condition of the transfer. The reinforcement of the nuclear export control regime should be appreciated from the viewpoint of preventing nuclear proliferation. However, this implies an

increased flexibility of the regime entailing difficulties of export control and a need of harmonization among participating countries. Some directions, such as introducing more rigorous rules, promoting information exchange and enhancing transparency, are suggested to improve the regime. (in Japanese)

**60: Nuclear Development in the "Knowledge Society"**

「知識社会」と原子力

**T. Murata and K. Kanda**

J. Atom. Energy Soc. of Japan, Vol.40, No.12, pp.946-954, 1998.

日本原子力学会誌、第40巻、第12号、頁946-954、1998年

In considering various issues which the nuclear development is coping with in these days, viewpoints from the context of changing society provide with the clear understanding of the requirements for the nuclear development to be harmonious with the society. Although vast amount of the knowledge itself spread widely and rapidly in the knowledge society, each individual in general suffers from scarcity in the quality of information for the reasonable decision making. Such a double structure in the knowledge society requires the nuclear development to be much more accountable and self-descriptive. And enhancement of accountability and self-description of the nuclear development must be one of the main part of nuclear policies. (in Japanese)

**61: The Demise of National COCOM and the Establishment of the Wassenaar Arrangement**

コCOMの終焉とワッセナー・アレンジメントの成立

**Hiroshi Kuniyoshi**

J. National Defense, Vol.26, No.2, pp.94-111, 1998.

新防衛論集、第26巻、第2号、頁94-111、1998年

The Wassenaar Arrangement is usually explained as a successor of COCOM and often called the Post-COCOM regime. However, it is not appropriate to understand the Wassenaar Arrangement as a simple replacement of COCOM. The Wassenaar Arrangement has a different nature of regime from COCOM. Its origin as an export control regime for conventional arms and their dual-use goods and technologies can be traced back to the G7 negotiations outside COCOM long before the end of COCOM. In 1990, COCOM started to change its nature from confrontation between the East and the West to their cooperation to cope with the new threat from third world countries such as Iraq. In 1994, corresponding to a request by Russian President Boris Yeltsin, it rang down the curtain on its 45 years history. The Wassenaar Arrangement was established in 1996 after protracted discussions. The issues in dispute were: a) whether to seek Russian participation who was exporting arms to Iran; b) whether to control the transfer of arms themselves in addition to dual-use goods; c) whether the notification of the transfer of controlled items should be made in advance or after the fact; d) whether to specify targeted countries. The settlement of these issues identified the nature of the Wassenaar Arrangement, which is rather flexible and respects

each country's discretion: (in Japanese)

**62: A Ripple of the "Atomausstieg" Policy of the New German Government**

ドイツ新政権の原子力政策の波紋

**Takashi Murata**

Nikkan-Kogyo Production 'Nuclear Viewpoints', Vol.45, No.2, pp.34-37, 1998

日刊工業出版プロダクション「原子力eye」、第45巻、第2号、頁34-37、1998年

New German Government was established after the general election of Bundestag in last September. Established in October, new red (SPD)-green (Grünen) coalition decided their new energy policy which is characterized by "Atomausstieg". Since one third of the total electricity in Germany comes from nuclear power plant, the formulation and implementation of the drastic policy to seek the society without the use of nuclear energy need long way to go. In Japan some discussion simply refers to the fact that Germany has decided not to use nuclear energy, but in reality their policy is strictly linked with geo-political situation in the central Europe. This paper provides the idea not only the basic framework of German new policy and its limitation. (in Japanese)

**63: \* Multiplicity and Energy of Neutrons from  $^{235}\text{U}(n, f)$  Fission Fragments**

**K. Nishio\*, Y. Nakagome, H. Yamamoto\* and I. Kimura\* \*)Dept. Nucl. Eng., Kyoto Univ.**

Nucl. Phys., Vol.A632, pp.540-558, 1998

The correlation between fission fragments and prompt neutrons from the reaction  $^{235}\text{U}(n, f)$  was measured with improved accuracy. The results determined the neutron multiplicity and emission energy as a function of fragment mass and/or total kinetic energy. The average multiplicity as a function of fragment mass followed a saw-tooth distribution and the distribution of average energy with mass had a bell-shaped distribution centered about the equal-mass split. The slope of the neutron multiplicity with kinetic energy had a saw-tooth distribution with a minimum at  $m^* \sim 130$ . The total excitation energy implied by the measurements was consistent with energy conservation and had a concave distribution with heavy-fragment mass, with a flat minimum between  $m^* \sim 132$  and 152, suggesting that fragment pairs are preferentially formed in a compact configuration at the scission point.

**64: \* Multi-parametric Measurement of Prompt Neutrons and Fission Fragments for  $^{233}\text{U}(\text{nth},\text{f})$** 

**K. Nishio\*, M. Nakashima\*, I. Kimura\* and Y. Nakagome \*) Dept. Nucl. Eng., Kyoto Univ.**

J. Nucl. Sci. Technol., Vol.35, No.9, pp.631-642, 1998

The multiplicity and the energy of prompt neutrons from the fragments for  $^{233}\text{U}(\text{nth},\text{f})$  were measured as functions of fragment mass and total kinetic energy. Average neutron energy against the fragment mass showed a nearly symmetric distribution about the half mass division with two valleys at 98 and 145 u. This shape formed a contrast with a saw-tooth distribution of the average neutron multiplicity. It indicates that the shell-effects, which are pronounced for the fragments having the proton number or neutron number close to the magic-number of 50 or 82, affected the neutron emission process. The slope of the neutron multiplicity with total kinetic energy depended on the fragment mass and showed the minimum at about 130 u. The obtained neutron data were applied to determine the total excitation energy of the system, and the resulting value in the typical asymmetric fission lied between 22 and 25 MeV. The excitation energy agreed with that determined by subtracting the total kinetic energy from the Q-value within 1 MeV, thus satisfied the energy conservation. In the symmetric fission, where the mass yield was drastically suppressed, the total excitation energy is significantly large and reaches to about 40 MeV, suggesting that fragment pairs are preferentially formed in a compact configuration at the scission point.

**65: Fission Fragment Configurations at the Scission Point of  $^{233}\text{U}$ ,  $^{235}\text{U}$  and  $^{239}\text{Pu}(\text{nth},\text{f})$** 

**K. Takamiya\*, T. Inoue\*, K. Nakanishi\*, A. Yokoyama\*, N. Takahashi\*, T. Saito\*, H. Baba\* and Y. Nakagome \*) Graduate School of Science, Osaka Univ.**

J. Radioanal. Nucl. Chem., Vol.239, No.1, pp.117-122, 1999

In order to estimate the deformation rate of fission fragment at the scission point for thermal neutron-induced fission of  $^{233}\text{U}$ ,  $^{235}\text{U}$  and  $^{239}\text{Pu}$ , double-velocity and double-energy measurements were carried out. As the result of the estimation of the deformation rate, two types of scission point configurations were found. One type is composed of deformed light and heavy fragments, and the other type is a combination of deformed light and spherical heavy fragments. Mass and total kinetic energy distributions were sorted in two distributions by means of the type of configuration.

**66: MOX Fuel Core Physics Experiments and Analysis -Aiming for Plutonium Effective Use-**

MOX 燃料炉物理試験と解析の現状 —プルトニウムの有効利用に向けて—

**K. Kanda, T. Yamamoto\*1, H. Matsuura\*1, M. Tatsumi\*2, K. Sakurada\*3, M. Sasaki\*4 and H. Maruyama\*5** \*1) NUPEC, \*2)NFI, Ltd., \*3)Toshiba Co., \*4)MHI, Ltd., \*5)Hitachi Co.

J. Atom. Energy Soc. Japan, Vol.40, No.11, pp.834-854, 1998.

日本原子力学会誌、第40巻、第11号、頁834-854、1998年

In order to utilize plutonium effectively in APWR and ABWR, a conceptual study on the well moderated light water reactor, which can increase fissile plutonium consumption, has been performed as Japan-France Joint Study supported by the Ministry of International Trade and Industry. This project is called the MISTRAL program between NUPEC (Nuclear Power Engineering Corporation) and CEA (French Atomic Energy Agency), which supports the analysis of the well moderated reactor core. The program started in 1996 and continues until 2000. NUPEC also obtained the physics data for the current light water core called EPICURE project, which was done by CEA. This report describes the outline of project and the interim result. Physics analysis results by both countries are also introduced.

**67: Neutron activation analysis of ivory of Africa elephants**

**Takayuki Takeuchi Yukihiro Nakano Hiroko Koike\***

Journal of Radioanalytical and Nuclear Chemistry, Vol. 235, Nos 1-2, 1998, 273-277.

Instrumental neutron activation analysis was applied to 80 samples from various African countries and 81 samples from the Kruger National Park in the Republic of South Africa. Twelve elements such as Br, Ca, Cl, Co, Cs, Fe, Mg, Mn, Na, Sc, Sr, and Zn, were determined in all samples. The factor scores of each sample were calculated from those elemental concentrations for the first and second factors to clarify the differences of samples from various African countries with those from Kruger Park. The results were compared with those by stable isotope analysis ( $^{13}\text{C}$  and  $^{15}\text{N}$ ).

## II Department of Fundamental Energy Science

(エネルギー基礎科学専攻)

### 68: Effect of Aging on Yttria-Stabilized Zirconia

#### I. A Study of Its Electrochemical Properties

**Junya Kondoh<sup>a</sup>, Tsuyosi Kawashima<sup>b</sup>, Shiomi Kikuchi<sup>c</sup>, Yoichi Tomii<sup>d</sup> and Yasuhiko Ito<sup>d</sup>**

<sup>a</sup>Department of Energy Science and Engineering, Graduate School of Engineering, Kyoto University

<sup>b</sup>Tokyo Gas Company, Limited, Fundamental Technology Research Laboratory

<sup>c</sup>Department of Materials Science, School of Engineering, The University of Shiga Prefecture

<sup>d</sup>Department of Fundamental Energy Science, Graduate School of Energy Science, Kyoto University

Journal of the Electrochemical Society, Vol.145, No.5, p.1527-1536, 1998

The causes of decrease in electrical conductivity with aging in Y<sub>2</sub>O<sub>3</sub>-stabilized zirconia, an oxygen-ion conductor, were studied. This study was carried out using the dc four-probe technique for measuring electrical conductivity and the activation energy for the migration of oxygen ions. The results show that conductivity decreased with aging below certain temperatures in all specimens. Moreover, it was found that conductivity decreases significantly as the temperature decreases. Samples that were aged at relatively low temperatures exhibited a decrease in conductivity and an increase in activation energy. It was concluded that short range ordering of oxygen ion vacancies toward the zirconium to relax the anisotropy of the lattice distortion is the cause of the decrease in electrical conductivity and the increase in activation energy. When aging was carried out at a relatively high temperature, fully stabilized zirconia showed no change in activation energy and only a slight increase in conductivity. This is because oxygen ion vacancies are in the disordered state and the cubic phase is the only phase at this temperature. Short range ordered of oxygen ion vacancies are takes such a long time presumably because these oxygen ion vacancies are still able to move after aging. This was explained using the concept of mean first passage time.

**69: Effect of Aging on Yttria-Stabilized Zirconia****II. A study of Effect of the Microstructure on Conductivity**

**Junya Kondoh<sup>a</sup>, Shiomi Kikuchi<sup>b</sup>, Yoichi Tomii<sup>c</sup> and Yasuhiko Ito<sup>a,c</sup>**

<sup>a</sup>Division of Energy Science and Engineering, Graduate School of Engineering, Kyoto University, Sakyo-ku, Kyoto 606-01, Japan

<sup>b</sup>Department of Materials Science, School of Engineering, The University of Shiga Prefecture, 2500 Hassaka, Hikone, Shiga 522, Japan

<sup>c</sup>Department of Fundamental Energy Science, Faculty of Energy Science, Kyoto University, Sakyo-ku, Kyoto 606-01, Japan

Journal of the Electrochemical Society, Vol.145, No.5, p.1536-1550, 1998

Microstructural changes in yttria-stabilized with aging were investigated by X-ray diffraction, high resolution transmission electron microscopy (TEM), energy dispersive X-ray spectroscopy under TEM, and electron diffraction. First, various microstructural changes reported in the literature as the causes of the decrease in conductivity were carefully examined. As a result, almost all of them proved not to be direct cause. Therefore, the changes with aging were analyzed mainly by calling attention to a characteristically broad area that appears on the left shoulder of the X-ray diffraction peaks as well as the superlattice reflections and diffuse scattering seen on electron diffraction patterns, and the relationship between microstructural changes and conductivity was clarified. It is concluded that various phenomena due to aging at relatively lower temperatures are caused by short range ordering of oxygen ion vacancies, which occurs in order to relax the anisotropy of periodical lattice distortion. We also studied changes in microstructures occurring with changing dopant concentrations and concluded that the changes in microstructures responsible for the decrease in conductivity associated with increasing dopant concentration are caused by short range ordering of oxygen ion vacancies in order to relax the anisotropy in strain fields, similar to those with aging.

**70: Effect of Aging on Yttria-Stabilized Zirconia****III. A study of Effect of the Local Structures on Conductivity**

**Junya Kondoh<sup>a</sup>, Shiomi Kikuchi<sup>b</sup>, Yoichi Tomii<sup>c</sup> and Yasuhiko Ito<sup>a,c</sup>**

<sup>a</sup>Division of Energy Science and Engineering, Graduate School of Engineering, Kyoto University, Sakyo-ku, Kyoto 606-01, Japan

<sup>b</sup>Department of Materials Science, School of Engineering, The University of Shiga Prefecture, 2500 Hassaka, Hikone, Shiga 522, Japan

<sup>c</sup>Department of Fundamental Energy Science, Faculty of Energy Science, Kyoto University, Sakyo-ku, Kyoto 606-01, Japan

Journal of the Electrochemical Society, Vol.145, No.5, p.1550-1560, 1998

Changes in local structure with aging in yttria-stabilized zirconia were examined by extended x-ray absorption fine structure (EXAFS) and internal friction measurement. An analysis of EXAFS shows that a decrease in the first nearest neighbor coordination number of Zr ions, which means short range ordering of oxygen ion vacancies, a decrease in distance between a Zr ion and its first nearest atoms, and an increase in distance between a Zr ion and its second nearest atoms occurred in aged 8YSZ. Aging caused a noticeable decrease in the relaxation peak of internal friction in 8YSZ. These phenomena are attributed to the short range ordering of oxygen ion vacancies around a Zr ion that results from relaxation in the anisotropy of periodical lattice distortion. Therefore, it is concluded that the trapping of oxygen ion vacancies at Zr ions in order to relax such distortion is responsible for a decrease in conductivity with aging. The relaxation peak of internal friction before aging changed with increasing dopant concentrations, and the behavior of this change from 8YSZ to 10YSZ was very similar to that when 8YSZ was aged, and that from 10YSZ to 15YSZ was similar to that when a single crystal of 10YSZ was aged. This marked similarity indicates that the changes in crystal structure which cause the decrease in conductivity with increasing dopant concentration are caused by the short range ordering of oxygen ion vacancies brought about by relaxation of the distortion, similar to those when conductivity decreases with aging.

**71: \* Protonic and Native Conduction in Sr-Substituted  $\text{LaPO}_4$  Studied by Thermoelectric Power Measurements**

**Koji Amezawa<sup>\*</sup>, Signe Kjelstrup<sup>†</sup>, Truls Norby<sup>‡</sup> and Yasuhiko Ito<sup>\*</sup>**

**<sup>\*</sup>Graduate School of Human and Environmental Studies, Kyoto University, Sakyo-ku, Kyoto 606-8501, Japan**

**<sup>†</sup>Department of Physical Chemistry, Norwegian University of Science and Technology, N-7034 Trondheim, Norway**

**<sup>‡</sup>Center for Materials Science, University of Oslo, N-0371 Oslo, Norway**

**<sup>\*</sup>Graduate School of Energy Science, Kyoto University, Sakyo-ku, Kyoto 606-8501, Japan**

Journal of the Electrochemical Society Vol. 145, No.10 pp. 3313-3319, 1998

Measurements of the thermoelectric power were applied to investigate the electrical conductivity in 5 mol% Sr-substituted  $\text{LaPO}_4$  as a function of temperature (600 to 900°C), water vapor partial pressure (0.2 to 6 kPa), and oxygen partial pressure (4 to 100 kPa). Expressions of the thermoelectric power for materials conducting protons, oxide ions, and electronic defects were derived, based on a thermodynamic treatment of entropy production by heat and charge transfer. The experimental data for 5 mol% Sr-substituted  $\text{LaPO}_4$  were interpreted in terms of protonic conduction, and some additional conduction, possibly by electron holes. In air, the proton transport number is unity at 600°C when  $p_{\text{H}_2\text{O}} > 1\text{kPa}$ , and at 700°C when  $p_{\text{H}_2\text{O}} > 3\text{kPa}$ . In wet atmospheres, the transported entropy of protons in this material was found to be nearly constant,  $112 \pm 2 \text{ J mol}^{-1}\text{K}^{-1}$  at 600 to 800°C in wet atmospheres.

**72: \* INTERMITTENT HEAT TRANSPORT USING HYDROGEN ABSORBING ALLOYS****K. NASAKO<sup>\*†</sup>, Y. ITO<sup>\*</sup> and M. OSUMI<sup>†</sup>****\*Department of Fundamental Energy Science, Graduate School of Energy Science, Kyoto University, Yoshida, Sakyo-ku, Kyoto 606, Japan****†Mechatronics Research Center, Sanyo Electric Co. Ltd, 1-8-13, Hashiridani, Hirakata City, Osaka 573, Japan**

Int. J. Hydrogen Energy, Vol. 23, No.9, pp. 815-824, 1998

Hydrogen absorbing alloys enable heat to be transported over long distances using hydrogen as the transport medium, with theoretically very little heat loss. This report describes the system structure of a newly proposed heat transport system and an analysis of heat transport efficiency, and offers proof that a high efficiency of about 60% can be maintained by the system regardless of distance. Analytical results of a comparison between our transport method and a conventional method using heated water for the long-distance transport of intermittent heat (such as solar heat and plant waste heat) clearly show that transport by hydrogen enables the use of a more compact pipeline diameter for long-distance transport, that the rise time for heat transport is very short, that small-scale (2kW) heat can be transported over a long distance, and that transport by hydrogen is much more efficient than transport by heated water for large-scale (100 kW) heat transport at distances over 2 km.

**73: \* LONG-DISTANCE HEAT TRANSPORT SYSTEM USING A HYDROGEN COMPRESSOR****K. NASAKO<sup>†</sup>, Y. ITO<sup>\*</sup> and M. OSUMI<sup>†</sup>****\*Department of Fundamental Energy Science, Graduate School of Energy Science, Kyoto University, Yoshida, Sakyo-ku, Kyoto, Japan****†Mechatronics Research Center, Sanyo Electric Co. Ltd, 1-8-13, Hashiridani, Hirakata City, Osaka, Japan**

Int. J. Hydrogen Energy, Vol. 23, p.911, 1998

A heat transport system using hydrogen absorbing alloys offers several advantages, such as enabling the use of more compact long-distance transport pipes, maintaining a constant level of efficiency regardless of transport distance, and enabling rapid transport. On the other hand, the system supplies heat to a load through a heat pump with a 20 K difference. The system therefore cannot be used for heat loads that require a higher temperature difference. Then, in order to increase heat load applications, we have proposed a hybrid heat transport system that uses a hydrogen compressor. We also developed a system structure and achieved a heat pump with a 40 K difference by using a 0.2-kW experimental system. Furthermore, we focused on using the same structure on the heat source side for supplying various heat

loads, and have proposed a basic concept for a wide-area heat utilization system that transports heat to various loads from centralized heat sources.

#### 74: RELAXATION OF INTERNAL STRESS GENERATED IN HYDROGEN ABSORBING ALLOY VESSELS

K. NASAKO\*†, Y. ITO\*, N. HIRO† and M. OSUMI†

\*Department of Fundamental Energy Science, Graduate School of Energy Science, Kyoto University, Yoshida, Sakyo-ku, Kyoto, Japan

†Mechatronics Research Center, Sanyo Electric CO. Ltd, 1-8-13, Hashiridani, Hirakata City, Osaka, Japan

Int. J. Hydrogen Energy, Vol. 23, No. 10, pp.921-929,1998

Hydrogen absorbing alloys cause internal stress in reaction vessels due to the expansion that occurs when they absorb hydrogen. This stress is affected not only by the amount of reacting hydrogen but also by ab/desorption cycles. In this paper, we analyze the reaction distribution in a reaction vessel through simulations and show that locally excess internal stress occurs near the heat media inlet. We also show that this excess stress is decreased by unifying the reaction ratio by exchanging heat between the heat media inlet and the outlet in the reaction vessel.

#### 75: Stability of $\text{LiAlO}_2$ as electrolyte matrix for molten carbonate fuel cells

Seiji Terada<sup>a,\*</sup>, Ikuo Nagashima<sup>a</sup>, Kenjin Higaki<sup>a</sup> and Yasuhiko Ito<sup>b</sup>

<sup>a</sup>Kawasaki Heavy Industries, 1-1, Kawasaki-cho, Akashi, Hyogo, 673-8666, Japan

<sup>b</sup>Graduate School of Energy Science, Kyoto University, Sakyo-ku, Kyoto, 606-8501, Japan

Journal of Power Sources vol.75, p.223-229, 1998

In order to prolong the life of molten carbonate fuel cells, the amount of electrolyte in the matrix must be maintained at an appropriate level over long-term operation. Lithium aluminate, the state-of-the-art material for the matrix substrate, still presents some problems, such as crystal phase stability and particle growth. The mechanism of phase transformation and particle growth of lithium aluminate under various conditions (temperature, gas composition, carbonate composition) are investigated. Moreover, the effect of several additives for inhibiting particle growth are investigated. It is found that the allotropic phase transformation and particle growth occurs via a 'dissolution-deposition' mechanism. The results obtained suggest that lower temperature, higher partial pressure of  $\text{CO}_2$  or lower basicity of carbonates are preferable to control the particle growth of lithium aluminate and that  $\alpha$ -lithium aluminate appears more stable under typical MCFC operating conditions. Potassium tungstate inhibits the particle growth

of the lithium aluminate containing  $\beta$ -phase.

**76: Formation of Fine Nickel Particles by Discharge Electrolysis in Molten Chloride System**

**Hiroyuki Kawamura<sup>\*1</sup>, Kimikazu Moritani<sup>\*2</sup> and Yasuhiko Ito<sup>\*3</sup>**

<sup>\*1</sup>Department of Energy Science and Engineering, Graduate School of Engineering, Kyoto University, Yoshidahonmachi, Sakyo-ku, Kyoto 606-8501

<sup>\*2</sup>Department of Nuclear Engineering, Graduate School of Engineering, Kyoto University, Yoshidahonmachi, Sakyo-ku, Kyoto 606-8501

<sup>\*3</sup>Department of Fundamental Energy Science, Graduate School Of Energy Science, Kyoto University, Yoshidahonmachi, Sakyo-ku, Kyoto 606-8501

Journal of the Japan Society of Powder and Powder Metallurgy Vol. 45, No. 12, p.1142-1147, 1998

A stationary discharge was generated in molten chloride by simple apparatus and successfully applied at electrolysis. Fine nickel particles were obtained using a LiCl-KCl-NiCl<sub>2</sub> melt under atmospheric argon gas. From the grading analysis which was estimated through the SEM observation of fine nickel particles, the particles were almost spherical, and the particle sizes were found to depend on the concentration of NiCl<sub>2</sub> and the charge. For the growth of fine nickel particles, the particle sizes were compared with numerical solutions of a Brownian collision-coalescence in colloidal suspensions.

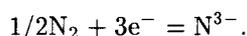
**77: \* Electrochemical reduction of nitrogen gas in a molten chloride system**

**Takuya Goto and Yasuhiko Ito**

Department of Fundamental Energy Science, Graduate School of Energy Science, Kyoto University, Sakyo-ku, Kyoto, 606-8501. Japan

Electrochimica Acta, Vol.43, No. 21-22, pp.3379-3384, 1998

Electrochemical reduction of nitrogen gas in the molten LiCl-KCl system has been studied by electrochemical measurements combined with gas analysis using a nitrogen gas electrode. It was found that nitrogen gas was electrochemically reduced to produce nitride ions almost quantitatively according to the following reaction:



It was confirmed that the use of a nitrogen gas electrode as counter electrode allows us to supply nitride ions successively during anodic surface nitriding in LiCl-KCl systems.

**78: \* Thermodynamic and Kinetic Properties of the N<sub>2</sub> Gas Electrode in a Molten LiCl-KCl-Li<sub>3</sub>N System**

**Y. Ito and T. Goto**

**Department of Fundamental Energy Science, Graduate School of Energy Science, Kyoto University, Sakyo-ku, Kyoto 606-8501, Japan**

Molten Salt Forum Vols.5-6, pp.279-286, 1998

Recently, We have found that N<sub>2</sub> gas is subject to a cathodic reduction to form N<sup>3-</sup> ion in molten chloride system. This new finding is encouraging us to consider the possibility of several energy conversion related electrochemical processes, ie., thermally regenerative fuel cell with Li-N<sub>2</sub> couple, ammonia synthesis from N<sub>2</sub> and H<sub>2</sub>O, and electrochemical implantation of N atom into metal surface to form energy material. In order to provide available data for considering these possibilities, cathodic reduction of N<sub>2</sub> gas and anodic oxidation of N<sup>3-</sup> ion in molten chloride were investigated in detail.

**79: \* Discharge electrolysis in molten chloride: formation of fine silver particles**

**Hiroyuki Kawamura<sup>a</sup>, Kimikazu Moritani<sup>b</sup>, Yasuhiko Ito<sup>a\*</sup>**

**<sup>a</sup>Department of Energy Science and Engineering, Graduate School of Engineering, Kyoto University, Sakyo-ku, Kyoto606, Japan**

**<sup>b</sup>Department of Nuclear Engineering, Graduate School of Engineering, Kyoto University, Sakyo-ku, Kyoto606, Japan**

Plasmas & Ions Vol.1, p.29-36, 1998

A relatively stationary discharge was generated in molten chloride utilizing a simple apparatus and successfully achieved at electrolysis. Fine silver particles were obtained using a LiCl- KCl-AgCl eutectic melt in an argon atmosphere. SEM observations of the silver particles showed them to be almost spherical and the size to be strongly dependent on the experimental conditions. This new kind of discharge electrolysis is expected to be adopted as a new method for metal powder production.

**80: First-nearest-neighbour interatomic potentials for light-actinide metals**

**Kan Hachiya, Yasuhiko Ito**

**Department of Fundamental Energy Science, Graduate School of Energy Science, Kyoto University, Sakyo-ku, Kyoto 606-8501, Japan**

Physica B, Vol.262, p.233-239, 1999

We present first-nearest-neighbour interatomic potentials within a framework of the nearly-free-electron-tight-binding-bond model. Angular dependence of the potential is included as a very simple form to account for the directional f-bonding interactions. Parameters are adjusted to reproduce the experimental interatomic separation and the bulk modulus of the FCC Th ( $\alpha$  phase) and Pu ( $\delta$  phase). Elastic constants are calculated and compared with the available experimental data. The derived potential gives a very good agreement with the experimental data for all the calculated elastic constants for FCC Th, and for the bulk modulus for FCC Pu.

**81: Molecular dynamics simulations of the self-diffusion phenomena in Ni<sub>2</sub>Y intermetallic phase**

**Kan Hachiya, Yasuhiko Ito**

**Department of Fundamental Energy Science, Graduate School of Energy Science, Kyoto University, Yoshida, Sakyo-ku, Kyoto 606-8501, Japan**

Journal of Alloys and Compounds, Vol.279, p.171-178, 1998

We present a molecular dynamics study of the diffusion phenomena in Ni<sub>2</sub>Y, transition-metal intermetallic phase via nearly-free-electron-tight-binding-bond interatomic interaction model. Interpretations of the dynamic structures from the calculations of the mean square displacements and spectral densities of velocity show that the rapid growth of this intermetallic phase found in the experimental study is mainly due to the high-rate self-diffusion in and near the grain-boundaries and independent of the vacancy. Therefore, the standard vacancy-based diffusion process is found to be not essential in this phase.

**82: Clustering Process of the Cuprate Phase in Ag-Added BPSCCO Composites**

**Katsukuni Yoshida, Michiaki Matsukawa\* and Koshichi Noto\***

**\*(Faculty of Engineering, Iwate University)**

Materials Letters, Vol.36, pp.7-10 (1998).

The clustering of cuprate grains in sintered composites of Ag-added (Bi, Pb)-Sr-Ca-Cu-O ( $T_c \approx 110\text{K}$ ) has been investigated in comparison with the behavior of coexisting Ag-clusters. The specimens were prepared by sintering the mixture of superconducting cuprate of (Bi, Pb)<sub>2</sub>Sr<sub>2</sub>Ca<sub>2</sub>Cu<sub>3</sub>O<sub>x</sub> (2223 phase) and Ag<sub>2</sub>O. The resistivity  $\rho$  at 77 K is a decreasing function of Ag-volume fraction  $f$ , the contribution from the superconducting clusters being concealed. However, when the temperature  $T$  is further lowered enough,  $\rho$  changes stepwise into an increasing function, showing the obvious contribution from the superconducting clusters. This transition is realized when the superconducting weak-link is enhanced by lowering  $T$ , and is featured by the two dimensional character of the percolation process of the cuprate clusters.

**83: Behavior of Percolative Transport Paths in Pr-Doped  $Y_1Ba_2Cu_3O_y$** 

**Katsukuni Yoshida and Tomohiro Goya**

Proceedings of World Ceramics Congress and Forum on New Materials (9th CIMTEC, Florence, 1998), Vol. K, pp. 569-575 (1999).

The percolation process when Pr concentration is increased in  $Y_{1-x}Pr_xBa_2Cu_3O_{7-\delta}$  has been investigated in particular reference to the behavior of transport paths contributing to the conductivity and the diamagnetic susceptibility. From the observation of the electric and diamagnetic behavior, a characteristic range is found as  $0.55 \geq x \geq 0.44$ , where the diamagnetic susceptibility  $\chi$  is markedly influenced by applying magnetic fields  $h$  (ac), implying the presence of superconducting current-paths as are easily deteriorated by  $h$ . This compound can be regarded as a 2D discrete site percolation system with structural resolution on nanometer scale. However the range shown above is narrower than the range  $0.59 \geq x \geq 0.41$  as specified by the percolation thresholds based on the nearest-neighbor and the second-nearest neighbor connections between superconducting sites. This variance indicates that a Y-site unit cell weakens in its peculiarity when contacting the Pr-site unit cells.

**84: Synthesis of Functional Ceramic Materials from Aqueous Solutions**

**Takeshi Yao**

Journal of Materials Research, Vol. 13, No. 5, pp. 1091-1098, 1998

Methods for synthesizing ceramic materials from aqueous solutions at ordinary temperature and pressure are advantageous because of the applicability to making films with wide areas and/or complicated shapes with no requirement of vacuum or high temperature, and because of lower cost. Powder of  $ZrO_2$  or  $LnMeO_3$  ( $Ln=La, Nd$ ;  $Me=Cr, Mn, Fe, Co$ ) perovskite was dissolved in hydrofluoric acid and a solution of fluoro-complex ions was obtained. Boric acid was added to the solution, the fluoride ions were consumed by the formation of  $BF_4^-$ , and then the fluoro-complex ions were hydrolyzed to  $ZrO_2$  or  $LnMeO_3$  in order to increase the amount of fluoride ions. A number of synthesized particles of  $ZrO_2$  or  $LnMeO_3$  were observed on the substrates in scanning electron microscope images.

**85: Hydrothermal Synthesis and Crystal Structure of Barium Hewettite:  $\text{BaV}_6\text{O}_{16} \cdot n\text{H}_2\text{O}$** 

Yoshio Oka\*, Takeshi Yao, Shoichi Sato\*\*, Naoichi Yamamoto\*\*\*

\*Faculty of Integrated Human Studies, \*\*Rigaku Corporation, \*\*\*Graduate School of Human and Environmental Studies

Journal of Solid State Chemistry, Vol. 140, No. 2, pp. 219-225, 1998

Ba analogues of hewettite ( $\text{CaV}_6\text{O}_{16} \cdot 9\text{H}_2\text{O}$ ) were synthesized by the hydrothermal methods. The compounds exhibit two phases formulated by  $\text{BaV}_6\text{O}_{16} \cdot n\text{H}_2\text{O}$  and  $\text{Ba}_{1+x}\text{V}_6\text{O}_{16} \cdot n\text{H}_2\text{O}$  ( $x \approx 0.2$ ,  $n \approx 3$ ), and the structure of  $\text{BaV}_6\text{O}_{16} \cdot n\text{H}_2\text{O}$  has been determined from a single crystal study. It crystallizes in the orthorhombic system  $Pnmm$  with  $a = 12.162(3)$  Å,  $b = 10.841(4)$  Å,  $c = 17.035(4)$  Å, and  $Z=6$  and the structure refinements led to  $R = 0.066$  and  $R_w = 0.076$  for 1480 reflections with  $I > 3\sigma(I)$ . The structure is basically analogous to that of  $\gamma\text{-Li}_{1+x}\text{V}_3\text{O}_8$  or  $\text{CaV}_6\text{O}_8 \cdot 9\text{H}_2\text{O}$ , consisting of  $\text{V}_6\text{O}_{16}$  layers and interstitial hydrated Ba atoms. The  $\text{V}_6\text{O}_{16}$  layers stack along the  $c$  axis with 8.518-Å spacing which is half of the  $c$  axis; adjacent layers are mirror images of each other. Ba atoms reside in three kinds of sites with totally different oxygen coordinations. Their interlayer distributions result in another long period along the  $b$  axis which is triple the ordinary 3.6-Å period of the hewettite compounds. This is the first single-crystal structural study of the synthetic hewettite compounds.

**86: Crystal Structure and Metal Distribution of  $\alpha\text{-CoV}_3\text{O}_8$** 

Yoshio Oka\*, Takeshi Yao, Naoichi Yamamoto\*\*, Yutaka Ueda\*\*\*

\*Faculty of Integrated Human Studies, \*\*Graduate School of Human and Environmental Studies, \*\*\*Institute for Solid State Physics, University of Tokyo

Journal of Solid State Chemistry, Vol. 141, No. 1, pp. 133-139, 1998

Single crystals of  $\alpha\text{-CoV}_3\text{O}_8$ , a mixed-valence compound of  $\text{V}^{\text{IV/V}}$ , were hydrothermally synthesized. It crystallizes in the orthorhombic system  $Ibam$  with  $a = 14.3298(6)$  Å,  $b = 9.8906(6)$  Å,  $c = 8.3950(8)$  Å, and  $Z = 8$ . The structure was refined to  $R = 0.034$  and  $R_w = 0.030$  for 1558 reflections with  $I > 3\sigma(I)$ . There are three kinds of metal sites, namely, octahedral  $M(16k)$  for  $M=\text{Co}$ ,  $\text{V}(1)$ , tetrahedral  $\text{V}(2)$  ( $8j$ ), and trigonal-bipyramidal  $\text{V}(3)$  ( $8j$ ), where the  $M$  site was found to consist of half-occupied Co and V(1). Its polyhedral framework is built up of  $\text{MO}_6$  slabs and  $\text{V}(2)\text{O}_4\text{-V}(3)\text{O}_5$  units. The  $\text{MO}_6$  slab is constructed by linking zigzag chains of edge-sharing  $\text{MO}_6$  octahedra running along the  $c$  axis. The linkage is made along the  $b$  axis by sharing common vertices of O(5) and thus the slab stands in the  $bc$  plane. The  $\text{V}(2)\text{O}_4\text{-V}(3)\text{O}_5$  unit, playing a role in bridging  $\text{MO}_6$  slabs, is made of an edge-sharing  $\text{V}(3)\text{O}_5$  pair to which two  $\text{V}(2)\text{O}_4$  are attached. Valence states of metals were evaluated as  $\text{Co}^{\text{II}}$ ,  $\text{V}(1)^{\text{IV}}$ ,  $\text{V}(2)^{\text{V}}$ , and  $\text{V}(3)^{\text{V}}$ . The metal distribution over the  $M$  site is basically random but is constrained by a rule to form a  $\text{Co-O}(5)\text{-V}(1)$  group at the linkage of  $\text{MO}_6$  chains, which accounts for the half-occupancies of Co and V(1) as well as a positional shift of O(5). The structure is compared with those of  $\alpha\text{-ZnV}_3\text{O}_8$  and

$\beta$ -MgV<sub>3</sub>O<sub>8</sub> in particular reference to metal distributions. The magnetic susceptibility curve of  $\alpha$ -CoV<sub>3</sub>O<sub>8</sub> exhibits a sharp peak at 8 K, suggesting the onset of antiferromagnetic order.

### 87: Crystal Structures and Transition Mechanism of VO<sub>2</sub>(A)

Yoshio Oka\*, Shoichi Sato\*\*, Takeshi Yao, Naoichi Yamamoto\*\*\*

\*Faculty of Integrated Human Studies, \*\*Rigaku Corporation, \*\*\*Graduate School of Human and Environmental Studies

Journal of Solid State Chemistry, Vol. 141, No. 2, pp. 594-598, 1998

Structures of VO<sub>2</sub>(A) have been redetermined by single-crystal diffractometry for low- (LTP) and high-temperature (HTP) phases at 298 and 473 K, respectively. The LTP adopts the tetragonal system  $P4/ncc$  with  $a = 8.4403(9)$  Å,  $c = 7.666(1)$  Å, and  $Z = 16$ , whereas the HTP adopts the body-centered tetragonal system  $I4/m$  with  $a = 8.476(2)$  Å,  $c = 3.824(2)$  Å, and  $Z = 8$ . The refinements led to  $R/R_w = 0.031/0.032$  for LTP and  $0.012/0.033$  for HTP. The structures of both phases consist of edge-sharing VO<sub>6</sub> octahedra and exhibit quite similar oxygen frameworks. Through the transition the V<sup>4+</sup>-V<sup>4+</sup> bonding in LTP with a distance of  $2.7695(8)$  Å is dissociated in HTP to a distance of  $3.0794(3)$  Å. The transition occurs with cooperative movements of the V atoms, namely, a rotation around the  $c$  axis and a shift along the  $c$  axis. Strangely, twinning is induced on the LTP to HTP transition but disappears on the reverse transition.

### 88: Metal-Insulator Transition and Crystal Structure of La<sub>1-x</sub>Sr<sub>x</sub>CoO<sub>3</sub> as Functions of Sr-Content, Temperature, and Oxygen Partial Pressure

Atsushi Mineshige\*, Masafumi Kobune\*, Satoshi Fujii\*, Zempachi Ogumi\*\*, Minoru Inaba\*\*, Takeshi Yao, Kenji Kikuchi\*\*\*

\*Department of Applied Chemistry, Himeji Institute of Technology, \*\*Graduate School of Engineering, \*\*\*Department of Materials Science, University of Shiga Prefecture

Journal of Solid State Chemistry, Vol. 142, No. 2, pp. 374-381, 1999

Electrical properties of La<sub>1-x</sub>Sr<sub>x</sub>CoO<sub>3</sub> (LSC) change with variations in Sr content, temperature, and oxygen partial pressure. With a change in each variable, LSC showed metal-insulator transition (MIT). The changes in electrical properties of LSC were correlated here with those of its crystal structure. The variations of crystallographic parameters such as the length of  $a$ -axis, the rhombohedral angle, the Co-O distance, and the Co-O-Co angle ( $\theta$ ) were precisely determined by powder X-ray Rietveld analysis. Of these, the variation of  $\theta$  described most consistently the variation of conduction state, metallic or insulating, of LSC. The Co-O-Co angle increased whenever the conduction state changed from insulating to metallic by changing each variable, Sr content, temperature, and oxygen partial pressure. In addition, MIT took place at a critical Co-O-Co angle of ca.  $165^\circ$  in each case. It was concluded that the transition

from insulator to metal is caused by the closing of the charge transfer band gap, induced by broadening of the electronic bandwidths of the Co-3d and O-2p bands with an expansion of the Co-O-Co angle.

**89: Superstructure of Strontium Vanadium Oxide,  $\text{Sr}_{0.5}\text{V}_2\text{O}_5$ : Their Twinning, Groupoid Symmetry and Interpretation as OD Structure**

**Katsuo Kato\***, **Yasushi Kanke\***, **Yoshio Oka\*\***, **Takeshi Yao**

**\*National Institute for Research in Inorganic Materials, \*\*Faculty of Integrated Human Studies**

Zeitschrift für Kristallographie, Vol. 213, No. 7-8, pp. 399-405, 1998

The title compound has been considered to be isotypic with  $\text{Ag}_{0.68}\text{V}_2\text{O}_5$ , a typical  $\delta$  vanadium bronze crystallizing in space group  $C2/m$ . Through hydrothermal synthesis, however, crystals were obtained showing superlattice reflections. Triclinic,  $C\bar{1}$  (No. 2),  $a = 23.536(2) \text{ \AA}$ ,  $b = 7.3985(3) \text{ \AA}$ ,  $c = 8.801(1) \text{ \AA}$ ,  $\alpha = 90^\circ$ ,  $\beta = 88.28(1)^\circ$ ,  $\gamma = 90^\circ$ ,  $Z = 16$ . The structure was determined based on 2160 reflections of a specimen twinned about  $[010] \mid (010)$ ;  $R(F) = 0.032$ ,  $R_w(F) = 0.024$ . Twinning about  $[100]$  or  $(001)$  was also observed. The structure includes  $\text{V}_2\text{O}_5$  layers with Sr atoms sandwiched between them. The perfectly ordered arrangement of the Sr atoms leads to the superstructure. The V(V) and V(IV) positions can be distinguished. The structure has an idealized symmetry of a Brandt groupoid  $C2/m \{t(1/4, 3/4, 0)\}$ . An interpretation as OD structure is given to explain the mechanism of twinning.

**90: Structure of Strontium Vanadium Oxyhydrates,  $\text{SrV}_{12}\text{O}_{27} \cdot 3\text{H}_2\text{O}$ : A Vanadium Oxide Bronze with New Vanadate Framework**

**Katsuo Kato\***, **Yasushi Kanke\***, **Yoshio Oka\*\***, **Takeshi Yao**

**\*National Institute for Research in Inorganic Materials, \*\*Faculty of Integrated Human Studies**

Zeitschrift für Kristallographie, Vol. 213, No. 10, pp. 532-536, 1998

$\text{SrV}_{12}\text{O}_{27} \cdot 3\text{H}_2\text{O}$  was synthesized hydrothermally. Monoclinic  $P2_1/m$ ;  $a = 11.684(2) \text{ \AA}$ ,  $b = 11.126(2) \text{ \AA}$ ,  $c = 9.052(2) \text{ \AA}$ ,  $\beta = 110.94(2)^\circ$ ;  $Z = 2$ .  $R(F) = 0.049$ ,  $R_w(F) = 0.039$  for 3756 observed reflections. The structure includes a new vanadate framework  $\text{V}_4\text{O}_9$ , similar to the  $\text{V}_2\text{O}_5$  in vanadium bronzes  $\beta\text{-}A_x\text{V}_2\text{O}_5$ . The  $\text{V}_4\text{O}_9$  framework, forming a substructure with  $b' = b/3$ , consists of  $2 \times 3$  columns of edge-sharing  $\text{VO}_6$  octahedra and chains of edge-sharing  $\text{VO}_5$  trigonal bipyramids. The columns and the chains run parallel to  $[010]$  and are connected through common corners of  $\text{VO}_6$  and  $\text{VO}_5$ . The columns neighbouring in  $[001]$  direction share two corners of octahedra per  $b'$  period. The Sr atoms and  $\text{H}_2\text{O}$  molecules are accommodated in the wide  $[010]$  tunnels characteristic of the  $\text{V}_4\text{O}_9$  framework.

**91: Optimization of Preparation Conditions of Spinel  $\text{Li}_{4/3}\text{Mn}_{5/3}\text{O}_4$  as a Cathode Material for Rechargeable Lithium Battery****Kiyoshi Kanamura\*, Hidetoshi Naito\*, Takeshi Yao, Zen-ichiro Takehara\*****\*Graduate School of Engineering**

Denki Kagaku, Vol. 66, No. 12, pp. 1182-1187, 1998

$\text{Li}_{4/3}\text{Mn}_{5/3}\text{O}_4$  was prepared under various conditions to optimize its discharge and charge characteristics as cathode materials for rechargeable lithium batteries. We found that the oxidation state of Mn ions and crystallinity of  $\text{Li}_{4/3}\text{Mn}_{5/3}\text{O}_4$  strongly depended on the preparation temperature. The best rechargeability was obtained for the sample prepared at 550°C in oxygen atmosphere. The  $\text{Li}_{4/3}\text{Mn}_{5/3}\text{O}_4$  sample exhibited unique electrochemical and structural characteristics which were the very flat discharge and charge curves and the negligible structure change during the discharge and charge cycling.

**92: Novel Method for Zirconium Oxide and Rare Earth-Transition Metal Perovskite Oxides Synthesis from Aqueous Solutions****Takeshi Yao, Yoshiharu Uchimoto, Koichi Kajihara**

Hydrogen Energy Progress XII, edited by J.C. Bolcich and T.N. Veriroglu, pp. 2139-2148, 1998

Zirconium oxide:  $\text{ZrO}_2$  and rare earth-transition metal perovskite oxides:  $\text{LnMeO}_3$  (Ln = La, Nd; Me = Cr, Mn, Fe, Co) have many technological uses including such as oxygen sensors, catalysts, electrocatalysts, oxygen permeating membranes, and now are paid a great attention as electrolyte, cathode and interconnect materials for solid oxide fuel cells and high temperature steam electrolysis cells. Methods for forming films from an aqueous solution is expected to be advantageous because no vacuum, no high temperature and no expensive apparatus will be required, and substrates, even those with wide areas and/or complicated shapes, are available. From this point of view, we have considered it important to find out methods for synthesizing these oxides from aqueous solutions. In this study, we will present methods for synthesizing  $\text{ZrO}_2$  and  $\text{LnMeO}_3$  from aqueous solutions at ordinary temperature and ordinary pressure. We have tried to deposit  $\text{LaMnO}_3$ , the candidate of electrode material, on yttria stabilized zirconia: YSZ, the major electrolyte material, by using this method.

**93: Effect of Doping Strontium to LaMnO<sub>3</sub> on the Electrode Properties**

Yoshiharu Uchimoto, Takeshi Yao, Tsutomu Ioroi\*, Zempachi Ogumi\*, Zen-ichiro Takehara\*

\*Graduate School of Engineering

Proceedings of the 4th Intern. symp. on Ionic and Mixed Conducting Ceramics, Vol. 97, No. 2, pp. 2177-2182, 1997

Complex AC impedance and steady state polarization measurements have been conducted on dense and thin LaMnO<sub>3</sub> and La<sub>0.85</sub>Sr<sub>0.15</sub>MnO<sub>3</sub> film electrodes and porous-sintered LaMnO<sub>3</sub> and La<sub>0.85</sub>Sr<sub>0.15</sub>MnO<sub>3</sub> electrodes in air at elevated temperatures between 873 and 1273 K to investigate the reaction mechanism at the La<sub>1-x</sub>Sr<sub>x</sub>MnO<sub>3</sub> electrode of a SOFC. By fitting impedance spectra to the appropriate equivalent circuit, the oxygen chemical diffusion coefficient through the La<sub>1-x</sub>Sr<sub>x</sub>MnO<sub>3</sub> film electrode and the interfacial reaction resistance for oxygen reduction have been determined. These results suggest that the interfacial reaction at the electrode surface is the rate determining step for the electrochemical reduction of oxygen in a practical porous La<sub>1-x</sub>Sr<sub>x</sub>MnO<sub>3</sub> electrode for SOFCs.

**94: Kinetics of Vapor-Phase Electrolytic Deposition of Yttria-Stabilized Zirconia Thin Films**

Yoshiharu Uchimoto, Kazushi Tsutsumi\*, Tsutomu Ioroi\*, Zempachi Ogumi\*, Zen-ichiro Takehara\*

\*Graduate School of Engineering

Journal of Electrochemical Society, Vol. 145, pp. 4277-4281, 1998

The kinetic aspects of the Vapor-phase Electrolytic Deposition (VED) process are discussed. This new technology, which is similar to the electrochemical vapor deposition process, is based on electrolytic deposition using a glow-discharge plasma as the conductive medium. After reaction for 2 h at a DC current density of 2.82 mA cm<sup>-2</sup>, a uniform cubic fluorite YSZ layer containing about 8 mol% Y<sub>2</sub>O<sub>3</sub> of thickness about 7 μm was deposited. The thickness of the deposited layer was directly proportional to the reaction time, indicating that the VED process is consistent with Faraday's Law. In VED, the deposition rate of YSZ depends only on the O<sub>2</sub>-flux (the DC current density) through the YSZ layer.

**95: Preparation of Perovskite-Type  $\text{La}_{1-x}\text{Sr}_x\text{MnO}_3$  Films by Vapor-Phase Processes and Their Electrochemical Properties. Part 2. Effects of Doping Strontium to  $\text{LaMnO}_3$  on the Electrode Properties**

**Tsutomu Ioroi\*, Tatsunori Hara\*, Yoshiharu Uchimoto, Zempachi Ogumi\*, Zen-ichiro Takehara\***

**\*Graduate School of Engineering**

Journal of Electrochemical Society, Vol. 145, pp. 1999-2004, 1998

Complex AC impedance and steady state polarization measurements have been conducted on dense and thin  $\text{LaMnO}_3$  and  $\text{La}_{0.85}\text{Sr}_{0.15}\text{MnO}_3$  film electrodes and porous-sintered  $\text{LaMnO}_3$  and  $\text{La}_{0.85}\text{Sr}_{0.15}\text{MnO}_3$  electrodes in air at elevated temperatures between 873 and 1273 K in order to study the reaction mechanism of oxygen reduction at  $\text{La}_{1-x}\text{Sr}_x\text{MnO}_3$  electrode of SOFC. By fitting impedance spectra to an appropriate equivalent circuit, chemical diffusion coefficient of oxygen and interfacial reaction resistance of the  $\text{LaMnO}_3$  and  $\text{La}_{0.85}\text{Sr}_{0.15}\text{MnO}_3$  film electrodes were determined. The chemical diffusion coefficient was scarcely affected by Sr-doping, while the interfacial reaction resistance considerably decreased by Sr-doping. Steady state polarization behavior of the porous-sintered  $\text{La}_{1-x}\text{Sr}_x\text{MnO}_3$  were dramatically improved by doping Sr, while those of the dense  $\text{La}_{1-x}\text{Sr}_x\text{MnO}_3$  film were almost unchanged by Sr-doping. These results suggested that the electrochemical reduction of oxygen at the porous  $\text{La}_{1-x}\text{Sr}_x\text{MnO}_3$  electrode takes place around the TPB and the reaction rate is controlled by the surface reactions at close to the TPB region.

**96: Preparation of Macroporous Titania Films by a Sol-Gel Dip-Coating Method from the System Containing Poly(ethylene glycol)**

**Koichi Kajihara, Kazuki Nakanishi\*, Katsuhisa Tanaka\*, Kazuyuki Hirao\*, Naohiro Soga\***

**\*Graduate School of Engineering**

Journal of the American Ceramic Society, Vol. 81, No. 10, pp. 2670-2676, 1998

Macroporous titania ( $\text{TiO}_2$ ) films have been prepared via a sol-gel dip-coating method from a titanium tetraisopropoxide solution that contains poly(ethylene glycol) (PEG). The macroporous morphology—i.e., the size, distribution and shape of the macropores—is controlled by varying the content and molecular weight of PEG, the withdrawal speed, and the temperature of the dipping solution. The morphology of the  $\text{TiO}_2$  film is determined by competitive contributions of the following factors: (i) decrease in fluidity, because of the evaporation of solvent; (ii) network formation by polycondensation reactions; and (iii) domain formation during phase separation into gel phases and solvent phases.

**97: Macroporous Morphology of the Titania Films Prepared by a Sol-Gel Dip-Coating Method from the System Containing Poly(ethylene glycol). I. Effect of Humidity****Koichi Kajihara, Takeshi Yao**

Journal of Sol-Gel Science and Technology, Vol. 12, No. 3, pp. 185-192, 1998

The influence of humidity upon the macroporous morphology of the titania films has been studied for a sol-gel dip-coating system containing poly(ethylene glycol) (PEG). The water adsorption from the ambient atmosphere modifies the polycondensation rate of  $\text{TiO}_2$  oligomer and the phase separation rate between the  $\text{TiO}_2$ -PEG complex and solvent mixture, and greatly varies the macroscopic morphology of the resultant  $\text{TiO}_2$  film.

**98: Macroporous Morphology of the Titania Films Prepared by a Sol-Gel Dip-Coating Method from the System Containing Poly(ethylene glycol). II. Effect of Solution Composition****Koichi Kajihara, Takeshi Yao**

Journal of Sol-Gel Science and Technology, Vol. 12, No. 3, pp. 193-201, 1998

The influences of water and alkoxide concentrations, as well as the relative humidity upon the macroporous morphology of the titania ( $\text{TiO}_2$ ) films have been studied for a sol-gel dip-coating system containing poly(ethylene glycol) (PEG). The distribution of resultant morphology against the withdrawal speed and relative humidity is varied significantly by mainly modifying the polycondensation and phase separation processes during the dipping operation, even by the small change in starting composition of the dipping solution.

**99: Internal Disruptions in Heliotron E****Benjamin A. Carreras\*, Vicky E. Lynch\*, Hideki Zushi\*\*, Katsuji Ichiguchi\*\*\*, Mamahiro Wakatani****\* Oak Ridge National Labo**

Physics of Plasmas Vol.5, No.10, pp.3700-3707, 1998

In Heliotron E [K. Uo, Nucl. Fusion **25**, 1243 (1985)] shifted-in vacuum magnetic field configuration, the  $q$  profile varies from just above 2 at the magnetic axis to 0.4 at the plasma edge. For low- $\beta$  plasmas, resistive interchange modes are the dominant low- $n$  instabilities at the plasma core. They saturate at low

fluctuation levels. Above a threshold value, the ideal  $m/n = 2/1$  modes become unstable. They can be resonant or nonresonant modes depending on the value of  $q(0)$ . In either case, their nonlinear evolution leads to a sudden crash of the pressure within the  $r/a = 0.3$  radius (sawtooth oscillation). When beta is increased further, the  $q = 2$  surface moves out of the plasma, and the ideal  $m/n = 2/1$  modes are effectively stabilized when  $q(0) < 1.85$ . As a result, the sawtooth oscillations are suppressed.

#### 100: Damping of Surface Alfvén Wave in a Slab Plasma

**Tomoya Tatsuno, Mamahiro Wakatani**

Journal of the Physical Society of Japan, vol.67, No.7, pp.2322-2326, 1998

The MHD wave is studied when two steep density gradient regions exist at surfaces of slab plasma. In such a case, it is shown that the surface Alfvén wave has two branches with nearly the same damping rates, since the steep density gradients are located closely each other. However, for the sharp boundary plasma, the surface Alfvén wave does not damp. As the density profile is relaxed, the damping rates become larger, pass via extremum, and again they become small when the scale length of the density gradients extremely increases. These damping rates seem consistent with behavior of magnetic fluctuations observed in the Heliotron-E pellet injection experiment.

#### 101: Stabilization of Resistive Wall Mode Due to Shear Alfvén Resonance in a Cylindrical Plasma with a Uniform Longitudinal Flow

**Akira Yoshioka, Tomoya Tatsuno and Masahiro Wakatani**

Journal of the Physical Society of Japan, vol.67, No.11, pp.3794-3800, 1998

Resistive wall mode (RWM) is studied in a cylindrical plasma with a uniform longitudinal plasma flow. In order to simplify the analysis, two steps current profile model is employed with a constant current density  $j_0$  for the inner region  $0 \leq r \leq a_0$  and a constant current density  $j_1$  for the outer region  $a_0 \leq r \leq a$ . Also the resistive shell is assumed sufficiently thin. Current profiles from peaked ones to hollow ones are simulated by changing the ratio  $j_1/j_0$ . Based on the incompressible MHD model, it is shown that RWM can be stabilized by adjusting the resistive wall position, when the shear Alfvén resonance appears inside the plasma column, with the increase of the uniform flow velocity. In this case the free energy destabilizing the RWM is absorbed in the plasma column through the shear Alfvén resonance. However, except when the RWM is close to the marginal state without a plasma flow, the flow velocity for stabilization is comparable to the sound velocity.

**102: Gyrokinetic Particle Simulation Using the Orbit Average Electron Drift-Kinetic Equation****Yasuhiro Idomura, Sinji Tokuda\* and Masahiro Wakatani****\* Japan Atomic Energy Research Institute**

Journal of Plasma and Fusion Research Vol.75, No.2, pp.131-142, 1999

A new gyrokinetic particle simulation method using the orbit averaged electron drift-kinetic equation has been developed in a three dimensional slab geometry. Using the large discrepancy between the time scale of the low frequency fluctuations and the Courant-Friedrichs-Lewy condition determined by the electron ballistic mode, the transit time ordering,  $\omega/\omega_{tr} \sim \theta(\epsilon)$ , is introduced. The motion of the high energy transit electron is averaged over the periodic unperturbed orbit by means of the action-variation Lie perturbation method. In a new gyrokinetic Vlasov-Maxwell system, the drift-kinetic equation for the high energy part of the electron distribution function reduces to a two dimensional problem, which involves only the  $\mathbf{E} \times \mathbf{B}$  nonlinearity, and the adiabatic response to the low frequency fluctuation is renormalized in the field equation. The ballistic mode arising from the high energy transit electron is removed and a longer simulation time step is enabled.

**103: Integral Suppression of Pfirsch-Schlüter Current in the Inward Shifted Stellarator Plasma in Heliotron E****Sakae Besshou, Vladimir. D. Pustovitov,\* Norihito Fujita,\*\* Katsumi Kondo, Tohru Mizuuchi,\*\* Kazunobu Nagasaki,\*\* Masahiko Nakasuga, Tokuhiko Obiki,\*\* Hiroyuki Okada,\*\* Fumimichi Sano,\*\* Hideki Zushi \*Russian Research Centre, Kurchatov Institute, Russia \*\*Institute of Advanced Energy, Kyoto University**

Journal of Plasma Fusion Research SERIES, Vol. 1 , pp.452-455, 1998

Observation of the complete suppression of integral effect of Pfirsch-Schlüter current in Heliotron E plasmas is reported. Poloidal magnetic field was measured to control the plasma boundary position. We found that pressure-induced plasma shift, an observable characteristic of Pfirsch-Schlüter current, depends strongly on the initial position of magnetic axis. When it was moved by the vertical field inside the torus, finite- $\beta$  shift became smaller. Complete suppression of finite- $\beta$  shift was achieved in a deeply inward shifted configuration: 7 cm from the standard position  $R_{axis}=2.20$  m. Observed effect is explained by MHD equilibrium theory for planar circular axis stellarator plasma with a high magnetic hill and deep inward shift.

**104: \* Physical Property of Plasmas in the L=1 Heliotron**

**Yuji Nakamura, Masahito Wakatani, Masayuki Yokoyama (National Institute of Fusion Science) and Heliotron E Group**

Journal of Plasma and Fusion Research SERIES, Vol.1, 433-436 (1998)

The design study of the L=1/M=4 helical axis heliotron device is now undertaken at Kyoto University. This device will have an L=1 helical coil with two sets of toroidal coils and three sets of poloidal coils to control the rotational transform, toroidal mirror component of the magnetic field strength, plasma position and shape. Current status of the physical studies of plasmas in this device is presented using detailed and realistic parameters of the machine.

**105: \* Local Stability of High Beta Low Aspect Ratio Tokamak with Negative Shear**

**Masaru Furukawa (Department of Nuclear Engineering, Faculty of Engineering, Kyoto University), Yuji Nakamura and Masahiro Wakatani**

Journal of Plasma and Fusion Research, Vol.74, No.6, 598-606 (1998)

Magnetohydrodynamic (MHD) equilibrium and local stability are studied for low aspect ratio tokamaks with an aspect ratio  $A=1.25$ . Particular interest is in equilibria with substantial negative shear region. Almost all MHD equilibria with negative shear region are paramagnetic for low aspect ratio tokamaks. Shafranov shift is reduced in case of the negative shear for the same  $q_{min}$  and it becomes difficult to produce a region with a closed  $|B|=const.$  surface, which is favorable for particle confinement under the effect of toroidal ripples, even for  $\beta(0) \sim 50\%$ . Here  $q_{min}$  is the minimum value of safety factor and  $\beta(0)$  is a central beta value. Mercier criterion is checked for MHD equilibria obtained with the VMEC (Variational Moment Equilibrium Code) by changing ellipticity and triangularity. A low aspect ratio configuration with a moderate triangularity is proposed to obtain a high plasma current in a high beta plasma, which has an advantage to confine charged fusion products.

**106: \* Formation and Termination of High Ion Temperature Mode in Heliotron/Torsatron Plasmas**

**Katsumi Ida\***, **Katsumi Kondo**, **Kazunobu Nagasaki\*\***, **Hideki Zushi**, **Yuji Kurimoto\*\*\***, **Takateru Hamada\*\*\***, **Fumimichi Sano\*\***, **Tohru Mizuuchi\*\***, **Hiruyuki Okada\*\***, **Sakae Besshou**, **Hikomichi Funaba\*\*\***, **Sigeru Hidekuma\***, **Kiyomasa Watanabe\***, and **Tokuhiro Obiki\*\***

**\*National Institute for Fusion Science \*\*Institute of Advanced Energy, Kyoto University \*\*\*Faculty of Engineering, Kyoto University**

Plasma Physics and Controlled Fusion, 40, pp.793-797, 1998

The physics of the formation and the termination of high ion temperature mode (high  $T_i$  mode) is studied by controlling density profiles and radial electric field. High ion temperature mode is observed for neutral beam heated plasmas in heliotron/torsatron plasmas (Heliotron-E). This high  $T_i$  mode plasma is characterized by a peaked ion temperature profile and is associated with a peaked electron density profile produced by neutral beam fuelling with low wall recycling. This high  $T_i$  mode is terminated by flattening of the electron density caused either by gas puffing or by second-harmonic ECH (core density 'pump out').

**107: \* Experiments on Li Pellet Injection into Heliotron E**

**Vladimir Y. Sergeev\***, **Konstantin V. Khlopenkov\***, **Boris V. Kuteev\***, **Shigeru Sudo\*\***, **Katsumi Kondo**, **Hideki Zushi**, **Sakae Besshou**, **Fumimichi Sano\*\*\***, **Hiroiyuki Okada\*\*\***, **Tohru Mizuuchi\*\*\***, **Kazunobu Nagasaki\*\*\***, **Tokuhiro Obiki\*\*\***, and **Yuji Kurimoto\*\*\*\***, **\*State Technical University, St Petersburg, Russia \*\*National Institute for Fusion Science \*\*\*Institute of Advanced Energy, Kyoto University \*\*\*\* Faculty of Engineering, Kyoto University**

Plasma Physics and Controlled Fusion 40, pp.1785-1801, 1998

Li pellets of large size were injected into electron cyclotron resonance (ECR) heated plasmas and neutral beam injection (NBI) heated plasmas of Heliotron E. The discharge behaviour, pellet ablation and wall conditioning were studied. The electron pressure is doubled after injection into the NBI plasma and remains unchanged in the case of ECR heating. This may be due to the energy exchange between the electrons and thermal ions with the fast ions from the neutral beam. The observed discrepancy between the experimental and modelled ablation rates may be caused by both the plasma cooling due to pellet ablation and ablation stimulated by the fast ions in the NBI-heated regime and by the fast electrons in the ECR-heated regime. In preliminary experiments on wall conditioning by Li pellet injection, no improvement of plasma performance after Li pellet injection was observed in the divertor or limiter configuration, with the limiter radii  $r_L = 24-25$  cm.

**108: Sawtooth Control by On-Axis Electron Cyclotron Current Drive on the WT-3 Tokamak**

**Makoto Asakawa\***, **Kazunori Tanabe\***, **Mitsuru Watanabe**, **Masahiko Nakamura\*\***, **Hitoshi Tanaka**, **Takashi Maekawa**, **Yasushi Terumichi\***

**\*(Fac. of Science, Kyoto Univ.)**, **\*\* (Osaka Institute of Technology)**

Proc. 17th IAEA Fusion Energy Conference, Yokohama, 1998, paper No. CN-69/CDP/06

The experiments on control of sawtooth oscillations (STO) by electron cyclotron current drive (ECCD) have been performed on the WT-3 tokamak. Stabilization and excitation of STO are observed for counter-ECCD and co-ECCD, respectively, when the position of the power deposition is located inside the inversion radius. These results are due to the modification of the current profile near the magnetic axis.

**109: \* Formation and Confinement of Non-neutral Electron Plasmas in a Multi-Ring Electrodes Trap Using with a Field Emitter Array Cathode**

**Hitoshi Tanaka**, **Tatsuya Sodekoda**, **Takashi Maekawa**, **Souichiro Yamaguchi\***, **Tamio Nagatomo\***, **Makoto Asakawa\***, **Yasushi Terumichi\***, **Akihiro Mohri\*\***

**\*(Fac. of Science, Kyoto Univ.)**, **\*\* (Institute of Physical and Chemical Res.)**

Proc. of 1998 ICPP & 25th EPS Conf. on Contr. Fusion and Plasma Phys., Praha, 1998, ECA Vol.22C, pp.11 – pp.14.

A Field Emitter Array (FEA) cathode is used to form a non-neutral electron plasma in a multi-ring electrodes trap by the multi-pulse stacking method. The time evolution of the accumulation is investigated. When a  $m = 1$  or 2 rotating electric field at frequency range of the electrostatic mode is applied, the plasma radius decreases and the confinement time becomes one order of magnitude longer.

**110: \* Experiments on Non-Neutral Long Spheroidal Electron Plasmas in a Multi-Ring-Electrode Trap**

**Akihiro Mohri\***, **Hiroyuki Higaki\*\***, **Yohei Yamazawa\*\*\***, **Hitoshi Tanaka**, **Toshinori Michishita\*\*\*\***, **Tetsumori Yuyama\*\*\*\***

**\*(Institute of Physical and Chemical Res.)**, **\*\* (Institute of Physics, University of Tokyo)**, **\*\*\* (Graduate School of Environmental Human Studies, Kyoto Univ.)**, **\*\*\*\* (Fac. of Integrated Human Studies)**

Proc. of 1998 ICPP & 25th EPS Conf. on Contr. Fusion and Plasma Phys., Praha, 1998, ECA Vol.22C, pp.67 – pp.70.

A nonneutral spheroidal plasma with a longer axial length can be stably trapped in a shallower electrostatic hyperbolic (or harmonic potential) well in the presence of a uniform magnetic field. This feature brings a possibility to construct a fusion reactor scheme using nonneutral plasma composed of ions only. Here, the potential well might be formed within a feasible strength of the electric field. Long spheroidal plasmas are also very useful for fundamental studies of plasma physics, especially of electrostatic waves. Traps equipped with many electrodes of a ring shape, named by Multi-Ring-Electrode Trap: MRE, have been developed for the above mentioned purpose and experiments have been performed. This report describes experimental results obtained from a new trap named MRE-4.

### 111: Profile Control Studies on Heliotron E

Tokuhiro Obiki, H.Okada, K.Kondo, F.Sano, H.Zushi, K.Hanatani, T.Mizuuchi, S.Besshou, K.Nagasaki, M.Wakatani, Y.Nakamura, M.Nakasuga, Y.Ijiri, T.Senju, K.Yaguchi, S.Kobayashi, K.Toshi, K.Sakamoto, Y.Kurimoto, T.Hamada, S.Sudo\*, M.Sato\*, K.Ida\*, H.Funaba\*, S.Kado\*, B.J.Peterson\*, K.Muraoka\*\*, HSugai\*\*\*, H.Toyota\*\*\*, K.Sasaki\*\*\*, H.Kokura\*\*\*, K.Matsuo\*\*\*\*, V.Yu.Sergeev\*\*\*\*\*, K.V.Khlopenko\*\*\*\*\*, V.V.Chechkin\*\*\*\*\*, V.S.Voitsenya\*\*\*\*\*

\* National Institute for Fusio Science

\*\* Interdisciplinary Graduate School of Eengineering Science, Kyushu Univ.

\*\*\* Faculty of Engineering, Nagoya Univ.

\*\*\*\* Faculty of Engineering, Fukuoka Institute of Technology

\*\*\*\*\* State Technical Univ., Russia

Kharkov Institute of Physics and Technology, Ukraine

Journal of Plasma and Fusion Research SERIES, Vol.1, pp.27-29, 1998

In Heliotron-E device, the effects of combined heating with ECR and NBI on profile formation and confinement have been studied. The various profiles can be obtained by the control of the heating power, the heating method and the density. With the high power NBI, the peaked electron density and ion temperature profiles are achieved simultaneously. On the contrary, the peaked electron temperature and flat density profile is brought by ECH. The profile effects on the global energy confinement in the medium density region are discussed in this paper.

### 112: Structure of the Edge Magnetic Field of the $\ell = 1$ Helical Axis Heliotron

T.Mizuuchi, M.Nakasuga, Y.Nakamura, F.Sano, K.Kondo, H.Okada, K.Nagasaki, S.Besshou, K.Hanatani, M.Wakatani and T.Obiki

Journal of Plasma and Fusion Research SERIES, Vol.1, pp.209-212, 1998

The structure of the edge magnetic field of the  $\ell = 1$  Helical-Axis Heliotron, Which is designed at the Institute of Advanced Energy, is numerically analyzed. In contrast to the Heliotron E case, the edge magnetic field structure of this low shear device is strongly affected by "natural-islands" such as

$n/m=4/5, 4/6, 4/7$  or  $4/8$  near the outermost magnetic surface. By changing the vertical field strength, we observe “wall-limiter”, “island-divertor” and “local divertor” configurations.

### 113: ECH Launching Conditions in Helical System

**K. Nagasaki, A. Ejiri\*, T. Mizuuchi, S. Besshou, H. Funaba\*, K. Ida\*, K. Kondo, H. Morioka, T. Obiki, H. Okada, F. Sano and H. Zushi**

\* National Institute for Fusion Science

Journal of Plasma and Fusion Research SERIES, Vol.1, pp.114-117, 1998

Launching conditions for electron cyclotron heating (ECH) are studied on Heliotron E. In heliotron/torsatron configurations, the polarization of the launched wave should be determined by taking into account the effect of magnetic shear. The best-localized heating is obtained when the electric field of the launched wave is off-normal to the resonant magnetic field even for perpendicular beam injection. The experimental results are in good agreement with the numerical calculation results including the magnetic shear terms.

### 114: In-Situ Surface Modification by ECH Plasma in Heliotron E

**Norihito Fujita, K.Nishimura, T.Mizuuchi, T.Kito, K.Kondo, K.Nagasaki, H.Okada, F.Sano, T.Obiki, K.Kokura\*, H.Toyoda\* and H.Sugai\***

\* Department of Electrical Engineering, Nagoya Univ.

Journal of Plasma and Fusion Research SERIES, Vol. 1, pp.306-309, 1998

This paper describes in-situ surface modification methods by using ECH plasmas. A localized deposition of a B-film was observed for the ECH boronization in Heliotron E. The reason of the local deposition and how to improve the uniformity of a B-film are discussed. On the other hand, a unique evaporation technique of lithium by a “plasma-assisted heating” was examined in a small linear device for the ECH “lithiumization”.

### 115: The New Helical Plasma Device at IAE, Kyoto University

**Fumimichi Sano, T.Obiki, N.Inoue, A.Kohyama, K.Kondo, M.Wakatani, K.Hanatani, T.Mizuuchi, Y.Katoh, Y.Nakamura, M.Ohnishi, A.Otsuki, H.Okada, K.Nagasaki, S.Besshou, M.Nakasuga, M.Yokoyama\* and K.Higahi**

\* National Institute for Fusion Science

Journal of Plasma and Fusion Research SERIES, Vol. 1, pp.168-171, 1998

Studies of the confinement optimization of heliotron such as Heliotron E have led to the concept of "helical-axis heliotron" which is characterized by reduced neoclassical transport and enhanced beta limit with small bootstrap current. Based on these novel theoretical results, the L=1 helical-axis heliotron experiment is being planned at the Institute of Advanced Energy, Kyoto University, with a goal of demonstrating the capability of this confinement line. The related physics and engineering design issues are discussed.

**116: Numerical analysis of small movable ICRF antenna loading resistance in Heliotron-E**

**H.Okada, T.Kotani, T.Mutoh\*, F.Sano, K.Kondo, M.Wakatani and T.Obiki**

**\* National Institute for Fusion Science**

Journal of Plasma and Fusion Research SERIES, Vol.1, pp.322-325, 1998

In order to study the dependence of the angle between the antenna RF current and the magnetic field line on the plasma loading resistance in Ion Cyclotron Range of Frequency(ICRF) heating, a small loop antenna was fabricated and introduced into Heliotron-E device. The loading resistance decreased gradually with the distance between the antenna and the plasma edge as expected. When the antenna was rotated, the loading resistance became very large value unexpectedly at the angle near 70 degrees between the antenna and the magnetic field. To understand the result, we developed the numerical code including the magnetic field direction in the model of the calculation. The angular dependence from the calculation has broader peak than that observed in the experiment.

**117: Integral Suppression of Pfirsch-Schluter Current in the Inward Shifted Stellarator Plasma in Heliotron E**

**S. Besshou, V.D. Pustovitov\*, N. Fujita, K. Kondo, T. Mizuuchi, K. Nagasaki, M. Nakasuga, T. Obiki, H.Okada, F. Sano, H. Zushi**

**\* Russian Research Centre, Kurchatov Institute**

Journal of Plasma and Fusion Research SERIES, Vol.1, pp.452-455, 1998

Observation of the complete suppression of integral effect of Pfirsch-Schlüter current in Heliotron E plasmas is reported. Poloidal magnetic field was measured to control the plasma boundary position. We found that pressure-induced plasma shift, an observable characteristic of Pfirsch-Schlüter current, depends strongly on the initial position of magnetic axis. When it was moved by the vertical field inside the torus, finite- $\beta$  shift became smaller. Complete suppression of finite- $\beta$  shift was achieved in a deeply inward shifted configuration: 7 cm from the standard position  $R_{axis} = 2.20$  m. Observed effect is explained by MHD equilibrium theory for planar circular axis stellarator plasma with a high magnetic field and deep inward shift.

**118: Studies of Magnetic Surface Control and Electron Orbit Loss in Heliotron DR**

Morimoto Shigeyuki\*,  
 K.Matsushita\*\*, S.Niwa\*, M.Nauki\*, T.Minamigaw, F.Yamashita\*, M.Masaki\* and  
 T.Obiki

\* Kanazawa Institute of Tecnology

\*\* National Institute for Fusion science

Journal of Plasma and Fusion Research SERIES, Vol.1, pp.195-198, 1998

Magnetic surface control by  $n/m = 1/1$  helical windings and electron orbit loss measurement by stellarator method have been carried out in Heliotron DR. Magnetic island of  $m = 1$  is effectively corrected by  $n/m = 1$  helical windings but  $m = 2$  like island structure is remained uncorrected. Electron confinement is observed to be deteriorated for high pitch angle Electrons at the outboard side of the torus and also improved by inward shift of the magnetic axis.

**119: Influence of Magnetic Configuration and Heating Methods on Distribution of Diverted Plasmas in Heliotron E**

T.Mizuuchi, V.V.Chechkin\*, V.S.Voitsenya\*, H.Zushi, K.Nagasaki, M.Nakasuga,  
 H.Okada, S.Besshou, A.Hayakawa, H.Funaba, T.Hamada, S.Masuzaki\*\*, K.Kondo,  
 F.Sano, O.Motojima\*\*, T.Obiki

\* Kharkov Institute of Physics and Technology

13th International Conference on Plasma Surface Interactions in Cntralled Fusion  
 Devices, San Diego, California, 18-22 may, 1998

A study on the distribution of the amount of diverted plasma along torus in Heliotron E was performed for NBI and ECH plasma under different experimental conditions. A Strong up-down asymmetry of the diverted plasma flux was observed contrary to what should be expected from the vacuum magnetic configuration. The degree of this asymmetry depends on the discharge conditions. This result indicates that the knowledge of only vacuum field traces in a divertor region is not enough to predict how much ratio of the total diverted plasma comes to a concerning divertor section in the heliotron/torsatron devices.

**120: Dependence of Plasma Profiles on ECH Power Absorption in Heliotron-E**

Kazunobu Nagasaki, T. Mizuuchi, S. Besshou, H. Funaba\*, K. Ida\*, K. Kondo, H.  
 Morioka, T. Obiki, H. Okada, F. Sano and H. Zushi

\* National Institute for Fusion Science

Jornal of the Physics of Japan, Vol.67, pp.1625-1635, 1998

Dependence of plasma profiles on the power absorption of electron cyclotron heating is experimentally studied in the Heliotron-E helical device. A focused Gaussian beam with controllable polarization makes it possible to change the power absorption. The electron density and temperature profiles are sensitive to the single pass absorption rate. The electron temperature profile is peaked and the density profile is hollow as the single pass absorption increases. The resonance position is also important for determining their profiles. The electron temperature profile is changed from a peaked one to a hollow one, depending on the resonance position. The non-diffusive outward flow, which is necessary to form a hollow temperature profile, is estimated by using a simple heat transport model.

**121: Effects of Magnetic Shear on Electron Cyclotron Resonance Heating in Heliotron/Torsatron Configurations**

**Kazunobu**

**Nagasaki, A.Ejiri\*, T.Mizuuchi, T.Obiki, H.Okada, F.Sano, H.Zushi, S.Besshou and K. Kondo**

**\* National Institute for Fusion Science**

Physics of Plasmas, Vol.6, pp.556-564, 1998

Effects of magnetic shear on electron cyclotron resonance heating (ECRH) are studied in heliotron/torsatron configurations. In such configurations, the poloidal magnetic field is comparable to the toroidal magnetic field, and varies spatially along the minor radius, making a strong magnetic shear. When high power millimeter waves are launched into a plasma, it is coupled to propagating modes at the plasma peripheral region. The existence of a transition layer between the core plasma region and the vacuum region, where the magnetic field direction is largely changed, requires accurate polarization control for good single pass absorption. The mode conversion between the propagation modes due to the magnetic shear also affects the launching conditions. The polarization control experiment by using second harmonic ECRH in Heliotron E [T.Obiki, Fusion Technol. 17, 101(1990)] are compared with the numerical calculation in which one dimensional second order coupled equations are solved. The polarization dependence experimentally measured is in good agreement with the numerical results including the magnetic shear terms.

**122: Oblique Launching Experiment for ECH and ECCD in Heliotron-E**

**Kazunobu Nagasaki, T.Mizuuchi, H.Okada, F.Sano, K.Kondo, S.Besshou, N.Hashimoto, Y.Manabe, N.Fukumoto\*, T.Obiki**

**\*Faculty of Electrical Engineering**

1998 ICPP & 25th EPS Conf. on Contr. Fusion and Plasma Physics, Praha, ECA  
Vol.22C, pp.1210-1213, 1998

The oblique launching experiment of high power millimeter waves in the toroidal direction were made to investigate the density limit and ECCD in the Heliotron E helical device. The ECH plasma is subject

to radiation collapse at high density, and the accessible density decreases with an increase of launching angle. The density limit may be determined by the wave refraction of the second harmonic X-mode. Another heating scenario such as second harmonic O-mode would be required to extend the accessible density regime at the oblique launching case. The EC driven current was measured at low density, and its dependence on toroidal launching angle and magnetic field strength was investigated. The experimental results showed that the current drive efficiency was rather lower than that of tokamaks, and its direction contradicted a simple linear theory.

### 123: Divertor Studies in Heliotron/torsatrons

V.Ye.Bykov\*, V.V.Chechkin\*, I.P.Fomin\*, L.I.Grigor'ea\*, A.V.Khodyachikh\*,  
N.I.Nazorov\*, R.O.Pavlichenko\*, V.G.Peletninskaya\*, V.V.Plyusnim\*,  
K.S.Rubtsov\*, V.A. Rudakov\*, A.I.Skibenko\*, M.S.Simirnova\*, E.L.Sorokovoj\*, V.S.  
Voitsenay\*, E.D.Volkov\*, T.Mizuuchi, K.Nagasaki, H.Okada, A.Hayakawa, H.Funaba,  
T.Hamada, F.Sano, T.Obiki, H.Zushi, M.Naksuga, S.Bessou, K.Kondo, S.Masuzaki\*\*,  
O.Motojima\*\*

\* Institute of Plasma Physics, National Science Center, "Kharkov Institute of Physics and Technology"

\*\* National Institute for Fusion Science

1998 ICPP & 25thEPS Conf. on Contr. Fusion and Plasma Physics, Praha, ECA  
Vol.22C, pp.464-467, 1998

1. Experimentally measured spatial distributions of diverted plasma flows can substantially differ in their magnitude and position from those, which are expected proceeding from the calculated distributions of the divertor field lines. In the  $l = 2$  Heliotron E device, under NBI and ECH conditions a strong up-down asymmetry of DFs is observed. At least two factors seem to be responsible for this asymmetry: (1) a distortion of the magnetic structure of the divertor layer due to inaccuracies in manufacturing and installation of the helical coils resulting in an additional stochastization of the field lines in the SOL (by analogy with a double-null divertor in a tokamak [5]); (2) a vertical asymmetry of the helical magnetic field ripple in the top and bottom parts of the torus [6,7] resulting in a spatial re-distribution of groups of locally trapped high energy ions and electrons drifting vertically in opposite directions. In the  $l = 3$  Uragan-3M device, to create and heat the plasma, RF fields are used generated by the antennae, which are crossed by the DFs. The proximity of the antenna to the probes and deposition of a fraction of RF power outside the OMS have a substantial effect on the measured DF distribution. 2. In both H-E and U-3M, the flow of diverted plasma increases with heating power irrespective of the kind of heating (NBI with different injection angles, fundamental and 2nd harmonic ECH, Alfvén heating). The rate of DF increase seems to depend on the power deposition profile. In whole, the DF increase with heating power can be considered as a manifestation of so-called power degradation of plasma confinement, the effect common for both tokamaks and stellarators [8]. 3. In the H-E device, intense charge particle flows (electric currents) arise parallel to the diverted field lines. These currents always have opposite directions in the top and bottom parts of the torus, thus evidencing the existence of a poloidal electric field in the SOL plasma. The magnitude of any non-ambipolar DF is a rising function of the total absorbed power and does not depend on the kind of heating and the toroidal position of the heating source in the first approximation. The above-mentioned vertical asymmetry of the helical magnetic field ripple resulting

in the vertical drift of the locally trapped electrons and ions in opposite directions might be a possible reason for the observed spatial distribution of the non-ambipolar DFs.

#### 124: Experiments on Li pellet injection into Heliotron E

V.Yu.Sergeev\*, K.V.Khlopenkov\*, B.V.Kuteev\*, S.Sudo\*\*, K.Kondo, H.Zushi, S.Besshou, F.Sano, H.Okada, T.Mizuuchi, K.Nagasaki, T.Obiki and Y.Kurimoto\*\*\*

\* State Technical Univ., Russia

\*\* National Institute for Fusion Science

\*\*\* Faculty of Engineering, Kyoto Univ.

Plasma Physics and Controlled Fusion, Vol.40, pp.1785-1801, 1998

Li pellets of large size were injected into electron cyclotron resonance (ECR) heated plasmas and neutral beam injection (NBI) heated plasmas of Heliotron E. The discharge behaviour, pellet ablation and wall conditioning were studied. The electron pressure is doubled after injection into the NBI plasma and remains unchanged in the case of ECR heating. This may be due to the energy exchange between the electrons and thermal ions with the fast ions from the neutral beam. The observed discrepancy between the experimental and modelled ablation rates may be caused by both the plasma cooling due to pellet ablation and the ablation stimulated by the fast ions in the NBI-heated regime and by the fast electrons in the ECR-heated regime. In preliminary experiments on wall conditioning by Li pellet injection, no improvement of plasma performance after Li pellet injection was observed in the divertor or limiter configuration, with the limiter radii  $r_L = 24 - 25$  cm.

#### 125: Complete integral suppression of Pfirsch-Schluter current in a Stellarator plasma in Heliotron E

S. Besshou, V.D. Pustovitov\*, N. Fujita, K. Kondo, T. Mizuuchi, K. Nagasaki, M.nakasuga, T.Obiki, H.Okada, F.Sano and H.Zushi

\* Russian Research Center "Kurchatov Institute"

Physics of Plasmas, Vol.5, pp.481-485, 1998

The poloidal magnetic field was measured to detect the plasma boundary position. It was found that the pressure-induced plasma shift, an observable characteristic of the Pfirsch-Schlüter current, depends strongly on the initial position of the magnetic axis. When the axis was moved by the vertical field inside the torus, the finite- $\beta$  became smaller. Complete suppression of the finite-deeply inward shifted configuration: 7 cm from the standard position  $R_{axis} = 2.20$ m. This effect is explained by magneto-hydrodynamic (MHD) equilibrium theory for stellarator toroidal plasma with a large magnetic hill and deep inward shift.

**126: The new helical plasma device at IAE, Kyoto University**

**F.Sano, T.Obiki, N.Inoue, A.Kohyama, K.Yoshikawa, K.Kondo, M.Wakatani, K.Hanatani, T.Mizuuchi, Y.Katoh, Y.Nakamura, M.Ohnishi, A.Otsuki, H.Okada, K.Nagasaki, S.Besshou, M.Nakasuga, M.Yokoyama\* and K.Higashi**

**\*(National Institute for Fusion Science)**

J.Plasma Fusion Res. SERIES, Vol.1, pp.168-171, 1998

Studies of the confinement optimization of heliotron such as Heliotron E have led to the concept of "helical-axis heliotron" which is characterized by reduced neoclassical transport and enhanced beta limit with small bootstrap current. Based on these novel theoretical results, the L=1 helical-axis heliotron experiment is being planned at the Institute of Advanced Energy, Kyoto University, with a goal of demonstrating the capability of this confinement line. The related physics and engineering design issues are discussed.

**127: Heliotron J experimental program**

ヘリカル軸ヘリオトロン装置 (ヘリオトロン J) 実験計画

**F.Sano, T.Obiki, K.Hanatani, T.Mizuuchi, H.Okada, K.Nagasaki, K.Kondo, M.Wakatani, Y.Nakamura, M.Nakasuga, S.Besshou and M.Yokoyama\***

**\*(National Institute for Fusion Science)**

プラズマ・核融合学会誌、Vol.75、pp.222-229、1999

Heliotron J is an L=1 helical-axis heliotron being constructed at Kyoto University, and the first experimental test of the "helical-axis heliotron" line. The design feature of Heliotron J is, as compared with that of Heliotron E, the reduced neoclassical transport and enhanced beta limit with small bootstrap current, which carries the potential for developing the currentless "quasi-isodynamic" configuration in a helical-axis heliotron. To refine its design principle, Heliotron J is planned to offer a high experimental flexibility by using (i) the auxiliary poloidal and toroidal coils to control the bumpiness and the magnetic well and (ii) the existing heating systems such as ECH, NBI and ICRF. The first plasma will be produced in FY1999. (in Japanese)

**128: Stellarator transport simulation using  $\delta f$  Monte Carlo algorithms**

**K.Hanatani**

J.Plasma Fusion Res. SERIES, Vol.1, pp.472-475, 1998

Several versions of Monte Carlo codes based on  $\delta f$  methods are under development for studying transport in nonaxisymmetric toroidal plasmas. This paper reports initial progress of the development. The  $\delta f$  simulations of neoclassical diffusion and bootstrap current in a stellarator are presented together with the results of benchmark using a tokamak geometry. Comparisons with conventional Monte Carlo methods are also made.

**129: Numerical analysis of small movable ICRF antenna loading resistance in Heliotron-E**

**H.OKada, T.Kotani, T.Mutoh\*, F.Sano, K.Kondo, M.Wakatani and T.Obiki**  
**\*(National Institute for Fusion Science)**

J.Plasma Fusion Res. SERIES, Vol.1, pp.322-325, 1998

In order to study the dependence of the angle between the antenna RF current and the magnetic field line on the plasma loading resistance in Ion Cyclotron Range of Frequency(ICRF) heating, a small loop antenna was fabricated and introduced into Heliotron-E device. The loading resistance decreased gradually with the distance between the antenna and the plasma edge as expected. When the antenna was rotated, the loading resistance became very large value unexpectedly at the angle near 70 degrees between the antenna and the magnetic field. To understand the result, we developed the numerical code including the magnetic field direction in the model of the calculation. The angular dependence from the calculation has broader peak than that observed in the experiment.

**130: Experiments on Li pellet injection into Heliotron E**

**V.Yu.Sergeev\*, K.V.Khlopenkov\*, B.V.Kuteev\*, S.Sudo\*\*, K.Kondo, H.Zushi, S.Besshou, F.Sano, H.Okada, T.Mizuuchi, K.Nagasaki, T.Obiki and Y.Kurimoto\*\*\***  
**\*(State Technical Univ., Russia)**  
**\*\* (National Institute for Fusion Science)**  
**\*\*\* (Faculty of Engineering, Kyoto Univ.)**

Plasma Phys. Control. Fusion, Vol.40, pp.1785-1801, 1998

Li pellets of large size were injected into electron cyclotron resonance (ECR) heated plasmas and neutral beam injection (NBI) heated plasmas of Heliotron E. The discharge behaviour, pellet ablation and wall conditioning were studied. The electron pressure is doubled after injection into the NBI plasma and remains unchanged in the case of ECR heating. This may be due to the energy exchange between the electrons and thermal ions with the fast ions from the neutral beam. The observed discrepancy between the experimental and modelled ablation rates may be caused by both the plasma cooling due to pellet ablation and the ablation stimulated by the fast ions in the NBI-heated regime and by the fast electrons in the ECR-heated regime. In preliminary experiments on wall conditioning by Li pellet injection, no improvement of plasma performance after Li pellet injection was observed in the divertor or

limiter configuration, with the limiter radii  $r_L = 24 - 25$  cm.

**131: Metal deposition into a porous silicon layer by immersion plating: Influence of halogen ions**

**Takashi Tsuboi, Tetsuo Sakka, Yukio H. Ogata**

Journal of Applied Physics, Vol. 83, pp. 4501-4506, 1998.

Metal deposition into a porous silicon (PS) layer by immersion plating has been studied. Ag and Cu were found to deposit on PS, while Ni was found not to deposit. The dependence of the amount of Cu deposition on  $\text{Cu}^{2+}$  concentration, halogen ion concentration, and immersion time was investigated using chelatometric titration. Copper deposition from halide solutions exhibited an unusual behavior; the amount increased with increasing concentration, then decreased, and no copper deposited at high concentration. This is because adsorption of chloride and bromide ions inhibits the copper deposition process. We have also discussed the metal deposition mechanism on the basis of x-ray diffraction, Fourier transform infrared spectroscopy, and x-ray photoelectron spectroscopy measurements. They revealed that metal deposition occurred simultaneously with the oxidation of silicon to  $\text{SiO}_2$ . Copper crystals with 30-80 nm in diameter deposited on the oxidized PS surface rather than on the unoxidized PS surface.

**132: \* Dopant and fluence effects on the ablation of silicon surfaces under pulsed  $\text{CO}_2$  laser irradiation**

**Tetsuo Sakka, Kokichi Hotta, Satoshi Akiba, Akira Kuroyanagi, Yukio H. Ogata, Mahito Mabuchi\***

**\*(Niihama National College of Technology)**

Applied Surface Science, Vol. 127-129, pp. 71-75, 1998.

Effects of impurity doping and laser-pulse fluence on the laser ablation of silicon wafers are studied by using a TEA  $\text{CO}_2$  laser. Silicon ions with charge from 1 to 4 au were observed in the ablation species. The average ion charge increased with dopant concentration and the laser fluence. The velocity of the ions depends on the fluence and slightly on the dopant concentration. The electric current flowing from a target into the ground level was also measured and showed dopant and fluence effects. The correlation among these experiments is examined and the ablation mechanism is discussed.

**133: \* Characteristics of the species ablated from silicon surface by pulsed CO<sub>2</sub> laser irradiation**

**Tetsuo Sakka, Kokichi Hotta, Akira Kuroyanagi, Satoshi Akiba, Mahito Mabuchi,\*  
Yukio H. Ogata**

**\*(Niihama National college of Technology)**

Japanese Journal of Applied Physics, Vol. 37, pp. 2666-2669, 1998.

Laser ablation of silicon surfaces with various dopant concentrations is studied by the irradiation of TEA CO<sub>2</sub> laser. Silicon ions with the charge from 1 to 4 au were observed in the emitted species. The fraction of multiple charged ions increased with increasing dopant concentration. The kinetic energy of Si ions determined by time-of-flight measurement extended up to ca. 300 eV, and was almost independent of the dopant concentration. The results seem to be explained by a positive charging of the irradiated spot during the laser irradiation.

**134: Magnetic shielding tensor calculations of cluster models and comparison with nuclear magnetic resonance spectra of porous silicon**

**Takashi Tsuboi, Tetsuo Sakka, Yukio H. Ogata**

Proceeding of the Special Symposium on Advanced Materials, pp. 203-206, Nagoya,  
May 12-15, 1998.

Magnetic shielding tensor of cluster models were estimated using *ab initio* molecular orbital calculations to investigate the <sup>29</sup>Si nuclear magnetic resonance (NMR) spectra of porous silicon (PS). We calculated three cluster models: SiH, SiH<sub>2</sub>, and (SiH)<sub>2</sub> dimer configurations. The isotropic shielding of SiH was larger than that of SiH<sub>2</sub>. In addition, (SiH)<sub>2</sub> dimer had almost the same isotropic shielding as SiH<sub>2</sub>. On the other hand, the anisotropy of (SiH)<sub>2</sub> dimer was much larger than those of the others. Comparison with the NMR spectra of PS resulted in the assignments that signals at -85 and -94 ppm from tetramethylsilane are due to SiH<sub>2</sub> and SiH, respectively. Annealing PS did not change the peak position of NMR spectra, but the chemical shift anisotropy increased with annealing time. These behaviors can be explained in terms of the calculated isotropic shielding and anisotropy. The annealing desorbs hydrogen from SiH<sub>2</sub> species in PS surface and a part of SiH<sub>2</sub> species produces (SiH)<sub>2</sub> dimer structure during the annealing.

**135: Diffusivity and Solubility of Hydrogen in Ti-Al Alloys**

Shizuo Naito, Masahiro Yamamoto, Minoru Doi,\* Masao Kimura,\*\* Yukio H. Ogata  
\*(Nagoya Institute of Technology)  
\*\*(Nippon Steel Co.)

Proceeding of the Special Symposium on Advanced Materials, pp. 408-412, Nagoya,  
May 12-15, 1998.

Diffusion coefficients,  $D$  for H in Ti,  $\text{Ti}_{88}\text{Al}_{12}$  and  $\text{Ti}_3\text{Al}$  have been measured in the temperature range 873-1298 K. It has been found that the activation energy for diffusion in  $\text{Ti}_3\text{Al}$  (0.84 eV) is nearly twice those in Ti (0.45 eV) and Al (0.42 eV), and in  $\text{Ti}_{88}\text{Al}_{12}$  (0.57 eV) it is closer to that in Ti than in  $\text{Ti}_3\text{Al}$ . The relatively large activation energy for  $\text{Ti}_3\text{Al}$  is explained by the presence of ordered Al atoms in  $\text{Ti}_3\text{Al}$ . The  $D$  of  $\text{Ti}_{88}\text{Al}_{12}$  is modeled, assuming distributions of prefactor and activation energy of  $D$  resulting from the disordered Al atoms. Solubility has been studied by measuring pressure-composition isotherms of the Ti- and  $\text{Ti}_{94}\text{Al}_6$ -H systems in the temperature range 673-973 K. The plateaux of the isotherms, which correspond to the  $\alpha + \beta$ -phase region, have been found to slope upward in the  $\text{Ti}_{94}\text{Al}_6$ -H system. The observed sloping plateaux are shown to be explicable by a Gaussian distribution of energies of H atoms in the metals.

**136: \* Changes in the environment of hydrogen in porous silicon with thermal annealing**

Yukio H. Ogata, Fumio Kato, Takashi Tsuboi, Tetsuo Sakka

Journal of the Electrochemical Society, Vol. 145, pp. 2439-2444, 1998.

Changes in hydrogen environments in porous silicon prepared from a p-type silicon wafer with thermal annealing were studied to make an exact assignment of the infrared absorption spectrum and to clarify the fine structures of hydrogen in porous silicon. Annealing makes it possible to desorb the  $\text{SiH}_3$  and  $\text{SiH}_2$  states from porous silicon. The results, with the help of the vibrational analysis by molecular orbital calculations, revealed the following. First, an absorption band at  $2100\text{ cm}^{-1}$  is composed of seven fine structures and their assignment is clarified. Second, the wagging mode of  $\text{SiH}_2$  contributes an absorption band at  $667\text{ cm}^{-1}$ , and finally it is confirmed that the strongest absorption band at  $626\text{ cm}^{-1}$  belongs to the bending vibration of SiH. Further, oxidation behavior under wet environments of porous silicon in which hydrogen is partially desorbed is compared with that without the desorption. Acceleration of the oxidation is explained in terms of strained Si-Si bonding.

**137: \* Absorption of pulsed CO<sub>2</sub> laser in silicon and resulting laser ablation and surface damage formation**

**Tetsuo Sakka, Satoshi Akiba, Akira Kuroyanagi, Kokichi Hotta, Yukio H. Ogata, Mahito Mabuchi\***

**\*(Niihama National College of Technology)**

Plasmas and Ions, Vol. 1, pp. 23-28, 1998.

Fluence dependence of the absorption of TEA CO<sub>2</sub> laser in silicon wafers with various dopant concentration is studied. The transmittance decreases with increasing fluence, and the effect of the dopant concentration was small. The time profile of the pulse intensity after transmitting through a sample showed a narrowing of the width. The results suggest a build-up of some photo-induced absorbance in the middle of a pulse, leading to the absorption of the later part of the pulse, and also suggest that this effect is not sensitive to the ground state absorbance of the silicon samples.

**138: \* Structural study of porous silicon and its oxidized states by solid-state high-resolution <sup>29</sup>Si NMR spectroscopy**

**Takashi Tsuboi, Tetsuo Sakka, Yukio H. Ogata**

Physical Review B, Vol. 58, pp. 13863-13869, 1998.

<sup>29</sup>Si nuclear magnetic resonance (NMR) spectra were measured to characterize porous silicon (PS) structures. <sup>29</sup>Si nuclei close to surface were selectively detected both in cross-polarization (CP) and non-CP spectra. The spectra were different from those for amorphous silicon and amorphous hydrogenated silicon. Therefore PS is different from amorphous materials in the structural character. The resonant peaks were, however, much broader than the peaks observed for crystalline silicon. There exists distribution of bonding conformation in PS layer. Origin of the linewidth in the NMR spectra has been discussed. The contribution of each broadening mechanism to the width has been estimated theoretically and experimentally. The <sup>29</sup>Si NMR spectra for oxidized PS species have been assigned as follows: -50 ppm due to O<sub>2</sub>SiH<sub>2</sub>, -85 ppm due to O<sub>3</sub>SiH, -111 ppm due to SiO<sub>2</sub>, and -101 ppm due to Si(OH)<sub>x</sub> or <sup>29</sup>Si located between O<sub>y</sub>SiH<sub>x</sub> and SiO<sub>2</sub>. The signals of SiH<sub>x</sub> species have been assignable to -85 and -94 ppm; however further study should be done for the detailed assignment.

**139: \* Structure of as-prepared and annealed porous silicon surface studied by nuclear magnetic resonance spectroscopy****Takashi Tsuboi, Tetsuo Sakka, Yukio H. Ogata**

Journal of the Electrochemical Society, Vol. 146, pp. 372-375, 1999.

Structures of as-prepared and annealed porous silicon samples have been characterized by  $^{29}\text{Si}$  nuclear magnetic resonance (NMR) spectroscopy. Magnetic shielding tensors have also been calculated using *ab initio* molecular orbital calculations to help the characterization. After the annealing at  $300^\circ\text{C}$  for 4 hours, the NMR peak position shifted slightly and the chemical shift anisotropy increased. Hydrogen desorption during the annealing gives  $(\text{SiH})_2$  dimer structure from  $\text{SiH}_2$  configuration. The assignments of NMR signals are as follows:  $-94\text{ ppm}$  due to  $\text{SiH}$ ,  $-85\text{ ppm}$  due to  $\text{SiH}_2$ , and about  $-85\text{ ppm}$  due to  $(\text{SiH})_2$ . The  $(\text{SiH})_2$  dimer has large chemical shift anisotropy and small magnetic shielding, which are caused by the strained conformation of the dimer.

**140: \* Chemical etching of porous silicon in diluted hydrofluoric acid****Takashi Tsuboi, Tetsuo Sakka, Yukio H. Ogata**

Solid State Communications, Vol. 109, pp. 195-199, 1999.

Chemical etching of *n*-type porous silicon in diluted hydrofluoric acid has been studied by Fourier transform infrared spectroscopy. A new peak was observed at  $616\text{ cm}^{-1}$  after the etching, which is assigned to Si-H bending of  $\text{H-Si}[\text{SiH}(\text{Si})_2]_2[\text{Si}(\text{Si})_3]$  configuration. The absorption at  $627\text{ cm}^{-1}$ , due to Si-H bending of  $\text{H-Si}[\text{Si}(\text{Si})_3]_3$  structure, was narrowed by the etching. The etching produces  $\{011\}$  microfacets, which are absent in as-prepared porous silicon. These features can be interpreted in terms of the dissolution chemistry and the pore morphology of *n*-type porous silicon.

**141: Long-Range Attractive Interaction between Macroparticles in a Binary Fluid Mixture****Masahiro Kinoshita**

Molecular Physics, Vol.84, No.3, pp.485-494, 1998

In a previous paper we analyzed the interaction between macroparticles immersed in a binary fluid mixture using the reference hypernetted-chain theory. The bulk mixture separates into two immiscible

phases in a certain composition regime, but the thermodynamic state considered was far from the spinodal line and the mixture was stable as a single phase. The singular behavior of the reduced density profiles of mixture components near the macroparticle surface and the potential of mean force between macroparticles, which was revealed in the previous paper, have been examined further. It has been found that the thickness of the surface-induced layer and the range of macroparticle interactions suddenly grow to a submacroscopic scale which is far longer than molecular dimensions (but not infinitely long) near the singular point. The macroparticle interactions always become strongly attractive. This is a transition phenomenon and can be interpreted as "partial wetting" of one of the components accompanied by "partial drying" of the other. It has been pointed out that trace amounts of impurity can affect the macroparticle interactions to a drastic extent. For instance, presence of trace amounts of small, nonpolar solutes in water can cause aggregation of large, hydrophobic molecules or particles.

#### 142: Calculation of Solvation Free Energy Using RISM Theory for Peptide in Salt Solution

Masahiro Kinoshita, Yuko Okamoto\*, and Fumio Hirata\* \*(Institute for Molecular Science)

Journal of Computational Chemistry, Vol.19, No.15, pp.1724-1735, 1998

We have developed a robust, highly efficient algorithm for solving the full reference interaction site model (RISM) equations for salt solutions near a solute molecule with many atomic sites. It is obtained as an extension of our previously reported algorithm for pure water near the solute molecule. The algorithm is a judicious hybrid of the Newton-Raphson and Picard methods. The most striking advantage is that the Jacobian matrix is just part of the input data and need not be recalculated at all. To illustrate the algorithm, we have solved the full RISM equations for a dipeptide (NH<sub>2</sub>-CHCH<sub>3</sub>-CONH-CHCH<sub>3</sub>-COOH) in a 1M-NaCl solution. The extended simple point charge (SPC/E) model is employed for water molecules. Two different conformations of the dipeptide are considered. It is assumed for each conformation that the dipeptide is present either as an unionized form or as a zwitterion. The structure of the salt solution near the dipeptide and salt effects on the solvation free energy have also been discussed.

#### 143: Singular Behavior of the RISM Theory Observed for Peptide in Salt Solution

Masahiro Kinoshita, Yuko Okamoto\*, and Fumio Hirata\* \*(Institute for Molecular Science)

Chemical Physics Letters, Vol.297, No.5,6, pp.433-438, 1998

We examine the reference interaction site model theory applied to a peptide-salt solution system, with the assumption that a zwitterionic dipeptide (Ala-Ala) is present in NaCl solution at the infinite-dilution limit. For some sets of the potential parameters for the peptide-salt solution, the theory exhibits singular

behavior: as the salt concentration decreases, the ionic concentration around the peptide increases and the theory eventually loses its solution. The singularity is interpreted as the wetting of ions accompanied by the drying of water molecules. A trend of aggregation of peptide molecules is also found. For other sets of the potential parameters, however, no such singularity occurs. The qualitative aspects of the conclusions are thus very sensitive to the potential parameters employed.

**144: \* Interaction between Macroparticles in a Binary Fluid Mixture: Anomalous Effects Due to the Bulk Composition**

**Masahiro Kinoshita**

Molecular Physics, Vol.96, No.1, pp.71-80, 1999

The interaction between macroparticles in a binary fluid mixture has been analyzed using the reference hypernetted-chain (RHNC) theory. The mixture is composed of particles interacting through attractive potential (component 1) and hard spheres (component 2). Particles of different components interact through hard-sphere potential. Significantly high affinity is considered between the macroparticle surface and component 1. Two cases have been studied: case 1 where the bulk mixture unavoidably separates into two immiscible phases in the regime  $x_{1P} < x_1 < x_{1Q}$  ( $x_1$  is the mole fraction of component 1, and  $x_{1P}$  and  $x_{1Q}$  denote values at the spinodal points); and case 2 where the bulk mixture is miscible in the entire composition range. As  $x_1$  increases from  $x_1 = 0$  or  $x_1$  decreases from  $x_1 = 1$  in case 1, the macroparticle interaction always shifts to the more attractive side. As  $x_1 \rightarrow x_{1R;1-0}$  or  $x_1 \rightarrow x_{1S;1+0}$  ( $x_{1R;1}$  and  $x_{1S;1}$  are threshold values;  $x_{1R;1} < x_{1P}$  and  $x_{1S;1} > x_{1Q}$ ) the range of the interaction exhibits sudden growth to a scale that is far longer than molecular dimensions, and the interaction becomes strongly attractive. This behavior is ascribed to the surface-induced phase transition, "partial wetting" of one of the components accompanied by "partial drying" of the other. Even in case 2, similar behavior has been observed as  $x_1 \rightarrow x_{1R;2-0}$  or  $x_1 \rightarrow x_{1S;2+0}$  ( $x_{1R;2}$  and  $x_{1S;2}$  are threshold values). In the regime  $x_{1R;2} < x_1 < x_{1S;2}$  the RHNC theory possesses no solutions. The interaction between UNLIKE macroparticles, whose surfaces have high affinity only with component 1 and only with component 2, respectively, has also been analyzed. While the interaction between LIKE macroparticles is strongly attractive except at very small separations, the interaction between unlike macroparticles is st

**145: Analysis on Conformational Stability of C-Peptide of Ribonuclease A in Water Using the Reference Interaction Site Model Theory and Monte Carlo Simulated Annealing**

**Masahiro Kinoshita, Yuko Okamoto\*, and Fumio Hirata\* \*(Institute for Molecular Science)**

The Journal of Chemical Physics, Vol.110, No.8, pp.4090-4100, 1999

Solvation structure and conformational stability of the C-peptide fragment of ribonuclease A in pure water, have been analyzed using the full reference interaction site model (RISM) theory. The charged groups in the side chains of Lys-1+, Glu-2-, Lys-7+, Arg-10+, and His-12+ (in particular, the four like-charged groups) play substa

**146: First-Principles Calculations of Light Elements/Metal Surface and Liquid/Metal Interface Systems**

**Masahiro Yamamoto, Shizuo Naito, and Masahiro Kinoshita**

Proceedings of the Special Symposium on Advanced Materials, Nagoya Garden Palace, Nagoya, Japan, May 12-15, 1998, pp.373-376

Atomistic structure and behavior of the transition metal surface and the noble metal/liquid interface have been studied theoretically. We have investigated the hydrogen, carbon, nitrogen, and oxygen adsorption [1X1 structure] on Zr(0001) surface using the first-principles pseudopotential calculation with the mixed-basis method. The favorable adsorption sites are the octahedral sites below the surface except the hydrogen adsorption. The structure and workfunctions calculated for the surface are in good agreement with experimental results. The physical origin of the underlayer adsorption is discussed. For the liquid/metal interface we have used the combination of the first-principles calculation of Pt(111) surface and a statistical-mechanical model of liquid water. The self-consistent solution of the electrostatic field of the interface gives a good description of the density profile and orientational ordering of dipole moments for the water side.

**147: \* Solvation Structure of Solutes in Supercritical Fluids Analyzed by the HNC Theory**

**Masahiro Kinoshita and Ken Kuwamoto**

Proceedings of the Sixth Workshop on Separation Phenomena in Liquids and Gases, Nagoya Congress Center, Nagoya, Japan, October 18-21, 1998, pp.371-379

The solvation structure of a solute in a supercritical solvent (in medium- and high-density regions near the critical temperature) has been analyzed using an integral equation theory. The solvent and solute molecules are Lennard-Jones particles. The solvation free energy is discussed by dividing it into two terms: the work required for creating a cavity large enough to accommodate a solute molecule (term 1); and the energy of interaction between the solute molecule and the surrounding solvent (term 2). In the high-density region, term 1 dominates and the solvation free energy is usually higher for a larger solute. The solvent structure around a solute molecule is rigid and not significantly influenced by the solute-solvent interaction. In the medium-density region, term 2 dominates and the solvation free energy becomes lower as the solute size increases. The solvent structure around a solute molecule is greatly dependent on the solute-solvent interaction. When the solute-solvent attractive interaction is sufficiently strong in the

medium-density region, the solvation structure exhibits unique characteristics. For example, the solvent confined between a pair of solute molecules becomes denser and more stabilized as the distance between the solute molecules decreases, and an attractive interaction is induced between the solute molecules.

**148: \* Selective Separation of Trypsin from Pancreatin Using Bioaffinity in Reverse Micellar System Composed of a Nonionic Surfactant**

**Motonari Adachi\*, Kengo Shibata, Akihisa Shioi, Makoto Harada**

Biotechnology and Bioengineering, vol. 58, pp.649-653, 1998

Selective separation of trypsin from a mixture involving many kinds of contaminating proteins, i.e., pancreatin, was achieved using trypsin inhibitor immobilized in reverse micelles, which were composed of a nonionic surfactant, tetra-oxyethylene monodecylether. To determine the efficient operations throughout the whole separation processes we examined the operating conditions, which affect the immobilization efficiency of trypsin inhibitor and also forward and backward extractions of trypsin. Fifty percent of the recovery of trypsin from pancreatin was realized with no loss of activity of the recovered trypsin.

**149: \* Structure and Properties of Fluids Composed of Polyelectrolyte and Ionic Surfactant in Organic Phase: Poly(acrylic acid) and Didodecyldimethyl Ammonium Bromide**

**Akihisa Shioi, Makoto Harada, Motoharu Obika and Motonari Adachi**

Langmuir, vol. 14, pp. 4737-4743, 1998

The structure and properties of the oil-rich microemulsion (L2 phase) containing anionic polyelectrolyte, poly(acrylic acid) (PAA-H,  $M_w=450\ 000$ ) and its sodium salt PAA-Na ( $M_w=30\ 000$ ), were investigated. The cationic surfactant, didodecyldimethyl ammonium bromide (DDAB), which generates the rodlike aggregates in cyclohexane, was selected. Small-angle X-ray scattering, dynamic light scattering, electric conductivity, and viscosity measurements were performed. The rodlike structure was unchanged upon dissolving the polymers. PAA-Na is a strong polyelectrolyte, which takes a rather extended conformation in the bulk aqueous solution. However, PAA-Na adsorbed DDAB molecules by electrostatic interaction in the microemulsions. Then, the extended conformation was loosened in the microemulsion and was dissolved within the water pool of the DDAB aggregates. The characteristic size of the PAA-Na dissolved within the water pool of the DDAB aggregates was similar to that of the original DDAB aggregates. High-molecular weight polymer PAA-H was also dissolved within the water pool, and the polymer chain connected the rodlike aggregates. However, the diameter of the rodlike constituent for the connected structure is almost the same as that of the original DDAB aggregates.

**150: \* Structure and Properties of Fluids Composed of Polyelectrolyte and Ionic Surfactant in Organic Phase: Poly(allylamine) and Sodium Bis(2-ethylhexyl) Sulfosuccinate**

**Akihisa Shioi, Makoto Harada, Motoharu Obika and Motonari Adachi**

Langmuir, vol. 14, pp. 5790-5794, 1998

The structure and properties of an oil-rich microemulsion containing the cationic polyelectrolyte poly(allylamine) hydrochloride, PAAN, were investigated. An anionic surfactant, sodium bis(2-ethylhexyl) sulfosuccinate AOT, was selected. The patterns of the small-angle X-ray scattering SAXS were drastically changed from those of the polymer-free AOT microemulsions. Electric conductivity and the SAXS patterns indicated the formation of the pearl-necklace structure in the polymer-containing microemulsion. Two kinds of the characteristic size, R1 and R2, were evaluated from the SAXS patterns. R1 was the droplets (pearl) size that was essentially controlled by water-to-surfactant mole ratio W0. R2 was the size of the polymer chain connecting the droplets. R2 of the salt-free system was near the end-to-end distance of an uncharged polymer chain whose degree of polymerization was the same as that of used PAAN. PAAN behaved like an uncharged polymer due to strong electrostatic interaction with AOT. This was supported by the dynamic light scattering experiment. R2 was affected by the salt concentration in the aqueous solution, which was attributed to the change in the strength of the electrostatic interaction between AOT and PAAN. The AOT aggregates retained the original form even in the presence of the polymer strongly interacting with AOT.

**151: \* Formation Processes of Silica-Microstructures in Micellar and Reverse-Micellar Solutions**

**M. Harada, M. Adachi, A. Shioi, S. Itakura and T. Harada**

The Third International Conference on Materials Engineering for

Surfactant-directed structure formation is important for preparing nano-meso materials such as porous materials. The understanding of microstructure formation is necessary for rational design of the materials. In this work, we elucidated the formation processes of silica microstructures in two surfactant systems, laurylamine hydrochloric acid(LAH) and didodecylmethylammonium bromide(DDAB). The silica source was tetraethoxysilane(TEOS). In LAH-aqueous solution system, the amphiphilic molecules composed of LAH and partially hydrolyzed TEOS self-assemble into rod-like micelles, which are elongated with the proceeding of the silanol-condensation. Finally, the elongated rods are entangled with each other to yield gel. A simple model of hydrocarbon-chain packing in the inner parts of the micelles can explain well the changes in the microstructure. We succeeded in the preparation of long tubules with nano-scale diameter by combining the silanol groups on the microstructure with trimethylchlorosilane. In DDAB/cyclohexane

system, the generated reverse-micelles directed the rod-like microstructure of silica. The reverse micelles functioned as the template for fiber-silica with nanometer diameter.

**152: \* Preparation of Cadmium Sulfide Ultrafine Particles with Sharp Size-Distribution Using Cadmium Diolelyphosphate Microemulsion**

**Kiyoshi Suzuki, Noriaki Mizutani and Makoto Harada**

Journal of Chemical Engineering of Japan, vol. 32, pp.31-39, 1999

Cadmium Diolelyphosphate (CDOLP) and sodium diolelyphosphate (SDOLP) are expected to form rigid microemulsion droplets. They were used as surfactants in place of sodium bis(2-ethylhexyl) sulfosuccinate (AOT), which has been often used for the preparation of cadmium sulfide (CdS) ultrafine particles in microemulsion (ME). CdS ultrafine particles were prepared by mixing hydrogen sulfide solution with the ME composed of CDOLP and SDOLP. The growth process of the particles through their coagulation is restricted more strongly, and the size distribution of the obtained particles was sharper than those in AOT-ME. Furthermore, in CDOLP/SDOLP-ME, the average number of cadmium ions per microemulsion droplet is larger and the number of contaminating "empty" ME droplets which contain no particle is much smaller than in AOT-ME system. Diolelyphosphates are proper surfactants for the preparation of ultrafine particles with sharp size distribution, because particle coagulation is restricted in the system. The restriction of the coaguration between larger particles is attributed to two mechanisms: 1) It is hard for larger particles to be exchanged between two fusing ME droplets through the "open channel" between them. 2) The ME droplets with the larger particles can hardly coalesce with the other ME droplets.

**153: \* A Molecular Dynamics Study of the Stereoselective Interaction between an Enantiomeric Amino Acid Ester and an L-Histidine-containing Catalyst in the Bilayer Membrane**

**Koji Maekawa, Shigeru Ishikawa\*, Hitoshi Ishida\*\*, Setsuko Nakagawa\*\*\*, Katsutoshi Ohkubo, Tokio Yamabe\*\*\*\***

**\* Tokai University, \*\* Kumamoto University, \*\*\* Institute for Fundamental Chemistry, \*\*\*\* Graduate School of Engineering, Kyoto University**

Molecular Engineering 8, pp.9-24, 1998

Molecular dynamics simulations were performed to investigate the stereoselective interaction between an enantiomeric amino acid substrate (*N*-acylated-L-phenylalanine-*p*-nitrophenyl ester) and an L-histidine-containing dipeptide catalyst (*N*<sup>α</sup>-(*N*-benzyloxycarbonyl-L-leucyl)-L-histidine) in the bilayer of cationic surfactants (*N,N*-bis(dodecyl)-*N,N*-dimethylammonium chloride). We found that a catalyst-substrate

complex, which had an interamide hydrogen bond, was formed spontaneously in vacuum at 500 K. This complex was found to be stable both in vacuum and in the bilayer membrane for 100 ps at 300 K. The distances between the hydrophobic side chains in the complex were consistent with experimental results. The interamide hydrogen bond was retained in the hydrophobic core of the membrane. These results suggest that the catalyst-substrate complex found in this work is relevant to the stereoselective hydrolysis of the L-enantiomer of the substrate.

**154: \* Identification of Lipid Inhibitor of Mammalian Phospholipase D**

**Koichi Kawabe\***, **Tsutomu Kodaki**, **Kazuhisa Katayama\***, **Shin-ichi Okamura\***,  
**Masatomo Mori\***, **Satoshi Yamashita\***

**\* Gunma University**

Journal of Biochemistry 123, pp.870-875, 1998

Phospholipase D (PLD) is implicated in important cellular processes, such as hormone action, inflammation, secretion, mitogenesis, and neural activity. Recent studies using cell-free systems have shown that the enzyme activity is modulated by both positive and negative regulators. During an attempt to purify PLD from pig colon mucosa, we noted the presence of a PLD inhibitor in the tissue extract. The inhibitor was purified and identified as comprising lysophosphatidylserine, phosphatidylinositol, and lysophosphatidylinositol, of which lysophosphatidylserine was the most potent. These lipids affected all of the PLD isoforms examined, oleate-dependent PLD, ARF-dependent PLD (PLD1a, PLD1b), and phosphatidylinositol 4,5-bisphosphate-dependent PLD (PLD2), in the concentration range of the 1 or 10  $\mu$ M order. In contrast to lysophosphatidylserine, the diacyl counterpart phosphatidylserine was without effect in the same concentration range. PLD inhibition by lysophosphatidylserine could not be reversed by an increase in the concentration of the substrate phosphatidylcholine or activator phosphatidylinositol 4,5-bisphosphate.

**155: \* Enhanced Levels of Oleate-dependent and Arf-dependent Phospholipase D Isoforms in Experimental Colon Cancer**

**Makoto Yoshida\***, **Shin-ichi Okamura\***, **Tsutomu Kodaki**, **Masato Mori\***, **Satoshi Yamashita\***

**\* Gunma University**

Oncology Research 10, pp.399-406, 1998

Phospholipase D (PLD) (EC 3.1.4.4) is one of the intracellular signal transduction enzymes and plays an important role in a variety of cellular functions. In order to clarify the role of PLD in proliferation and tumorigenesis of colon cancer, we investigated the activities of oleate-dependent and ADP-ribosylation factor (Arf)-dependent types of PLD in experimental colon cancer of the rat. We produced colon cancer in

Wistar rats by injecting the carcinogen, dimethylhydrazine dihydrochloride (DMH). The control rats were injected with physiological saline. Mucosal scrapings from the colon were homogenized and centrifuged to obtain the microsomal or membrane fraction. We measured the two types of PLD activities in these fractions using the transphosphatidylolation reaction. Both oleate-dependent and Arf-dependent PLD activities were significantly higher in the colon cancer tissue than normal colonic mucosa. The mean specific activity of oleate-dependent PLD in colon cancers was  $1.66 \pm 0.75$  (SD) nmol/min/mg whereas the value for normal colonic mucosa was  $0.18 \pm 0.09$  nmol/min/mg ( $P < 0.01$ ; Mann-Whitney U-test). On the other hand, the mean specific activity of Arf-dependent PLD in colon cancers was  $76.36 \pm 29.37$  pmol/min/mg whereas the value for normal colonic mucosa was  $19.90 \pm 11.97$  pmol/min/mg ( $P < 0.01$ ; Mann-Whitney U-test). These results suggest that PLD is implicated in the proliferation and tumorigenesis of colon cancer. The present study provides the first evidence for the enhanced levels of two types of PLD in colon cancer and raises the possibility that these PLDs can be used as the potential target for the treatment of colon cancer.

**156: Time-spatial neutron measurement by using position-sensitive  $^3\text{He}$  proportional counter**

**Y. Kitamura, T. Misawa, H. Unesaki, S. Shiroya, A. Uritani(Nagoya Univ.), and K. Ishitani(Nagoya Univ.)**

Nuclear Instruments and Methods in Physics Research A, 422, 64-68 (1999)

Time-spatial neutron measurement was carried out by using a position-sensitive  $^3\text{He}$  proportional counter (PSPC) in the Kyoto University Critical Assembly. The data of the output pulses from the PSPC were acquired by a data acquisition system which was based on the LN-9000 system of Laboratory Equipment Corporation. In this system, the time and the position data of the neutron detection pulses were simultaneously accumulated by a personal computer. In the present study, the Rossi- $\alpha$  method, which was derived for time-domain neutron correlation analysis, was extended in order to process the measured two-dimensional data of time and space. The processed experimental results and a theoretical formula based on the one-group diffusion approximation neglecting the higher modes agreed well with each other, which indicates the present system is applicable for reactor physics experiments including reactor kinetics.

**157: Modified Explicit Higher Order Perturbation Method with Two Energy Groups**

**Cheol Ho Pyeon, Yoshihiro Yamane(Nagoya Univ.), Tsuyoshi Misawa and Seiji Shiroya**

Annals of Nuclear Energy, 26, 833-844 (1999)

The Explicit High Order Perturbation method is among various perturbation methods, and its main

feature is to expand neutron flux of a perturbed system in a series of the  $\lambda$ -mode eigenfunctions in an unperturbed system. Although various perturbation methods using  $\lambda$ -mode eigenfunctions have been proposed in the past, it was difficult to calculate accurately the perturbed flux and the reactivity with multi energy groups. To overcome this problem, we derived a new perturbation formulation unlike the Flux Reconstructed Explicitly by Neutronic Calculated Harmonies method based on the Explicit Higher Order Perturbation Method, and applied it to a simplified core system. To show the validity of this new perturbation method, numerical calculations with two energy groups in an x-y geometry were carried out and it was found that the perturbed flux and the reactivity could be accurately obtained by this new perturbation method.

**158: \* Formulation of Data Synthesis Technique for Feynman- $\alpha$  Method**

**Y. Yamane(Nagoya Univ.), T. Misawa, S. Shiroya and H. Unesaki**

Annals of Nuclear Energy, Vol.25, 141-148 (1998)

We intend to develop a subcriticality monitor based on the Feynman- $\alpha$  method, which detects a change in the prompt neutron decay constant caused by a change in the reactivity of a system containing nuclear fuel materials. For the practical use of this method, quick data processing is necessary to facilitate a real time measurement and it needs to be applicable to a wide range of count rates in the neutron detector. The Feynman- $\alpha$  method, based on pulse counting, has a serious problem relating to the counting statistics, namely the count loss effect due to the dead time of counter itself and the following counting circuit. To eliminate the count loss effect, especially in a high count rate region, a quick correction technique should be established to ensure accurate measurement. As a candidate for this, we have developed the data-synthesis technique which processes synthesized data generated by adding multiple time-series data acquired by independent neutron detectors. The present paper provides the derivation of a formula for this data-synthesis technique and the result of a numerical examination on its applicability

**159: Variance-to-Mean Method Generalized by Linear Difference Filter Technique**

**K. Hashimoto(Kinki Univ.), H. Ohsaki(Kinki Univ.), T. Horiguchi(Kinki Univ.), Y. Yamane(Nagoya Univ.) and S. Shiroya**

Annals of Nucl. Energy, Vol.25, No.9, 639-652 (1998)

The conventional variance-to-mean method (Feynman- $\alpha$  method) seriously suffers the divergency of the variance under such a transient condition as a reactor power drift. Strictly speaking, then, the use of the Feynman- $\alpha$  is restricted to a steady state. To apply the method to more practical uses, it is desirable to overcome this kind of difficulty. For this purpose, we propose an usage of higher-order difference filter technique to reduce the effect of the reactor power drift, and derive several new formulae taking account

of the filtering. The capability of the formulae proposed was demonstrated through experiments in the Kyoto University Critical Assembly. The experimental results indicate that the divergency of the variance can be effectively suppressed by the filtering technique, and that the higher-order filter becomes necessary with increasing variation rate in power

**160: Analysis of KUCA Critical Experiments Using MVP Code and JENDL-3.2**

**Hironobu Unesaki and Seiji Shiroya**

Proc. of International Conference on the Physics of Nuclear Science and Technology,  
Oct. 5-8, 1998, New York, pp. 1587-1592

Criticality analysis of critical experiments at Kyoto University Critical Assembly (KUCA) have been performed using the continuous energy Monte Carlo code MVP together with the latest evaluated nuclear data library JENDL-3.2. The C/E values of the effective multiplication factors for the polyethylene moderated / reflected cores were 1.010 ~ 1.020, whereas the C/E values for the light-water moderated / reflected cores were 0.997 ~ 1.006.

**161: Research Needed for Core Design of Thorium Cycle Reactors Including Accelerator Driven Subcritical Reactors**

トリウムサイクルと加速器駆動型未臨界炉の炉設計のために必要な研究

原子核研究、VOL 43、NO 1、27-36、1998

**162: Time-spatial neutron measurement by using position-sensitive 3-He proportional counter**

**Y. Kitamura, T. Misawa, H. Unesaki, S. Shiroya, A. Uritani(Nagoya Univ.), and K. Ishitani(Nagoya Univ.)**

Proc. of the Ninth Symposium on Radiation Measurements and Applications, Ann Arbor, MI, May 11-14, 1998, pp. 64-68

Time-spatial neutron measurement was carried out by using a position-sensitive 3-He proportional counter (PSPC) in the Kyoto University Critical Assembly. The data of the output pulses from the PSPC were acquired by a data acquisition system which was based on the LN-9000 system of Laboratory Equipment Corporation. In this system, the time and the position data of the neutron detection pulses were simultaneously accumulated by a personal computer. In the present study, the Rossi- $\alpha$  method,

which was derived for time-domain neutron correlation analysis, was extended in order to process the measured two-dimensional data of time and space. The processed experimental results and a theoretical formula based on the one-group diffusion approximation neglecting the higher modes agreed well with each other, which indicates the present system is applicable for reactor physics experiments including reactor kinetics.

**163: Study on Conceptual Neutronics Design of "Neutron Factory" as a Future Facility in Kyoto University Research Reactor Institute (KURRI)**

**Seiji Shiroya and Hironobu Unesaki**

Proc. of the Ninth International Conference on Emerging Nuclear Energy Systems,  
Tel-Aviv, Israel, Jun.28-Jul.2, 1998, pp.289-296

In accordance with the recent development in the field of neutron science including the application of neutrons, demands to utilize so-called "controlled neutrons" are becoming much stronger in order to promote new researches of a higher grade. Kyoto University Research Reactor Institute (KURRI), a future plan of a main facility for joint use program among university researchers is being investigated by organizing a working group, as a substitute of the 5 MW research reactor (KUR) which has been operated since 1964. At the present stage, a synergetic system of a proton or deuteron accelerator and a spectrum controlled type research reactor named as "Neutron Factory" is considered to be leading candidate of a future neutron source in KURRI. In "Neutron Factory", the accelerator and the reactor can be operated either independently or in combination to generate various kinds of "controlled neutrons" both in the energy and time spaces. In the design study, the neutron flux levels in several irradiation or experimental ports in the research reactor were examined through neutronic calculations.

**164: Burnup Study of Reactor Grade Plutonium in Molten Salt Reactor**

**Naohiro Hirakawa(Tohoku Univ.), Koshi Mitachi(Toyohashi Inst. of Technol.),  
Tsuyoshi Misawa, and Ahmed Aboanber(Tohoku Univ.)**

Proc. of the Ninth International Conference on Emerging Nuclear Energy Systems,  
Tel-Aviv, Israel, Jun.28-Jul.2, 1998, pp.439-446

Burnup characteristics of MSR for converting Pu from light water reactors into  $^{233}\text{U}$  was studied. A cylindrical model which is composed of hexagonal graphite moderator columns and has cylindrical fuel path at the center was adopted. The fuel salt composition was selected as  $\text{LiF} - \text{BeF}_2 - \text{ThF}_4 - \text{PuF}_3 = 72-16-11.4-0.6$  mol % which corresponds to  $V_F/V = 0.2$ . For this model, burnup characteristics up to 2250 days which corresponds to 86MWD/kgHM for initial loading were calculated for both with  $^{123}\text{Xe}$  and without  $^{135}\text{Xe}$  feeding Pu continuously. It was found that if we tune the feeding rate of Pu more carefully, it would be possible to keep  $k_{\text{eff}}$  almost unity. Since this System consumes about 2.6 times of

initially loaded Pu and makes the fissile Pu content from 74 % to 33 % in 2250 days, it looks promising to constrain Pu.

**165: \* Experimental Study on Thorium Fuel Cycle by Using the Kyoto University Critical Assembly (KUCA)**

**Seiji Shiroya**

Genshikaku Kenkyu, Vol.43, No. 5, 41-47, 1999

It was recognized from the early days of nuclear energy history that thorium (Th) would become a practical energy source, although the transmutation of  $^{232}\text{Th}$  into  $^{233}\text{U}$  is inevitable in the Th fuel cycle. An experimental study on the Th fuel cycle was initiated in 1977 by using the Kyoto University Critical Assembly (KUCA) established in 1974 for the joint use program among Japanese universities including the research and education of reactor physics. Thereafter, the experimental study on the Th fuel cycle has been performed in the KUCA by using Th metal plates. A solid moderator core is utilized for the series of critical experiments on the Th fuel cycle. In addition, basic experiments on Th hybrid reactors were performed by using a Cockcroft-Walton type accelerator installed in the KUCA. In order to promote the experimental study on the Th fuel cycle in the KUCA, a future plan is being investigated to perform various experiments by introducing the  $^{233}\text{U}$  fuel from US.

**166: \* Verification of Neutron Radiographic Measurement of Void Fraction by Monte Carlo Simulation**

**Hironobu Unesaki, Takashi Hibiki, Kaichiro Mishima**

Nuclear Instruments and Methods in Physics Research, vol.A405, pp.98-104, 1998

Neutron radioscopic images have been simulated using the Monte Carlo method to verify the sigma-scaling method used in void fraction measurement of two-phase flow. Continuous energy Monte Carlo code MCNP was used for the accurate treatment of the test section with complex geometry. Radioscopic images of water-layer thickness distribution in a concentric triple-tube test section were successfully reproduced by the Monte Carlo simulation. The simulated images at various distances between the test section and the converter were obtained using an ideal monodirectional (parallel) beam and realistic beam with unparallelness defined by the L/D ratio, thus enabling the separate treatment of the unsharpness of the image caused by the scattered neutrons and the unparallelness of the incident neutron beam. The treatment of the scattered component and the unparallelness of incident beam employed in the sigma-scaling method was verified to be appropriate through the simulation, which shows that the sigma-scaling method could be successfully adopted for the quantitative measurement of void fraction of two-phase flow.

**167: \* Evaluation of Scattered Neutron Component in Thermal Neutron Radiography Image: Influence of Scattered Neutrons and Unparallelness of Incident Neutron Beam****Hironobu Unesaki, Takashi Hibiki, Kaichiro Mishima**

Nuclear Instruments and Methods in Physics Research, vol. A413, pp. 143-150, 1998

Analysis of thermal neutron radiographic images are performed using neutronic methods. Analytical expressions for the behavior of scattered neutron component and image distortions due to the unparallelness of the incident neutron beam are shown. Numerical results are compared with the neutron radiographic images of simple rectangular polystyrene test sections of various thickness. Suggestions for the optimum distance between the test section and the converter have been given.

**168: Local Measurements of Interfacial Area, Interfacial Velocity and Liquid Turbulence in Two-Phase Flow****Takashi Hibiki, Steven Hogsett\*, Mamoru Ishii\* \* Purdue University**

Nuclear Engineering and Design, vol. 184, pp.287-304, 1998

Double sensor probe and hotfilm anemometry methods were developed for measuring local flow characteristics in bubbly flow. The formulation for the interfacial area concentration measurement was obtained by improving the formulation derived by Kataoka and Ishii. The assumptions used in the derivation of the equation were verified experimentally. The interfacial area concentration measured by the double sensor probe agreed well with one by the photographic method. The filter to validate the hotfilm anemometry for measuring the liquid velocity and turbulent intensity in bubbly flow was developed based on removing the signal due to the passing bubbles. The local void fraction, interfacial area concentration, interfacial velocity, Sauter mean diameter, liquid velocity, and turbulent intensity of vertical upward air-water flow in a round tube with inner diameter of 50.8 mm were measured by using these methods. A total of 54 data sets were acquired consisting of three superficial gas flow rates, 0.015, 0.076 m/s, and three superficial liquid flow rates, 0.600, 1.00, and 1.30 m/s. The measurements were performed at the three locations:  $L/D=2, 32, \text{ and } 62$ . This data is expected to be used for the development of reliable constitutive relations which reflect the true transfer mechanisms in two-phase flow.

**169: Scaling Parameter of CHF under Oscillatory Flow Condition**

**Hisashi Umekawa\*, Mamoru Ozawa\*, Tamotsu Mitsunaga\*, Kaichiro Mishima, Takashi Hibiki, Yasushi Saito \* Kansai University**

Transactions of the Japan Society of Mechanical Engineers, vol. 64, pp. 161-166, 1998

Critical heat flux (CHF) was reduced by flow oscillations, and the reduction of CHF was significantly influenced by the flow oscillation period, amplitude, heat capacity of test tube and mean inlet mass flux. A scaling parameter of temperature response of tube wall was derived based on a lumped-parameter model of tube wall heat capacity. Applying this scaling parameter to the CHF data under flow oscillation, the experimental data of CHF was successfully correlated.

**170: Effect of Flow-Induced Vibration on Local Flow Parameters of Two-Phase Flow**

**Takashi Hibiki, Mamoru Ishii\* \* Purdue University**

Nuclear Engineering and Design, vol. 184, pp.183-201, 1998

A preliminary study was conducted experimentally in order to investigate the effect of flow-induced vibration on flow structure in two-phase flow. Two kinds of experiments were performed; "reference" (no vibration) and "vibration" experiments. In the reference experiment, an experimental loop was fixed tightly by three structural supports, whereas the supports were loosen a little in the vibration experiment. In the vibration experiment vibration was induced by flowing two-phase mixture in the loop. For relatively low superficial liquid velocity, flow-induced vibration promoted the bubble coalescence but liquid turbulence energy enhanced by the vibration might not be enough to break up the bubble. This led to the marked increase of Sauter mean diameter, and the marked decrease of interfacial area concentration. Accordingly, flow-induced vibration changed the void fraction profile from "wall peak" to "core peak" or "transition", which increased distribution parameter in the drift-flux model. For high superficial liquid velocity, shear-induced liquid turbulence generated by two-phase flow itself might be dominant for liquid turbulence enhanced by flow-induced vibration. Therefore, the effect of flow-induced vibration on local flow parameters was not marked as compared with that for low superficial liquid velocity. Since it is anticipated that flow structure change due to flow-induced vibration would affect the interfacial area concentration, namely interfacial transfer term, further study may be needed under the condition of controlled flow-induced vibration.

**171: Development of High-Frame-Rate Neutron Radiography and Quantitative Measurement Method for Multiphase Flow Research****Kaichiro Mishima, Takashi Hibiki**

Nuclear Engineering and Design, vol. 184, pp. 183-201, 1998

In relation to the establishment of thermal neutron radiography as a measurement method with high accuracy and reliability, this paper reviewed the present status on the development of high-frame-rate neutron radiography with a steady thermal neutron beam and its application to multiphase flow researches. This review included also the present progress on the quantification of neutron radiographic image at Kyoto University, that is, (1) quantitative method to measure void fraction of two-phase flow with thermal neutron radiography (S-scaling method), (2) influence of scattered neutrons on void fraction measured by neutron radiography, (3) measurement error of neutrons in a low neutron flux field, (4) error in void fraction measurement due to low gray level, and (5) measurement error due to low imaging speed. Moreover, a new experimental approach on a total macroscopic cross section for thermal neutrons measurement by neutron radiography was presented. This paper revealed neutron radiography to be a promising visualization and measurement method in thermal hydraulic research.

**172: \* The Review of the Application of Neutron Radiography to Thermal Hydraulic Research****Kaichiro Mishima, Takashi Hibiki, Yasushi Saito, Hideo Nakamura\*, Masahito Matsubayashi\* \* Japan Atomic Energy Research Institute**

Nuclear Instruments and Methods in Physics Research, vol. A424, pp.55-72, 1999

This paper is concerned with the establishment of thermal neutron radiography as a high accuracy measurement method. This paper reviews the present status on the development of high-frame-rate neutron radiography with a steady thermal neutron beam and its application to multiphase flow research performed at the Research Reactor Institute of Kyoto University in collaboration with the Japan Atomic Energy Research Institute.

**173: \* Application of High-Frame-Rate Neutron Radiography to Steam Explosion Research**

**Yasushi Saito, Kaichiro Mishima, Takashi Hibiki, Akihiro Yamamoto, Jun Sugimoto\*, Kiyofumi Moriyama\* \* Japan Atomic Energy Research Institute**

Nuclear Instruments and Methods in Physics Research, vol. A424, pp. 142-147, 1999

To understand the behavior of dispersed molten metal particles dropped into water during the premixing process of steam explosion, preliminary experiments were performed by using heated stainless-steel particles simulating dispersed molten metal particles. Newly developed high-frame-rate neutron radiography was successfully employed for visualization and void fraction measurement. Visualization was conducted by dropping heated stainless-steel particle into heavy water filled in a rectangular tank with the particle diameter (6, 9, and 12 mm) and temperature (600, 700, 800, and 1000 °C) as parameters. Steam generation due to direct contact of heated particle and heavy water was successfully visualized by the high-frame-rate neutron radiography at the recording speed of 500 frames/s. The following results were deduced from the void fraction measurement: Steam was generated in proportion to the particle size and temperature. It is expected that the thickness of vapor film around a molten fuel may be decreased as the molten fuel is broken into small fragments in a premixing process. This thin steam film would easily collapse due to a pressure wave. On the other hand, the molten fuel with high temperature and large size generates thick steam film, which would be stable against the pressure wave.

**174: \* Visualization and Measurement of Gas-Liquid Metal Two-Phase Flow with Large Density Difference Using Thermal Neutrons as Microscopic Probes**

**Kaichiro Mishima, Takashi Hibiki, Yasushi Saito, Hideaki Nishihara, Yoshiharu Tobita\*, Kensuke Konishi\*, Masahito Matsubayashi\*\* \* Japan Nuclear Cycle Development Institute, \*\* Japan Atomic Energy Research Institute**

Nuclear Instruments and Methods in Physics Research, vol. A424, pp. 229-234, 1999

In a core melt accident of a fast breeder reactor, there is a possibility of boiling of the fuel-steel mixture in the containment pool. In relation to safety evaluation on severe accident, it is indispensable to evaluate the possibility of re-criticality of melted core. Gas-liquid two-phase flow with a large liquid-to-gas density ratio is formed due to the boiling of fuel-steel mixture. Although it is anticipated that the large density ratio may affect the basic characteristics of two-phase flow, little work has been performed so far on two-phase flow with a large liquid-to-gas density ratio. In this study, visualization and void fraction measurement of gas-liquid metal two-phase flow were performed by using neutron radiography and image processing techniques. Then, the effect of large density difference between gas and liquid phases on the basic flow characteristics of two-phase flow was clarified.

**175: Local Flow Measurements of Vertical Upward Air-Water Flow in a Round Tube****Takashi Hibiki, Mamoru Ishii\*, Zheng Xiao\* \* Purdue University**

Proceedings of the Third International Conference on Multiphase Flows '98, 1998

Recently, the concept of the interfacial area transport equation has been proposed to develop the constitutive relation on the interfacial area concentration in relation to model the interfacial transfer terms in the two-fluid model. Accurate data sets on axial development of local flow parameters such as void fraction, interfacial area concentration, interfacial and liquid velocities and turbulent intensity are indispensable to verify the modeled source and sink terms in the interfacial area transport equation. From this point of view, local flow measurements of vertical upward air-water flows in a round tube with an inner diameter of 50.8 mm were performed at three axial locations by using the double-sensor probe and the hot film probe. The combined data from the double-sensor probe and the hot film probe give near complete information on the time averaged local hydrodynamic parameters of two-phase flow. This data can be used for the development of reliable constitutive relations which reflect the true transfer mechanisms in two-phase flow.

**176: Flow Regime Transition Criteria for Vertical Upward Two-Phase Flow in Narrow Rectangular Ducts****Kaichiro Mishima, Takashi Hibiki**

Proceedings of the Third International Conference on Multiphase Flows '98, 1998

In relation to the cooling system of high performance microelectronics, a high power research reactor with plate type fuels and plasma facing components of a fusion reactor, study of two-phase flow in a narrow rectangular duct has been paid considerable attention, recently. For the two-fluid model, direct geometrical parameters such as the void fraction should be used in flow-regime criteria. From this point of view, flow-regime transition criteria for vertical upward flows in narrow rectangular ducts have been developed considering the mechanisms of flow-regime transitions. The basic concept of the present modeling followed the Mishima & Ishii model for vertical upward two-phase flows in round tubes. Newly developed criteria have been compared with the existing experimental data for air-water flows in narrow rectangular ducts with the gaps from 1 to 17 mm. The present criteria showed satisfactory agreements with those data.

**177: Axial Development of Liquid Turbulence and Interfacial Area in Bubbly Two-Phase Flows**

**Takashi Hibiki, Mamoru Ishii\* \* Purdue University**

Proceedings of the 5th ASME/JSME Thermal Engineering Joint Conference, 1999

In relation to the development of the interfacial area transport equation, local measurements of the void fraction, interfacial area concentration, interfacial velocity, and Sauter mean diameter using the double sensor probe method as well as the liquid velocity and turbulence intensity using hotfilm anemometry were performed extensively for vertical upward bubbly air-water flows in a round tube with an inner diameter of 25.4mm at three axial locations of  $L/D=12.0$ , 65.0 and 125, and fifteen radial locations from  $r/R=0$  to 0.95. The data set obtained in this study will eventually be used for the development of reliable constitutive relations which reflect the true transfer mechanisms in bubbly flow systems.

**178: \* Study on Flow Characteristics in Gas-Molten Metal Mixture Pool Simulating Core Disruptive Accident of FBR**

**Takashi Hibiki, Kaichiro Mishima, Yasushi Saito, Yoshiharu Tobita\*, Kensuke Konishi\*, Masahito Matsubayashi\*\* \*Japan Nuclear Cycle Development Institute, \*\* Japan Atomic Energy Research Institute**

Proceedings of the 5th ASME/JSME Thermal Engineering Joint Conference, 1999

As part of basic research on the flow characteristics of two-phase mixture pool with a large liquid-to-gas density ratio under severe accident of fast breeder reactor (FBR), visualization and measurement of N<sub>2</sub>-molten Pb/Bi two-phase flow in a rectangular pool were performed by using neutron radiography technique. Measurements of drag coefficient of a single bubble and bubble shape regime suggested that the relationship between the shape, size and the rising velocity of a single isolated bubble with a large liquid-to-gas density ratio is not much different from that for ordinary one. Appropriate correlation for drift velocity and drag coefficient between phases were recommended from the drift flux correlation of measured pool void fraction. One- and two-dimensional analyses were performed by using a next generation computational code for safety analysis of severe accident of FBRs, SIMMER-III with various drag coefficient models. It was revealed that Kataoka-Ishii's equation was suitable basically for estimation of drift velocity, namely drag force between phases.

**179: Mechanism of Periodical Dryout under Oscillatory Flow Condition**

**Hisashi Umekawa\*, Mamoru Ozawa\*, Ryuta Murakami\*, Kaichiro Mishima, Takashi Hibiki, Yasushi Saito \* Kansai University**

Proceedings of the 5th ASME/JSME Thermal Engineering Joint Conference, 1999

Critical Heat Flux (CHF) is a very important design factor of boiling systems. Many investigations have been conducted so far, but almost all these investigations were conducted under steady flow conditions. CHF was strongly influenced by flow condition, and the reduction of CHF under unsteady flow oscillation was more than 60 condition. In this investigation the CHF experiment was conducted by using the boiling channel equipped with a mechanical flow oscillator. The experiment was conducted under upward, downward and horizontal flow conditions. The superimposed flow oscillation included the strong flow reversal condition at the tube inlet, and the oscillation period was 2 - 6 s. The simulation based on the lumped-parameter model and the calculation using the Mini-TRAC code developed by JAERI was also conducted. These simulation methods interpreted the experimental results reasonably.

**180: Visualization of Molten-Metal/Water Interaction Using High-Frame-Rate Neutron Radiography**

**Hideo. Nakamura\*, Yasuteru Shibamoto\*, Yoshinari Anoda\*, Yutaka Kukita\*\*, Kaichiro Mishima, Takashi Hibiki \* Japan Atomic Energy Research Institute, \*\* Nagoya University**

Nuclear Technology, vol. 125, pp.213-224, 1999

High-frame-rate neutron radiography was applied to observe the behavior of high-temperature (773K) molten Pb-Bi alloy dropped into a water-containing or an empty vessel. Using a high-speed camera combined with an image intensifier and a high-flux neutron source, the interactions among the molten and solidified alloy with water and steam were visualized at a rate of 500frame/s. The behavior of the melt and steam bubbles was observed clearly by contrast with water. Observation of tracer particles in the molten metal dropped into the empty vessel was also successful. The velocity distribution in the melt was measured successfully by using AuCd3 tracer particles. This visualization technique proved to be a promising tool for observation and measurement of rapid and complex phenomena of metal-gas-liquid mixture.

**181: \* Experimental Study on Interfacial Area Transport in Bubbly Two-Phase Flows**

**Takashi Hibiki, Mamoru Ishii\* \* Purdue University**

International Journal of Heat and Mass Transfer, vol. 42, pp.3019-3035, 1999

In relation to the development of the interfacial area transport equation, local measurements of the void fraction, interfacial area concentration, interfacial velocity, and Sauter mean diameter using the double sensor probe method as well as the liquid velocity and turbulence intensity using hotfilm anemometry were performed extensively for vertical upward bubbly air-water flows in a round tube with an inner diameter of 25.4 mm at three axial locations of  $L/D=12.0$ , 65.0 and 125, and fifteen radial locations from  $r/R=0$  to 0.95. The liquid flow rate and the void fraction ranged from 0.292 m/s to 3.49 m/s and from 3 will eventually be used for the development of reliable constitutive relations which reflect the true transfer mechanisms in bubbly flow systems.

**182: Experimental Study on Two-Phase Natural Circulation and Flow Termination in a Loop**

**Juei-Tsuen Hsu\*, Mamoru Ishii\*, Takashi Hibiki \*Argonne National Laboratory**

Nuclear Engineering and Design, vol. 186, pp.395-409, 1998

In order to study the two-phase natural circulation and flow termination during a small break loss of coolant accident in LWR, a hot leg U-bend simulation loop has been built based on the two-phase flow scaling criteria developed under this program. The nitrogen-water system has been used to isolate the key hydrodynamic phenomena from heat transfer problems. Various tests were carried out to establish the basic mechanism of the flow termination and reestablishment as well as to obtain essential information on scale effects of various parameters such as the loop frictional resistance, thermal center, U-bend curvature, and inlet geometry. It was found that the permanent termination of the natural circulation was related to the head balance between the hot and cold legs. The local flow condition at the inverted U-bend could produce intermittent flow, however was not related to the permanent flow termination. The void distribution in a hot leg, flow regime and natural circulation rate have been measured in detail for various conditions. Significant effects of the inlet geometry on these were observed. Near the flow termination condition, large amplitude flow oscillations occurred. The occurrence of this type of flow instability is important for safety analyses, because it may lead to loop-to-loop oscillations or flow excursions in a prototype system which has a multi-loop configuration.

**183: \* Visualization Study of Molten Metal-Water Interaction by Using Neutron Radiography**

**Kaichiro Mishima, Takashi Hibiki, Yasushi Saito, Jun Sugimoto\*, Kiyofumi Moriyama\* \* Japan Atomic Energy Research Institute**

Nuclear Engineering and Design, vol.189, pp. 391-403, 1999

The purpose of this study is to visualize the behavior of molten metal dropped into water during the premixing process by means of neutron radiography which makes use of the difference in the attenuation characteristics of materials. For this purpose, a high-sensitive, high-frame-rate imaging system using neutron radiography was constructed and was applied to visualization of the behavior of molten metal dropped into water. The test rig consisted of a furnace and a test section. The furnace could heat the molten metal up to 650 ° C. The test section was a rectangular tank made of aluminum alloy. The tank was filled with heavy water and molten Wood's metal was dropped into heavy water. Visualization study was carried out with use of the high-frame-rate neutron radiography to see the breakup of molten metal jet or lump dropped into heavy water pool. In the images obtained, water, steam or air bubbles, molten metal jets or droplets, cloud of small particles of molten metal after atomization could be distinguished. The debris of Wood's metal was collected after the experiment, and the relation between the break-up behavior and the size and the shape of the debris particles was investigated.

**184: \* Application of Photocatalytic Reactions Caused by TiO<sub>2</sub> Film to Improve the Maintenance Factor of Lighting Systems**

**H. Honda, A. Ishizaki, R. Soma, K. Hashimoto, and A. Fujishima**

J. Illuminating Eng. Soc., Winter, 42-49 (1998).

The buildup of stains on lamps and luminaires causes extreme decreases of light output lighting systems when used in a dusty environment. For example, in tunnel lighting, the glass covers of luminaires suffer from a great deal of contamination due to dust, dirt, grime, and vehicle exhaust fumes. This staining can cause the rapid deterioration in various types of light output. Therefore, frequent cleaning is necessary to maintain an adequate luminance level. Ever since the Fujishima-Honda effect, involving photoelectrochemical reactions of a semiconducting TiO<sub>2</sub> electrode, was reported in 1972, attention has been focused on TiO<sub>2</sub> as a precious photocatalyst, and it has been applied to a variety of environmental problems in addition to water and air purification. In the last few years, research and application on this photocatalyst have been increasing in Japan. This is because we have proven that only a small amount of UV radiation from various types of lamps such as fluorescent lamps is sufficient for the photocatalytic decomposition of nearly all contaminants in indoor environments. Additionally, it has been demonstrated that the TiO<sub>2</sub> photocatalyst is effective for deodorization, sterilization of bacteria, and the decomposition of oil spills.

**185: \* Electrochemical Behavior of Highly Conductive Boron-Doped Diamond Electrodes for Oxygen Reduction in Alkaline Solution**

T. Yano, D. A. Tryk, K. Hashimoto, and A. Fujishima

J. Electrochem. Soc., 145 (6), 1870-1876 (1998).

Highly conductive boron-doped polycrystalline diamond thin films ( $\rho \approx 10^{-3} \Omega \text{cm}$ ) were prepared via microwave plasma chemical vapor deposition (CVD). The electrochemical behavior for oxygen reduction was examined in 0.1 MKOH using linear sweep voltammetry. Oxygen reduction was found to be highly inhibited, the cathodic voltammetric peak being observed at  $\sim -1.2$  V vs. Ag/AgCl, compared with the standard potential for the two-electron reduction of oxygen  $\text{O}_2 + \text{H}_2\text{O} + (2e^- = \text{HO}_2^- + \text{OH}^-)$ ,  $E^\circ = -0.234$  V vs. Ag/Cl at pH 13. This demonstrates that even in the presence of dissolved oxygen, diamond retains a relatively wide potential window, which could be advantageous in certain types of analytical applications. Possible interpretations for the high overpotential for oxygen reduction include a lack of adsorption sites for oxygen and/or reduced intermediates, a low density of states or a potential drop within a thin surface layer, all of which have also been proposed for highly ordered pyrolytic graphite. The experimental data were fitted using digital simulation, which showed that the reduction peak appearing at ca.  $-1.2$  V vs. Ag/AgCl is predominately due to the reduction of oxygen to peroxide. Rotation disk electrode measurements were also consistent with an overall two-electron process. Experiments involving the addition of superoxide dismutase also supported this conclusion. The oxygen reduction reaction is proposed to occur on the sp carbon component of the surface, with a very small contribution from sp carbon impurities at smaller overpotentials.

**186: \* Metal Black Pattern Formation on Photofunctional ZnO Thin Films by Electroless Deposition**

R. D. Sun, D. A. Tryk, K. Hashimoto, and A. Fujishima

Electrochem. Solid-State Lett., 1 (1), 29-31 (1998).

A novel method is presented for the preparation of patterned metallic black thin films under ambient pressure conditions and without the use of photoresist. This method makes use of the rough underside of a metal layer which was deposited on a ZnO thin film on a smooth glass substrate. This highly black metallic underside is achieved by controlling the surface texture of the ZnO thin film. The black pattern is prepared via a photopatterning method that was recently developed in our laboratory, in which a Pd pattern is first produced by the photocatalytic reaction of the ZnO film, and then a metal, e. g. Cu, is selectively electroless deposited on the patterned Pd. The metal patterns produced in this fashion exhibit very high optical densities and relatively high adhesive strength, which makes it possible to use this method to fabricate high quality black matrices for use in liquid crystal color displays at lower cost.

**187: \* AFM Observation of Surface Reconstruction of C<sub>60</sub> Single Crystals**

**Y. Kim, L. Jiang, T. Iyoda, J. Li, K. Kitazawa, K. Hashimoto, and A. Fujishima**

Appl. Phys. A, 66, S763-S766 (1998).

We report an atomic force microscopic (AFM) examination of the photo-induced surface reconstruction of C<sub>60</sub> single crystals. The (111) and the (000) faces of C<sub>60</sub> single crystals were illuminated with photons with energies below the band gap (generation of Frenkel-type excitons) or above the band gap. In the case of sub-band-gap illumination, reconstructed surfaces formed on the crystals. Thereconstruction was represented by fringes running in the [112] and [010] directions on the (111) and (001) surfaces, respectively. As a result of supra-band-gap illumination, however, there appeared only cracks, without any fringes, which were oriented in directions characteristic of each face. The results suggest that the photo-induced surface reconstruction of C<sub>60</sub> single crystals is induced via the recombination of Frenkel-type excitons.

**188: \* Photoelectrochemical Reduction of CO<sub>2</sub> at High Current Densities at p-InP Electrodes**

**K. Hirota, D. A. Tryk, K. Hashimoto, M. Okawa, and A. Fujishima**

J. Electrochem. Soc., 145 (5), L83-L84 (1998).

High-rate cathodic photoelectrolysis of CO<sub>2</sub> was conducted in a high pressure CO<sub>2</sub> + methanol medium at p-InP electrodes. Current densities up to 100 mA cm<sup>-2</sup> were achieved, with current efficiencies up to 93% for CO production. The photoelectrochemical reduction of CO<sub>2</sub> in the highly concentrated CO<sub>2</sub><sup>-</sup> methanol solution was limited at the higher current densities (50-100 mA cm<sup>-2</sup>) by light intensity and not by the mass transport of CO<sub>2</sub>.

**189: \* Adhesion Mechanism of Electroless Copper Film Formed on Ceramic Substrates Using ZnO Thin Film as an Intermediate Layer**

**H. Yoshiki, K. Hashimoto, and A. Fujishima**

J. Electrochem. Soc., 145 (5), 1430-1434 (1998).

Electroless Cu layers with pull strengths of greater than 2.5 kg/mn<sup>2</sup> were fabricated on smooth ceramic substrates (glass, Al<sub>2</sub>O<sub>3</sub>, AIL) without surface etching ( $R_a \leq 0.05 \mu\text{m}$ ). High adherence was achieved using

ZnO thin films (ca. 1  $\mu\text{m}$  thickness), prepared by spray pyrolysis as an intermediate layer between the ceramic substrates and the Cu layers. It was shown from the interfacial analysis that the high adherence was due to both strong van der Waals forces acting at the Cu/ ZnO interface and a chemical-type bond acting at the ZnO/ceramic interface. The adhesive forces at the Cu/ZnO interface were enhanced by numerous small pores ( $< 0.5 \mu\text{m}$  diam) formed on the ZnO thin film during catalyzation. In contrast, the ZnO/ceramic adhesion was due to the thermal diffusion of Zn into the substrate during the preparation of the ZnO thin film, which involves chemical bonding forces. As a result, the ZnO thin film acts as a highly effective adhesive layer between the electroless Cu layer and the ceramic substrate.

**190: \* Observation of Electrochemical  $\text{C}_{60}$  Reduction of a Diamond Thin Film Electrode at Room Temperature**

**Z. Wu, T. Yano, D. A. Tryk, K. Hashimoto, and A. Fujishima**

Chem. Lett., 503-504 (1998).

Highly conductive boron-doped diamond thin film electrodes were used for the first time to examine the cyclic voltammetric behavior of  $\text{C}_{60}$  reduction at room temperature as a demonstration of the relatively wide potential window in nonaqueous media. Five reduction peaks were observable on diamond electrodes at room temperature, while four reduction peaks were observed on Pt.

**191: \* Examination of the Photoreaction of *p*-Nitrobenzoic Acid on Electrochemically Roughened Silver Using Surface-Enhanced Raman Imaging (SERI)**

**X. M. Yang, D. A. Tryk, K. Hashimoto, and A. Fujishima**

J. Phys. Chem., B, 102, 4933-4943 (1998).

The present work is the first report of the use of surface-enhanced Raman scattering (SERS) for two-dimensionally spatially resolved, chemically selective monitoring of the course of a surface-catalyzed photoreaction. We have recently developed the surface-enhanced Raman imaging (SERI) technique, which is chemically selective, has monolayer sensitivity, and can be used under ambient conditions. *p*-Nitrobenzoic acid (PNBA) deposited on an electrochemically roughened silver surface was used as a model system. In order to examine the dependence of the photoreaction on the state of aggregation of the molecules, two-types of sample were prepared, one in which the compound was uniformly adsorbed as a monolayer and another in which there was a combination of monolayer plus crystallites. In the form of a uniformly adsorbed monolayer, the SERS image (based on the  $1348 \text{ cm}^{-1}$  band) exhibited a relatively uniform intensity level over the sample surface, due to uniform roughness, but there were slight variations that are related to small differences in the surface roughness, as measured with atomic force microscopy (AFM). A photoreaction, induced by the  $\text{Ar}^+$  illumination (514.5nm), involving PNBA is known to be strongly

catalyzed by metallic silver and is strongly suspected to produce azodivenzoate. The extent of this photoreaction, which was successfully mapped using SERI, was found to depend upon whether the PNBA was in the form of a monolayer or multilayers (i.e., crystallites). The time dependence of the SERS intensity clearly shows that the photocatalytic reaction, as monitored by both the  $1348\text{ cm}^{-1}$  reactant peak and the  $1437\text{ cm}^{-1}$  product peak, takes place to a much larger ( $\sim 80\%$ ) when PNBA is adsorbed as a monolayer, while the reaction proceeds to a much lesser extent (10-20%) when the compound is present as small crystallites on the surface, even for the molecules that are in direct contact with the Ag surface, due to steric limitations. However, work of others has shown that PNBA molecules in the form of an adsorbed layer but separated from the Ag surface by  $\sim 1.8\text{ nm}$  can still undergo photoreaction, showing that an electromagnetic-type mechanism may also be operative for surface-catalyzed photoreactions.

**192: \* External Magnetic Field Effect on the Photoinduced Magnetization in a Cobalt Iron Cyanide**

**Y. Einaga, S. Ohkoshi, O. Sato, A. Fujishima and K. Hashimoto**

Chem. Lett., 585-586 (1998).

We studied the external magnetic field effects on the photoinduced magnetization of a cobalt iron cyanide,  $\text{K}_{0.4}\text{Co}_{1.3}[\text{Fe}(\text{CN})_6]5\text{H}_2\text{O}$ . Photoinduced magnetization value was increased ca. 20% at maximum under the magnetic field of 50000G at 5K. In addition, in the ferrimagnetic region ( $T < T_c = 26\text{K}$ ), the external magnetic field accelerated the rate of photoinduced spin generation. Those data suggest that external magnetic field increases magnetic interaction between the excited state and spin clusters.

**193: \* Electrochemical Reduction of  $\text{CO}_2$  in Micropores**

**T. Yamamoto, K. Hirota, D. A. Tryk, K. Hashimoto, A. Fujishima, and M. Okawa**

Chem. Lett., 825-826 (1998).

$\text{CO}_2$  electroreduction was examined on high area nickel electrocatalysis supported on activated carbon fibers, which contain slit-shaped pores with widths on the order of nanometers. The current efficiency for  $\text{CO}_2$  reduction to CO reached values of 70%. In contrast, much smaller amounts of CO were generated for the same type of high area nickel catalyst supported on non-activated carbon fibers. The enhancement of the  $\text{CO}_2$  reduction selectivity with the microporous support is thought to include a nanospace effect, which gives rise to high pressure-like effects at ambient pressure.

**194: \* AFM Study of Surface Phenomena Based on C<sub>60</sub> Film Growth**

**Y. Kim, L. Jiang, T. Iyoda, K. Hashimoto, and A. Fujishima**

Appl. Sur. Sci., 130-132, 602-609 (1998).

The surface phenomena of C<sub>60</sub> films were investigated using atomic force microscopy (AFM). The films were grown epitaxially on cleaved KBr(001) substrates under various conditions. For thin films (< 50 nm), single crystalline C<sub>60</sub> islands oriented randomly on the substrate due to the lattice mismatch between C<sub>60</sub> and substrate. Peculiar features were observed on the thin films, i.e., concave top surface, fivefold twinning and screw dislocation of the islands. The thick films (> 500 nm) showed different surface phenomena from the thin films. One of these is the spiral growth originated in screw dislocation. We observed both single and double spirals. Another is the surface reconstruction on the thick films. Furthermore, deposition-rate-dependence studies revealed that morphological changes from the (001) faces to the (111) faces depend on an increase in the deposition rates.

**195: \* Soliton Superlattices on the (0001) Surface of C<sub>70</sub> Single Crystals**

**L. Jiang, T. Iyoda, D. A. Tryk, N. Kino, K. Kitazawa, A. Fujishima, and K. Hashimoto**

Sur. Sci., 408, 112-122 (1998).

Soliton-type superlattices were directly observed on the (0001) face of C<sub>70</sub> single crystals using atomic force microscopy. The images show a stressed surface, with parallel fringes along the < 210 > direction, which represent a ( $p\sqrt{3} \times 1$ ) superstructure, with  $p=14\sim 16$  in the < 010 > direction. Monolayer steps and platelets containing superstructures were also observed on the superstructure surface, consistent with a multilayer reconstruction model. The observed structure also appears to represent a novel example of a one-dimensional sine-Gordon soliton superlattice on the surface of a molecular crystal. The parallel fringes, with a dominant peak-to-peak spacing (half of the full width of the soliton structure) of  $27.5 \pm 1$  nm ( $\sim 32\sqrt{3} \times 1$  superstructure) and corrugation height difference of  $0.3 \pm 0.03$  nm, were found to be domain walls between face-centered cubic stacking regions and those with hexagonal close-packed stacking on the surfaces of the C<sub>70</sub> single crystals. Molecular resolution images, which were obtained on the surface of the superstructure, support the proposed molecular arrangement model of the soliton superlattice.

**196: \* Effect of Adsorbed Water on the Photoelectrorheology of TiO<sub>2</sub> Particle Suspensions****N. Sakai, Y. Komoda, T. N. Rao, D. A. Tryk, and A. Fujishima**

J. Electroanal. Chem., 445, 1-6 (1998).

The photoelectrorheological properties of several types of TiO<sub>2</sub> samples having widely varying surface water contents were examined in order to understand the role of water in the photoelectrorheology of TiO<sub>2</sub>- based fluids. The particles having low water contents showed an increase in the ER effect upon illumination, which is due to a polarization by photogenerated charges. The diminution in the photoeffect with increasing water content on the particles is attributed to the partial removal of photogenerated charges which have been trapped as a result of reactions involving water, adsorbed OH groups and oxygen, e.g. reduction of adsorbed hydroxyl radicals and oxidation of adsorbed superoxide. The resulting photoelectrophoretic effect is believed to dominate the electrorheological force, thus reducing the photoeffect.

**197: \* Bactericidal and Detoxification Effects of TiO<sub>2</sub> Thin Film Photocatalysts****K. Sunada, Y. Kikuchi, K. Hashimoto, and A. Fujishima**

Environmental Sci. &amp; Technology, 32 (5), 726-728 (1998).

To examine the special features of the antibacterial effect for a thin transparent titanium dioxide (TiO<sub>2</sub>) film, the photocatalytic degradation of endotoxin, which is a pyrogenic constituent of *Escherichia coli* (*E.Coli*), as well as its bactericidal activity, was investigated. The TiO<sub>2</sub> films were prepared from titanium isopropoxide solution, annealing at 500 degree. The bactericidal activity for *E.Coli* cells was estimated by survival ratio calculated from the number of viable cells which form colonies on the nutrient agar plates. The endotoxin concentration was determined by the *Limulus* tests. When *E.Coli* cells were killed by the TiO<sub>2</sub> photocatalyst under UV irradiation, the endotoxin from the cells was also degraded efficiently. This result shows that the TiO<sub>2</sub> photocatalyst has both bactericidal activity and decomposing activity for the endotoxin. The bactericidal effect of the TiO<sub>2</sub> thin films results from both inactivating the viability of the bacteria and the destruction of the *E.Coli* cells. This feature renders TiO<sub>2</sub> photocatalysts to be applicable to environmental protections, especially in medical facilities where the endotoxin is needed to control.

**198: \* Photoinduced Dislocation Lines on the (111) Face of C<sub>60</sub> Single Crystals**

L. Jiang, T. Iyoda, D. A. Tryk, J. Li, K. Kitazawa, A. Fujishima, and K. Hashimoto

J. Phys. Chem. B, 102 (33), 6351-6359 (1998).

We report an atomic force microscopic (AFM) study of photoinduced dislocation lines (DLs) on the (111) face of C<sub>60</sub> single crystals via excitation of the Frenkel exciton transition of solid C<sub>60</sub>. Under illumination, DLs appeared along the [112] direction on the (111) face of the C<sub>60</sub> single crystals. These DLs consist of pairs of substructures that are separated by a shallow region with a width of  $30.0 \pm 0.5$  nm and a depth of  $0.08 \pm 0.02$  nm, while the height difference between the topmost regions of the substructures and the surrounding face-centered cubic (fcc) regions is  $0.30 \pm 0.03$  nm. The two substructures correspond to ridge-like domain walls enclosing narrow strips of metastable hexagonal-close-packed (hcp) domains on the surrounding fcc surface. It was also observed that the pair of substructures constituting the DLs is terminated by a U-shaped growing tip. The photodriven growth of these DLs displayed unique dynamic surface reconstruction behavior. They also exhibited different types of collision processes depending on the growth rate. The driving force for the dynamic process is considered to be the recombination of excitons at surface defects or at the growing tip of each DL. Furthermore, a threshold light intensity value of  $0.8$  mW/mm<sup>2</sup> was found for the generation of DLs, which indicates that multiexciton relaxation is a prerequisite for the photoinduced dislocation.

**199: \* Surface-Enhanced Raman Imaging (SERI) as a Technique for Imaging Molecular Monolayers with Chemical Selectivity Under Ambient Conditions**

X. M. Yang, D. A. Tryk, K. Hashimoto, and A. Fujishima

J. Raman Spectroscopy, 29, 725-732 (1998).

Surface-enhanced Raman imaging

**200: \* Surface Functionalization of Doped CVD Diamond via Covalent Bond. An XPS Study on the Formation of Surface-bound Quaternary Pyridinium Salt**

B. Ohtani, Y. H. Kim, T. Yano, K. Hashimoto, A. Fujishima, and K. Uosaki

Chem. Lett., 953-954 (1998).

Lightly boron-doped polycrystalline diamond thin films prepared on single crystal silicon wafers via

chemical vapor deposition (CVD) were treated with chlorine ( $\text{Cl}_2$ ) under ultraviolet ( $> 200$  nm) photoirradiation and then heated in boiling pyridine. *Ex situ* X-ray photoelectron spectroscopic measurements suggested the plausible formation of surface bound chloride species and quaternary pyridinium salt by these chemical processes.

**201: \* Normally Aligned  $\pi$ -conjugated Langmuir-Blodgett Films of Oligo-acene Amphiphiles**

**K. Ishibashi, T. Iyoda, K. Hashimoto, and A. Fujishima**

Thin Solid Films, 325, 218-222 (1998).

Preparation and properties of novel oligo-acene Langmuir-Blodgett films without alkyl chain were investigated. Oligo-acene skeleton is used for the hydrophobic part, instead of conventional long alkyl chains, and substituted with weak hydrophilic groups at the 2- or 3-position. In addition to an amphiphilic balance between the hydrophilic and hydrophobic parts of the molecule, it was revealed that the number of aromatic rings and van der Waals cohesive forces in oligo-acene are crucial for stable monolayer formation. Tetracene-2, 3-dialdehyde forms stable condensed monolayer on pure water subphase. This amphiphile gave a Z-type multilayer film on a hydrophilic substrate. The absorption spectra of the multilayer indicated large intermolecular  $\pi - \pi$  interaction between the neighboring amphiphiles.

**202: \* Effect of Ultrasonic Treatment on Highly Hydrophilic  $\text{TiO}_2$  Surfaces**

**N. Sakai, R. Wang, A. Fujishima, T. Watanabe, and K. Hashimoto**

Langmuir, 14 (20), 5918-5920, (1998).

Glass surfaces coated with polycrystalline titanium dioxide ( $\text{TiO}_2$ ) films were found to exhibit a  $0^\circ$  water contact angle when the surfaces were illuminated with UV light in the air. This highly hydrophilic surface was maintained for more than 1 week in the dark in air. However, ultrasonic treatment in pure water decreased the degree of surface hydrophilicity, yielding a contact angle of approximately  $11^\circ$ . X-ray photoelectron spectroscopic measurements indicated that hydroxyl groups and molecular water adsorption, which govern the surface wettability, were partially removed from the surface by the ultrasonic treatment. The effect of ultrasonic treatment was ascribed to the generation of OH radicals that reoxidized the photoreduced surface, accompanied by the removal of surface-adsorbed water. This has been confirmed by adding acrylamide, a typical OH radical scavenger, to pure water to effectively suppress the hydrophilic-to-hydrophobic reconversion on the  $\text{TiO}_2$  surface.

**203: \* Preparation of Electrolessly Plated Au Films with High Adhesive Strength Using a TiO<sub>2</sub>-ZnO Composite Film as an Adhesive Layer**

**H. Yoshiki, K. Kanazawa, K. Hashimoto, and A. Fujishima**

Electrochem. Solid-State Lett., 1 (4), 162-164 (1998).

Electrolessly plated Au films with adhesive strength suitable for practical use were obtained on 96 % alumina substrates without etching the surface. This was accomplished through the use of a chemically stable TiO<sub>2</sub>-ZnO composite film prepared on the substrate, which serves as an adhesive layer between the substrate and the Au film. The adhesion of the electroless Au film to the substrate depended on the TiO<sub>2</sub>/ZnO ratio in the composite film. Specifically, the electroless Au film with the highest adhesive strength was obtained using a film with a molar ratio TiO<sub>2</sub>:ZnO of 8:2. The adhesive strength of the Au film on this composite film also depended on the coverage of photocatalytically deposited palladium nuclei on the TiO<sub>2</sub>-ZnO film. The adhesive strength achieved under optimal conditions was greater than ca. 3.2 kg/mm<sup>2</sup> in terms of pull strength.

**204: \* Titanium Oxide-Coated Glass: Self-Cleaning and Anti-Fogging Properties and Applications**

**A. Fujishima, D. A. Tryk, T. Watanabe, and K. Hashimoto**

International Glass Review-Flat Glass Processing, 114-116 (1998).

Glass coated with a thin film of titanium dioxide exhibits two intriguing properties when illuminated with UV light: the first is photocatalytic (light-induced) breakdown on organic compounds that come into contact with it, making it self-degreasing, and the second is a very high affinity for water, so that water does not bead up but forms a continuous sheet. Together, these properties make it possible to produce glass that is both self-cleaning and anti-fogging. Ever since the first glass window was made, people have been trying to ways to make them self-cleaning. Let's face it- few of us actually enjoy washing windows. During the last hundred years, with the advent of tall buildings, washing windows has become downright dangerous and expensive. For almost as long, people have also been trying to think of ways of making both windows and mirrors anti-fogging. During the past three years, we at the University of Tokyo have been working with the TOTO Company in Japan to develop just such technologies, and the first commercial applications are now starting to hit the market.

**205: \* New Mesostructured Porous TiO<sub>2</sub> Surface Prepared Using a Two-Dimensional Array-Based Template of Silica Particles**

S. I. Matsushita, T. Miwa, D. A. Tryk, and A. Fujishima

Langmuir, 14 (22), 6441-6447 (1998).

Mesoporous photocatalytic titanium dioxide films with periodic structures were prepared by molding from two-dimensionally ordered arrays of monodisperse SiO<sub>2</sub> particles. The morphology of the porous structures in these films was dependent upon the annealing temperature. The photocatalytic activity of the films was confirmed, as evidenced by the photodeposition of silver on the textured film surfaces. Attachment of the free-standing films to rigid supports allowed us to locate specific microscopic areas at will and to monitor the progress of the silver photodeposition in these areas using optical microscopy and scanning electron microscopy, with both secondary electron and backscattered electron detection. However, the repeated electron beam exposure in these selected areas was found to adversely affect the photoreducibility. Although the detailed film morphology did not affect the macroscopic photocatalytic activity, we found subtle differences in the silver nucleation process which depended upon the pore wall thickness.

**206: \* Formation of Catalytic Pd on ZnO Thin Films for Electroless Metal Deposition**

R. D. Sun, D. A. Tryk, K. Hashimoto, and A. Fujishima

J. Electrochem. Soc., 145 (10), 3378-3382 (1998).

The formation process of highly dispersed Pd on ZnO thin films as a catalyst for electroless metal deposition was studied in detail by means of adsorption experiments combined with X-ray photoelectron spectroscopy measurements. The chemical state of the yellow-brown species adsorbed on ZnO thin film during the catalyzation process in acidic PdCl<sub>2</sub> solution (pH 2.5) was determined to be Pd(OH)<sub>2</sub>. It was found that the adsorption of Pd on the ZnO thin film is closely related to the partial dissolution of ZnO in acidic solution, which results in an increase of the pH in the vicinity of ZnO surface, while the pH of the overall PdCl<sub>2</sub> solution remains essentially unchanged (~ 2.5) within the period of the catalyzation treatment (< 10 min). This pH increase results in partial hydrolysis of Pd-containing ions, and thus Pd(OH)<sub>2</sub> is formed near the surface of the ZnO thin film. The Pd(OH)<sub>2</sub> thus produced is then efficiently adsorbed on the ZnO surface, which has been made highly porous by its partial dissolution in the acidic solution. In the subsequent electroless metal deposition step, Pd(OH)<sub>2</sub> is first reduced to Pd<sup>(0)</sup> by the reductant, e.g., HCHO, contained in the deposition bath, and then the Pd particles act as catalytic nuclei for the deposition reaction. The Pd catalyst prepared in this fashion was found to be highly dispersed and can initiate several types of electroless metal deposition reactions.

**207: \* Photocatalytic Degradation of Gaseous Formaldehyde Using TiO<sub>2</sub> Film**

**T. Noguchi, A. Fujishima, P. Sawunyama, and K. Hashimoto**

Environmental Sci. & Technology, 32 (23), 3831-3833 (1998).

The photocatalytic degradation of gaseous formaldehyde—a major cause of sick building syndrome—was studied using a TiO<sub>2</sub> thin film. Thin films have many unique photoinduced properties, for example, self-cleaning, anti-fouling, and anti-bacterial functions. UV illumination of the TiO<sub>2</sub> thin film placed in a gaseous formaldehyde/air environment resulted in the total mineralization of formaldehyde to CO<sub>2</sub> and H<sub>2</sub>O. We invoked a Langmuir-Hinshelwood kinetic model to analyze the dependence of reaction rates on the concentration of formaldehyde. In addition, the overall decomposition rate constant for formaldehyde was comparable to that of acetaldehyde for initial concentrations of up to 1000 ppmv. However, the apparent adsorption constant  $K_{app}$  of formaldehyde onto TiO<sub>2</sub> was ca. 2.5 times larger than that of acetaldehyde. Thus in the low concentration regime, the reactivity of formaldehyde appeared to be greater than that of acetaldehyde. In like manner, a dark adsorption experiment also showed the high adsorption capacity of TiO<sub>2</sub> for formaldehyde. Therefore, we conclude that TiO<sub>2</sub> serves as both a good adsorbent and a photocatalyst for the elimination of gaseous formaldehyde.

**208: \* Photoelectrochemical Reduction of CO<sub>2</sub> in a High-Pressure CO<sub>2</sub>+Methanol Medium at p-Type Semiconductor Electrodes**

**K. Hirota, D. A. Tryk, T. Yamamoto, K. Hashimoto, M. Okawa, and A. Fujishima**

J. Phys. Chem. B, 102 (49), 9834-9843 (1998).

Photoelectrochemical CO<sub>2</sub> reduction was examined in a high-pressure (40 atm) CO<sub>2</sub>+ methanol medium using the p-type semiconductor electrodes p-InP, p-GaAs, and p-Si. With the p-InP photocathodes, current densities up to 200 mA cm<sup>-2</sup> were achieved, with current efficiencies of over 90% at low levels. At high current densities and CO<sub>2</sub> pressures, the CO<sub>2</sub> reduction current was found to be limited principally by light intensity. Of the various factors that were found to influence the product distribution, including the concentrations of added water and strong acid, CO<sub>2</sub> pressure was the most critical factor. We propose that the adsorbed (CO<sub>2</sub>)<sub>2</sub> radical anion complex reaches high coverages at high CO<sub>2</sub> pressure and is responsible for both the high current efficiencies observed for CO production and the low values observed for H<sub>2</sub> evolution. Furthermore, we propose that this adsorbed complex is responsible for stabilizing all three semiconductor electrode materials at high CO<sub>2</sub> pressures, even at current densities as high as 100 mA cm<sup>-2</sup>.

**209: \* Grain Size of a Hard Molecule-Based-Magnet of Manganese Porphyrin-Tetracyanoethylene Charge Transfer Salt**

**K. Nagai, L. Jiang, T. Iyoda, A. Fujishima, and K. Hashimoto**

Thin Solid Films, 331, 165-169 (1998).

This paper describes one-dimensional charge-transfer-type manganese porphyrin-tetracyanoethylene as the hardest molecule-based-magnet. The coercive forces of the magnets consisting of manganese (tetraphenylporphyrin)(MnTPP) and manganese (tetraethoxyphenylporphyrin)(MnTEtOPP) were 8000 Oe and 20000 Oe at 2 K, respectively. The high coercive forces resulted from their metamagnetism, where both interchain ferromagnetic and antiferromagnetic interactions are balanced. Although the saturation magnetization of millimeter size crystal of MnTPP-TCNE is equal to that of powder, the initial magnetization processes are different owing to their domain structures. Almost consistent domain size of several decade nanometers was estimated from the powder X-ray diffraction and atomic force microscopy. Conventional relationships between the coercive force and the domain size hold true in the present molecule-based magnets.

**210: \* Mosbauer Study on Characterization of  $\text{Co}[\text{Fe}(\text{CN})_5\text{NH}_3] \cdot x\text{H}_2\text{O}$** 

**Y. Einaga, Z. Z. Gu, Y. Kobayashi, O. Sato, T. Iyoda, F. Ambe, K. Hashimoto, and A. Fujishima**

Hyperfine Interaction, 116, 159-166 (1998).

The electronic states of Fe atoms in  $\text{Co}[\text{Fe}(\text{CN})_5\text{NH}_3] \cdot x\text{H}_2\text{O}$  were studied by means of  $^{57}\text{Fe}$  Mosbauer spectroscopy. The Mosbauer spectra of  $\text{Co}[\text{Fe}(\text{CN})_5\text{NH}_3] \cdot 6\text{H}_2\text{O}$  show the coexistence of mixed valences for the Fe atoms and a magnetic relaxation at 4 K. When water molecules were removed, electron transfer from Co to Fe occurred.

**211: \* Continuous-Flow Photoreactor Packed with Titanium Dioxide Immobilized on Large Silica Gel Beads to Decompose Oxalic Acid in Excess Water**

**K. Kobayakawa, C. Sato, Y. Sato, and A. Fujishima**

J. Photochem. Photobiol. A: Chem., 118, 65-69 (1998).

A tubular continuous-flow photoreactor consisting of a pyrex glass tube 8mm in diameter packed with titanium dioxide photocatalyst immobilized on 2mm diameter silica gel beads was constructed to

efficiently decompose water contaminants at high-flow rate. To fix titanium dioxide using sol-gel without destroying silica gel beads, the beads were exposed to ethanol vapor and then wetted with ethanol before being dipped into the TiO<sub>2</sub> precursor sol. Photoreactor performance was evaluated for how it decomposed aqueous oxalic acid solution as a model contaminant.

**212: \* Influence of the Rotation Rate of a Rotary Viscometer on the Photoelectrorheological Properties of TiO<sub>2</sub> Particle Suspensions**

**Y. Komoda, T. N. Rao, D. A. Tryk, and A. Fujishima**

J. Electroanal. Chem., 459, 155-165 (1998).

The influence of the rotation rate of a rotary viscometer on the photoelectrorheological (PER) properties of two types of TiO<sub>2</sub> powder dispersed in silicone oil was investigated. Type P-25 TiO<sub>2</sub> (water content, 1.2wt %) particle suspensions exhibited a positive photoeffect on the viscosity, i.e. the combination of UV illumination and an electric field produced a larger increase in the fluid viscosity than that produced by the electric field alone. The positive effect was enhanced with increasing rotation rate. Type ST-01 TiO<sub>2</sub> (water content, 10 wt %) particle suspensions exhibited behavior in which there was a negative photoeffect (UV illumination produced a decrease in the field-enhanced viscosity) when the rotation speed was low ( $\leq 50$  rpm), and a positive photoeffect when the rotation speed was high ( $\geq 100$  rpm).

**213: \* Effect of ZnO Film Thicknesses on the Adhesive Strength of Electroless Cu Deposits**

**R. D. Sun., D. A. Tryk, K. Hashimoto, and A. Fujishima**

Chem. Lett., 11-12 (1999).

The effect of ZnO film thickness on the adhesive strength of electrodes Cu deposited on ZnO-coated glass substrates was examined. An increase of adhesive strength of the Cu deposits with increasing ZnO film thickness was observed. Excellent adhesion was obtained on ZnO films thicker than 0.6  $\mu\text{m}$ , which is considered to be associated with the formation of rougher, more porous structures. XPS data combined with SEM and AFM measurements showed that in addition to the surface area effect, the mechanical anchoring effect caused by Cu depositing deeply within the ZnO film may also play an important role in obtaining the excellent adhesion of the Cu deposits on thicker ZnO films.

**214: \* ZnO Thin Film-Based New Electroless Metal Deposition**

**R. D. Sun, H. Yoshiki, D. A. Tryk, K. Hashimoto, and A. Fujishima**

Electrochemistry, 67 (1), 11-17 (1999).

Electroless metal deposition plays an important role in the fabrication of printed circuit boards mainly due to its ability to produce uniform metal films on insulating substrates (e.g. ceramics, glass, polymers). However, the adhesion of the electrolessly deposited metal films, particularly coinage metals (Cu, Ag, Au) on ceramic substrates is usually poor, even on roughened substrates. Nevertheless, using our newly developed electroless metal deposition process, which is characterized by the use of a ZnO thin film as an intermediate layer between the substrate and the metal deposit, metal films with high adhesive strength can be achieved, even on smooth glass substrates. In addition, this new process possesses the advantage of 1) simple processing procedures and 2) the ability to fabricate fine metal patterns in a fully additive fashion based on the photosensitivity of the ZnO films. New functions based on this process have been discovered in our recent research. In the present paper, the processing steps involved in this new method, the formation mechanism of catalytic Pd particles, the adhesion mechanism, as well as its possible applications in pattern fabrication, are briefly reviewed, based on our recent work.

**215: \* Electrochemical Reduction of  $\text{Cu}^{2+}$  without Surface Trapping on Synthetic Conductive Diamond Electrodes**

**S. Nakabayashi, D. A. Tryk, A. Fujishima, and N. Ohta**

Chem. Phys. Lett., 300,409-413 (1999).

The electrochemical reduction of metal ions is commonly referred to as electrodeposition because the reduced metal is trapped on the surface, and a new solid phase is formed. We present evidence for a clear deviation from this general concept on the conductive boron-doped CVD diamond electrode, where the electrochemical reduction of copper proceeds with negligible deposition of the metal on the electrode and the product is a colloid composed of the metal clusters.

**216: \* Band-Edge Movements of Semiconducting Diamond in Aqueous Electrolyte Induced by Anodic Surface Treatment**

**T. N. Rao, D. A. Tryk, K. Hashimoto, and A. Fujishima**

J. Electrochem. Soc., 146 (2), 680-684 (1999).

Photoelectrochemical characterization of semiconducting diamond was carried out in a weakly UV-absorbing aqueous electrolyte using suprabandgap illumination in order to examine the influence of electrochemical oxidative surface treatment on the energetic positions of bandedges. Anodic treatment of diamond photoelectrodes resulted in a positive shift in both the photocurrent onset potential and the flatband potential obtained from Mott-Schottky plots, indicating the displacement of the bandedges. A corresponding increase in the photovoltage was also observed. The pH dependence of the flatband potential of anodically treated diamond indicates an acid-base equilibrium at the interface, suggesting the formation of oxygen-containing groups. The presence of the latter was confirmed using X-ray photoelectron spectroscopy. These results suggest that the changes in the potential drop in the Helmholtz layer are due to oxygen functional groups, and the loss of surface and subsurface hydrogen are mainly responsible for the observed shifts in the flatband potentials.

**217: \* Photoelectrodeposition of Copper on Boron-Doped Diamond Films: Application to Conductive Pattern Formation on Diamond. The Photographic Diamond Surface Phenomenon**

**S. Yoshihara, K. Shinozaki, T. Shirakashi, K. Hashimoto, D. A. Tryk, and A. Fujishima**

*Electrochimica Acta*, 44, 2711-2719 (1999).

The photoelectrodeposition of copper on semiconducting B-doped films was investigated. There were clear morphology differences between photoelectrodeposited and electrodeposited copper. Photoelectrodeposition proceeded by a uniform two-dimensional growth process, whereas electrodeposition involved isolated random deposition. By applying this effect we have succeeded in forming a conductive copper pattern on semiconducting B-doped diamond with the aid of a photo-mask. Interestingly, it was further found that changes occurring on the diamond surface during photoelectrochemical polarization in the absence of copper in solution facilitate subsequent copper electrodeposition in the dark, possibly due to the formation of subsurface hydrogen. We refer to this as the photographic diamond surface phenomenon.

**218: \* Selective Electrochemical Detection of Dopamine in the Presence of Ascorbic Acid at Anodized Diamond Thin Film Electrodes**

**E. Popa, H. Notsu, T. Miwa, D. A. Tryk, and A. Fujishima**

*Electrochem. Solid-State Lett.*, 2 (1), 49-51 (1999).

Selective highly stable determination of dopamine (DA) was achieved in cyclic voltammetric and chronoamperometric measurements carried out at electrochemically treated conductive diamond film electrodes. The treated electrodes exhibited substantial shifts in the positive direction for the peak potential

for ascorbic acid (AA) oxidation, thus making it possible to discriminate between the DA and AA responses. Linear calibration curves were obtained for both a lighter concentration range (1-70  $\mu\text{M}$  DA, 1 mM AA) and a lower range (0.1-1  $\mu\text{M}$  DA, 0.1 mM AA) using voltammetry and chronoamperometry respectively. The detection limit appears to be on the order of 50 nM, which is among the lowest values reported thus far. Selectivity was also achieved in pH 7.0 aqueous solution using more stringent electrochemical treatment but the effect was relatively short-lived.

**219: \* Electrochemical Behavior of Highly Conductive Boron-Doped Diamond Electrodes for Oxygen Reduction in Acid Solution**

**T. Yano, E. Popa, D. A. Tryk, K. Hashimoto, and A. Fujishima**

J. Electrochem. Soc., 146 (3), 1081-1087 (1999).

The electrochemical behavior of highly conductive, boron-doped polycrystalline diamond thin films for oxygen reduction was examined in 0.5 M  $\text{H}_2\text{SO}_4$  using linear sweep voltammetry. When the potential sweep is confined to the region negative of 0.0 V vs. Ag/AgCl oxygen reduction is highly inhibited with cathodic current being observed at -0.6 V vs. Ag/AgCl, as compared with the standard potential for the two-electron reduction of oxygen ( $\text{O}_2 + 2\text{H}^+ + 2\text{e}^- = \text{H}_2\text{O}_2$ ,  $E^\circ = 0.47$  V vs. Ag/AgCl at pH 0). The extreme inhibition of oxygen reduction may be due to an absence of catalytic sites. When the potential is swept to potentials positive +1.4 V vs. Ag/AgCl the subsequent sweep into the negative region shows a reduction peak due to oxygen reduction. In this case, catalytic oxygen-containing functional groups can be formed on  $\text{sp}^2$  carbon impurities. Relatively mild conditions are required to deactivate the catalytic functional groups, but strong oxidative treatment in base appears to substantially remove the  $\text{sp}^2$  carbon impurities. The oxygen reduction behavior in acid solution could be useful in characterizing diamond electrodes, i.e., as a diagnostic for the presence of  $\text{sp}^2$ -type carbon on chemical-vapor-deposited diamond thin-film electrodes. It is proposed that diamond electrode surfaces free of  $\text{sp}^2$  carbon are highly insensitive to oxygen, which could be a useful feature in electroanalysis.

**220: \* Studies of Surface Wettability Conversion on  $\text{TiO}_2$  Single-Crystal Surfaces**

**R. Wang, N. Sakai, A. Fujishima, T. Watanabe, and K. Hashimoto**

J. Phys. Chem. B, 103 (12), 2188-2194 (1999).

Reversible surface wettability conversion on titanium dioxide ( $\text{TiO}_2$ ) single crystals has been achieved, and its mechanism has been examined by means of contact angle measurement and X-ray photoelectron spectroscopy (XPS). A UV light illuminated  $\text{TiO}_2$  single-crystal surface exhibited a  $0^\circ$  contact angle for both water and oil, indicative of a highly amphiphilic surface against its native hydrophobic surface. This was ascribed to photoreduction of surface  $\text{Ti}^{4+}$  to  $\text{Ti}^{3+}$  at definite sites, leading to preferential adsorption

of dissociative water on top. A long-term storage of the highly amphiphilic surface resulted in reconversion of the surface wettability. It was found that the amphiphilic-to-hydrophobic reconversion is due to the replacement of the adsorbed hydroxyl groups by oxygen, which returns the surface geometric and electronic structures similar to the native  $\text{TiO}_2$  surface. The result of angle-resolved XPS measurement revealed that the surface reactions occurred at the uppermost layers of the single crystals. By comparing the reactivities of (110), (100), and (001) single-crystal surfaces, it was concluded that oxygen bridging sites played an important role in the surface wettability conversions.

### III Department of Energy Conversion Science

(エネルギー変換科学専攻)

#### 221: Effect of Exhaust Gas Recirculation and Injection Pressure on Exhaust Emissions from a Diesel Engine

**Makoto Ikegami, Takuji Ishiyama, Koichiro Nakatani, Tomohiro Ohtani, Shunsaku Nakai**

Proc. Int. Symp. COMODIA98, pp87-92, 1998

To clarify optimal combination of high-pressure injection and exhaust gas recirculation (EGR) for simultaneous reduction of nitric oxides (NO<sub>x</sub>) and particulate (PM) emissions in the diesel engine exhaust, experimental and theoretical studies were performed on a single cylinder test engine. The measured tendencies of NO<sub>x</sub> and PM were evaluated in terms of spray characteristics under various injection conditions and of exhaust recirculation rate. The results suggest that enhancement of air entrainment and turbulent mixing effectively reduce the PM without deterioration of NO<sub>x</sub> at a high exhaust recirculation rate. From an analysis based on a stochastic diesel combustion model, this phenomenon is caused by a change of maximum temperature at which the mixture can arrive.

#### 222: Spatial Distribution of Initial Droplets of a Diesel Spray

ディーゼル噴霧の初期液滴群の空間分布

**Kei Miwa<sup>1)</sup>, Takuji Ishiyama, Liu Yumin<sup>2)</sup>, Tomohiro Okubo<sup>3)</sup>**

**1) The University of Tokushima, 2) Isuzu Ceramics Reseach Co.Ltd., 3) Miurakogyo Co.Ltd.**

Trans. Jpn. Soc. Mech. Eng. (B), Vol.64, No.624, pp.2715-2721, 1998

日本機械学会論文集(B編), 64巻, 624号, pp.2715-2721, 1998

Spatial characteristics of fine droplets formed at an initial injection stage has a great influence on mixture formation and ignition of diesel sprays. In this paper, a size and shape of each droplet near a nozzle tip has been analyzed by the back light illumination photography using a nano-spark light technique. The results show that fine droplets are formed immediately after 50 microseconds from the commencement of the injection near the nozzle tip regardless of different nozzle hole sizes. Then, at the early stage of the injection period, the structure like a branch occurs at the periphery of a dense spray behind a spray tip and a number of the droplets were produced in this region. (in Japanese)

**223: Reduction of Nitrogen Oxides of Diesel Engines by Exhaust-Gas-Selective Recirculation**

**Masanori Fukuda<sup>1)</sup>, Koji Yamane<sup>2)</sup>, Tohru Neichi<sup>3)</sup>, Makoto Ikegami**

**1) Tsuyama College of Technology, 2) The University of Shiga Prefecture, 3) Mitsubishi Motors Co.Ltd.**

Proc. Int. Symp. COMODIA98, pp93-98,1998

Exhaust-gas-selective recirculation is proposed for the purpose of reducing the emission of nitrogen oxides from diesel engines. In this method, either carbon dioxide or water is extracted from the exhaust gas and is fed directly into the intake air. These gases work to decrease the combustion temperature due to their greater heat capacities, thereby reducing the exhaust oxides of nitrogen remarkably. Therefore, it is expected that a diesel engine with exhaust-water-selective recirculation, EWR, may achieve a reduction in NO while maintaining thermal efficiency and exhaust particulates. In the case of exhaust-carbon-dioxide-selective recirculation, ECDR, a greater NO reduction might be attained with less amount of recirculating gas than EWR, although the ECDR requires a complicated system because of the difficulty in regenerating carbon dioxide.

**224: \* Flame Stability and NOx Formation in a High-Intensity Swirl Burner**

強旋回流バーナの火炎安定性および NOx 生成

**Masahiro SHIOJI, In-Su KIM, Makoto IKEGAMI, Kensuke MURAKAMI**

Trans. Jpn. Soc. Mech. Eng. (B), Vol.64, No.621, pp.1506-1511, 1998

日本機械学会論文集 (B 編), 64 巻, 621 号, pp.1506-1511, 1998

Flame modes and blow-off limits at a high-intensity swirl burner are systematically studied by changing swirl intensity, fuel-flow rate, nozzle structure, the length of combustion tube and combustor pressure. Result shows that there exists a critical point( $S=0.6$ ) above which high-intensity swirl well stabilizes the flame even at an elevated combustor pressure. A further investigation of the NOx concentration in relation to the swirl intensity shows that a stronger swirl has a capability to reduce NOx level especially with the nozzle which discharges fuel to the vertical direction under atmospheric condition. The nozzle which discharges fuel to the horizontal direction shows the lowest NOx level(when  $\phi \geq 0.8$ ,  $S=3.2$ ) and the most wide lean burn combustion range among three types of nozzles tested under atmospheric condition. As combustor pressure is elevated, the position of maximum NOx shifts toward to the fuel lean range. (in Japanese)

**225: \* CFD Simulation for Predicting Combustion and Pollutant Formation in a Homogeneous-Charge Spark-Ignition Engine****Hiroshi Kawanabe, Masahiro Shioji, Takashi Tsunooka, Yusoff Ali\*****\* Department of Mechanical Engineering UKM ,Malaysia**

Proc. Int. Symp. COMODIA98, pp233-238, 1998

A Flame Area Evolution (FAE) model was integrated into a CFD simulation program so as to predict combustion and pollutant formation in homogeneous-charge spark-ignition engines. Gas flows and combustion in a natural-gas engine was simulated by a fully three-dimensional numerical calculation with FAE model and k-e turbulence model. Pressure changes were successfully reproduced with those measured in the corresponding experiments for a variety of conditions. Based on the spatial profiles of velocity, local heat-release rate, temperature and the local production rate of NO, effects of gas flows and turbulence on flame propagation and pollutant formation were investigated with special attention to the mixing of heat and mass. In addition, the wall- quenching effect was also investigated to elucidate the mechanism of formation of unburned hydrocarbon in the combustion processes.

**226: Discussion on Accuracy of PIV Measurement****H. Kawanabe, M. Shioji, K. Kawasaki**

Proc. of the 3rd Japan-Central Europe Joint Workshop on Modelling and Simulation of Non-linear Engineering Systems and Related Phenomena, pp222-225, 1998

Accuracy of PIV (particle image velocimetry) is assessed using simulated images to clarify the advantage of the cross-correlation method. The results show that to suppress an error due to appearance and disappearance of particles, it is desirable to distribute particles uniformly in the test section, whereas to suppress an error due to random motions and rotational motions, heterogeneous particle- distribution is preferable. Furthermore, time- sequential analysis is attempted to obtain mean velocity and turbulence intensity and the results are compared with the HWA (hot-wire anemometry) measurement to assess the accuracy of PIV measurement.

**227: Performance and NO<sub>x</sub> Formation in a Hydrogen Premixed-Charge Engine****Masahiro Shioji, Naoki Inoue**

Proc. of the 12th World Hydrogen Energy Conference, pp1469-1478, 1998

This study demonstrates the feasibility of a hydrogen premixed-charge spark-ignition engine with special attention paid to a rapid combustion due to the large burning velocity of hydrogen mixture. Engine performance and NO<sub>x</sub> emissions are experimentally investigated using a single-cylinder test engine for a set of parameters. A hydrogen engine can smoothly operate in a very lean mixture with low NO<sub>x</sub> level, whereas the extremely rapid combustion causes not only an abnormal combustion but also a lower thermal efficiency due to an increase in heat loss. The improvement of the engine performance can be attained in the case when the diluted hydrogen fuels with nitrogen and the water injection into hydrogen mixture are employed so as to suppress a rapid combustion. Also, a backfire is never observed at the dilution fuels. In addition, NO<sub>x</sub> formation are theoretically discussed based on a thermodynamic model using the measured rates of heat release, in which the histories of temperature distribution and NO<sub>x</sub> concentration are well calculated.

**228: Gas-Flow Measurements in a Jet Flame Using Cross-Correlation of High-Speed Particle-Images**

**Masahiro Shioji, Kiyoshi Kawasaki, Hiroshi Kawanabe, Makoto Ikegami**

5th ASME-JSME Thermal Engineering Joint Conference, pp283, March 15-19, 1999

Time changes of a two-dimensional distribution of velocities in a methane jet flame and a nitrogen jet are measured by cross-correlation particle image velocimetry (PIV). From the measured results in a jet flame and a cold jet, it is shown that the velocity gradient at the shear layer in the reacting zone is increased due to the local acceleration by buoyancy, resulting in higher turbulence intensities compared with those in a non-reacting jet. Also, from the change of the distribution of velocity vectors with time, it is observed that the turbulence eddies are carried downstream along the gas motion with a little transformation. The time scale of turbulence at every location in the flow is obtained from the autocorrelation function of the velocity fluctuations. Furthermore, this also allows estimation of the turbulence length-scale. It is shown that the characteristic length-scales of a flaming jet are about 1.5 times greater than those of a non-flaming jet.

**229: \* A Laminar Flamelet Model for Turbulent Pre-mixed Combustion**

乱流予混合燃焼の層流火炎片モデル

**Masahiro SHIOJI Hiroshi KAWANABE Makoto IKEGAMI Kenichi KASE**

Trans. of JSME B, 65-631, 1089-1094, 1999-3.

日本機械学会誌 (B 編), 65-631, 1089-1094, 1999-3

A fully three-dimensional numerical model for the combustion process in a spark-ignition engine was established using the combustion submodel described of the flame area evolution. Computations carried out the process of premixed combustion and they were compared with the results using the combustion submodel of the eddy break-up. The combustion in a disc-chamber of constant volume was simulated.

The results show that the course of flame propagation is well predicted. The calculations for different conditions in a natural-gas engine are performed. It is shown that the effects of fuel-air equivalence ratio and swirl intensity on flame propagation are described. The cylinder pressure histories are agreed with measured one, and the distributions of velocity vectors and temperature in a cylinder are revealed.

**230: \* Performance and NO<sub>x</sub> Formation in a Hydrogen Premixed-Charge Engine**

**Masahiro Shioji Naoki Inoue**

Proc. of the 12th World Hydrogen Energy Conference, 1469-1478, 1998.

**231: \* Deformation of Spherical Living Tissue Cells by Using Shock Waves**

**Masaaki Tamagawa, Teruaki Akamatsu**

Proc. of the 3rd World Congress of Biomechanics, Sapporo, p.405, 1998

In this study, the damage experiments of the living tissue cells (red blood cells and cancer cells) [M. Tamagawa and T. Akamatsu, Proc.20th Int. Shock Wave Symp., Pasadena, USA, 517-518 (1995)], and the experimental model for cells (microcapsules including dye stuff) by plane shock waves are executed. It is shown from the results that using a microcapsule is an effective method for sensing injury to living tissue cells. To explain these phenomena, the living tissue cells are modeled mathematically as one and two spherical elastic shells filled with liquid toward the shock wave. Using stationary and transient analysis of a spherical shell, the dynamic characteristics of the one living tissue cell and two with a mutual interaction are evaluated. The results show that damage to living tissue cells depends on: (1) the elastic modulus of the cell, (2) the bulk modulus of intracellular material, (3) the thickness of the cell membrane, (4) the distance between the cells on shock-induced damage, and (5) the rise time of the shock wave.

**232: \* Macro- and Microscopic Simulation of Materio-Thermo-Mechanical Fields**

**Tatsuo Inoue**

Metals and Materials, Vol.4, No.3, pp.227-234, 1998

Two kinds of computer simulation are made for some engineering processes incorporating phase transformation. One is the macroscopic or continuum mechanics approach based on the theory of metal-thermo-mechanics developed by the authors, and the other is the microscopic, or atomic level simulation

by use of molecular dynamics. In each case, emphasis is focussed on the effect of coupling among material structures, temperature and stress/strain during in- solid or liquid-solid phase transformations. Some illustrative examples are presented.

**233: \* Computer Simulation of Residual Stresses/distorsion and Structural Change in the course of Scanning Induction Hardening**

高周波移動焼入れ過程における残留応力・ひずみおよび組織のコンピューターシミュレーション

**Fumiaki Ikuta\***, **Takashi Horino\***, **Tatsuo Inoue** \*Neturen Co.

J. Society of Materials Science, Japan, Vol.47, No.9, pp.892-898, 1998

材料, 47 卷, 9 号, pp.892-898, 1998

Simulated results of structure change, residual stresses and distorsion are presented for carbon steel cylinder in the scanning type induction hardening process by a CAE system HEARTS. The results under different scanning velocity as well as the magnitude and pattern of the heat source from induction coil are compared with the experimental data of distorsion, volume fraction of martensite phase as well as residual stresses. (in Japanese)

**234: Residual Stress and Distortion — Metallo-thermo-mechanics Simulation of Engineering Processes incorporating Phase Transformation**

**Tatsuo Inoue**

Mathematical Modelling of Weld Phenomena, (ed. H. Cerjak), Vol.4, pp.547-575, 1998

Governing equations for the evolution of metallurgical structures, temperature, and stress/strain relevant to describing both in-solid and liquid- solid phase transformation are presented by taking into account the effect of metallo-thermo-mechanical coupling. The inelastic constitutive equations are established and applied to numerical simulation of some engineering processes such as quenching, welding and casting by means of the finite element technique.

**235: Stress-strain Relation of CuAlNi SMA Single Crystal under Biaxial Loading - Constitutive Model and Experiments**

**D.N. Fang\***, **W. Lu\***, **W.Y. Yan\***, **K.C. Hwang\***, **T. Inoue**

\* Tsinghua University

Acta Materialia, Vol.48. No.1, pp.269-280, 1999

In the previous work of one of the authors, a generalized micromechanics constitutive model was developed to describe thermoelastic martensitic transformation. In order to verify the theory and to investigate basic properties of thermoelastic martensitic transformation in shape memory alloys, uniaxial and biaxial loading tests under different combined loads at a constant temperature were performed on cruciform specimens of a SAM CuAlNi single crystal. The crystallographic theory for martensitic transformation has been employed to calculate the orientations of martensite variants and the transformation plastic strain. Experimental data were compared with theoretical calculation based on the generalized micromechanics constitutive model. The results show that the constitutive theory can describe the complex thermodynamic processes, such as the forward transformation, reverse transformation and reorientation happening simultaneously, and the theoretical predictions consist well with experiments.

**236: \* Simulation of Dual Frequency Induction Hardening Process of a Gear Wheel**

**Tatsuo Inoue, Hiroyuki Inoue, Fumiaki Ikuta\*, Takashi Horino\***

**\* Neturen Co.**

Proceedings of the 3rd International Conference on Quenching and Control of Distortion, Prague, pp.243-250, 1999

As one of efficient methods to harden the surface of a gear wheel, the induction heating technique with two different frequency is applied: The gear is induction-heated by medium frequency to the deep region for several seconds and is reheated by high frequency for so short period only on the surface followed by quenching by water spray. The pattern of frequency used in the present experiments is 3kHz for 1.8sec in preheating and 150kHz for 0.18sec during subsequent heating. This new technique provides the thin-surface hardening with little distortion and high compressive residual stress which leads to long durability. The paper motivate to simulate the metallo-thermo- mechanical fields as well as magnetic field to evaluate heat generation during the heating and quenching process by use of the developed code HEARTS for heat treatment simulation and also MAGNA for electromagnetic field analysis. Some results of the transformed microstructures, residual stresses and distortion of a spur gear are compared with the experimental data, and careful discussion is made for the advantage of the technique relative to the conventional one with a single frequency of 25kHz for 2.8sec.

**237: \* Progress of Phase Boundaries and Walls in Thermo-deformable Solids: A Canonical Approach**

**Gerard Maugin\*, Tatsuo Inoue**

**\* University of Paris VI**

Proceedings of EUROMECH-MECHAMAT : 3rd European Mechanics of Materials Conference, Oxford, 1998

Four approaches at different scales or levels of understanding are proposed to study the propagation

of phase boundaries and domain walls in thermo-deformable solids ; (i) a microscopic one relying on the lattice model that yields the representation of the thin transition zone as a solitonic structure, (ii) a thermodynamic macroscopic one that is based on the use of jump relations associated with the canonical formulation of continuum mechanics on the material manifold, (iii) a mesoscopic continuum approach using directly a mixed viscosity-strain-gradient modelling, and (iv) a global quasi-particle viewpoint which, although accounting structure of the transition zone, is also canonical and allows for the study of transient motions of these zones, The common points and respective ineterests of the approaches are discussed.

**238: \* Molecular Dynamics Simulation of Change in Surface Shape and Microstructure of Thin Film during Melting and Solidification Process**

薄膜の溶融・凝固過程における表面形状と微視構造変化の分子動力学シミュレーション

**Takuya Uehara, Tatsuo Inoue**

Trans. Japan Soc. Mech. Eng., Vol.64, No.626, pp.2448-2455, 1998

日本機械学会論文集 A 編, Vol.64, No.626, pp.2448-2455, 1998

Changes in surface shape and microstructure of thin film induced by heating and cooling are simulated by means of molecular dynamics method. A simple three-dimensional model of iron atoms as an example of bcc metal with periodic boundary condition is employed to identify the temperature for melting and crystallization and the rate by use of Finnis-Sinclair potential function. Following simulations of heating and cooling of thin film are carried out with a model which has free surface and fixed boundary in one direction and periodic boundaries in other two directions being a model of optical disk of phase-change type such as DVD system. A rippled shape is observed when a concentrated part of the surface heated to be molten state, while planer surface is achieved by flat heat source. Such difference comes from the surface tension and surface energy. The surface tension decreases as increasing temperature, and the tension of solidified crystal reveals to be larger than that of liquid. The potential energy near the molten surface takes higher value comparing to the bulk, and it may minimize the surface area. Amorphous structure is obtained by rapid cooling in the molten region while it becomes crystal by moderate cooling, which causes the small amorphous spot on the surface corresponding to a memory digit, and the digit vanishes by the subsequent reheating. (in Japanese)

**239: \* Molecular Dynamics Simulation of Melting/Solidification and Induced Stresses**

**Tatsuo Inoue, Takuya Uehara**

Proceedings of IUTAM Symposium on Variations of Domain and Free-Boundary Problems in Solid Mechanics, pp.103-111, 1998

Molecular dynamics simulations are carried out to investigate the microscopic, or atomic scale mechanism of melting/solidification in relation to the macroscopic *materio-thermo-mechanics*. A simple model

with 2-D array of atoms is treated, and uniform temperature distribution is considered. After evaluating the melting point and some other material properties for the model, mode of volume dilatation and generation of latent heat due to melting and hysteresis of temperature are simulated. The results represent that the feature of phase transformation depends on heating and cooling rates. Simulation of non-uniform heating process is followed where thermal stress is induced. The variation of temperature is compared with the solution of normal heat conduction equation, which shows good correspondence with MD simulation.

**240: \* Phase Transformation and Related Thermo-Mechanical Behavior — A Molecular Dynamics Approach**

**Tatsuo Inoue, Takuya Uehara**

Proceedings of EUROMECH-MECHAMAT : 3rd European Mechanics of Materials Conference, Oxford, 1998

Melting and solidification behaviour is simulated by the molecular dynamics method in order to investigate the complicated phenomena associated with the process such as volume dilatation and generation of latent heat. The effect of latent heat on the variation of temperature is evaluated during homogeneous and inhomogeneous heating; Fundamental characteristics are clarified in the homogeneous heating, and thermal stresses are evaluated in the latter case caused by induced temperature gradient. Simulated result of microscopic heat conduction is compared with macroscopic one by solving the original heat conduction equation. Both results are proved to correspond with each other when they are plotted against non-dimensional time or Fourier number

**241: \* Simulation of Materio-Thermo-Mechanical Fields — Macro- and Microscopic Approach**

**Tatsuo Inoue, Takuya Uehara**

Proc. 7th JSPS-VCC Seminar on Integrated Eng., pp.257-262, 1998

Two kinds of computer simulations are made for some engineering processes incorporating phase transformation. One is the macroscopic or continuum mechanics approach based on the theory of metal-thermo-mechanics developed by the authors, and the other is the microscopic or atomic-level simulation by use of the molecular dynamics method. In each case, emphasis is focused on the effect of coupling among material structures, temperature and stress/strain during in-solid or liquid-solid phase transformations. An example of macroscopic simulation, the quenching process of a Japanese sword is simulated, and it is revealed that the variation of temperature and martensitic and pearlitic transformation causes the complicated change in distortion and stress distribution in quenching process. Melting and solidification on a thin-film surface is taken as an example of microscopic simulation, and the changes in the

microstructure and surface shape are simulated which corresponds to the data-recording/erasing process on a phase-change optical disk.

**242: \* Experiment and Simulation for Thick-Plate Bending by High Frequency Inductor**

**Shoji Imatani, Yasuhiro Okuno, Tatsuo Inoue**

Proceedings of 3rd Sino-Japanese Bilateral Symposium on High Temperature Strength of Materials, pp.120-125, 1998

In order to produce thick plate with complicated curved surface, a prototype bending machine by use of high frequency inductor is developed. The bending mechanism is based on the localized thermal stresses which are induced from the difference of temperature in thickness by the high frequency inductor. The operating speed and the thickness of plate are examined from the experiment, and the variation of temperature is measured. Finite element analysis is carried out, in the second part, based on the experimentally obtained temperature distribution. So-called "Mindlin plate element" is used in order to perform the simulation efficiently. We discuss the strategy to produce such curved surface in the practical process and describe further perspective of the production system.

**243: \* Stress Analysis of Quenching Process Following Draw Forming**

**Shoji Imatani, Tatsuo Inoue**

Proceedings of EUROMECH 385 Colloquium on Inelastic Analysis of Structures under Varying Loads, pp.161-163,1998

Several steps of forming processes, such as casting, drawing as well as heat treatment are successively carried out for the materials utilized in structural components. Since residual stresses are inevitably induced through each step of the processes, the final products undergo very complicated thermo-mechanical loading history. This paper deals with the stress analysis of both prior draw forming and subsequent quenching processes on axisymmetric bars. The discussion is focused on the effect of residual stresses in the prior draw forming on the final properties of the material through the quenching process.

**244: Measurement of Static Strain Distribution Using Piezoelectric Polymer Film (Principle and Application to a Holed Plate)****Keisuke Katsumi<sup>†</sup>, Shiro Biwa<sup>†</sup>, Eiji Matsumoto, Toshinobu Shibata<sup>†</sup>****<sup>†</sup> Graduate School of Engineering, Kyoto University**

JSME International Journal, Ser.A, Vol.42, No.1, pp.11-16, 1999

The objective of the present study is to exploit the feasibility of piezoelectric polymer film sensors to evaluate in-plane strain distributions of structural components. In contrast to ordinary use of piezoelectric films as strain and strain-rate sensors detecting electric charges and currents potentials induced in the piezoelectric film mounted on the surface of a structural component in account the piezoelectric constitutive law of film materials. As an illustrative example, thin films of polarized polyvinylidene fluoride (PVDF) are mounted on a holed elastic plate subjected to in-plane loading, and the induced potential distributions are measured on the film surface by an electrostatic voltmeter of non-contact type. It is demonstrated that the determined strain distributions are in fair conformity with those analytically predicted.

**245: Stress Magnetization Properties of Low Carbon Steel (SM490A) and Ni****Tadafumi Nishimura<sup>†</sup>, Eiji Matsumoto, Toshinobu Shibata<sup>†</sup>****<sup>†</sup> Graduate School of Engineering, Kyoto University**

Proceedings of the Seventh Magnetodynamics Conference, pp.211-214, 1998

Magnetization change of ferromagnetic materials due to stress under constant magnetic field is studied as well as the stress dependence of the magnetization curve. Such magnetoelastic properties are not known so well for structural steel and Ni as silicon steel. It is found that the magnetizations of low carbon steel (SM490A) and Ni under constant magnetic field show the hysteresis according to the applied stress, in a different manner from the case of silicon steel. Rate-type constitutive equations are proposed to describe the phenomena and to show the relationship between the stress magnetization properties and stress dependence of the magnetization curve. (in Japanese)

**246: Magnetic Impedance of Fe-28% Mn-Si-Cr Shape Memory Alloy****Katsuyuki Kinoshita, Eiji Matsumoto, Toshinobu Shibata<sup>†</sup>****<sup>†</sup> Graduate School of Engineering, Kyoto University**

Proceedings of the Seventh Magnetodynamics Conference, pp.63-66, 1998

This paper describes magnetic impedance of Fe-28(SMA) which depends on Martensite phase transformation. This SMA changes the impedance in the range of high frequency AC according to the magnitude of the external magnetic field. Since the magnetic impedance depends on the extend of the martensite phase transformation, it is expected that this SMA can be used as a sensor for the stress or the temperature by measuring the magnetic impedance. The prediction is verified by the measurement of the impedance under the magnetic field. (in Japanese)

**247: Effects of Stress on Magnetostriction and Magnetization Curve of Ferromagnetic Materials**

強磁性体の磁気ひずみ, 磁化曲線の応力依存性

**Kunio Asai<sup>†</sup>, Eiji Matsumoto, Toshinobu Shibata<sup>†</sup>**

**<sup>†</sup> Graduate School of Engineering, Kyoto University**

Transaction of Japan Society of Mechanical Engineers, Ser.A, Vol.64, No.624, pp.2183-2190, 1998

日本機学会論文集 (A 編), 64 巻, 624 号, pp.2183-2190, 1998

This paper describes magnetic impedance of Fe-28(SMA) which depends on Martensite phase transformation. This SMA changes the impedance in the range of high frequency AC according to the magnitude of the external magnetic field. Since the magnetic impedance depends on the extend of the martensite phase transformation, it is expected that this SMA can be used as a sensor for the stress or the temperature by measuring the magnetic impedance. The prediction is verified by the measurement of the impedance under the magnetic field. (in Japanese)

**248: Effect of Specimen Geometry on Strength in Engineering Ceramics**

**Toshihiko Hoshide, Jun Murano, Ryosuke Kusaba**

Engineering Fracture Mechanics, Vol.59, No.5, pp.655-665, 1998

Four-point bending tests of a pressure-less sintered alumina and a gas pressure sintered silicon nitride were conducted using notched specimens with different notch shapes as well as smooth specimens of distinct sizes, and the effect of the specimen geometry on the bending strength was experimentally clarified. The mean strength in the alumina was correlated with the effective volume independently of specimen geometry. In the silicon nitride, however, the mean strength could not be correlated with the effective volume; the mean strength in notched specimens shifted toward the lower strength side compared with the relation for smooth specimens. The poor correlation in the silicon nitride was suggested to be caused by the fact that the flaw distribution in smooth and notched specimens was different. To discuss the efficiency of the effective volume, a Monte Carlo simulation in the framework of fracture mechanics was also carried out by assuming the same characteristics of crack distribution in a material. The simulated result revealed that the effect of the specimen geometry on the strength was explained by using the

effective volume. The effective volume, however, was found to be inefficient because of failure of the basic assumptions in the Weibull theory when the Weibull modulus was not consistent or the flaw density was extremely low in a material.

**249: \* Bending Strength of Borosilicate Glass Coated with Alumina and Silicon Carbide by RF Magnetron Sputtering**

**Toshihiko Hoshide, Akira Nebu, Kenji Hayashi**

JSME International Journal, Series A, Vol.41, No.3, pp.332-337, 1998

Bending strength of ceramics coated glass was investigated from two aspects, concerning effects of the sputtering condition and the difference of target material on the strength. In this work, a borosilicate glass was coated with an alumina or a silicon carbide by a radio-frequency magnetron sputtering method under various conditions. Three-point bending tests of coated materials and the glass substrate were carried out. The strength of coated material was improved compared with that of the glass substrate. The scatter in the strength of coated materials appeared to be comparable with or less than the strength scatter of the glass substrate. Although monolithic alumina is usually weaker than monolithic silicon carbide, the strength of alumina coated materials was found to be higher than that of silicon carbide coated materials. This tendency was explained by a tensile thermal stress generated in silicon carbide coated materials, in which substrates were initially pre-heated.

**250: Interrelation Analyses of Mechanical Properties in Commercial Ceramics Using Cataloged Data**

**Toshihiko Hoshide**

Materials Science Research International, Vol.4, No.3, pp.179-185, 1998

Under conditions specified in this work, mechanical properties of commercial alumina, silicon carbide, silicon nitride and zirconia ceramics were selected from published manufacturers' catalogs. Numerical data of the selected properties for materials of 254 kinds in total were finally compiled in a computer-readable database. Interrelations among these properties were analyzed by using the database, and analyzed results were discussed. The selected properties of Young's modulus, linear thermal expansion coefficient, bending strength, Vickers hardness and fracture toughness were correlated with an apparent porosity derived from the theoretical and bulk density. Relationships of the selected properties to the porosity were fitted to exponential functions, and a good fitness was confirmed in most of the cases with a few exceptions. In general, every mechanical property tended to decrease with increasing the porosity. Although the hardness variation with respect to the bending strength was expressed by a proportional relationship for alumina and silicon carbide, a power relation was more adequate for silicon nitride and

zirconia. The relation between the fracture toughness and the bending strength was fitted to a power function. In this case, a good fitness was identified for silicon carbide and zirconia, though a poor correlation was found for alumina and silicon carbide. A specific crack length, which was used to modify a fracture mechanics criterion for small cracks, was well correlated with the bending strength by a power function.

**251: \* Estimation of Residual Stress with Non-Uniform Distribution by Indentation-Fracture Method in Ceramics**

**Toshihiko Hoshide**

Materials Science Research International, Vol.4, No.4, pp.294-296, 1998

In ceramic materials, the residual stress, which remarkably affects strength properties, is usually generated in sintering and machining processes. Although an X-ray stress measurement method is successfully used to estimate the residual stress in various ceramics, alternative simple methods may be applicable to the residual stress estimation especially in ceramics. A possible candidate for the residual stress estimation is an indentation-fracture (IF) method, which is a procedure to evaluate a fracture toughness of ceramics. Since experimental results show that a distribution of residual stress due to grinding is non-uniform in ceramics, it should be clarified how the non-uniform distribution of residual stress affects its estimation. In this work, an estimation of residual stress by using the IF method was presented for assumed non-uniform distributions of residual stress. By applying the present procedure to the case of ground silicon nitride, it was revealed that compressive residual stresses estimated for non-uniform stress distributions were almost twice as large as those for the uniform stress distribution. A larger residual stress was estimated in the material ground using a rougher wheel. Comparing results by X-ray stress measurements, it was suggested that the residual stress was reasonably estimated by the present procedure.

**252: Public Acceptance of Fusion Energy and Scientific Feasibility of a Fusion Reactor III Summary**

核融合エネルギーの社会的受容性と科学的見通し III まとめ

**N. Inoue, Y. Ogawa**

Journal of Plasma and Fusion Research, Vol.74, No.9, pp.957-966, 1998

プラズマ・核融合学会誌, Vol.74, No.9, pp.975-966, 1998

In these articles, public acceptance of the fusion reactor has been examined from the viewpoint of energy resources, radioactive wastes, safety, non-proliferation of nuclear weapons, cost of electricity, and the spin off of fusion science and technologies. These inspections have resulted the advantages of the fusion reactor among various energy sources, even though its cost of electricity is somewhat higher than that of the nuclear power reactor. Referring to the results of presently available tokamak fusion reactor

design, the achievement of the first commercial fusion reactor is estimated by comparing the assumed physics and technology levels in the designed fusion power reactors with those of the ITER. A diagram of the trends in the development of large superconducting coils indicates that these coils will be available for practical use by 2035; the practical negative ion source will also be completed by this year. Results of the reactor design study indicate that the low cost reactor requires an advanced plasma operation scenario and structural materials that can withstand high fluence irradiation of 14 MeV neutrons. It is concluded that the operation of commercial fusion power plant will be feasible by the middle of the next century.

**253: Design of a Steady-State Tokamak Device with Superconducting Coils for a Volumetric Neutron Source**

Yuichi Ogawa<sup>1)</sup>, Kunihiro Okano<sup>2)</sup>, Nobuyuki Inoue, T. Amano<sup>3)</sup>, Y. Asaoka<sup>2)</sup>, R. Hiwatari<sup>1)</sup>, Yosiki Murakami<sup>4)</sup>, K. Takemura<sup>1)</sup>, K. Tokimatsu<sup>1)</sup>, K. Tomabechi<sup>2)</sup>, T. Yamamoto<sup>1)</sup>, T. Yosida<sup>2)</sup>

1) Tokyo Univ., 2) Central Research Institute of Electric Power Industry, 3) National Institute for Fusion Science, 4) Toshiba Research and development Center

Fusion Engineering and Design 41, pp.469-475, 1998

We designed a volumetric neutron source for testing large-scale blanket components, based on a steady-state tokamak device with superconducting coils. It is found that a neutron flux of approximately  $1.0 \text{ MWm}^{-2}$  is available in the medium-size device ( $R = 4.5, a = 1.0 \text{ m}, k = 1.8, I_p = 5.6 \text{ MA}$ ) under the conditions of  $H \sim 2$  and  $\beta_N \sim 3$  with a neutral beam injection (NBI) power of about 60 MW. We demonstrate the controllability of the current profiles required for high-beta plasma up to  $\beta_N = 3-3.8$  with the combination of bootstrap current and NB-driven current ( $E_b = 1.0 \text{ MeV}$ ). If an advanced performance scenario such as a reversed shear configuration is available, a neutron flux of  $1.4 \text{ MWm}^{-2}$  is achievable. We install the breeding blanket of Li-Pb only at outboard and upper regions, and find that a local tritium breeding ratio (TBR) of 1.5 is achievable and a net TBR of 0.8 could be available. The analysis of shielding materials at the inboard region shows that the proper combination of tungsten, steel and boric water yields a reduction of the nuclear irradiation of TF coil by a factor of approximately 10.

**254: Inertial Electrostatic Confinement Fusion Simulation**

Masami Onishi, Chikara Hoshino, Kiyoshi Yoshikawa, Kai Masuda and Yasushi Yamamoto

Proceedings of Int. Symp. on Environment-Conscious Innovative Materials Processing with Advanced Energy Sources, pp.355-359, Nov.24-27, 1998

We developed the spherical one-dimensional code to study numerically the profiles of potential built in the center and the neutron generation in an inertial electrostatic confinement fusion device. The potential

well structure we obtained by the code was "double well", that is a negative potential well nested inside a positive potential well, but unstable. The fusion reactions occurred mainly between a background gas and fast particles, i.e. accelerated deuterium ions and charge exchanged neutrals. The total number of neutrons was consistent with the experimental results obtained in our device.

### 255: Experimental Results of Inertial- Electrostatic Confinement Fusion

**Y. Yamamoto, M. Ohnishi, M. Hasegawa, T. Koyama, T. Taruya, H. Toku, K. Yoshikawa**

Proceedings of Int. Symp. on Environment-Conscious Innovative Materials Processing with Advanced Energy Sources, pp.599-602, Nov.24-27, 1998

Inertial-electrostatic confinement fusion (IECF) experimental studies are carried out using 35-cm diameter spherical chamber with about 6-cm diameter cathode. We have measured  $5 \times 10^6$  n/s the D-D fusion neutrons with an applied voltage of 52.5 kV and the discharge current of 20 mA. It was found that the neutron production rate depends linearly on discharge currents. The normalized neutron yield, defined as neutron yield divided by multiples of the D-D fusion cross-section, pressure, and discharge current, is found to show dependence on 1.2 power of discharge voltage. D-D proton measurements using Solid State Detector (SSD) were also carried out. Preliminary results show that good agreement between dependence of neutron/proton production rate on applied voltage.

### 256: Decay Rate Measurements in a Negative Ion Rich Plasma

**Kouichi Jimbo, Masashi Iima\***

**\* The National Institute for Fusion Science**

Review of Scientific Instruments, Vol.69, No.10, pp.3551-3554, 1998

By artificially terminating the hydrogen arc discharge in the sheet plasma experiments, the decay rates of the negative and the positive saturation currents of a Langmuir probe could be measured. This technique made it possible to observe, under a deep potential well geometry, two single decay curves of saturation currents, which decayed at the same rate reciprocally with time in the negative ion dominant cold region. This result illustrates that the negative saturation current, which consisted of chiefly electrons, was still proportional to negative ion density.

**257: Study of the Performance Characteristics of a Travelling-Wave RF-Gun**

**K.Yoshikawa, D.Tsukahara, T.Inamasu, K.Masuda, M.Sobajima, J.Kitagaki,  
Y.Yamamoto, H. Toku, M.Ohnishi**

Nuclear Instruments And Methods in Physics Research, A407, pp.364-369, 1998

To understand the behavior of electrons in a travelling-wave-type RF gun using the thermionic cathode with expectation of less backstreaming effects, gun electrode structures were studied to improve the electron beam properties for FELs. Electron trajectories in an RF gun were calculated by a 2-D simulation code newly developed with full Maxwell equations with space-charge effects taken into account self-consistently to evaluate RF gun performance characteristics, in particular, the effects due to backstreaming electrons and defocusing effects in the vicinity of the electrodes. Although several advantageous features are shown, the emittance for the TW RF gun is found inferior to the SW RF gun, due not to space-charge effects, but to defocusing electric fields in the vicinity of the disk aperture. Several methods for emittance improvements are proposed and shown successfully by numerical calculations.

**258: Improvements of a Staggered-Array Undulator by Tapered Iron Disks**

**M.Ohnishi, S.Shimada, J.Kitagaki, K.Okada, M.Sobajima, K.Masuda, Y.Yamamoto,  
H.Toku, K.Yoshikawa**

Nuclear Instruments And Methods in Physics Research, A407, pp.434-438, 1998

A staggered-array undulator consists of two rows of simply stacked iron and aluminum disks alternately set in a solenoid coil. Its performance characteristics studied by the 2-D code show insufficient beam transverse focusing. Also, the original arrangement of iron disks at the entrance of the undulator is found not adequate for electron beam walk-off. Reduction of the beam walk-off effects is provided successfully by an addition of an auxiliary iron disk at the entrance, but the deviation of electrons in the transverse x-direction is found crucial even in this improved undulator. A tapered iron disk is qualitatively found to provide focusing effects in the x-direction, and optimization is made by a newly developed 3-D numerical code for magnetic fields using FEM and the reduced scalar potential. The focusing forces due to these methods will play an important role, in particular, in the ultra-long staggered-array undulator for shorter wavelength FELs.

**259: Numerical Study on Improvements of Beijing FEL Lasing Performances through Modifications of the Beam-Duct Geometry**

**M.Sobajima, Yonggui Li, Jialin Xie, K.Yoshikawa, M.Ohnishi, Y.Yamamoto, H.Toku, K.Masuda, J.Kitagaki, T.Nakamura**

Nuclear Instruments And Methods in Physics Research, A407, pp.121-125, 1998

In January 1997, the first lasing at 8-18  $\mu\text{m}$  was observed at Beijing FEL (BFEL). However, the output powers were found not large enough especially in the longer wavelength regime, where the laser power loss on the relatively narrow beam-duct wall is not expected to be small, and actually, the saturation of the laser power was not seen. In order to evaluate and to improve the effects due to the beam duct, we have modified our three-dimensional FEL code to accommodate the finite beam-duct size. It is predicted that more than three times as large as the output power is theoretically achieved at an 18  $\mu\text{m}$  wavelength with newly designed beam ducts.

**260: Study on Inertial Electrostatic Confinement Fusion as a Portable Neutron Source**

**M.Ohnishi, Y.Yamamoto, M.Hasegawa, K.Yoshikawa, George H. Miley**

Fusion Engineering And Design 42, Part C, pp207-211, 1998

The scaling of neutron generation versus ion current is important in evaluating the prospect of an Inertial-Electrostatic Confinement fusion (IEC) as a neutron source. In this paper, the scaling of neutron generation versus ion current  $I$ , based on the results of both the experiments and the numerical simulations is discussed. The experiments show the scaling of  $I^2$ , while the numerical simulation gives the stronger scaling of  $I^3$ . The regime of current in the present experiments is limited by the capability of the available power supplies. As the current increases, the potential structure is numerically shown to be more unstable. The intermittent peaking of the density is accompanied with unstable potential behaviors and brings about the higher density in time averaging. This may be a reason why the numerical simulation gives a stronger scaling versus ion current. Experiments in higher ion current regime may be required to verify the scaling estimated by the numerical simulation.

**261: Accelerator Plasma-Target-Based Fusion Neutron Source**

**G.H.Miley, Y.Gu, J.DeMora, M.Ohnishi**

Fusion Engineering And Design 41, pp.461-467, 1998

The University of Illinois inertial electrostatic confinement (IEC) device provides  $10^7$  2.5-MeV D-D neutrons per second ( $n\ s^{-1}$ ), when operated with a steady-state deuterium discharge at 70 kV (G.H.Miley et al., Inertial electrostatic confinement neutron/proton source, in: M.Haines, A.Knight (Eds.), 3rd Int. Conf. Dense Z-pinchs, AIP Conf. Proc. 299, AIP Press, New York, 1994, pp. 675-689). Being compact and lightweight, the IEC potentially represents an attractive portable neutron source for activation analysis applications (R.A.Anderl et al., Development of an IEC neutron source for NDE, 16th IEEE/NPSS Symp. Fusion Engineering, IEEE, Piscataway, NJ., 1996, pp. 1482-1485). The plasma discharge in the IEC is unique, using a spherical grid in a spherical vacuum vessel with the discharge formed between the grid and the vessel wall, while the cathode grid also serves to extract high-energy ions. Two key features of the IEC discharge physics are discussed: (1) the formation of ion 'microchannels' that carry the main ion flow through grid openings; and (2) the potential well structure formed in the dense central core.

**262: \* Studies of Inertial Electrostatic Confinement Fusion Neutron Source**

**M.Ohnishi, K.Yoshikawa, Y.Yamamoto, K.Masuda, H.Toku, M.Hasegawa, C.Hoshino, T.Koyama, K.Taruya**

Fusion Technology, Vol.34, pp.207-211, 1998

The dependence of neutron generation on the discharge current as well as the voltage in an IEC device is experimentally. We consider that the fusion events mainly occur between the accelerated ions and the background neutral gas from the linear dependence of neutron yield on the discharge current. The result of neutron generation proportional to the  $3/2$  power of the applied voltage indicates that the current within the hollow cathode may be limited by space charge. The particle simulation shows that the perveance in the experiments satisfies the conditions for space charge.

**263: Evolution of Field Reversed Configuration Plasma with Rotating Magnetic Field**

**M.Ohnishi, J.Kitagaki, Y.Yamamoto, K.Yoshikawa**

Proceedings of 1997 International Symposium on Plasma Dynamics in Complex Electromagnetic Fields, Institute of Advanced Energy, Kyoto University, pp.189-192, 1998

We have numerically studied that the flux enhancement of an FRC plasma by applying the rotating magnetic field with the frequency which is time-varying or constant but initially asynchronous with the electron motion. It was demonstrated that the FRC plasma can be sustained by applying the rotating magnetic field with a time-varying frequency, and controlling the axial magnetic field.

**264: Development of an Improved Two-Dimensional Finite-Element Code for Cylindrically Symmetric Eigenmodes**

**K.Masuda, K.Yoshikawa, M.Ohnishi, Y.Yamamoto, H.Toku, M.Sobajima, J.Kitagaki**

IEEE Trans. Microwave Theory Tech., 46-8, pp.1180-1182, 1998

A new two-dimensional finite-element (FE) eigenmode solver has been developed, which is suitable for calculating cylindrically symmetric modes. The quantity  $H_\theta/\gamma$  is used in the code to describe the electromagnetic fields instead of  $H_\theta$  or  $\gamma H_\theta$ , which is preferentially used in the existing codes, and the new formation with  $H_\theta/\gamma$  is found to show higher accuracy and smoother convergence with respect to the number of mesh points. Comparison is also made between linear and quadratic elements, resulting in remarkably higher accuracy by the latter.

**265: Experimental Studies of Inertial Electrostatic Confinement Fusion at Institute of Advanced Energy**

**Y.Yamamoto, M.Ohnishi, T.Koyama, K.Taruya, K.Yoshikawa**

Proceedings of U.S-Japan Workshop on IEC Neutron Sources, Los Alamos National Laboratory, September 14-15, pp.23-46, 1998

To verify fusion neutron measurements by  $^3\text{He}$  counter, fusion proton measurements using SSD are carried out. Preliminary results show that dependence of fusion proton production rate on the discharge voltage is in good agreement with that of fusion neutron production rate. But due to limitation of experimental setups, (1) simultaneous measurements of fusion proton and neutron could not be made, (2) discharge at high voltages ( $> 25\text{kV}$ ) were not stable enough, which resulted in low proton count rates. To solve these problems, we installed additional equipments and new cathodes, which were made of thin molybdenum/tantalum plate. Discharge characteristics of new cathodes and comparisons of neutron production rate with proton's will be presented at workshop.

**266: \* Numerical Studies of Inertial Electrostatic Confinement Fusion Taking Account of Atomic Processes**

**M.Ohnishi, C.Hoshino, K.Yoshikawa, K.Masuda, Y.Yamamoto**

Proceedings of U.S-Japan Workshop on IEC Neutron Sources, Los Alamos National Laboratory, September 14-15, pp.277-301, 1998

The numerical simulations are carried out in order to study the performance characteristic of an

inertial electrostatic confinement fusion device. We numerically solve the motion equations of ions and electrons for one dimension of the coordinate space and two dimension of the velocity space in the spherical coordinates as well as the Poisson equation by using the particle-in-cell model. The numerical results explain well the neutron yield and the dependencies on the discharge current and voltage, and show that the fusion events occur mainly between the accelerated deuterium ions and background deuterium gas. The effects of the atomic processes such as the charge exchange, dissociation and ionization are also studied on the performance of neutron generation.

### **267: Perspective of Inertial-Electrostatic Confinement Fusion**

**K. Yoshikawa**

Proceedings of Japan-U.S Workshop on Fusion Power Plants and Related Advanced Technologies, Kyodai Kaikan, Kyoto University, March 24-26, pp.287-297, 1998

Establishment of the scaling law of neutron generation a function of various parameters, such as, the cavity geometry, dimension of the hollow cathode, electrode-configuration, applied voltage, ion current, and gas pressure is very important in evaluating the prospect of an Inertial-Electrostatic Confinement fusion (IEC) as a neutron source, as well as the future power reactors. The current status of IEC as well as the innovative laser-induced fluorescence method by making use of Stark effect are presented.

### **268: Dependence of Ductile-Brittle Transition Behavior on the Specimen Size and Location of Notch in the HAZ of Welded A533B PVS**

**Akihiko Kimura, Tetsuya Suzuki, Morio Jincho\*, Hideki Matsui\***

**\* Tohoku University**

ASTM STP 1329, pp.110-122, 1998

The dependence of ductile-brittle transition (DBT) behavior of welded A533B pressure vessel steel (PVS) on the specimen size and location of notch in the heat affected zone (HAZ) has been investigated utilizing small specimen technique. Submerged arc welded thick plate for plant-use was supplied by Japan Steel Works, LTD. Standard size, one-third size and 1.5mm size Charpy V-notch (CVN) specimens were prepared so as to place the notches at the base metal (M15) and the deposit (D15) 15mm away from fusion boundary and 1 mm inside the base metal (M1) from the boundary. It is interesting that the M1 specimen shows better DBT behavior, namely a larger upper shelf energy (USE) and a lower ductile-brittle transition temperature (DBTT), than the M15 and D15 specimens independent of the specimen size. To investigate the dependence of the DBT behavior on the location of notch in the HAZ in more detail, impact tests were carried out for the one-third size specimens with notches at different distance from the fusion boundary ( $x=0$ ), that is,  $x=-15, -6, -5, -4, -3, -2, -1, 0, +1, +2, +3, +15$  mm from the boundary. Again the DBTT is the lowest and the USE is the highest for the M1 specimen. On the contrary, impact properties

are the worst at a HAZ location 4mm away from the boundary (M4). Normalization of the USE is successfully done by a curve fitting method. There observed linear relationships between DBTTs obtained using standard and sub-sized specimens of base metal, deposit and HAZ.

**269: Dependence of Impact Properties on Irradiation temperature in Reduced Activation Martensitic steels**

**Akihiko Kimura, Minoru Narui<sup>1)</sup>, Toshihei Misawa<sup>2)</sup>, Hideki Matsui<sup>1)</sup>, Akira Kohyama**

**1) Tohoku University, 2) Muroran Institute of Technology**

Journal of Nuclear Materials, 258-263, pp1340-1344, 1998

Ductile-brittle transition(DBT)behavior of 9%Cr-2%W reduced-activation martensitic (RAM) steels has been investigated following neutron irradiation in the fast flux test facility, materials open test facility (FFTF/MOTA) at different temperatures. Both the irradiation at 663 and the 733 K cause an increase in DBTT temperature, while the irradiation at 633 K induces the hardening and the softening at 733 K. Microstructural observation by transmission electron microscope (TEM) revealed that small dislocation loops existed in the specimen irradiated at 663K and no such loop, but relatively large M<sub>6</sub>C carbides and Laves phase were formed by the irradiation at 733 K. There appears to be a linear dependence between  $\Delta$ DBTT and  $\Delta\sigma_y$  in neutron irradiated RAM steels when irradiation induces the hardening. Irradiation embrittlement accompanied by the softening is considered to be due to reduction of cleavage fracture stress caused by the irradiation -induced recovery of the martensitic structure, namely decrease dislocation density and formation of large precipitates.

**270: \* Enhancement of Irradiation Hardening by Nickel Addition in the Reduced-Activation 9Cr-2W Martensitic Steel**

**Ryuta Kasada, Akihiko Kimura, Hideki Matsui\* , Minoru Narui\***

**\* Tohoku University**

Journal of Nuclear Materials, 258-263, pp.1199-1203, 1998

Reduced-activation martensitic (RAM)steels with and without an addition of 1%Ni were irradiated in a so called multisection-multidivision controlled irradiation capsule in the JMTR at 220 degree C up to 0.15 dpa. The 1/4 power dependence of the irradiation hardening on neutron dose was observed for the specimens irradiated in the controlled capsule. A part of the specimens were simultaneously irradiated in the capsule out of the reactor core where the irradiation temperature was considered to be lower than 170 degree C. The out of-reactor core irradiation induced a tremendous irradiation hardening as much as 350 Mpa in the Ni added RAM steel but only 120MPa of the hardening in the unadded RAM steel. The tremendous irradiation hardening was never observed following the irradiation at 220 degree C. As for the

results of positron annihilation measurements, no significant effect of the Ni addition was observed in the life time spectrum. Post-irradiation annealing studies indicate that the irradiation hardening observed in the Ni added RAM steel begins to recover at 190 degree C and diminishes after the annealing at 250 degree C.

#### **271: Swelling Behavior of V-Fe Binary and V-Fe-Ti Ternary Alloys**

**Kennichi Fukumoto\*, Akihiko Kimura, Hideki Matsui\***

**\* Tohoku University**

Journal of Nuclear Materials, 258-263, pp.1431-1435, 1998

Titanium addition to the swelling was very remarkable. One atom V-Fe binary alloys with different Fe concentrations, i. e., V-1, 3 and 5 at.% Fe, and V-5% Fe alloy added with 1, 3 and 5 at % of Ti were irradiated in EBR- at 380-615 degree C to about 11 dpa .TEM observation was performed after irradiation. A systematic increase in cavity size was observed with increasing iron concentration in the binary alloys, especially at 510 degree C And 615 degree C irradiation .On the other hand, the density of cavities decreased with increasing iron concentration and irradiation temperature. .Maximum swelling in V-Fe system occurred between 500 degree C and 600 degree C and the amount of swelling was up to 30% at a damage level of 11 dpa. The alloy containing only 1% Fe already showed substantial swelling. The effect of c percent of titanium addition to V-5 at. % Fe significantly suppressed cavity formation, and 3 at.% of titanium Addition entirely suppressed swelling, There seems to be a threshold titanium concentration for suppression of swelling in V-5 at. % Fe. Radiation-induced precipitation of titanium oxide may be one reason why titanium additions suppress the swelling in vanadium alloys. Homogeneous titanium oxide precipitates were not observed so that the titanium in solution is more likely to be playing an important role for suppression of swelling.

#### **272: Production of Low Activation Steel; JLF-1, Large Heats-Current Status and Future Plan**

**Akira Kohyama, Yutaka Kohno\*, M. Kuroda, Akihiko Kimura, F. Wan**

**\* University of Tokyo**

Journal of Nuclear Materials, 258-263, pp.1319-1323, 1998

Based on the excellent basic properties prior to neutron irradiation and under neutron irradiation up to 100 dpa, the 9Cr-2W type low activation ferritic steel (LAF). JLF-1, had been selected as one of the reference materials to the IEA low activation ferritic steels R&D activity. This paper provides the general information about the second large heat of JLF-1 steel. The basic property of thick plates (24 and 12mm in thickness) and their welded joints together with the information about microstructure are

also provided.

**273: \* Assessment of Helium Embrittlement of Reduced-Activation 9Cr Martensitic Steels**

**Ryuta Kasada, Akihiko Kimura, Taro Morimura\*, Akira Hasegawa\***

**\* Tohoku University**

Proc. of ECOMAP 98, pp.625-628, 1998

Helium implantation technique is one of powerful methods to study the effect of helium on the material performance, of which reduced activation martensitic steels have been investigated by means of Small Punch (SP) test. Helium of concentration up to 580 at.ppm was implanted by 36 MeV alpha-particle between 353 and 423K, which produced the displacement damage of 0.226 d damage by 14MeV neutron irradiation but also effects of transmutation helium. Though it has been well known that reduced-activation martensitic steels, which have been candidate beyond DEMO reactor, have supe In fusion reactor environment, structural materials suffered from not only displacement rior resistance to irradiation-induced embrittlement and void swelling under the fission irradiation of low helium concentration, not made clear the effects of helium

**274: Factors Controlling Kinetics of Hydrogen Embrittlement of Intermetallic Compounds**

**Akihiko kimura, Ryuta kasada, Masahiro Yamamoto, Taro morimura, Akihisa Koya**

Proc. of ECOMAP-98, pp.347-350, 1998

Vital efforts have been made to develop advanced intermetallic compounds as high temperature structural materials. Environmental embrittlement, which has been considered to be due to hydrogen, is one of the critical issues in intermetallics research and development. Hydrogen embrittlement of intermetallic compounds is classified into two categories; 1) time-dependent embrittlement which is so called environmental embrittlement caused by hydrogen decomposed from water vapor in air, 2) time-independent embrittlement caused by residual hydrogen in the materials. In the former case, there are so many processes controlling the kinetics of hydrogen embrittlement, such as adsorption of water vapor, decomposition of water vapor, absorption of hydrogen, hydrogen diffusion, deformation and transportation of hydrogen. In order to determine the main factor controlling the embrittlement of intermetallics, time-dependent brittle fracture behavior was investigated for Co<sub>3</sub>Ti alloys. The obtained data indicates that rate determining process of hydrogen embrittlement of Co<sub>3</sub>Ti alloys is hydrogen transportation by dislocations to grain boundaries. As for the later case, brittle fracture behavior depends on only the amount of residual hydrogen. Out-gassing treatment of TiAl alloys resulted in an increase in impact fracture energy and mass-spectroscopy measurements revealed that hydrogen was released during heating, which suggested

that the out-gassing reduced the hydrogen concentration at crack nucleation sites in TiAl alloys.

**275: Advanced Experimental Techniques for Material Engineering Workability Evaluation Technique – Evaluation of High Temperature Dynamic Fracture Toughness**

材料工学の先端実験技術（分担）加工特性解析技術 – 高温動的破壊靱性評価法

**Akihiko Kimura**

日本金属学会誌, pp.282-287, 1998

Evaluation technique of high temperature dynamic fracture toughness of intermetallic compounds is introduced along with small specimen technology. Focus is placed on the evaluation of intrinsic fracture toughness which is often degraded by environmental effects in many intermetallic compounds. In order to measure the fracture toughness of intermetallic compounds, which is strongly influenced by the environment, impact test is recommended in a variety of environments at high temperatures. High temperature impact test machine is produced and examples of the test results are shown for some intermetallic compounds. (in Japanese)

**276: Magnetic Nondestructive Evaluation of Fatigue Damage of Ferromagnetic Steels for Nuclear Fusion Energy Systems**

**Attila Gilanyi\*, Kazunori Morishita, Toshio Sukegawa\*, Mitsuru Uesaka\*, Kenzo Miya\***  
\* University of Tokyo

Fusion Engineering and Design, 42, pp.485-491, 1998

An inspection method is proposed for structural metal components of fusion reactors based on magnetic properties measurement. This integrity inspection is very important because structural materials are fully damaged by neutron radiation, heat load, thermal and mechanical stresses. Present work shows that magnetic hysteresis is sensitive to microstructural changes caused by high cycle fatigue, even at a stress level below the yield stress. The fatigue-induced degradation in the microstructure mainly has its fingerprint on the upper part of the hysteresis curve, where the rotation of magnetization is predominant. The changes in magnetic properties are well represented by the decreasing remanent induction with fatigue cycling. A microscopic study was also performed using transmission electron microscopy (TEM) to investigate the microstructural changes in the fatigued specimen. The TEM images show an increase in dislocation density in the ferrite phase.

**277: Round-robin Test for Nondestructive Evaluation of Steel Components in Nuclear Power Plants**

Mitsuru Uesaka<sup>1)</sup>, Attila Gilanyi<sup>1)</sup>, Tosio Sukegawa<sup>1)</sup>, Kenzo Miya<sup>1)</sup>, Koji Yamada<sup>2)</sup>, Storu Toyooka<sup>2)</sup>, Naoko Kasai<sup>3)</sup>, Akihiko Chiba<sup>4)</sup>, Siki tkahashi<sup>4)</sup>, Kazunori Morishita, Katsuyuki Ara<sup>5)</sup>, Noriya Ebine<sup>5)</sup>, Yoshihiro Isobe<sup>6)</sup>

1) University of tokyo, 2) Saitama University, 3) Electrotechnical Lab, 4) Iwate University, 5) JAERI, 6) Nuclear Fuel Industry

Electromagnetic Nondestructive Evaluation(II) (R.Albanese et al. Eds.), IOS Press, pp.39-48, 1998

The Round-robin test to evaluate degradation of low allow steel (A533B) for a pressure vessel in nuclear power plants was performed. Tensile and fatigue load tests were performed for plate and cylindrical specimens of A533B in order to increase microscopic dislocation density. WE adopted the laser speckle interferometry, Superconducting Quantum Interference Device (SQUID), Hall sensor, Barkhausen noise, macroscopic B-H curve measurement, microscopic observation by Transmission Electron Microscope (TEM) and Vickers hardness measurement to evaluate the degradation of the specimens. Generation and propagation of the Luders band was observed by the laser speckle interferometry, SQUID and Hall sensor. Different changes of the B-H curve were observed for small and large plastic deformations, which is related to microscopic structure of dislocations observed by TEM.

**278: \* Magnetic Nondestructive Evaluation of Accumulated Fatigue Damage in Ferromagnetic Steels for Nuclear Plant Component**

Kazunori Morishita, Attila Gilanyi\*, Toshio Sukegawa\*, Mitsuru Uesaka\*, Kenzo Miya\*  
\* University of Tokyo

Journal of Nuclear Materials, 258-263, pp.1946-1952, 1998

We performed the measurement of magnetic properties of ferromagnetic steels that were degraded by tensile plastic deformation and cyclic loading, where lattice imperfections were produced in the steels. Magnetic hysteresis curves were changed depending on the load conditions. The changes in coercive force, residual magnetic flux density and permeability were obtained as functions of the magnitude of residual strain for the tensile tests and the number of loading cycles for the fatigue test; In the case of the tensile deformation, the coercive force increased and the residual magnetic flux density decreased with increasing the residual strains. In the case of fatigue damage accumulated by the cyclic loading, the residual magnetic flux density decreased with increasing the number of cyclic loading, while the coercive force remained constant. The changes in hysteresis curves were well consistent with the TEM observation results of microstructural changes in the steels. We concluded that the magnetic property was enough sensitive to microstructural changes caused by mechanical deformation.

**279: Intelligent Beam Transforming Earthquake Force into Vibration Control Force and Its Optimal Design****Kosuke Nagaya, Toshiyuki Fukushima\*****\* Gunma University**

Journal of Sound and Vibration, Vol.218, No.3, pp.445-461, 1998

This paper presents a method of vibration control for a beam carrying a mass at its tip subjected to earthquakes. A vibration isolation mechanism consisting of gear train for the beam is presented. Theoretical analysis for the beam is developed, and to validate the method and analysis, experimental tests are carried out for a model of the present mechanism. It is clarified that the vibration displacements and the moments in the beam are suppressed significantly in comparison with the general beam without the mechanism. A method of optimal design has been also presented, and numerical calculations have been carried out for the beam with actual sizes. In the present beam, energies for controlling vibrations are not required, because the earthquake force is utilized as a control force. Therefore, the structure using the beam has advantages as compared with the structure having active vibration control system.

**280: Method for Reducing Sound Radiated From Structures Using Vibration Absorbers Optimized with a Neural Network****Kosuke Nagaya, Lian-Jin Li\*****\* Gunma University**

Journal of the Acoustical Society of America, Vol.104, No.3, pp.1466-1473, 1998

The usual design methods for the vibration absorbers are applicable to suppress vibrations of machines and structures, but they are invalid for reducing sounds. This study discusses a method for reducing sound radiated from structures by use of vibration absorbers. In this study, the peaks of sound power in the frequency domain are considered to be cost functions. Hence, the equations for obtaining optimal parameters of the absorbers become nonlinear expressions. In order to have the optimal parameters, a neural network procedure is applied. A new technique is also developed for obtaining rapid convergence.

**281: Piezoelectric Sensor and Electromagnetic Linear Actuator System and Its Application to Vibration Control of a Motor on a Flexible Structure**

圧電素子とリニアモーター一体型センサ・アクチュエータ系の開発とそれによる柔軟構造物に搭載されたモータの振動制御

**Sigeo Ikai<sup>1)</sup>, Hiroshi Kashimoto<sup>2)</sup>, Keiichi Ohsawa<sup>1)</sup>, Kosuke Nagaya**

**1) Gunma University, 2) Gunma College of Technology**

Transactions of the Japan Society of Mechanical Engineers, Ser.C, Vol. 64, No.623, pp.2542-2549, 1998

日本機械学会論文集、C編、Vol. 64, No.623, pp.2542-2549, 1998

This paper presents an actuator with a sensor for controlling vibrations of machines. It consists of a voice coil type electromagnetic actuator connected to piezoelectric sensor and a coil spring. The actuator is used for controlling a motor laid on the beam. The disturbance force due to the centrifugal force of the motor is detected by the sensor, and the force which is equivalent to the disturbance force is applied to the motor and the beam by the actuator. This implies that the disturbance force is canceled. The control technique as just mentioned has advantages because it reduces the vibration in the low frequency region, in addition, the actuator becomes compact, and the control force becomes small. But the control is insufficient for controlling the resonance peak. The PD control is available for reducing the resonance peak, but the displacement and velocity sensors are required. In the present article, a method of vibration control of disturbance cancellation combining the PD control is presented in which both the displacement and velocity sensor are not required.

**282: \* Nonlinear Vibration Control for a High-Tc Superconducting Levitation System**

高温超電導浮上系の非線形振動制御

**Kosuke Nagaya, Masato Tsukagoshi<sup>1)</sup>, Yasuhiro Kosugi<sup>1)</sup>, Masato Murakami<sup>2)</sup>**

**1) Gunma University, 2) Superconductivity Research Laboratory**

Trans. Jpn Soc. Mech. Engr., Ser.C, Vol.64, No.623, pp.2520-2527, 1998

日本機械学会論文集、C編、Vol.164, No.623, pp.2520-2527, 1998

The present article discusses a modeling and control of high-Tc superconducting nonlinear levitation system. The paper clarifies analytical expressions for obtaining nonlinear levitation force given by the present author. A method of nonlinear vibration control is developed. In the method, an addition of a square of the displacement and currents in a frequency domain is taken to be a cost function. Then optimal nonlinear control can be performed by using the method presents. Numerical calculations have been carried out for some typical problems. To validate the present method, experimental tests also have been carried out (in Japanese).

**283: Vibration Control of Spindles of Machine Tools by Using Piezoelectric Actuators Under the Disturbance Cancellation and H-Infinity Control**

柔軟な腕に取り付けられた軸の圧電アクチュエータを用いた外乱相殺と $H_\infty$ による振動制御

Shigeo Ikai<sup>1)</sup>, Kenichi Shimada<sup>1)</sup>, Hiroshi Kashimoto<sup>2)</sup>, Kosuke Nagaya

1) Gunma University, 2) Gunma College of Technology

Journal of the Japan Society of Applied Electromagnetics and Mechanics, Vol.6, No.3, pp.258-266, 1998.

日本 AEM 学会誌, Vol.6, No.3, pp.258-266, 1998

This paper discusses vibration control problem of a spindle of machines with flexible arm. When the arm of the spindle is flexible, vibration displacements become 20  $\mu$  m to 100  $\mu$  m, and the frequencies involve high frequency components. Hence high response actuator with large displacements is required in the control of the spindle, but actuators which cover the frequencies and the displacements have not been presented. In this article, an actuator consisting of piezoelectric ceramics with flexible displacement enlargement mechanism is presented, then a control method is discussed. In this case, three forces apply to the spindle simultaneously. One of the force is generated by the driving mechanism. It applies to the spindle passing through the arm of the machine. The second is a centrifugal force, and the third is the cutting force which apply to the spindle directly. For the fine cutting, the cutting force is small, so that a controller can be designed with consideration of first two vibration forces. In the present article, the vibration by the driving mechanism is controlled by using the disturbance cancellation method given in our previous work, and the vibration due to the centrifugal force is controlled by the H-infinity control. (in Japanese)

**284: Vortex Shedding Resonance From a Rotationally Oscillating Cylinder**

Nobuyuki Fujisawa<sup>1)</sup>, Kouichirou Ikemoto<sup>2)</sup>, Kosuke Nagaya

1) Niigata University, 2) Gunma University

Journal of Fluids and Structures, Vol.12, pp.1041-1053, 1998.

Vortex shedding resonance of a circular cylinder wake to a forced rotational oscillation has been investigated experimentally by measuring the velocity fluctuations in the wake, pressure distributions over the cylinder surface, and visualizing the flow field with respect to cylinder oscillations. It is clarified that the vortex shedding resonance occurs near the natural shedding frequency at small amplitude of cylinder oscillations, while the peak resonance frequency shifts to a lower value with an increase in oscillation amplitude.

**285: Active Control of Vortex Shedding from Circular Cylinder by Rotary Oscillations (Optimized with Neural Network)**

円柱の回転運動による渦放出のアクティブ制御に関する研究 (ニューラルネットを用いた最適化)

**Nobuyuki Fujisawa<sup>1)</sup>, Takamitsu Nakabayashi<sup>2)</sup>, Koichiro Ikemoto<sup>2)</sup>, Kosuke Nagaya**  
**1) Niigata University, 2) Gunma University**

Trans. Jpn Soc. Mech. Engrn., Ser.B, Vol.64, No.621, pp.1293-1298, 1998

日本機械学会論文集, B編, Vol.64, No.621, pp.1293-1298, 1998

The active control of vortex shedding from a circular cylinder by rotary oscillations is studied experimentally using neural networks, which optimizes automatically the control parameters such as the phase lag and the feedback coefficient. The optimization procedure is applied to find out an optimum position of reference probe to attenuate the vortex shedding effectively. The attenuation effect of vortex shedding under this control is investigated by measuring the velocity fluctuations in the cylinder wake and the unsteady pressure distributions over the cylinder surface. It is found that the drag and lift forces acting on the cylinder are reduced under the optimum reference control in comparison with the control under other reference positions as well as those of the stationary cylinder. (in Japanese)

**286: Micro-Vibration Suppression Mechanism and Adaptive Control for a Milling Machine Spindle**

フライス盤スピンドルの微振動除振機構の開発とその適応制御

**Kosuke Nagaya, Sigeo Ikai<sup>1)</sup>, Yasuhide Hano<sup>1)</sup>, Hiroshi Kashimoto<sup>2)</sup>, Nobuyuki Fujisawa<sup>3)</sup>**

**1) Gunma University, 2) Gunma College of Technology, 3) Niigata University**

Journal of the Japan Society of Applied Electromagnetics and Mechanics, Vol.7, No.1, pp.76-81, 1998

日本 AEM 学会誌, Vol.7, No.1, pp.76-81, 1998

A mechanism for controlling micro-vibrations of a spindle of milling machine is presented in which sandwiched piezo electric elements are used as actuators. An auto-tuning control method by using the mechanism is presented. To validate the mechanism and the control method, experimental tests have been carried out for a milling machine in which a lower bearing is improved by use of the actuators as just mentioned. It is clarified that the vibrations of the spindle can be controlled to be significantly small. (in Japanese)

**287: Control for Passing Through Critical Speeds of a Superconducting Radial Bearing by Using Electromagnetic Actuators**

高温超電導ラジアル軸受の電磁アクチュエータによる共振乗り越し制御

**Kosuke Nagaya, Kouichi Kannno<sup>1)</sup>, Nobuyuki Hayashi<sup>1)</sup>, Eiichi Tejima<sup>2)</sup>, Mitsuru Morita<sup>2)</sup>, Sinji Ikeda<sup>3)</sup>**

**1) Gunma University, 2) Sin-Nippon Steel Company, 3) Japan Servo Co. LTD**

Journal of the Japan Society of Applied Electromagnetics and Mechanics, Vol.7, No.1, pp.90-95, 1999

日本 AEM 学会誌, Vol.7, No.1, pp.90-95, 1999

The high-T<sub>c</sub> superconducting levitation system is stable in both radial and axial directions without contacts, so it has been applied as bearings of an energy storage flywheel. To have high efficiency, the rotating speed of the wheel is significantly high, and it is necessary to pass through critical speeds. The rotating tail stocks are often attached at both ends of the shaft, and those are removed after passing through the critical speeds. But the method is complex in practical use. The present article discusses a method for passing through the critical speeds by using a magnetic bearing as an actuator. The analytical result for the system under the PD control are obtained. To validate the present system and the method, experimental tests have been carried out. (in Japanese)

## IV Department of Energy Science and Technology

(エネルギー応用科学専攻)

### 288: Design of a Bit-Serial Word-Parallel Functional Memory with Ferroelectric Capacitor

**Yoshiro Fujii, Hiroshi Nozawa, Kazutoshi Kobayashi\*, Keikichi Tamaru\*, Kazuhiro Hoshiba\*\* and Isao Matsumoto\*\***

**\*: Graduate School of Information, Kyoto University, \*\*: Rohm Co.,LTD.**

Proceedings of the 1999 IEICE General Conference, C-12-84, p 182, March 1999

The functional memory type parallel processor is studied enthusiastically, because it enables massively parallel computing inside a memory, and it has a capability to break the Von Neumann bottleneck. In this paper, we designed the bit-serial word parallel functional memory with ferroelectric capacitor. That was based on 1 transistor and 1 capacitor (1T1C) ferroelectric memory. We designed and fabricated a test LSI to examine the operation of read/write and bit-serial word-parallel processing using ferroelectric capacitor. The LSI had 2 Processing Element (PE), which consisted of 4bit words, and an ALU for logical operation. It was confirmed that the test chip could operate the read and write operation and bit-serial word-parallel processing in 150ns. We also simulated this ferroelectric memory cell and discussed about plate line drive current and bit line voltage. ( in Japanese)

### 289: Simulation on Thermionic Electron Emission Rate Considering Local Field in Ferroelectric Thin Film

**Dai Nagasawa and Hiroshi Nozawa**

Extended Abstracts, The 46th Spring Meeting, The Japan Society of Applied Physics, 31a-K-7, p 596, March 1999

We investigated the origin of imprint mechanism of the ferroelectric thin films such as PZT or SBT by considering thermionic field emission under local fields. The electric fields of the ferroelectric films inside are represented. Since the poled ferroelectric capacitors had strong local field inside, thermionic field emission rate is enhanced by tunneling effect (Thermionic Field Emission). The emission rate is estimated by taking thermionic field emission into account. The dependence of imprint phenomenon on the emitted electron from trap was made detailed explanation. We calculated the voltage shift that was results of imprint phenomenon. Comparing the result with the experiments, we successfully explained imprint phenomenon based on pinning. ( in Japanese)

**290: Crystal growth of layered perovskite  $\text{Sr}_2\text{Nb}_2\text{O}_7$  and  $\text{Sr}_2\text{Ta}_2\text{O}_7$  film by sol-gel technique****K. Okuwada\*, S. Nakamura\*, H. Nozawa****\*: Toshiba Corporation**

Journal of Materials Research, Volume 14, No.3, March 1999

High dielectric and low loss capacitor thin films of  $\text{Sr}_2\text{Nb}_2\text{O}_7$  (SN),  $\text{Sr}_2\text{Ta}_2\text{O}_7$  (ST), and their solid solution  $\text{Sr}_2(\text{Nb}_x\text{Ta}_{1-x})_2\text{O}_7$  (SNT) were investigated using the sol-gel technique. The SN film grows with the (0n0) orientation in the case of heating at over 700 °C. Heat treatment at a lower temperature results in the polycrystal ST-type structure. The SNT at  $x < 50\%$  also resulted in the ST-type. The dielectric constant for the SN film was 45, within 10% was 0.3~0.5%. The small variation in dielectric constant and the paraelectricity with low loss are suitable for capacitor applications.

**291: \* Importance of Metal-Metal Bondings at the Interface of MgO and 3 d-Transition Metals****I. Tanaka, M. Mizuno (Dept. of Materials Science and Engineering, Kyoto University),****H. Adachi (Dept. of Materials Science and Engineering, Kyoto University)**

Acta mater. Vol. 46, No. 18, pp.6511-6520, 1998

First principles cluster calculations of  $\text{MgO}(001)//\text{M}(001)$  (M-Sc to Cu) interfaces have been systematically made using numerical atomic orbitals as basis functions. Detailed analysis of bond overlap populations (BOP) found the M-Mg covalent bond predominantly determines the interfacial bond-strength. M atoms prefer to be located on top of O atoms, not because the first nearest-neighbor M-O covalent bond is stronger than the m-Mg bond at the same bond-length, but because the M-Mg bond prefers to be at the second nearest-neighbor distance in order to increase the number of effective interfacial bonds from 1 to 4. The equilibrium interfacial bond-length is found to be determined by the balance of M-Mg bond-reinforcement and weakening of the M-M bond. Atomic number dependence of the interfacial bond-strength is also determined by the variation of the M-Mg BOP. It decreases with rising atomic number mainly because of the contraction of M-orbitals. Theoretical electron energy loss near edge structures (ELNES) are given to help interpretation of experimental spectra to be acquired directly from the interface.

**292: \* Electronic Mechanism of Ag-Cluster Formation in AgBr and AgI**

**K. Matsunaga (Dept. of Materials Science and Engineering, Kyoto University), I. Tanaka, H. Adachi (Dept. of Materials Science and Engineering)**

Journal of Physical Society of Japan, Vol. 67, No.6, pp.2027-2036, 1998

We have carried out first principles molecular orbital calculations on an interstitial Ag in AgBr and AgI, using the discrete variational (DV)- $X\alpha$  method. Although AgBr and AgI are considered to be ionic compounds, Ag-4d orbitals are well admixed with anion- $p$  orbitals in their valence band. We have carried out first principles molecular orbital calculations on an interstitial Ag in AgBr and AgI, using the discrete variational (DV)- $X\alpha$  method. Although AgBr and AgI are considered band. In the presence of an interstitial Ag(Agi), an interstitial level appears within the band gap. The interstitial orbital is found to be more delocalized around the Agi in AgBr than in covalent bond in AgBr is stronger than any other covalent bonds around the Agi. On the other hand, the Agi-Ag covalent bond in AgI is much weaker than the Ag-I bond at normal sites. Since the formation of strong Agi-Ag bond is essential for the agglomeration of Ag atoms, an Ag cluster can be formed easier in AgBr than in AgI. In the presence of an interstitial Ag(Agi), an interstitial level appears within the band gap. The interstitial orbital is found to be more delocalized around the Agi in AgBr than in covalent bond in AgBr is stronger than any other covalent bonds around the Agi. On the other hand, the Agi-Ag covalent bond in AgI is much weaker than the Ag-I bond at normal sites. Since the formation of strong Agi-Ag bond is essential for the agglomeration of Ag atoms, an Ag cluster can be formed easier in AgBr than in AgI.

**293: \* Chemical Bonding at the Fe/TiX(X=C, N or O) Interfaces**

**M. Mizuno (Dept. of Materials Science and Engineering, Kyoto University), I. Tanaka, H. Adachi (Dept. of Materials Science and Engineering, Kyoto University)**

Acta. mater., Vol. 46, No.5, pp.1637-1645, 1998

First principles molecular orbital calculations for the Fe/TiX(X=C, N or O) interfaces have been made by the use of the spin-polarized discrete-variational  $X\alpha$  method. At the interfaces, no significant charge transfer occurs between the Fe and TiX layers. Ionic interaction is small and covalent bonding is predominant at the interface. The interfacial bond strength is stronger when Fe atoms are located on X atoms, that is, the Fe-on-X geometry of the Baker-Nutting orientation relationship. The Fe/TiX bond strength decreases with the rising atomic number of X. The anti bonding of the Fe-O bonds at the Fe/TiO interface is noteworthy. Although the Fe/TiO interface shows the smallest lattice mismatch among three interfaces, it is expected that the chemical bonding at the interfaces is weakest. The interfacial bond strength by the present calculation agrees well with the potency of TiX for intragranular ferrite nucleation in steels that was recently found experimentally.

**294: \* Electronic Structures and Chemical Bonding of  $\text{TiX}_2$  (X=S, Se, and Te)**

**Y-S. Kim (Dept. of Materials Science and Engineering), M. Mizuno (Dept. of Materials Science and Engineering), I. Tanaka, H. Adachi (Dept. of Materials Science and Engineering)**

Jpn. J. Appl. Phys., Vol. 37, pp. 4878-4883, 1998

A systematic study of the electronic structures and chemical bonding of the titanium dichalcogenide  $\text{TiX}_2$  (X=S, Se, and Te) layered structures is performed by a first-principles molecular orbital calculation using the discrete-variational (DV)- $X\alpha$  cluster method. The intra- and interlayer chemical bonding properties are also investigated using the bond overlap population. Valence band structures obtained by the calculation are in good agreement with experimental results obtained by X-ray photoemission spectroscopy. Each peak in the density of states (DOS) is identified from the viewpoint of chemical bonding. There is a considerably strong covalent bonding between Ti and chalcogen atoms in  $\text{TiX}_2$ . The covalency of chemical bonding is shown to increase and the ionicity to decrease in the series of  $\text{TiS}_2$ - $\text{TiSe}_2$ - $\text{TiTe}_2$ . Both in intra- and interlayer chalcogen-chalcogen bonding and intralayer Ti-Ti bonding are much weaker than Ti-chalcogen interlayer bonding. However, interlayer interaction is found to be not purely of the van der Waals type.

**295: \* Chemical Bondings around Intercalated Li Atoms in  $\text{LiTiX}_2$  (X=S, Se, and Te)**

**Y-S. Kim, Y. Koyama, Isao, Tanaka, H. Adachi**

Jpn. J. Appl. Phys., Vol. 37, pp.6440-6445, 1998

A systematic study of the electronic structure and chemical bonding of the Li-intercalated titanium dichalcogenides,  $\text{LiTiX}_2$  (X=S, Se, and Te), is performed by a first-principles molecular-orbital method using a model cluster composed of 75 atoms. The discrete-variational (DV)- $X\alpha$  method was employed and Mulliken's population analyses were thoroughly conducted. The net charge of Li is found to be approximately 0.1 independently of X-species. Net charges of Ti and X are not significantly affected by the Li intercalation. Strong covalent bonding is formed between Li and X with a bond-overlap population (BOP) of 0.173-0.176. The BOP of Ti-X bonding decreases by about 10% of Li. These results should be important for determining battery properties when the dichalcogenide are used for positive electrodes.

**296: \* Electronic Structure and Chemical Bondings of  $\text{TiS}_2$  by Cluster Calculation**

**Y-S. Kim, M. Mizuno, I. Tanaka, H. Adachi**

First-principles molecular orbital calculations for layered compound  $\text{TiS}_2$  have been made by the use of the discrete variational (DV)- $X\alpha$  method. Model clusters used are composed of 55 and 135 atoms. The magnitudes of individual chemical bondings are investigated by analyzing the bond overlap populations. The valence band structure measured by X-ray photoemission spectroscopy is well reproduced by the calculation, and each peak is identified from the viewpoint of chemical bonding. There is a considerably strong covalent bonding between Ti and S atoms in  $\text{TiS}_2$ . Both of the Ti-Ti and S-S bondings are found to be much weaker than the Ti-S bonding. The interlayer S-S bonding is also very weak, but virtually the interaction is not the van der Waals type.

**297: \* Analysis of Covalent Effects on the Multiplet Structure of Ruby Based on First-Principles Cluster Calculations**

**Kazuyoshi Ogasawara (Dept. of Materials Science and Engineering, Kyoto University), Takugo Ishii (Dept. of Materials Science and Engineering, Kyoto University), Yukiko Ito (Dept. of Materials Science and Engineering, Kyoto University), Isao Tanaka, Hirohiko Adachi (Dept. of Materials Science and Engineering, Kyoto University),**

Jpn. J. Appl. Phys. Vol.37, pp.4590-4594, 1998

A general method to calculate multiplet structures in distorted molecular orbitals has been developed, in which the matrix elements of the electron-electron interaction are calculated numerically using the molecular orbitals obtained by cluster calculations. The multiplet structure of chromium-doped alumina (ruby) has been calculated from first principles using model clusters consisting of 7 to 41 atoms with or without cubic approximation. By comparing the results, it was discovered that the energy of the  ${}^2E$  state is sensitive to the trigonal distortion of the impurity -state wave functions and that the energies of the  ${}^2T_1$  and  ${}^2T_2$  states are sensitive to spatial extension of these wave functions over aluminum ions. The present calculation is an effective method not only for the first-principles calculation of multiplet structures beyond cubic or tetragonal approximations but also for analysis of the effects of covalency on multiplets structures.

**298: \* Electronic States of Solid State Materials Using Model Clusters (in Japanese)**

固体の機能とクラスターの電子状態

**Hirohiko Adachi (Dept. of Materials Science and Engineering, Kyoto University) Isao Tanaka**

Materia Japan, Vol.37, No.7, pp. 587-591, 1998

まてりあ, Vol.37, No.7, pp. 587-591, 1998

**299: \* Chemical bonding of 3d transition-metal disilicides**

**S. R. Nishitani\*, S. Fujii\*, M. Mizuno\*\*, I. Tanaka, H. Adachi\* \* Dept. of Materials Science and Engineering, Kyoto University \*\* Kobe steel Ltd.**

Physical Review B, Vol. 58, No. 15, pp. 9741-9745, 1998

The bonding properties of 3d transition-metal (TM) disilicides are explored by the use of the discrete variational  $X \alpha$  cluster method. The calculated density of states of whole 3d TM disilicides reproduce well the characters obtained by photoemission spectroscopy. Mulliken's population analysis reveals that the bonding is dominated by the comparable interactions of TM-Si and Si-Si. The main participant of TM-Si bonds shifts from 3d-Si bonding for the middle 3d TM disilicides to 4sp-Si bonding for the late 3d TM disilicides.

**300: \* Madelung energy of metal-metalloid compounds**

**S. R. Nishitani\*, S. Fujii\*, M. Mizuno\*\*, K. Tanaka\*, I. Tanaka  
Dept. of Materials Science and Engineering, Kyoto University  
\* Kobe steel Ltd.**

Computational Materials Science, Vol 14, pp. 62-66, 1999

Using the formula including charge transfers on sites, the binding energy can be described by the sum of the short-range energy, the on-site charge transfer energy and the long-range electrostatic energy. For discussing the 'ionic' contributions on the binding energy, Madelung energies are calculated for the complex compounds of 3d transition metal (M) and metalloid (B,Si) of  $MB_2$ ,  $MSi_2$  and  $MSi_2$  and are compared to the heat of formation.

- 301: \* Interaction between Oxygen and 3d Transition-metal Impurities on ZnO(10-10) Surface

**F. Oba\*, I. Tanaka, K. Ogasawara\*, H. Adachi\***  
Dept. of Materials Science and Engineering

Proceedings of US-Japan Workshop on Electrically Active Ceramic Interfaces, p141,  
1998

- 302: \* Calculation of Grain-Boundary Bonding in Rare-Earth-Doped  $\beta$ -Si<sub>3</sub>N<sub>4</sub>

**T. Nakayasu\*, T. Yamada\*, I. Tanaka H. Adachi\*\*, S. Goto\*\*\***  
UBE Industries, Ltd.

\* Dept. of Materials Science and Engineering, Kyoto University

\*\* Faculty of Engineering, Yamaguchi University

J. Am. Ceram. Soc., 81, pp. 565-570, 1998

- 303: \* Cluster Calculation of oxygen K-edge electron-energy-loss near-edge structure of NiO

**H. Kanada\*, M. Yoshiya\*, F. Oba\*, K. Ogasawara\*, H. Adachi\* and I. Tanaka**  
Dept. of Materials Science and Engineering, Kyoto University

Phys. Rev. B., 58, pp. 9693-9696, 1998

- 304: Steady and Unsteady Heat Transfer from a Flat Plate in Subcooled He II

**M. Shiotsu, K. Hata\*, Y. Takeuchi\* and K. Hama\***  
Institute of Advance Energy, Kyoto Univ.

Advances in Cryogenic Engineering, Vol.43 (1998), pp.1409-1416

Transient heat transfer caused by large stepwise heat inputs to a flat plate was measured in subcooled He II at atmospheric pressure for bulk liquid temperatures ranging from 1.9 to 2.1 K. The flat plate was made of Manganin, one side insulated, 10.3 mm in width, 40 mm in length and 0.1 mm in thickness.

Steady-state heat transfer and its critical heat flux were also measured by using quasi-steadily increasing heat inputs for the same experimental conditions. The steady-state critical heat fluxes for the liquid temperatures were well expressed by the authors' correlation based on the Gorter-Mellink equations. The lifetime of quasi-steady heat flux in Kapitza conductance regime, which corresponds to that of a certain point on the extrapolation of steady-state Kapitza conductance curve, was systematically measured: the quasi-steady state rapidly changes to film boiling regime after the depletion of lifetime. Comparisons of the results on the flat plate with those on the horizontal wires with the diameters ranging from 0.08 to 0.7 mm under the same condition already reported by the authors were made to clarify the effect of heater shape.

**305: Electrical Resistivity of a High-Tc Superconductor for Electric Current Higher Than  $I_c$**

M. Shiotsu, K. Hata<sup>1</sup>, A. Sakurai<sup>2</sup>, C. Suzawa<sup>3</sup>,  
S. Isojima<sup>3</sup>, K. Sato<sup>3</sup> and T. Fukui<sup>3</sup>

<sup>1</sup> Institute of Advanced Energy, Kyoto Univ.

<sup>2</sup> Future Energy Research Assoc.

<sup>4</sup> Sumitomo Electric Ind. Ltd.

Advances in Cryogenic Engineering, Vol.44 (1998), pp.623-629

The electrical resistivity of a high-Tc superconductor for  $I > I_c$  is not clarified until now as a function of electric current through the conductor,  $I$ , and temperature of the conductor,  $T$ , because  $T$  varies with  $I$  due to joule heating. An estimation method of the electric resistivity based on non-boiling heat transfer coefficients for exponentially increased heat inputs to the high-Tc test sample in LN2 was developed: exponential heat inputs,  $Q = Q_0 e^{t/\tau}$ , with the periods,  $\tau$ , ranging from 10 ms to 10 s were given to a silver sheathed BiPbSrCaCuO tape in LN2, and electrical current  $I$  through the sheathed tape and the terminal voltage  $V$  between potential taps on the tape during the transient heating were measured. An empirical equation for the electrical resistance  $R$  of the sheathed tape was obtained as a function of  $I$  and  $T$ : two constants in the equation were fitted iteratively so that the value of  $T$  at each time obtained from the measured values of  $I$  and  $V$  at the time by using the equation of  $R$  may agree with the theoretical solution of nonboiling heat transfer for the exponential period. The distribution ratio of the electric current through the superconductor and the Ag sheath,  $I_N/I$ , and the flow resistance of the superconductor itself were estimated.

**306: Incipient Boiling Superheat in Liquid Sodium**

M. Shiotsu, K. Hata<sup>1</sup>, Y. Takeuchi<sup>1</sup>, K. Hama<sup>1</sup> and T. Sakai<sup>2</sup>

<sup>1</sup> Institute of Advanced Energy, Kyoto Univ.

<sup>2</sup> PNC

Proceedings of the Eleventh International Heat Transfer Conference, Vol.2 (1998)  
pp.407-412.

The incipient boiling superheats (IBS) on a horizontal cylinder test heater of 7.6 mm in diameter in saturated liquid sodium caused by quasi-steadily increasing heat input were systematically measured for the cold trap temperatures ranging from 378 K to 433 K at the bulk liquid temperatures of 863 K and 973 K. The IBS for the bulk liquid temperature of 873 K was significantly affected by the cold trap temperature. The IBS became higher with the decrease in the cold trap temperature and it amounted to around 250 K for the cold trap temperatures lower than 383 K. For the bulk liquid temperature of 973 K, the IBS are scattered from about 40 K to 200 K but little systematic effect of the cold trap temperature was observed. For the IBS lower than around 70 K, the surface temperature of the test heater suddenly decreased after the initiation of boiling and nucleate boiling was realized. After that the heat flux increased in nucleate boiling regime up to the critical heat flux. For the IBS higher than 70 K, direct transition from non-boiling to film boiling occurred at the initiation of boiling. The heat flux at the IBS of around 100 K was almost equal to the critical heat flux of nucleate boiling for the same condition and that of around 250 K was about 2.5 times of the critical heat flux.

**307: Mechanisms of Subcooled Flow Boiling Critical Heat Fluxes on Vertical Cylinder Surface and on Short Tube Inner Surface in Water Flowing Upward at Various Pressures**

A. Sakurai<sup>1</sup>, M. Shiotsu, K. Hata<sup>2</sup> and K. Fukuda<sup>3</sup>

<sup>1</sup> Future Energy Research Assoc.

<sup>2</sup> Institute of Advanced Energy, Kyoto Univ.

<sup>3</sup> Kobe University of Maritime Marine

Proceedings of the Eleventh International Heat Transfer Conference, Vol.2 (1998)  
pp.351-356.

The flow boiling critical heat fluxes (CHF's) on the surface of a vertical cylinder with 1.2 mm diam. and 72 mm length located at a center line of a round tube of 38 mm inner diam. and 1425 mm length, and on the inner surface of a short tube of 9 mm inner diam. and 48 mm length with water flowing upward were measured for the wide ranges of flow velocities, subcoolings and pressures. The CHF's versus subcoolings at each flow velocity for various pressures for the test cylinder, which increased with an increase in subcooling, were clearly dependent on the pressures for the lower subcoolings; on the contrary, they were almost independent of the pressures for the higher subcoolings except those for the pressures near atmospheric. The similar trend of subcooling dependence was also observed in the CHF's on the test tube

for intermediate and high subcooling range. However, the CHF for low subcoolings became larger from the minimum value at the lowest subcooling for the intermediate range with a decrease in subcooling down to zero. The minimum value was dependent on the pressure. The CHFs for low subcoolings for the test cylinder and those for intermediate subcoolings for the test tube agreed within 5 % difference with the values derived from the authors' correlation for each shape of the test heater based on the hydrodynamic instability CHF model. On the other hand, the CHFs for high subcooling, that were considerably lower than the predicted values by the correlation, were explained by assuming that the CHFs occur due to explosive-like heterogeneous spontaneous nucleation in previously flooded cavities on the surface in nucleate boiling regime. This assumption was first made for the pool boiling CHFs for high subcoolings and already clarified experimentally, theoretically and photographically in the papers published by the authors.

**308: Transient Heat Transfer Caused by a Stepwise Heat Input to a Flat Plate in Pressurized He II**

**M. Shiotsu, K. Hata\*, Y. Takeuchi\*, K. Hama\* and Y. Shirai**

**\* Institute of Advanced Energy Kyoto Univ.**

Proceedings of the 17th International Cryogenic Engineering Conference, (1998) pp. 687-690.

The lifetime of quasi-steady state in Kapiza conductance regime caused by a large stepwise heat input to a flat plate was systematically measured for the liquid temperatures ranging from 1.8 to 2.1 K at atmospheric pressure: the quasi-steady state rapidly changes to film boiling regime after the depletion of lifetime. Width of the test heater plate was varied from 3.8 to 40 mm. The lifetime for a certain quasi-steady heat flux,  $q_s$ , beyond steady-state critical heat flux,  $q_{st}$ , is almost independent of the plate width, although  $q_{st}$  depends on it. The lifetime is proportional to  $q_s^{-4}$  for the  $q_s$  lower than that corresponding to  $t_L=1.2$  ms, and to  $q_s^{-2}$  for

**309: Critical Heat Flux on Various Sized Flat Plates in Pressurized He II**

**H. Tatsumoto, K. Hata\*, Y. Takeuchi\*, K. Hama\*, Y. Shirai and M. Shiotsu**

**\* Institute of Advanced Energy Kyoto Univ.**

Proceedings of the 17th International Cryogenic Engineering Conference, (1998) pp. 683-686.

Critical heat fluxes on four different sized horizontal flat plates with widths ranging from 3.8 to 40 mm were measured in pressurized He II at atmospheric pressure for the bulk liquid temperatures of 1.8, 1.9, 2.0 and 2.1 K. Each flat plate heater was made of Manganin whose one side was insulated by pasting it on FRP plate. The measured CHFs were higher for shorter width of the test plate and for lower liquid temperature. A correlation of CHF on the flat plate was presented by modifying the authors' theoretical

CHF correlation for a cylinder. The correlation can describe the CHF data on various sized flat plates within 20 % differences.

**310: A Model for the CHF of One-wall Heated Rectangular He II Channel Critical Heat Flux on Various Sized Flat Plates in Pressurized He II.**

**K. Hata<sup>\*</sup>, M. Shiotsu, Y. Takeuchi<sup>\*</sup> and K. Hama<sup>\*</sup>**

**\* Institute of Advanced Energy Kyoto Univ.**

Proceedings of the 17th International Cryogenic Engineering Conference, (1998) pp. 789-792.

A model for the critical heat flux on a heated inner wall of a short rectangular channel in pressurized He II was presented. The model consists of the Gorter-Mellink heat conduction in the channel and the heat transport from the cross sectional area at both opened ends of the channel to large He II pool. Heat transfer equation from a flat plate to a large pool of pressurized He II obtained by the authors was used for the latter heat transport equation. The model can describe well the effect of channel gap length on the critical heat fluxes (CHF) of short channel observed by Kobayashi et al. The analyzed liquid temperature at both ends of the channel under the condition of critical heat flux almost agrees with the bulk liquid temperature  $T_B$  for  $T_B$  higher than 2 K, but it becomes higher than  $T_B$  with the decrease in  $T_B$  from the value.

**311: Critical Heat Fluxes in Subcooled Boiling of Water Flowing Upward in a Vertical Tube for Wide Ranges of Liquid Velocity, Subcooling and Pressure .**

**K. Hata<sup>1</sup>, K. Fukuda<sup>2</sup>, M. Shiotsu, A. Sakurai<sup>3</sup>, N. Noda<sup>4</sup>, O. Motojima<sup>4</sup> and A. Iiyoshi<sup>4</sup>**

<sup>1</sup> **Institute of Advanced Energy Kyoto Univ.**

<sup>2</sup> **Kobe University of Mercantile Marine**

<sup>3</sup> **Future Energy Research Assoc.**

<sup>4</sup> **National Institute of Fusion Science**

Proceedings of the 6th International Conference on Nuclear Engineering, Paper No. ICONE-6362 (1998) pp.1-16.

The flow boiling critical heat fluxes (CHF) versus inlet subcoolings  $\Delta T_{sub,in}$  at a flow velocity for various pressures were clearly divided into first, second and third groups for low, intermediate and high  $\Delta T_{sub,in}$ . The CHF first decrease from the CHF at saturated condition,  $q_{cr,sat}$ , near zero  $\Delta T_{sub,in}$  down to the minimum CHF at the higher limit of  $\Delta T_{sub,in}$  for the first group, secondly increase up to the CHF at the higher limit of  $\Delta T_{sub,in}$  for the second group and thirdly also increase with the increasing rate of CHF for  $\Delta T_{sub,in}$  lower than that of the second group with an increase in  $\Delta T_{sub,in}$ . The CHF for lower and intermediate subcoolings were clearly dependent on the pressures; on the contrary those for high subcooling were almost independent of the pressure. The effects of outlet subcoolings, and tube inner

surfaces of rough and mirror on the high CHF's for high subcoolings were obtained by the comparison of the present CHF's with the corresponding predictions from existing correlations, the predictions revealed the inadequacy in the prediction of the anomalous trend of CHF's observed here. Three CHF correlations for low, intermediate and high subcoolings were derived as the fundamental database for high heat flux thermal management.

**312: \* Experimental Study on Superconducting Fault Current Limiter with Adjustable Trigger Current Level**

**Kazuhiro Fujikawa, Yasuyuki Shirai, Takeo Nishikawa, Tanzo Nitta\*, Masayuki Fukunishi\* and Toshikazu Shibata\*\***

**\*The University of Tokyo, \*\*Sumitomo Electric Industries, Ltd**

Proceedings of 15th International Conference on Magnet Technology, Part ONE, SCIENCE PRESS, pp.571-574, 1998.

Fault analyses of power systems including superconducting fault current limiters (SCFCLs) point out that accuracy of the trigger current level of an SCFCL should be in a few tens percents. An SCFCL with adjustable trigger current level is proposed. A trial SCFCL of this type is designed and made. Basic tests on the SCFCL were carried out. Availability of the proposed SCFCL is discussed experimentally in this paper.

**313: Thermoelectric Power Generation: Converting Low-Grade Heat into Electricity**

**Katsutoshi Ono, Ryosuke O. Suzuki**

Journal of Metals, Dec. pp.49-51, 1998.

This article describes some of the fundamental aspects of thermoelectric power generation, which employs low-temperature heat sources to create electricity. The focus is on a potential system design and viable thermocouple materials. regarding generator design, a system is proposed that uses forced-air circulation and a multistage heat-exchanger to efficiently convert the heat content of a low-grade heat source into useful electricity. As for thermocouple materials, both p-type Fe-12.8Al-12.7Si and n-type Fe-112.3Al conductors exhibit significant thermoelectric power-conversion capabilities, making them ideal candidates for use in the proposed power-generation system.

**314: Experimental Phase Diagram in the Ag-Cu<sub>2</sub>O-CuO System**

**Hiroshi Nishiura, Ryosuke O. Suzuki, Katutoshi Ono, Ludwig J. Gauckler\***

**\*: Swiss Federal Institute of Technology (ETH-Zurich)**

The Journal of American Ceramic Society, 81 [8] pp.2181-87, 1998.

Phase equilibria in the Ag-CuO-Cu<sub>2</sub>O system were experimentally determined using thermal analysis, and structural and compositional studies. Three reactions were observed in air: (1)  $L_1 = \text{CuO} + \text{Ag}$ , (2)  $L_2 = \text{CuO} + L_1$ , and (3)  $\text{Cu}_2\text{O} = \text{CuO} + L_2$ . The evolution and absorption of oxygen accompanied these reactions. At oxygen partial pressures below 0.02 bar, the reactions  $L_1 = \text{Cu}_2\text{O} + \text{Ag}$  and  $L_2 = \text{Cu}_2\text{O} + L_1$  were found. Based on isobaric projections in the Ag-CuO-Cu<sub>2</sub>O system, two invariant reactions,  $L_1 = \text{CuO} + \text{Cu}_2\text{O} + \text{Ag}$  and  $L_2 = \text{CuO} + \text{Cu}_2\text{O} + L_1$ , were deduced.

**315: Thermodynamic description of the Pb-O System**

**Daniel Risold, Jun-ichi Nagata, Ryosuke O. Suzuki**

Journal of Phase Equilibria, 19 [3] pp.213-233, 1998.

The phase relations and thermodynamic properties of the Pb-O system are reviewed and assessed. The transformation temperature between PbO and Pb<sub>3</sub>O<sub>4</sub> was also experimentally reinvestigated. A model description of the Pb-O system is then proposed and thermodynamic parameters are optimized. The values calculated from the resulting consistent set of Gibbs energy functions are compared with experimental data and discussed.

**316: Experimental Phase Equilibria in the PbO<sub>x</sub>-CaO System**

**Ryosuke O.Suzuki, Jun-ichi Nagata, Daniel Risold**

The Journal of American Ceramic Society, 81 [9] pp.2493-96, 1998.

Phase equilibria in the PbO<sub>x</sub>-CaO system at oxygen partial pressures of  $1.01 \times 10^5$  and  $1.01 \times 10^3$  Pa were experimentally investigated. The temperatures of the eutectic reaction between PbO and PbCa<sub>2</sub>O<sub>4</sub> and of the peritectic melting of PbCa<sub>2</sub>O<sub>4</sub> were measured via differential thermal analysis at five oxygen partial pressures. The phase transition in air between PbO and Pb<sub>3</sub>O<sub>4</sub> was not affected by the coexistence of PbCa<sub>2</sub>O<sub>4</sub>.

**317: Thermoelectric Properties of the Fe-Al and Fe-Al-Si Alloys for Thermoelectric Generation Utilizing Low-Temperature Heat Sources**

**Katsutoshi Ono, Masaki Kado, Ryosuke O. Suzuki**

steel research, 69 [9/98] pp.387-390, 1998.

The iron is intrinsically p-type conductor. When aluminum with three valence electrons is added to the iron, the d-subbands are occupied by electrons, so alloying with the aluminum transforms the iron to the n-type conductor, hence the p-n junction is made possible. Furthermore, when silicon is added to the n-type Fe-Al alloy, this alloy returns to the p-type conductor. Therefore, the thermoelectric p-n junctions with high thermoelectric power have been recognised:

Fe(p) - Fe12%Al(n):  $\Delta\alpha = 38 \mu\text{V/K}$

Fe12%Al12%Si(p) - Fe12%Al(n):  $\Delta\alpha = 70 \mu\text{V/K}$

(mass contents in %)

Thermoelectric generation offers possibility of a gigantic electric power generation utilising low-temperature sources of energy below 700 K such as exhaust heat from the central-station steam-electric plant, solar heat and terrestrial heat. The immense production of electricity by this principle is made possible exclusively by means of the conversion materials consisted of the iron and iron-based alloy because the generator can be manufactured on an efficient mass production basis, and the alloys mentioned above will meet this requirement. In this paper, the thermoelectric properties of these alloys such as Seebeck coefficient, thermal conductivity and electrical resistivity were experimentally determined in the temperature range between 300 and 700 K to provide basic data on the conversion materials with respect to the thermoelectric generation utilising low-temperature heat sources.

**318: Titanium Powder Production by TiCl<sub>4</sub> Gas Injection into Magnesium through Molten Salts**

**Tetsushi N. Deura, Masahiro Wakino, Tomoya Matsunaga, Ryosuke O. Suzuki, Katsutoshi Ono**

Metallurgical and Materials Transaction B, 29B [12] pp.1167-74, 1998.

A process to produce titanium powder continuously is proposed and its applicability is examined experimentally. The method is based on the chemical reaction in the conventional Kroll reduction process; however, TiCl<sub>4</sub> gas is injected into molten salt on which a molten magnesium layer is floated as the reductant. Bubbles of gaseous TiCl<sub>4</sub> can be reacted at the lower surface of the liquid Mg layer, while TiCl<sub>4</sub> gas reacts on the upper surface in the Kroll process. The fine Ti particles produced in this study were well separated from magnesium and could be recovered from the bottom of the molten salts. The particles were small and fine enough for use in powder metallurgy, while congregated lumps of about 20  $\mu\text{m}$  in size are obtained by the Kroll process. The composition of molten salts and an operation

temperature above 1073 K did not affect the morphology of the Ti particles, if suitable material for the reaction vessel was chosen.

**319: New Iron-Based Thermoelectric Junctions and Thermoelectric Generation Concept**

**Katsutoshi Ono, Ryosuke O. Suzuki**

Proceedings of 17th International Conference on Thermoelectrics (ICT98), pp.515-518, 1998.

This article describes a new concept of the thermoelectric power generation from the immense low-temperature heat sources. The thermoelectric junction to be used for the present purpose is a new p-n junction consisted of Fe<sub>12</sub>pctAl<sub>12</sub>pctSi(p) - Fe<sub>12</sub>pctAl(n) (pct. in weight) which exhibits a thermoelectric power as high as 70microV/K and relatively high electrical conductivity even at low temperatures, and which can be manufactured on an effective mass production basis. Important issue of this study is the heat-exchange type multi-stage thermoelectric generation system. Theoretical approach was dealt with in order to organize the system so as to make the electrical recovery efficiency close to 80 pct.

**320: Solid State Deoxidation of Niobium by Vacuum Deposited Titanium**

**Ryosuke O. Suzuki, Masayuki Aizawa, Katsutoshi Ono**

Journal of Alloys and Compounds, 284, [1-2], pp.222-227, 1999.

A two step deoxidation of niobium was proposed as an alternative for titanium external gettering. The proposal was experimentally confirmed. Titanium vapor from the melt was deposited in vacuum on the free surface of niobium samples, and subsequently the deposited samples were annealed to diffuse oxygen from the Nb bulk to the Ti coating layer. Due to the radiation heat during electron beam vacuum melting of Ti, the deoxidation by the Ti deposit occurred partially. Electric resistivity measurements showed a hundreds times faster deoxidation in the subsequent annealing than during external gettering. This fast deoxidation could prevent the Ti penetration into Nb. RRR measurements suggested that the annealing could be conducted at lower temperatures than for external gettering.

**321: Evaporation Process in Vacuum Metallurgy**

**Katsutoshi Ono, Ryosuke O. Suzuki**

Journal of the Mass Spectrometry Society of Japan, 47, [1], pp.38-41, 1999.

Born of necessity in the metallurgy of the reactive metals, vacuum technology is now being applied to the steel-making resulting in excellent quality control and properties not otherwise realizable. To provide an insight into the selection and evaluation of the experimental data, the authors have considered it advisable to present a systematic review of the principles and theories on evaporation phenomena. This article contains the basic aspect of the free evaporation under perfect vacuum, the vapor transfer through the thermal boundary layer under poor vacuum, the enhancement of evaporation, the restriction evaporation and the selective evaporation from multi-component bulk.

**322: Thermodynamic considerations of zirconia electrochemical sensors**

**Masanori Iwase**

Proceeding of Alex McLean Symposium, ISS/AIME, 1998, pp.217/222,

In this article an overview was made on the recent development of zirconia sensors for liquid metal control. It must be emphasized that considerable research together with in-plant evaluation is required in order to transform a fundamental scientific concept into a reliable sensing device which can be used as an integral component of a process control system. For truly effective technology transfer in the field of sensor development it is essential that basic studies be conducted in close co-operation with instrument manufacturers and the user community, as exemplified for high-carbon ferrochromium. With this tri-partite interaction, there is excellent opportunity for linkages between people within the research, development and utilization communities. Successful implementation of a new sensor can have a direct impact on conventional processes and also provide the essential knowledge required for the modeling and control of new processes for the 21-st century. Activities of this type are a critical link in the chain of quality and a mandatory requirement for intelligent processing.

**323: A thermodynamic study of Calcium cyanamide**

**Motoki Yamanka, Yoshiyuki Fujita, Alexander McLean, Masanori IWASE.**

High Temperature Materials and Processes, vol.20, 1999, pp.1/8

The equilibrium nitrogen pressures for the following reaction have been measured at temperatures between 1123 K and 1303 K:  $i\text{CaCN}_2 + i\text{C}_i = i\text{CaC}_2 + (\text{N}_2)$  The equilibrium nitrogen partial pressures above the mixture  $i\text{CaCN}_2 + i\text{C}_i + i\text{CaC}_2$  could be expressed as  $\log (P_{\text{N}_2} / \text{Pa}) = - 3660 / (T/\text{K}) + 6.98$  at temperatures between 1123 and 1303 K.

**324: Activities of phosphorous in Cu-Co-P alloys at 1573 K****M. Hasegawa, A. McLean and M. Iwase**

Scandinavian Journal of Metallurgy, vol.27, 1998, pp.219/222.

By employing an electrochemical technique incorporating magnesia-stabilized zirconia electrolyte, the activities of phosphorus in liquid Cu-Co alloys were determined at 1573K. With this technique liquid Cu-Co-P alloys were brought into equilibrium with Al<sub>2</sub>O<sub>3</sub> and AlPO<sub>4</sub>, and the oxygen partial pressures measured with the aid of a solid-oxide galvanic cell. At relatively low phosphorus concentrations, the solution of phosphorus in Cu-Co alloys obeys Henry's law. With the addition of 10 wt pct. Co the activity coefficient of phosphorus is decreased by a factor of 100.

**325: Equilibrium between aluminum and oxygen in Fe-36****1973 K における Fe-36****Hiroyasu FUJIWARA, Atsushi HATTORI, Eiji ICHISE**

Tetsu-to-Hagane · vol.85 · No.3 · pp.201-207 · 1999

鉄と鋼 · vol.85 · No.3 · pp.201-207 · 1999

The deoxidation equilibrium for aluminum in liquid iron and Fe-36 were carried out under pressure controlled H<sub>2</sub>/H<sub>2</sub>O gas at 1973 K. Within the composition range of [the interaction parameter between aluminum and oxygen in liquid iron and Fe-36] values of the equilibrium constant for the deoxidation reaction: Al<sub>2</sub>O<sub>3</sub>(s) = 2 Al(1wt for liquid iron and Fe-36 in logarithmic scale, respectively.

**326: Trends and Short-Term Prospects for Energy Consumption from a Statistical Point of View**

エネルギー資源統計から見たエネルギー消費動向の現状と近未来

**Shiro Kadoshin and Takashi Nishiyama**

Energy and Resources, Vol.20, No.2, pp.192-197, 1998

エネルギー · 資源、第20巻、2号、pp.192-197、1998

Energy consumption has been increasing remarkably over the past half century mainly due to increasing population and economic development. Short-term prospects for energy consumption in the selected 8 countries and 2 areas are embodied respectively using population estimates from the United Nations and GDP growth rates from the Institute of Energy Economics Japan. A linear relationship between per capita GDP and per capita energy consumption was found during the period, 1982-1993, after the world economy was rid of the economic crisis caused by oil shocks. According to an exploration of this trend, the demand for energy consumption for the year, 2005 and 2010 was calculated. Energy

consumption in the researched countries or areas will increase radically. Especially China and India, with large populations, will amount for a large amount of energy consumption. Energy consumption in most developed and industrialized countries, such as Japan, France, Germany and Korea will increase due to economic development rather than increasing population, while that in the USA will increase due to both components, economic development and increasing population. A substantial decline in energy consumption based on the effects of population in Germany and Japan will occur in the future. Energy consumption in developing countries, such as China, India, Indonesia and Latin America will also increase due to the 2 fundamental components. However, the increase in energy consumption due to economic development in China, India and Indonesia is higher compared to that due to increasing population. In Latin America, the effects of both factors are roughly equal. It is also significant that energy consumption in Africa is absolutely dependant on the effect of increasing population. However, the African contribution to the world energy consumption is small. On a worldwide scale, energy consumption will be most affected by economic development in the near future (in Japanese).

### **327: Instabilities in the Consumption and Production for Cobalt**

**Takashi Nishiyama and Hideki Fujii\* \*(Board of Audit)**

Nonrenewable Resources, Vol.7, No.4, pp.281-285, 1998

Cobalt is obtained mainly as a byproduct of the mining and metallurgical processing of copper and nickel. The amount of minable cobalt has a characteristic supply limit, which is dependent upon demand of copper and nickel. It is considered that cobalt consumption will be affected by the amount mined in the near future, because world demand has been gradually increasing, while the production from copper sulfide ore in Zaire and Zambia, major producing countries, has decreased for political, economical and technical reasons. The world demand for cobalt has surpassed the world mine production, and cobalt sales from the National Defense Stockpile of the United States and exports from Russia and cobalt recovered from stockpiled intermediates contributed to the supply in 1994. It is concluded, from a statistical point of view, that this trend of shortage and high prices for cobalt will continue in the near future.

### **328: \* Fluorescent Approach to Visualize Grout Injected into rock Masses**

蛍光法によるグラウト浸透状況の可視化

**Michinao Terada\*, Yoshiaki Iwamoto\*, Takashi Nishiyama and Youqing Chen \*(OKU-MURA CORPORATION)**

Tsuchi-to-Kiso, Vol.47, No.3, pp.29-32, 1999

土と基礎、第47巻、3号、pp.29-32、1999

A new fluorescent approach was developed to visualize grouting processes. Various types of grout mixtures containing fluorescent substance were observed under ultraviolet light, using a borehole television system or a microscope. The process of grouting, the occurrences of grout precipitated from the early to

late driving of grouting were visualized and clearly demonstrated. It is considered that this approach is useful for analysis of grouting (in Japanese).

### 329: Topographic Survey in Open-cut Mines by Using RTK-GPS

露天採掘鉱山の地形測量における RTK-GPS 測量の適用

Makoto Omura\*, Toshihide Ito\*\* and Takashi Nishiyama \*(Kochi Women's University)  
 \*\*(Kansai University)

Shigen-to-Sozai, Vol.114, pp.699-703, 1998

資源と素材、第 114 巻、pp.699-703、1998

RTK-GPS (Real Time Kinematic-Global Positioning System) was applied to topographic survey in open-cut mines. The operation of the survey involves great difficulties, such as obstacles caused by local topography and electromagnetic noises interfering with micro-wave from GPS-satellites. Therefore, the survey was carried out under conditions when a good GPS-satellite constellation was formed in the sky, limited by local topography in each working face. A clear data link between two GPS-receivers on the working face was also important. In a field experiment at an operating open-cut mine, about 190 points were surveyed in about 5 hours on two successive days. Repeatability was estimated to be about  $\pm 6$  cm in coordinates obtained by the RTK-GPS. Topographic changes by operation were well pointed out by examining plotted RTK-GPS surveyed points on the topographic map surveyed by the traditional method. Consistency in coordinates was estimated to be about  $\pm 9$  cm between traditional local coordinates and those obtained by the RTK-GPS. Usefulness of the RTK-GPS was clearly demonstrated by examining actual field data acquired in operating open-cut mines. Rapid and precise measurements by the RTK-GPS is more suitable than the traditional optical surveying method for monitoring the topographic change in working face and for providing digital topographic data required for computer systems (in Japanese).

### 330: Use of GPS for Generating Topographic Maps and Production Schedules of Open Pit Mines

GPS による露天採掘鉱山の地形図作成と採掘計画

Toshihide Ito\*, Makoto Omura\*\* and Takashi Nishiyama \*(Kansai University)  
 \*\*(Kochi Women's University)

Shigen-to-Sozai, Vol.114, pp.939-944, 1998

資源と素材、第 114 巻、pp.939-944、1998

Utilization of digital topographic data for open pit mines was analyzed, including topographic map generation, modification of maps and estimation of mine productivity. On previous topographic maps of open-pit mines generated by computer systems, construction details, such as working faces and roads, were difficult to identify from the contour lines. In these maps, many contour lines were drawn very close together due to large fluctuations in topographic features. The presence of large numbers of contour lines often obstructed construction details. To identify these construction details, the outlines of each construction were drawn, and the contour lines enclosed by these outlines were erased. Furthermore,

construction details, such as manufacturing plants and office buildings, which were not identified by the contour lines. were drawn using the same algorithm. Highly detailed maps that distinguished these construction details from contour lines were then created. This digital topographic data was useful for simulating scene changes and the extent of mining. Computer graphics allowed simulation of scene changes in advance, and provided basic data concerning future changes. Moreover, These maps allowed accurate estimates of mine production to be calculated. To generate these maps, GPS (Global Positioning System) was utilized to measure topographic changes only where the operations had taken place. Furthermore, construction details outlines were also obtained from the operator's input previously arranged by the rule, i.e. inputting a set of surveyed points for construction. This mapping system easily maintained monthly or annually updated data on topographic and construction changes. For production schedule simulation, topographic maps, computer graphics, and product estimations based on monthly or annually up-to-date digital topographic data were useful (in Japanese).

**331: Numerical Model for Gas-Liquid Two-Phase Mixture Flow in a Vertical Pipe with a Sudden Enlargement in Diameter**

管径が急拡大する鉛直管内における気液二相流の数値モデル

Natsuo Hatta, Masaaki Omodaka\*, Takahiro Takatsu\*\*, Hitoshi Fujimoto, Hirohiko Takuda, Jung-Seock Kang\*\*\*

\*(Nippon Steel Corp.), \*\*(NKK Corp.), \*\*\* (Korea Institute of Geology)

Journal of the mining and materials processing institute of Japan, Vol.114,  
No.7, pp.475-482, 1998

資源と素材, 114 巻 7 号, pp.475-482, 1998

This paper is concerned with a numerical model for the steady-state flow characteristics of the gas-liquid two-phase mixture flowing upward in a vertical pipeline with an abrupt enlargement in cross sectional area. The system of governing equations used is based upon the multifluid model and the transitions of gas flow pattern are taken into consideration. For the case of an abrupt enlargement in diameter in a coaxial pipeline, the procedure of the numerical calculation to obtain the flow characteristics in the pipeline has been proposed in the present investigation. At the same time, the experiments have also been performed using two kinds of lifting pipes in order to confirm the validity of the numerical model. As a result of the comparison of the calculated results with the experimental data, we have confirmed the applicability of the system of governing equations as well as the validity of the procedure of the numerical calculation proposed here to the prediction of the flow characteristics of the gas-liquid two-phase mixture in a vertical pipe with a sudden change in diameter.

**332: \* A Simple Approach to Plane Strain Extrusion with Dead Metal Zone Using Upper-Bound Theorem****Hirohiko Takuda, Natsuo Hatta**

Metals and materials, Vol.4, No.4, pp.737-741, 1998

This paper treats the upper-bound approach to the problem of rigid-plastic deformation in case where the configuration of the deformation zone is previously unknown. The plane strain forward extrusion process with the so-called dead metal zone is analysed by assuming a simple velocity field. The calculations are carried out for the material with or without strain hardening or strain rate sensitivity and for various reduction ratios. The numerical results show that the region of the dead metal zone becomes smaller with the increase in the reduction ratio. The calculated punch forces agree with the experimental one fairly well. Furthermore, it is found that the dead metal zone becomes larger with increasing the strain hardening as well as the strain rate sensitivity of the material.

**333: \* Modelling on Flow Stress of Mg-Al-Zn Alloys at Elevated Temperatures****Hirohiko Takuda, Hitoshi Fujimoto, Natsuo Hatta**

Journal of Materials Processing Technology, 80-81, pp.513-516, 1998

For the evaluation of flow stress of magnesium-based alloys AZ31 and AZ91 in hot working processes, a formula is derived by analysing the stress data measured at various temperatures and strain rates. The formula is expressed in a simple form by means of the temperature-compensated strain rate, i.e., the Zener-Hollomon parameter,  $Z$ . It is demonstrated that a linear equation of the logarithmic  $Z$  fits the flow stress of the alloys at elevated temperatures.

**334: \* Finite Element Analysis of Forming Limit in Bore Expanding of Aluminium Alloy Sheets****Hirohiko Takuda, Yoshimitsu Tanaka\*, Natsuo Hatta**

\*(Kubota Corp.)

Archive of Applied Mechanics, Vo.68, pp.566-576, 1998.

A recently proposed method to predict the forming limit of sheet metals is applied to the problem of bore expanding. Axisymmetric bore-expanding processes of various aluminium alloy sheets are simulated by the rigid-plastic finite element method. From the calculated histories of stress and strain, the forming

limit, i.e. the fracture initiation, is predicted by means of the ductile fracture criterion. The comparison with the experimental results shows that the fracture initiation site and the critical punch stroke are successfully predicted by the present approach.

**335: Collision Dynamics of a Water Droplet Impinging on a Hot Solid Surface**

**Natsuo Hatta, Hitoshi Fujimoto, Torahiko Yokotani\***

**\*(Tsubakimoto Chain Corp.)**

Steel Research, Vol.69, No.10/11, pp. 429-437, 1998.

The collision dynamics of a water droplet impacting on a solid surface heated above the Leidenfrost temperature are treated in this paper. Emphasis is placed upon the droplet disintegration process and the effect of the Reynolds number, as well as the solid surface temperature, on the droplet deformation process. As a result, it has been found that, for the case of low Weber number, but above the critical one, the droplet breaks up into some parts in the recoiling process and that as the Weber number is increased further, the droplet disintegration occurs in a spreading process. It has been confirmed that the effect of the Reynolds number on the droplet deformation is negligibly small in the earlier stage, but a little significant in the later stage just before/after rebounding from the surface. Furthermore, it has been clarified that there is almost no effect of the surface temperature, or the Reynolds number, on the maximum spreading diameter, the time needed for the spreading droplet reach a maximum diameter, and the time from the moment of collision to rebounding from the surface.

**336: \* Numerical Analysis of the Formability of an Aluminium 2024 Alloy Sheet and Its Laminates with Steel Sheets**

**Hirohiko Takuda, Natsuo Hatta**

Metallurgical and Materials Transactions A, Vol.29A, pp.2829-2834, 1998.

A criterion for ductile fracture is applied to the formability prediction of an aluminum 2024 alloy sheet and its laminated composite sheets. Axisymmetric deep-drawing processes of the 2024 sheet and the laminates clad by mild steel sheets are simulated by the finite-element method. From the calculated distributions and histories of stress and strain, the fracture initiation site and the forming limit are predicted by means of the ductile fracture criterion. The predictions so obtained are compared with experimental observations. The results show that the fracture initiation in the 2024 sheet with no appearance of necking is successfully predicted by the present numerical approach. Furthermore, it is found that the formability of the 2024 sheet is improved by sandwiching it with the mild sheets.

**337: \* Formability of a Commercially Pure Zirconium Sheet**

**Hirohiko Takuda, Shiomi Kikuchi\*, Natsuo Hatta**  
**\*(University of Shiga Prefecture)**

Journal of Materials Processing Technology, Vol. 84, pp. 117-121, 1998.

To examine the formability of sheet zirconium in forming processes, some fundamental sheet forming tests, i.e. the deep drawing, the Erichsen and the bore-expanding tests are carried out for a commercially-pure zirconium sheet. The tensile properties are also examined by uniaxial tension tests in the direction of  $0^\circ$ ,  $45^\circ$  and  $90^\circ$  to the rolling direction, and the relationship of them to the deformation behavior in sheet forming processes is discussed. Due to a large value of the normal anisotropy parameter,  $r$ , the zirconium sheet shows the quite high drawability, whilst the stretchability is low. Due to strong planar anisotropy, very large ears are formed in deep drawing. It is noted that the forming limits in the deep drawing and bore-expanding process decrease with the punch profile radius.

**338: Theoretical Analysis of Flow Characteristics of Multiphase Mixtures in a Vertical Pipe**

**Natsuo Hatta, Hitoshi Fujimoto, Makoto Isobe\*, Jung-Seock Kang\*\***  
**\*(Nippon Steel Corp.), \*\* (Korea Institute of Geology)**

International Journal of Multiphase Flow, Vol.24, pp.539-561, 1998

This paper is concerned with the theoretical analysis to obtain the flow characteristics of multiphase mixtures in a vertically fixed air-lifting pipe. The case is treated where a transition process from a solid-liquid two-phase mixture flow to a solid-gas-liquid three-phase mixture by injecting gas-phase into the riser through a gas injector is present. The transitions of the flow pattern of gas-phase from bubbly to slug flows and from slug to churn flows are taken into account in the system of governing equations. In order to verify the validity of the system of governing equations accounting for the flow patterns transitions of gas-phase, the calculated results have been compared with experimental data measured by other investigators. It has been found that the present theoretical model gives a good fit to the experimental data. Furthermore, it has been demonstrated that the present model can predict the maximum solid/liquid volumetric flux.

**339: \* Reduction of Noise Radiated from Supersonic Jet by Interaction between the Screech and Cavity Tones**

**Yoshikuni Umeda\* and Ryuuji Ishii**

**\* Graduate School of Engineering, Kyoto University**

ASME FEDSM98-5, pp.1-6, 1998.

The supersonic freejets radiate broad band noise, shock associated noise, and very intense screech tone simultaneously. In recent years, the reduction of noise radiated from the supersonic jet becomes very important thema in connection with the development of the supersonic passenger airplane of next generation. In this experimental study, the possibility of the reduction of very strong screech tone radiated from the supersonic jet by the interaction between the screech tone and cavity tone which is generated when the open cavities expose to high-speed flow, was investigated and it was found that when internal cavity was placed near the nozzle exit, the SPL of the screech tone as well as the OASPL of sound was reduced.

**340: \* Acoustic Characteristics of the Noise Radiated from Supersonic Multi-Jets**

**Yoshikuni Umeda\* and Ryuuji Ishii**

**\* Graduate School of Engineering, Kyoto University**

Proc. 16th International Congress on Acoustics, pp. 1967-1968, 1998.

The acoustical characteristics of the noise radiated from combined jets issuing from one main nozzle and 1, 2, 4 or 8 sub-nozzles which were placed closely to the main nozzle were investigated experimentally. From the frequency characteristics of the screech tone, it is found that in almost all cases, two oscillation modes appear, but when 8 sub-nozzles with diameter of  $a/d = 0.6$  were used, the screech tone was disappeared completely. From variations of the SPL of screech tone, it is observed that although the total cross sectional areas of the multiple nozzles was larger than that of the single jet, the SPL radiated from multi-jets becomes the same or lower than that from the single jet.

**341: Numerical Simulation of Unsteady Supersonic Circular Jet**

**Ryuuji Ishii and Masatoshi Yuhi\***

**\* Department of Civil Engineering, Kanazawa University**

Proc. 15th NAL Symposium on Aircraft Computation Aerodynamics, pp. 289-294, 1998.

Time evolution of unsteady supersonic circular jet is investigated numerically by using a TVD finite difference scheme for the Euler equations. It is shown that the supersonic jet injected into an ambient gas is unstable and rapidly evolves into turbulent field.

**342: \* Effect of Hydrolysed Metal Cations on the Liquid-Liquid Extraction of Silica Fines with Cetyltrimethylammonium Chloride**

**Eishi Kusaka, Yousuke Kamata, Yasuhiro Fukunaka and Yoshitaka Nakahiro (Fukui Inst. Technology)**

Colloids and Surfaces A: Physicochemical and Engineering Aspects, Vol. 139, No. 2, pp. 155-162, 1998.

Silica fines of  $<5 \mu\text{m}$  were liquid-liquid extracted from aqueous suspension containing cationic surfactant cetyltrimethylammonium chloride (CTAC) to the isooctane-water interface region. The silica depression on addition of hydrolysable metal cations Fe(III), Al(III) and La(III) was investigated to clarify the role of such cations in the hydrophile-lipophile transition of the silica fines together with CTAC. At an addition of only 5 mM CTAC, the silica fines were completely recovered in the dense emulsion phase from metal salt-free suspension in the entire pH range investigated. In contrast, addition of 1-mM total metal cations caused silica depression in a certain pH range, specific for the metal salt used. Speciation distribution diagrams for the respective metal-H<sub>2</sub>O systems indicate that decreases in percent recoveries of the silica in the lower pH range are in line with increases in concentrations of the metal hydroxo complexes. Furthermore, the silica depression disappears when the pH approaches the point-of-zero charge of the hydroxide precipitate. In these pH ranges, the neutral to negative metal precipitates are also extracted into the oil-water interface during the liquid-liquid extraction. It seems that lipophilic-to-hydrophobic transition, that is, depression by metal-salt addition of silica fines in cationic liquid-liquid extraction is controlled by the presence of metal-hydroxide species and their charges, attributable to the hydroxide coating on the silica surface.

**343: Recycling of Disposal Consumer Electronics Goods – Recovery of Copper Components from Disposed Print Wiring Boards by Hydrocyclone**

**Eishi Kusaka, Hussin B. Kamardin\*, Yasuhiro Fukunaka and Yoshitaka Nakahiro\*\***

**\* School of Materials and Miner. Resources Eng., Universiti Sains Malaysia, \*\* Fukui University of Technology**

Proc. 7th JSPS-VCC Seminar on Integrated Engineering, pp. 479-484, 1998.

Disposal substrate taken out from the consumer electronics goods or disposed PWB (Print Wiring Board) materials were crushed, sieved and magnetically separated. Sample was dissolved into aqua regia and analyzed with an atomic absorption method. Au, Ag and Cd were not detected. Copper content and

distribution ratio in -20+35 mesh fraction were 45.6 % and 40.8 %, respectively. Non-magnetic particles of the -8+14 and -20+35 mesh fractions were processed with dense-medium separation and hydrocyclone. It was found that the effect of water flow rate of the overflow was significant to effectively separate the copper components into concentrate and tailings. Concentrate of the underflow shows apparently metallic reflection. The copper content and distribution ratio were improved to be 67.5 % and 89.0 %, respectively.

**344: \* Two-Liquid Flotation of Fine Oxide Particles with 8-Hydroxyquinoline**

**Eishi Kusaka, Kouji Maegawa, Yasuhiro Fukunaka, Masakazu Niinae\* and Yoshitaka Nakahiro**

**\* Faculty of Engineering, Kyoto University**

The Canadian Journal of Chemical Engineering, Vol. 77, No. 1, pp. 62-68, 1999.

The two-liquid flotation of fine oxide particles has been investigated using a chelating-type collector of oxine and the isooctane-water two-liquids' system. The recovery was enhanced in a certain pH range. The oil-floatability during two-liquid flotation was concerned with the oxine adsorption on the solids. In addition, solution-chemical calculations indicated that the reactivity of the metal cation with oxine based upon a surface precipitation model was closely related to the adsorbability of oxine and, hence, to the oil- floatability of the solids. Also, the possible conditions for collection by two-liquid flotation were experimentally determined; and were well related to the solution-chemical criterion.

**345: \* Measurements of Concentration Profiles of  $\text{Cu}^{2+}$  and  $\text{H}^{+}$  Ion near a Plane Vertical Anode by Two-Wavelength Holographic Interferometry**

**Yasuhiro Fukunaka, Yuuji Nakamura and Youko Konishi**

J. Electrochem. Soc., 145, 3814-3820(1998)

Two-wavelength holographic interferometer was applied to simultaneously measure the concentration profiles of  $\text{Cu}^{2+}$  and  $\text{H}^{+}$  ion near a plane vertical anode placed in an unstirred  $0.05\text{M}\text{CuSO}_4\text{-}1.85\text{M}\text{H}_2\text{SO}_4$  aqueous solution. The measurement was carried out at a low current density, under which a uniform current density distribution along the vertical anode was assured. The measured concentration profiles were similar to those arising from cathodic natural convection, when the difference in the flow direction was taken into account. As long as the electrode surface is flat and no precipitation of copper sulfate is observed, a nondimensional cathodic correlation based on boundary layer theory can be reasonably applied to anodic natural convection. Moreover, the addition of excess  $\text{H}_2\text{SO}_4$  resulted in a larger concentration gradient of  $\text{Cu}^{2+}$  ion at the anode surface, which compensated the negligible contribution of migration to the ionic mass transfer rate.

**346: \* Physical Modelling of Top Injection Smelting**

**Yasuhiro Fukunaka, Eishi Kusaka, Zenjiro Asaki\* and Yoshitaka Nakahiro\*\* \*Dept. of Materials Eng., Faculty of Engineering \*\*Fukui Institute of Technology**

Proc. of Symp. on Materials Processing, MMIJ, D, 71-73(1998)

Physical modelling was designed to simulate the highly intensified smelting technology. Acrylic resin particles laden SO<sub>2</sub>-N<sub>2</sub> gas jet was blown onto the surface of or into H<sub>2</sub>O<sub>2</sub> aqueous solution. The absorption rate of SO<sub>2</sub> gas into H<sub>2</sub>O<sub>2</sub> solution was monitored with a ion chromatography. The experimental results showed that the absorption rate was controlled by the gas phase mass transfer rate. It is in contrast to the liquid phase mass transfer controlling step observed in CO<sub>2</sub>-NaOH system. However, the expected enhancement effect of absorption rate caused by particle impingement to the solution was not so significant. Then, the surface of acrylic resin particle was treated with a kind of interface active agent of saponin. The absorption rate of SO<sub>2</sub> gas into H<sub>2</sub>O<sub>2</sub> solution was considerably improved with this surface treatment technique. This suggests the importance of wettability of injected particles to the gas-liquid contact behavior in the metallurgical reaction, especially, the recycled dust is smelted.

**347: \* Electrodeposition of Copper under Microgravity Conditions**

**Yasuhiro Fukunaka, Kimitoshi Okano, Yoichi Tomii, Zenjiro Asaki\* and Kazuhiko Kuribayashi\*\* \*Dept. of Materials Eng., Faculty of Engineering \*\*Inst. of Space and Aeronautical Science**

J. Electrochem. Soc., vol. 1876-1881(1998)

Copper was electrodeposited from 0.9M CuSO<sub>4</sub> aqueous solution for 8 seconds during a free-fall experiment in a drop shaft. A horizontally-orientated quasi two-dimensional electrolytic cell, in which a 200 $\mu$ m thick electrolyte layer was sandwiched by two sheets of slide glass, fell in the shaft. Electrolysis was conducted at constant current densities from 0.05 to 0.3A cm<sup>-2</sup>, and the potential difference between electrodes was simultaneously monitored. A common-path microscopic interferometer was installed in the capsule. The time variation of interference fringe pattern, corresponding to the concentration profile due to the ionic mass transfer rate accompanied with copper electrodeposition, was measured in-situ around the periphery of a 1-mm- dia circular cathode. The morphology of copper electrodeposited under microgravity conditions was compared with that obtained in a ground-level experiment. The development of diffusion layer thickness measured by the interferometer increased with the square root of time during the 8s experiment. The transient diffusion model combined with the migration effect reasonably explained the development of diffusion layer thickness. Calculated surface concentrations corresponded with the measured time variation of potential difference between electrodes. Under the gravitational field, the radius of annular interference fringe pattern developed at a rate much faster than that under microgravity, beginning 1 or 3 s after initiation of electrodeposition. Natural convection was evident in

the ground-level experiment, even using such a shallow electrolyte layer. Under microgravity, lower-index planes preferentially grew to form a fewer number of larger grains, even though electrodeposition was conducted at 0.05 to 0.3 A cm<sup>-2</sup> only for 8 s.

**348: Electrochemical Interfacial Phenomena under Microgravity Part 1 Electrochemical Dissolution of Copper in Drop Shaft**

**Yasuhiro Fukunaka, Youko Konishi, Yoichi Tomii, Yoshitaka Nakahiro\* and Kazuhiko Kuribayashi\*\* \*Fukui Inst. of Technology \*\*Inst. of Space and Aeronautical Science**

Metall. Mater. Trans., B, 30B, 99-105(1999)

As part of a series of physical modeling studies on the electrochemical etching of a printed wiring board, copper foil was anodically dissolved in a small cavity. Coupling of the ionic mass transfer rate with the under-cutting phenomena must be precisely understood in order to finely control high aspect ratio anisotropic etching. Interferometry has been applied to the study of the ionic mass transfer rate accompanying electrochemical reactions and it may help in the visualization of the concentration profile of the metal ion within a narrow cavity. As an idealistic case, the electrochemical dissolution of copper in a purely diffusional field, especially the Cu<sup>2+</sup> ion transfer rate itself, is now the focus of attention. The copper anode was galvanostatically dissolved in an aqueous solution (0.1M CuSO<sub>4</sub>-1M H<sub>2</sub>SO<sub>4</sub>) contained in a quasi-two-dimensional electrolytic cell for 8 seconds during free fall in a drop shaft. A disk type of anode, 1 mm in diameter and 100 μm in thickness, and a flat shaped ring cathode 20 mm in inner diameter were sandwiched by two sheets of slide glass. The electrolyte layer was 200 μm in effective thickness. The interference fringe pattern accompanying the copper dissolution, was measured in-situ with a common path-type microscopic laser interferometer. Terrestrial experiments were also conducted with a horizontally installed cell under the same electrolytic conditions. No natural convection would be expected in the present electrolytic cell design with such a shallow and horizontal electrolyte layer. The distance between the anode surface and the location at which the outer interference fringe appeared was measured by the duration time. It increased linearly with the square root of time under microgravity, but started to deviate from this linearity a few seconds after starting the electrolysis in the terrestrial experiment. A significant difference in the growing distance between the environments had not been a priori anticipated for such a quasi-two dimensional cell. The local current density distribution along the smaller electrode surface may be influenced by induction of a kind of natural convection.

**349: Characteristics of the NIJI-IV FEL at the electron-beam energy of 263 MeV**

**N. Sei\*, T. Yamazaki, K. Yamada\*, S. Sugiyama\*, T. Mikado\*, and H. Ohgaki\* \*Electrotechnical Laboratory**

Nucl.Instr.& Meth., A407 (1998) pp.187-192

The electron-beam and free-electron laser (FEL) characteristics have been measured at the electron energy as low as 263 MeV in the JIJI-IV FEL system. The peak electron density in the low-current region was higher by 40 % than that in the case of normal operation with electron energy of 310 MeV, though it was suppressed in the higher-current region by beam instabilities. The transverse FEL modes up to TEM<sub>02</sub> were observed, and the typical average FEL power was measured to be 50  $\mu$ W.

**350: Positron annihilation induced Auger electron spectroscopy with an intense slow-positron beam**

**T. Ohdaira\*, R. Suzuki\*, T. Mikado\*, and T. Yamazaki \***Electrotechnical Laboratory

J. Electron Spectroscopy and Related Phenomena, 88-91 (1998) pp.677-681.

A time-of-flight positron annihilation induced Auger electron spectroscopy (TOF-PAES) system has been developed, which is capable of measurement with much higher resolution and counting rate than the existing system. It has been proved from measurement of MoS<sub>2</sub> and Si with clean surface and surface with oxygen that the system can analyse the outermost surface layer with quite high sensitivity and without destroying the material.

**351: The Development of Ferritic Steels for DEMO Blanket**

**Akira Kohyama, Akimichi Hishinuma\*, Yutaka Kohno\*\*, Kiyoyuki Shiba\*, Akio Sagara\*\*\***

**\*Tokai Establishment, Japan Atomic Energy Research Institute, \*\*Univ. of Tokyo,**

**\*\*\*National Institute for Fusion Science**

Fusion Engineering & Design, vol. 41, pp.1-6, 1998.

The development of low-activation ferritic/martensitic steels is a key to the achievement of nuclear fusion as a safe, environmentally attractive and economically competitive energy source. The Japanese and the European Fusion Materials programs have put low-activation ferritic and martensitic steels R & D at the highest priority for a demonstration reactor (DEMO) and the beyond. An international collaborative test program on low-activation ferritic/martensitic steels for fusion is in progress as an activity of the International Energy Agency (IEA) fusion materials working group to verify the feasibility of using ferritic/martensitic steels for fusion by an extensive test program covering the most relevant technical issues for the qualification of a material for a nuclear application. The development of a comprehensive data base on the representative industrially processed reduced-activation steels of type 8-9Cr-2WVTa is underway for providing designers a preliminary set of material data for the mechanical design of components, e.g. for DEMO relevant blanket modules. The current design status of FFHR and SSTR utilizing low-activation ferritic steels is reviewed and future prospects are defined.

**352: Progress in the Development of SiC/SiC Composites for Advanced Energy Systems:CREST-ACE Program**

**Akira Kohyama, Yutai Katoh, Tatsuya Hinoki, Wen Zang, Masaki Kotani**

European Conference on Composite Materials Science -Technologies and applications, Vol.4, pp.15-22, 1998

Under the title of "R & D of Environment Conscious Multi-Functional Structural Materials for Advanced Energy Systems", a new R & D activity to establish high efficiency and environmental conscious energy conversion systems, as one of the programs of Core Research for Evolutional Science and Technology (CREST), has been initiated from October 1997 to September 2002. This program cares for R & D of high performance materials and materials systems for severe environments and production of model components for energy conversion systems is carried out. The emphasis is on R & D of SiC/SiC, W/W with their system studies to establish sound material life cycles. The program outline and preliminary results on SiC/SiC are provided.

**353: Roles of Interfacial Microstructure on Interfacial Shear Strength of SiC/SiC**

**Tatsuya Hinoki, Wen Zhang, Yutai Katoh, Akira Kohyama, Hideo Tsunakawa\***  
**\*Engineering Research Institute, The Univ. of Tokyo**

European Conference on Composite Materials Science -Technologies and applications, Vol.4 (1998) pp.209-215.

**354: Microstructural Evolution of SiC/SiC Composite under Irradiation**

European Conference on Composite Materials Science -Technologies and applications, Vol.4 (1998) pp.351-357.

Silicon carbide fiber reinforced silicon carbide matrix composite (SiC/SiC composite) is a potential material for use in very severe environment in advanced energy systems. In this work, neutron radiation tolerance of advanced SiC fiber reinforced SiC/SiC composite fabricated through chemical vapor infiltration method was studied by means of dual-beam ion irradiation experiment. The irradiated material was subjected to microstructural examination by transmission electron microscopy following the thin film processing with a focus ion beam device. The result showed the superior radiation resistance of the advanced low-oxygen near-stoichiometric SiC fiber but suggested the need for further study on the synergistic effect of atomic displacement and transmutant helium production.

**355: Effect of Fiber Coating on Initiation and Growth Characteristics in SiC/SiC under Indentation Test**

**Wen Zang, Tatsuya Hinoki, Yutai Katoh, Akira Kohyama, Tetsuji Noda\***

**\*National Research Institute for Metals**

European Conference on Composite Materials Science -Technologies and applications, Vol.4 (1998) pp.359-366.

SiC/SiC composites are attractive materials for fusion application and other applications such as heat exchanger and turbines. The objective of this work is try find a way to improve the toughness of the materials by investigating the interface microstructure under indentation test. SiC/SiC composite were made by CVI method. Carbon coatings and multiple coatings were applied to be interphase between fibers and matrix for improving the toughness. The effect of the coatings were studied by analyzing crack behavior and fiber debond behavior after push-in test by use of SEM and TEM. It was found that the fiber coatings were a very important role for improving the toughness of the SiC/SiC composites by leading fibers debond. This work offered some base data for finding a optimum coating thickness on fiber.

**356: Evaluation of Low-Temperature Swelling in Austenitic Stainless Steels**

**Y.Katoh**

American Standard for Testing and Materials STP 1325, pp.783-793, 1999

Major portions of structural materials of near-term fusion blankets and light water reactor core components are subject to neutron irradiation at low temperatures and low fluxes compared to those in typical void swelling studies using fast reactors. Observed swelling in austenitic stainless steels at temperatures below 673K are generally very small under typical fast reactor irradiation conditions, however, the amount of swelling might be significantly influenced by neutron flux, helium generation rate, etc. In this work, using a reaction rate theory model of swelling, the influences of such key irradiation parameters on low temperature swelling behavior in austenitic stainless steels will be demonstrated to aid evaluating swelling at low temperature / low neutron flux conditions.

**357: \* The HFIR 14J SiC/SiC Composite and SiC Fiber Collaboration**

**G.E.Youngblood\* R.H.Jones\* Akira Kohyama, Yutai Katoh, Akira Hasegawa\*\*,  
R.Scholz\*\*\*, L.L.Snead\*\*\*\***

**\*Pacific Northwest National Lab., \*\*Tohoku Univ., \*\*\*European Joint Research Com-  
mission, \*\*\*\*Oak Ridge National Lab.**

Proc. of The Fusion Reactor Materials, DOE/ER-0313/24, U.S.Department of En-  
ergy, pp.115-121, 1998

A short introduction with references establishes the current status of research and development of SiC/SiC composite for fusion energy systems with respect to several key issues. The SiC fiber and composite specimen types selected for the JUPITER 14J irradiation experiment are presented together with the rationale for their selection.

**358: Analysis of Interfacial Shear Process of CMCs**

**Tatsuya Hinoki, Wen Zhang, Hisashi Serizawa\*, Yutai Katoh, Akira Kohyama  
\*Osaka Univ.**

Proc. of ACCM-1, Vol.II, pp.510.1-4, 1998

Ceramic matrix composites (CMCs) are expected to apply for not only a

**359: Weld Cracking Behavior of Neutron Irradiated Austenitic Stainless Steel**

**Akira Kohyama, Takanori Hirose, Tsutomu Suzuki\*, Minoru Narui\*\*,  
Yutai Katoh, \*Sumitomo Metal Industries, Ltd., \*\***

Proc. of International Symposium on Environment-Conscious Innovative Materials  
Processing with Advanced Energy Sources, (1998) pp.621-624.

In fission and fusion reactor applications, properties of welds and welded joints are key factors which limit the service conditions including their end-of-life. Where, an availability of reliable repair welding techniques is strongly required in order to improve cost of electricity. One of the most difficult and the unique characteristic, of which the repair welding has to overcome, is the radiation damaged microstructure including nuclear transformed gaseous atoms, such as helium atoms from the ( $n, \alpha$ ) reaction.

**360: Development of High Performance Composites for Environment-Conscious Energy Applications****Akira Kohyama**

Proc. of International Symposium on Environment-Conscious Innovative Materials Processing with Advanced Energy Sources, (1998) pp.286-291.

Under the title of "R & D of Environment Conscious Multi-Functional Structural Materials for Advanced Energy Systems", a new R & D activity to establish high efficiency and environmental conscious energy conversion systems, as one of the programs of Core Research for Evolutional Science and Technology (CREST), has been initiated from October 1997 to September 2002. This program cares for R & D of high performance materials and materials systems for severe environments. The important goal is to produce model components for energy conversion systems with sufficient attractiveness. The emphasis is on R & D of SiC/SiC, W/W with their system studies to establish sound material life cycles. The present status of the program and the future prospects are provided.

**361: Multiple Beams-Material Interface Research Facility at Kyoto University and Prospective Application to Advanced Energy Materials Study****Yutai Katoh, Akira Kohyama, Masami Ando, Kouichi Jimbo, Tetsuo Sakka, Akihiko Kimura, Fumimichi Sano, Tohru Mizuuc**

Proc. of International Symposium on Environment-Conscious Innovative Materials Processing with Advanced Energy Sources, (1998) pp.428-433.

For the purpose of exploring the dynamic behavior of solid materials under severe environments in advanced energy systems, a multiple beams - material interaction research facility has been planned and designed for the last three years and is presently being constructed at the Institute of Advanced Energy, Kyoto University. The initial configuration will be a 1.7MV tandem accelerator system with a pair of ion sources (a cesium sputter type heavy ion source and a duo-plasmatron type light ion source), a 1.0MV single-end accelerator system with a light ion source and a dual-beam target station. The facility with this configuration is scheduled to be completed by March 1999 and will then be made available for collaborative research in late 1999. The present paper outlines the engineering design and prospective specification of the facility and the perspective of research plans.

**362: Interfacial Fracture Behavior of SiC/SiC Composites for Fusion Application**

Tatsuya Hinoki, Hisashi Serizawa\*, Tamaki Shibayama\*\*, Wen Zhang, Yutai Katoh, Akira Kohyama

\*Joining and Welding Research Institute, Osaka University, \*\*Center for Advanced Res

Proc. of International Symposium on Environment-Conscious Innovative Materials Processing with Advanced Energy Sources, 1998, pp.571-576.

The importance of shear stress of fiber-matrix interfaces on mechanical properties of CMCs has long been emphasized. However, interfacial shear process of CMCs has not sufficiently been understood. The objective of this work is to reveal interfacial fracture behavior and evaluate interfacial shear stresses in CMCs. In order to clarify interfacial fracture mechanism of CMCs, SiC/SiC composites with various interfacial properties were fabricated and specimens with variational interphase layer thickness were prepared to evaluate interfacial shear process and interfacial shear stress. Interfacial shear process and shear stresses were analyzed based on the load-displacement properties of single fiber push-out and push-back tests using a mic

**363: Fatigue Property of Low Activation Ferritic Steel and Its Weld Joint**

Takanori Hirose, Akira Kohyama, Yutai Katoh, Hiroyasu Tanigawa\*, A. Nishimura\*\*, Cyusei Namba\*\*, Takeo Muroga\*\*

\*Japan Atomic Energy Research Institute, \*\*National Institute for Fusion Science

Proc. of International Symposium on Environment-Conscious Innovative Materials Processing with Advanced Energy Sources, (1998) pp.629-632.

Reduced activation ferritic/martensitic steels are the leading candidates for the first wall and blanket structures of the future D-T fusion reactors. Among their engineering issues of concern, fatigue properties are realized to be an important issue to be studied including neutron irradiation effects. For a clear understanding of fatigue properties under fusion environment anticipated, the effect of specimen size on the fatigue properties was studied utilizing a reduced activation ferritic steel; JLF-1 and its weldment. The correlation of the fatigue life characteristics and fracture mechanisms was investigated for full- and miniature-sized specimens. As the part of this research, a new fatigue testing machine for a hot-cell usage has been developed. The materials used were reduced activation steel (JLF-1) and its weldment by tungsten inert gas (TIG) arc welding. JLF-1 has been developed as an important activity of the Japanese fusion materials R&D program, supported by Japan/US collaborative FFTF/MOTA and JUPITER programs.

**364: Dislocation Evolution in an Austenitic Alloy Induced by Post-irradiation Micro-Indentation****Masami Ando, Yutai Katoh, Hiroyasu Tanigawa\*, Akira Kohyama****\*Japan Atomic Energy Research Institute**

Effects of Radiation on Materials, ASTM STP, M.L.Hamilton, et al., Eds., American Standard for Testing and Materials, in printing.

The hardening and ductility degradation due to irradiation are important engineering issues of materials for use in neutron environments. In this series of studies, the efforts have been made to evaluate the mechanical property changes in irradiated materials by means of micro-indentation testing following ion irradiation. The present work is intended to examine the irradiation - produced microstructures in structural materials and the records of their interaction with dislocation motions, as a complement to the phenomenological study on irradiation-induced hardening. The materials used include Fe-Cr-Ni austenitic stainless alloy, pure Fe and Fe-Cr-W low activation ferritic steel. Specimens of small coupon type were irradiated with 4MeV Ni ions with or without co-implantation of He ions at elevated temperatures, at the High-fluence Irradiation Facility, University of Tokyo (HIT Facility). This paper will take up a limited number of materials and irradiation conditions for the purpose of detailed discussion on microstructures. The irradiated specimens were then indentation-tested at loads as low as 0.98mN using an Akashi MZT-3 instrumented micro-indentation testing system. The specimens' regions right beneath the indents were made into thin films, with JEOL JFIB-2100 focused ion beam (FIB) processing system. Microstructural examination is currently underway using JEOL JEM-2010EX transmission electron microscope operating at 200kV. The details of specimen processing schemes developed in this work and the results of microstructural examination will be discussed in the paper.

**365: Effect of Fiber Coatings on Crack Behaviors in SiC/SiC****Wen Zhang, Tatsuya Hinoki, Yutai Katoh, Akira Kohyama, Tetsuji Noda\*****\*National Research Institute for Metals T. Shibayama (Hokkaido University)**

Proc. of International Symposium on Environment-Conscious Innovative Materials Processing with Advanced Energy Sources, (1998) pp.561-564.

SiC/SiC composites are attractive materials for nuclear fusion application and other applications such as heat exchanger and turbines. The objective of this work is to improve the toughness of the materials by investigating the interface microstructure under indentation test. SiC/SiC composites were made by CVI method. Carbon coatings and multiple coatings were applied to be interphase between fibers and matrix for improving the toughness. With the increasing of the carbon coating thickness on fiber, fibers were easier to debond. Also the type of the fibers and the constituent of the matrix influenced the debond behavior. TEM and EDS analysis were applied to confirm the effective of the various factors.

**366: Fabrication of High Performance SiC/SiC Composite by Polymer Impregnation and Pyrolysis Method**

**Masaki Kotani, Akira Kohyama, Kiyoto Okamura\*, T. Inoue\*\***

**\*Osaka Prefecture University, \*\*Osaka National Research Institute**

Proc. of International Symposium on Environment-Conscious Innovative Materials Processing with Advanced Energy Sources, (1998) pp.595-598.

In order to develop the performances of SiC/SiC, Poly(vinylsilane) which is new types liquid Poly(carbosilane) with a lot of Si-H functionality was adopted for matrix precursor in PIP process. As a preliminary study of fabricating a composite, thermal behaviors of PVS were investigated. Since the viscosity or hardness of PVS is greatly changed accompanied by a violent gas evolution in medium range temperature, effects of the process conditions such as curing temperature and pressure on bulk density and microstructure were investigated considering volume shrinkage and gas evolution due to the conversion of polymer precursor.

**367: CREST-ACE(R & D of Advanced Material Systems for Conversion of Energy) Program and Materials R & D Strategy for Nuclear Fusion Applications**

戦略的基礎研究 CREST-ACE と核融合炉材料開発戦略の概要

**Akira Kohyama**

超高温材料シンポジウム論文集—新しいエネルギー材料— pp.59-67.1998

Under the title of "R&D of Environment Conscious Multi-Functional Structural Materials for Advanced Energy Systems", a new R&D activity to establish high efficiency and environmental conscious energy conversion systems, as one of the programs of Core Research for Evolutional Science and Technology (CREST), has been initiated from October 1997 to September 2002.

This program cares for R&D of high performance materials and material systems for severe environments and production of model components for energy conversion systems has been targeted. The emphasis is on R&D of SiC/SiC, W/W with their system studies to establish sound material life cycles. The program outline and preliminary results on SiC/SiC are provided. As one of the most important applications, present status of nuclear fusion research is reviewed with the emphasis on the materials R&D strategy for nuclear fusion applications.

**368: Current Status and Future R&D for Reduced-Activation Ferritic/Martensitic Steels**

**Akimichi Hishinuma\***, Akira Kohyama, R.L.Klueh\*\*, D.S.Gelles\*\*\*, W.Diez\*\*\*\*, K.Ehrlich\*\*\*\*\*

\* Tokai Establishment,JAERI, \*\* Oak Ridge National Laboratory, \*\*\* Battelle Pacific Northwest Laboratory, \*\*\*\* Consultant,EC/DGXII/Fusion Program, \*\*\*\*\* Institute für Materialforschung I

Journal of Nuclear Materials, 258-263, pp.193-204, 1998

**369: \* Effect of Fiber Coating on Interfacial Shear Strength of SiC/SiC by Nano-indentation Technique**

**Tatsuya Hinoki, Akira Kohyama, Shinji Sato\*, Tetsuji Noda\*\***

\*Fukushima National College of Technology, \*\*National Research Institute for Metals

Journal of Nuclear Materials, 258-263, pp.1567-1571, 1998

In order to quantitatively evaluate mechanical properties of fibers, matrices and their interfaces in fiber reinforced SiC/SiC composites, fiber push-out tests have been carried out. From the indentation load vs. displacement relations, the fiber push-out process has been discussed in comparison with the C/C composites and the loads for fiber

**370: Crack Initiation and Growth Characteristics in SiC/SiC under Indentation Test**

**Wen Zhang, Tatsuya Hinoki, Yutai Katoh, Akira Kohyama, Tetsuji Noda\*, Takeo Muroga\*\*, Jinnan Yu\*\*\***

\*Tsukuba Laboratories, National Research Institute for Metals, \*\*National Institute for Fusion Science, \*\*\*China Institute of Atomic Energy

Journal of Nuclear Materials, 258-263, pp.1577-1581, 1998

The mechanical behavior of ceramic matrix composites (CMC) is known to be strongly influenced by fiber-matrix interfacial properties and there have been many efforts to clarify the interfacial characteristics. To understand the fracture mechanism of the materials it is necessary to clarify how the cracks initiate and propagate among fibers, interphase (coating) and matrix. The objective of this study is to investigate crack initiation and growth characteristics in SiC/SiC composites with variations in coating thickness and coating methods by means of micro-indentation technique. Micro-indentation tests and hardness tests were carried out on SiC/SiC composites produced by the CVI process. The intrinsic

catastrophic mode of failure of the brittle composite was prevented by application of single carbon and multiple coatings on fibers. Thinner coatings are sensitive to make fibers debonded and may improve the toughness of the composites.

**371: Current Status of SiC/SiC Composite R&D**

**P. Fenici\*, A.J. Frias Rebelo\*, R.H.Jones\*\*, Akira Kohyama, L.L.Snead\*\*\***

**\*CER, JRC Ispra, \*\*Pacific Northwest National Laboratory, \*\*\*Oak Ridge National Laboratory**

Journal of Nuclear Materials, 258-263, pp.215-225, 1998

Advantage of SiC-based ceramic matrix composites (CMCs) as structural materials in fusion applications rely on their high-temperature properties and stability, low density and reduced neutron activation. In recent years, experimental activities on industrial SiC CMCs have highlighted their main features under irradiation and provided important guidelines for further development of a radiation compliant material. Parallel efforts included design studies, development of advanced fibers and interfaces, alternative composite processing methods and joint development. In this paper, the current status of SiC/SiC R&D is reported and it is demonstrated that future activities require a strong collaboration with the industry as well as common efforts involving the different laboratories.

**372: Influence of Tantalum and Nitrogen Contents, Normalizing Condition and TMCP Process on Mechanical Properties of Low Activation 9Cr-2W-0.2V-Ta Steels for Fusion Application**

**Toshinaga Hasegawa\*, Y Tomita\*, Akira Kohyama**

**\* Nippon Steel Corporation**

Journal of Nuclear Materials, 258-263, pp.1153-1157, 1998

Ferritic and martensitic steels are advantageous in void swelling resistance, low thermal expansion coefficient, and high thermal conductivity compared with austenitic steels as structural materials for wall and blanket components of fusion reactors. Where important R&D issues are recognized to be irradiation induced embrittlement and irradiation creep/relaxation.

Candidate low activation ferritic and martensitic steels have been developed based on the conventional high-Cr heat-resistant steels with Mo replaced by W and Nb by Ta in order to reduce induced radioactivity. Among the candidate steels, 9Cr-2W-0.2V-0.07Ta steels, which have been developed in Japanese Universities fusion program designated as JLF-1 steels, are the most promising for their good irradiation-creep resistance and small irradiation embrittlement as well as good baseline properties.

For clarifying the reason of good creep and mechanical properties and improving the mechanical prop-

erties of the JLF-1 steels, influence of Ta, N contents, normalizing condition and TMCP process on the mechanical properties of the 9Cr-2W-0.2V-Ta steels was investigated in contrast with conventional heat-resistant steels (9Cr-1Mo-0.2V-Nb).

The creep strength of the 9Cr-2W-0.2V-Ta steels increases with increasing amount of Ta and N contents irrespective of manufacturing processes. Concerning with manufacturing processes, the increasing of normalizing temperature or the application of TMCP processes, which corresponds to hot rolling and tempering or direct quenching and tempering processes, can improve creep strength. However, the toughness of the steels decreases with increasing creep strength. It is hypothesized that the increase of creep strength due to the increasing of normalizing temperature or the application of TMCP processes is attributed to uniform distribution of fine (Ta, V)(C, N) precipitates.

In conclusion, the 9Cr-2W-0.2V-Ta steels have equivalent creep strength and better toughness compared with 9Cr-2W-0.2V-Ta steels have equivalent creep strength and better toughness compared with 9Cr-1Mo-0.2V-Nb steels. The good toughness of the 9Cr-2W-0.2V-Ta steels is attributed to their fine austenite grain size.

### **373: Dependence of Post - Irradiation Impact Properties on the Irradiation Temperature in Reduced Activation 9Cr-2W Martensitic Steels**

**Akihiko Kimura, Hideo Kayano\*, Toshihei Misawa\*\*, Hideki Matsui\*, Akira Kohyama**  
\* Tohoku Univ., \*\* Muroran Industrial Univ.

### **374: Glass-ceramic Joining and Coating of SiC/SiC for Fusion Applications**

**M. Ferraris\*, M. Salvo\*, C. Isola\*, M. Montorsi\*, Akira Kohyama**  
\*Polytechnic of Torino

Journal of Nuclear Materials, 258-263, pp.1546-1550, 1998

The aim of this work is the joining and the coating of SiC/SiC composites by a simple, pressureless, low cost technique. A glass-ceramic was chosen as joining and coating material, because its thermal and thermomechanical properties can be tailored by changing the composition. The glass-ceramic coatings can also act as oxidation shield for the carbon interface between fibre and matrix, and as self-sealing coatings at temperatures above the glass softening point. The glass-ceramic utilised in this work does not contain boron oxide (incompatible with fusion applications) and has high characteristic temperatures (softening point at about 1400 °C). Furthermore, the absence of silica makes this glass-ceramic particularly interesting as ceramic breeder-compatible (i.e. lithium-silicates, -alluminates or -zirconates) coating material. Coatings and joints were successfully obtained with Hi-Nicalon fibres-reinforced silicon carbide

matrix. The coated and joined samples were morphologically (SEM) and compositionally (EDS) analysed. Mechanical tests (shear strength) and ceramic breeder compatibility tests were performed.

### **375: Radiation Response of SiC-based Fibers**

**G.E. Youngblood\*, R.H. Jones\*, Akira Kohyama, L.L. Snead**  
**\*Pacific Northwest National Lab., \*\*Oak Ridge National Lab.**

Journal of Nuclear Materials, 258-263, pp.1551-1556, 1998

Loss of strength in irradiated fiber-reinforced SiC/SiC composite generally is related to degradation in the reinforcing fiber. To assess fiber degradation, the density and length changes were determined for four types of SiC-based fibers (Tyrano, NicalonCG, Hi Nicalon and Dow X) after high temperature (up to 1000 °C) and high dose (up to 80 dpa-SiC) irradiations. For the fibers with nonstoichiometric compositions (the first three types in the list), the fiber densities increased from 6% to 12%. In contrast, a slight decrease in density (<1%) was observed for the Dow X fiber with a quasi-stoichiometric composition. Fiber length changes (0.5-6% shrinkage) suggested small mass losses (1-6%) had occurred for irradiated uncoated fibers. In contrast, excessive linear shrinkage of the pyrocarbon-coated Nicalon CG and Tyrano fibers (7-9% and 16-32%, respectively) indicated that much larger mass losses (11-84%) had occurred for these coated fibers. Crystallization and crystal growth were observed to have taken place at fiber surfaces by SEM and in the bulk by XRD, more so for irradiated Nicalon CG than for Hi Nicalon fiber. The radiation response of the quasi-stoichiometric Dow X fiber was the most promising. Further testing of this type fiber is recommended.

### **376: Neutron Irradiation Experiments for Fusion Reactor Materials through JUPITER Program**

**Katsunori Abe\*, Akira Kohyama, Cyusei Namba\*\*, F.W. Wiffen\*\*\*, R.H. Jones\*\*\*\***  
**\*Tohoku Univ., \*\*National Institute for Fusion Science, \*\*\*U.S. Department of Energy,**  
**\*\*\*\*Pacific Northwest National Lab.**

Journal of Nuclear Materials, 258-263, pp.2075-2078, 1998

A Japan-USA Program of irradiation experiments for fusion research, "JUPITER", has been established as a 6 year program from 1995 to 2000. The goal is to study "the behavior of fusion reactor materials and their response to variable and complex irradiation environment". This is phase-three of the collaborative program, which follows RTNS-2 Program (Phase-1: 1982-1986) and FFTF/MOTA Program (Phase-2: 1987-1994). This program is to provide a scientific basis for application of materials performance data, generated by fission reactor experiments, to anticipated fusion environments. Following the systematic study on cumulative irradiation effects, done through FFTF/MOTA Program, JUPITER is emphasizing

the importance of dynamic irradiation effects on materials performance in fusion systems. The irradiation experiments in this program include low activation structural materials, functional ceramics and other innovative materials. The experimental data are analyzed by theoretical modeling and computer simulation to integrate the above effects.

**377: Materials Design and Relating R&D Issues for the Force-Free Helical Reactor (FFHR)**

**Akio Sagara\***, **Takeo Muroga\***, **Osamu Motojima\***, **Tetsuji Noda\*\***, **Sato Tanaka\*\*\***,  
**Takayuki Terai\*\*\***, **Akira Kohyama**, **Hideki Matsui**

**\*National Institute for Fusion Science**, **\*\*National Research Institute for Metals**,  
**\*\*\*Univ. of Tokyo**, **\*\*\*\*Tohoku Univ.**

Journal of Nuclear Materials Materials 258-263 (1998) pp.2079-2082.

Materials issues related to the Force-Free Helical Reactor (FFHR) design are presented. In FFHR, which uses the Flibe liquid breeder from the main reason of safety, if there is no need to replace in-vessel materials in the lifetime of 30 years, the reactor can be operated with not only the high safety margin but also a high availability of the plant, resulting in reducing not only the cost of electricity (COE) but also the total amount of radiative wastes. Nuclear properties of induced radioactivity, solid transmutation products, and decay heat at the 14MeV neutron fluence of 45 MWa/m<sup>2</sup> as well as materials compatibility with Flibe are investigated for JLF-1, V-alloy, SiC and high Z materials. In conclusion, control of metal impurities, transmutation of W and V, acceptable decay heat, and reaction kinetics with Flibe are pointed out as R & D issues.

**378: Coherent soft X-ray generation with femtosecond high-intensity lasers**

**Kenzo Miyazaki**

Proc. Int. Symp. on Laser Application to Muon Science (KEK, Tsukuba, November 1998) pp.32 - 36.

The fundamental aspects of high-order harmonic generation (HHG) in atomic and molecular gases are discussed on the basis of the experimental results obtained using femtosecond, high-intensity laser pulses. The HHG experiments were made at a focused intensity of  $10^{13}$  -  $10^{16}$  W/cm<sup>2</sup>, and the results have shown the characteristic behaviors that depend on the laser wavelength, intensity, polarization, focusing, pulse width, and nonlinear medium. The problem for the development of a compact, high-brightness coherent soft X-ray sources using the HHG is also discussed.

**379: Strong-field interaction for high-order harmonic generation**

**Kenzo Miyazaki**

Proc. the 1998 Int. Photonics Conf. (National Taiwan Univ., Taipei, 1998) pp.167 - 169.

We review the theoretical and experimental aspects of high-order harmonic generation in atomic gases exposed to a high-intensity laser field and discuss problems in the development of coherent soft X-ray sources using the nonlinear interaction.

**380: The white light supercontinuum is indeed an ultrafast white light laser**

**See Leang Chin (Laval Univ.), Stephane Petit (Laval Univ.), Frederic Borne (Laval Univ.) and Kenzo Miyazaki**

Jpn. J. Appl. Phys., Vol.38, No.2A (1999) pp.L126 - L128.

We identify the white light supercontinuum generated by femtosecond Ti-sapphire laser pulses as an ultrafast white light laser because the relative coherence lengths of all the wavelength components of the supercontinuum are essentially the same as that of the laser pulse when compared to an incoherent white light source.

**381: Coherent control of photoabsorption: Application to real atoms**

**Takashi Nakajima Jian Zhang\* P. Lambropoulos\***

**\* Max-Planck-Institute for Quantumoptics**

Laser Physics, Vol. 8, pp.29-33, 1998

After a brief review of the control of photoabsorption processes, we show numerical results for real atoms such as Na and Ca, showing the experimentally achievable control of photoionization yield into different ionic channels. A scheme utilizing the laser detunings instead of the laser phase is also briefly discussed.

- 382: \* Collisional relaxation of the 5d6p J=1 states of laser-ablated Ba in He gas at room temperature**

**Takashi Nakajima Yukari Matsuo\* Nobuaki Yonekura\* Masato Nakamura\* Michio Takami\***

**\* The Institute of Physical and Chemical Research (RIKEN)**

Journal of Physics B, Vol. 31, pp.1729-1740, 1998

The laser ablation method has been applied for the study of collisional relaxation of the laser-excited Ba atom in He gas at room temperature. When He buffer gas is introduced collisional relaxation processes take place, and as a result depolarization and quenching are seen in the laser-induced fluorescence signal. The depolarization cross sections of 5d6p  $^3D_1$ ,  $^3P_1$ , and  $^1P_1$  are found to be  $86 \pm 6 \text{ \AA}^2$ ,  $77 \pm 10 \text{ \AA}^2$ , and  $202 \pm 20 \text{ \AA}^2$ , respectively, in He gas at room temperature (295K).

- 383: \* Temperature-dependent depolarization cross sections of the 5d6p  $^3P_1$  and  $^3D_1$  states of laser-ablated Ba in He gas in the range of 10-300K**

**Takashi Nakajima Nobuaki Yonekura\* Yukari Matsuo\* Qin Hui\* Michio Takami\***

**\* The Institute of Physical and Chemical Research (RIKEN)**

Physical Review A, Vol.57, pp.3598-3602, 1998

We have applied the laser ablation technique for the study of depolarization effects of the 5d6p  $^3P_1$  and  $^3D_1$  states of Ba with He gas in the wide temperature range of 10 K-300 K. The depolarization cross sections of both states have been found to have a positive temperature-dependence, indicating that the responsible interaction is not a van der Waals type. A tentative and qualitative explanation for the difference of the temperature-dependence between 5d6p  $^3P_1$  and  $^3D_1$  is given in terms of electron density distribution.

- 384: \* Population transfer in N-level systems assisted by dressing fields**

**Takashi Nakajima**

Physical Review A, Vol.59, pp.559-568, 1999

Motivated by the recent work by Malinovsky and Tannor, we analyze N-level systems for population transfer by counterintuitive pulse delay, in which N-2 intermediate states are strongly coupled by dressing laser fields. We have carried out detailed specific analysis for the four-level and five-level systems using a

dressed-state picture, as representatives for even-N and odd-N systems, respectively. We have found that the dynamics of the systems are essentially different for odd-N and even-N systems, and that complete population transfer assisted by dressing fields is more restrictive for even-N systems than for odd-N systems.

**385: Radiative lifetimes and collisional deactivation cross sections of the 5d6p states of laser-ablated Ba in He gas**

**Yukari Matsuo\* Takashi Nakajima Tohru Kobayashi\* Michio Takami\***

**\*The Institute of Physical and Chemical Research (RIKEN)**

Physical Review A, Vol.59, pp.2071-2077, 1999

We have measured radiative lifetimes and collisional deactivation cross sections of the 5d6p excited states of Ba atoms in He buffer gas. Barium atoms are produced by laser-ablation of a solid Ba sample, whereby populating the 6s5d  $^3D_J$  metastable states about 0.1~1% of the total population. The 5d6p  $^{1,3}P^\circ$ ,  $^{1,3}D^\circ$ , and  $^{1,3}F^\circ$  states, most of which are not accessible from the ground state by single-photon transition, are excited from the metastable states by a laser, and radiative lifetimes as well as collisional deactivation cross sections are determined from the decay rates of the laser-induced-fluorescence.

**386: Origin of the phase lag in the modulation of photoabsorption products under two-color excitation**

**P. Lambropoulos\* Takashi Nakajima**

**\* Max-Planck-Institute for Quantumoptics**

Physical Review Letters , Vol.82, pp.2266-2269, 1999

We investigate the physical origin of the phase lag in the modulation of photoionization products under two-color phase-controlled fields. We show that the phase lag comes from two physical mechanisms: The resonance phase shift, which is already incorporated in the simplest model, i.e., a single discrete state embedded in two continua, and the coupling between continua due to intra-system interactions. Three specific examples using, respectively, a simple model, multichannel quantum defect theory, and an  $L^2$  basis set including configuration interaction are also provided to support the argument.

**387: Critical Heat Fluxes in Subcooled Boiling of Water Flowing Upward in a Vertical Tube for Wide Ranges of Liquid Velocity, Subcooling and Pressure**

**K. Hata, K. Fukuda, M. Shiotsu, A. Sakurai, N. Noda, O. Motojima and A. Iiyoshi**

Proceedings of the 6th International Conference on Nuclear Engineering, Paper No. ICONE-6362 (1998) pp.1-16.

The flow boiling critical heat fluxes (CHF) versus inlet subcoolings ( ) at a flow velocity for various pressures were clearly divided into first, second and third groups for low, intermediate and high . The CHF's first decrease from the CHF at saturated condition, , near zero down to the minimum CHF at the higher limit of for the first group, secondly increase up to the CHF at the higher limit of for the second group and thirdly also increase with the increasing rate of CHF for lower than that of the second group with an increase in . The CHF's for lower and intermediate subcoolings were clearly dependent on the pressures; on the contrary those for high subcooling were almost independent of the pressure. The effects of outlet subcoolings, and tube inner surfaces of rough and mirror on the high CHF's for high subcoolings were obtained by the comparison of the present CHF's with the corresponding predictions from existing correlations, the predictions revealed the inadequacy in the prediction of the anomalous trend of CHF's observed here. Three CHF correlations for low, intermediate and high subcoolings were derived as the fundamental database for high heat flux thermal management.

**388: Critical Heat Flux on Various Sized Flat Plates in Pressurized He III.**

**Tatsumoto, K. Hata, Y. Takeuchi, K.Hama, Y. Shirai and M. Shiotsu,**

Proceedings of the Seventeenth International Cryogenic Engineering Conference, Vol.1 (1998) pp. 683-686.

Critical heat fluxes on four different sized horizontal flat plates with widths ranging from 3.8 to 40 mm were measured in pressurized He II at atmospheric pressure for the bulk liquid temperatures of 1.8, 1.9, 2.0 and 2.1 K. Each flat plate heater was made of Manganin whose one side was insulated by pasting it on FRP plate. The measured CHF's were higher for shorter width of the test plate and for lower liquid temperature. A correlation of CHF on the flat plate was presented by modifying the authors' theoretical CHF correlation for a cylinder. The correlation can describe the CHF data on various sized flat plates within 20

**389: Transient Heat Transfer Caused by Stepwise Heat Input to a Flat Plate in Pressurized He II**

M. Shiotsu, K. Hata, Y. Takeuchi, K. Hama and Y. Shirai

Proceedings of the Seventeenth International Cryogenic Engineering Conference, Vol.1 (1998) pp. 687-690.

The lifetime of quasi-steady state in Kapiza conductance regime caused by a large stepwise heat input to a flat plate was systematically measured for the liquid temperatures ranging from 1.8 to 2.1 K at atmospheric pressure: the quasi-steady state rapidly changes to film boiling regime after the depletion of lifetime. Width of the test heater plate was varied from 3.8 to 40 mm. The lifetime for a certain quasi-steady heat flux,  $q_s$ , beyond steady-state critical heat flux,  $q_{s,t}$ , is almost independent of the plate width, although  $q_{s,t}$  depends on it. The lifetime is proportional to  $q_s^{-4}$  for the  $q_s$  lower than that corresponding to  $tL=1.2$  ms, and to  $q_s^{-2}$  for  $q_s$  larger than the value. Correlation of lifetime based on the two fluid model was given.

**390: A Model for the CHF of One-wall Rectangular He II Channel**

K. Hata, M. Shiotsu, Y. Takeuchi and K. Hama,

Proceedings of the Seventeenth International Cryogenic Engineering Conference, Vol.1 (1998) pp. 789-792.

A model for the critical heat flux on a heated inner wall of a short rectangular channel in pressurized He II was presented. The model consists of the Gorter-Mellink heat conduction in the channel and the heat transport from the cross sectional area at both opened ends of the channel to large He II pool. Heat transfer equation from a flat plate to a large pool of pressurized He II obtained by the authors [1] was used for the latter heat transport equation. The model can describe well the effect of channel gap length on the critical heat fluxes (CHFs) of short channel observed by Kobayashi et al. [2]. The analyzed liquid temperature at both ends of the channel under the condition of critical heat flux almost agrees with the bulk liquid temperature TB for TB higher than 2 K, but it becomes higher than TB with the decrease in TB from the value.

**391: Mechanisms of Subcooled Flow Boiling Critical Heat Fluxes on Vertical Cylinder Surface and on Short Tube Inner Surface in Water Flowing Upward at Various Pressures**

**A. Sakurai, M. Shiotsu, K. Hata and K. Fukuda,**

Proceedings of the Eleventh International Heat Transfer Conference, Vol.2 (1998)  
pp.351-356.

The flow boiling critical heat fluxes (CHF) on the surface of a vertical cylinder with 1.2 mm diam. and 72 mm length located at a center line of a round tube of 38 mm inner diam. and 1425 mm length, and on the inner surface of a short tube of 9 mm inner diam. and 48 mm length with water flowing upward were measured for the wide ranges of flow velocities, subcoolings and pressures. The CHF versus subcoolings at each flow velocity for various pressures for the test cylinder, which increased with an increase in subcooling, were clearly dependent on the pressures for the lower subcoolings; on the contrary, they were almost independent of the pressures for the higher subcoolings except those for the pressures near atmospheric. The similar trend of subcooling dependence was also observed in the CHF on the test tube for intermediate and high subcooling range. However, the CHF for low subcoolings became larger from the minimum value at the lowest subcooling for the intermediate range with a decrease in subcooling down to zero. The minimum value was dependent on the pressure. The CHF for low subcoolings for the test cylinder and those for intermediate subcoolings for the test tube agreed within 5

**392: Incipient Boiling Superheat in Liquid Sodium**

**M. Shiotsu, K. Hata, Y. Takeuchi, K. Hama and T. Sakai,**

Proceedings of the Eleventh International Heat Transfer Conference, Vol.2 (1998)  
pp.407-412.

The incipient boiling superheats (IBS) on a horizontal cylinder test heater of 7.6 mm in diameter in saturated liquid sodium caused by quasi-steadily increasing heat input were systematically measured for the cold trap temperatures ranging from 378 K to 433 K at the bulk liquid temperatures of 863 K and 973 K. The IBS for the bulk liquid temperature of 873 K was significantly affected by the cold trap temperature. The IBS became higher with the decrease in the cold trap temperature and it amounted to around 250 K for the cold trap temperatures lower than 383 K. For the bulk liquid temperature of 973 K, the IBS are scattered from about 40 K to 200 K but little systematic effect of the cold trap temperature was observed. For the IBS lower than around 70 K, the surface temperature of the test heater suddenly decreased after the initiation of boiling and nucleate boiling was realized. After that the heat flux increased in nucleate boiling regime up to the critical heat flux. For the IBS higher than 70 K, direct transition from non-boiling to film boiling occurred at the initiation of boiling. The heat flux at the IBS of around 100 K was almost equal to the critical heat flux of nucleate boiling for the same condition and that of around 250 K was about 2.5 times of the critical heat flux.

**393: Effect of Surface Conditions on Pool Boiling Critical Heat Fluxes in Saturated and Subcooled Liquid Nitrogen at Various Pressures**

**A. Sakurai, M. Shiotsu, K. Hata and K. Fukuda,**

Advances in Cryogenic Engineering, Vol. 43, Part B (1998) pp. 1305-1312.

Critical heat fluxes (CHF) in fully developed nucleate boiling (FDNB) regime were measured for a 1.2 mm diameter horizontal cylinder with commercial or rough surface (CS or RS) in a pool of liquid nitrogen for subcooling covering a range from 0 K to about 40 K at pressures ranging from 0.3 to 2 MPa. The CHF for the cylinders with two different surfaces were compared under the same experimental conditions. Measured all data of the CHF for both surface conditions were well explained by the two different CHF mechanisms: one is due to hydrodynamic instability (HI), and another is due to the heterogeneous spontaneous nucleation in originally flooded cavities. The CHF due to the HI obtained for both surface condition agree well with the values derived from the saturated and subcooled CHF correlations: the former was given Kutateladze and the latter was given by the authors, respectively. It was clarified that the CHF due to the HI are independent of the surface conditions. Little effect of the surface condition tested here was observed on the CHF due to the HSN except the CHF at a pressure of 2047 kPa for low subcooling near saturated conditions. An empirical correlation for the CHF due to the HSN is presented.

**394: Steady and Unsteady Heat Transfer from a Flat Plate in Subcooled Helium II**

**M. Shiotsu, K. Hata, Y. Takeuchi and K. Hama**

Advances in Cryogenic Engineering, Vol. 43, Part B (1998) pp. 1409-1416.

Transient heat transfer caused by large stepwise heat inputs to a flat plate was measured in subcooled He II at atmospheric pressure for bulk liquid temperatures ranging from 1.9 to 2.1 K. The flat plate was made of Manganin, one side insulated, 10.3 mm in width, 40 mm in length and 0.1 mm in thickness. Steady-state heat transfer and its critical heat flux were also measured by using quasi-steadily increasing heat inputs for the same experimental conditions. The steady-state critical heat fluxes for the liquid temperatures were well expressed by the authors' correlation based on the Goger-Mellink equations. The lifetime of quasi-steady heat flux in Kapiza conductance regime, which corresponds to that of a certain point on the extrapolation of steady-state Kapiza conductance curve, was systematically measured: the quasi-steady state rapidly changes to film boiling regime after the depletion of lifetime. Comparisons of the results on the flat plate with those on the horizontal wires with the diameters ranging from 0.08 to 0.7 mm under the same condition already reported by the authors were made to clarify the effect of heater shape.

**395: Electrical Resistivity of a High-Tc Superconductor for Electric Current Higher than  $I_c$** 

**M. Shiotsu, K. Hata, A. Sakurai, C. Suzawa, S. Isojima, K. Sato and T. Fukui,**

Advances in Cryogenic Engineering, Vol. 44 (1998) pp. 623-629.

The electrical resistivity of a high-Tc superconductor for  $I > I_c$  is not clarified until now as a function of electric current through the conductor,  $I$ , and temperature of the conductor,  $T$ , because  $T$  varies with  $I$  due to joule heating. An estimation method of the electrical resistivity based on non-boiling heat transfer coefficients for exponentially increased heat inputs to the high-Tc test sample in LN2 was developed: exponential heat inputs,  $Q = Q_0 e^{t/\tau}$ , with the periods,  $\tau$ , ranging 10 ms to 10 s were given to a silver sheathed BiPbSrCaCuO tape in LN2, and electrical current  $I$  through the sheathed tape and the terminal voltage  $V$  between potential taps on the tape during the transient heating were measured. An empirical equation for the electrical resistance  $R$  of the sheathed tape was obtained as a function of  $I$  and  $T$ : two constants in equation were fitted iteratively so that the value of  $T$  at each time obtained from the measured values of  $I$  and  $V$  at the time by using the equation of  $R$  may agree with the theoretical solution of non-boiling heat transfer for the exponential period. The distribution ratio of the electric current through the superconductor and the Ag sheath,  $I_N/I$ , and the flow resistivity of the superconductor itself were estimated by using this method.

## *C. Review Articles*

C. 総説

# Chapter 3

## Review Articles

### I Department of Socio-Environmental Energy Science

(エネルギー社会・環境科学専攻)

#### 1: Supercritical Fluids to Biomass Research

超臨界流体によるバイオマス研究の試み

**Shiro Saka**

Cellulose Communications, 5, No.3, 129-135, 1998

The supercritical water biomass conversion system was designed and devised in our laboratory to cover a range of up to 50 MPa in pressure and up to 500 °C in temperature. The reaction vessel with cellulose and wood samples were treated with this system at supercritical state of water ( $T_c; 374\text{ }^\circ\text{C}$ ,  $P_c; 22.1\text{ MPa}$ ) for designated period (3 to 120 sec). The recovered products of hydrolysates were then analyzed by high performance liquid chromatography, indicating that a high amount of glucose can be achieved from cellulose for 10 sec supercritical treatment. However, with the longer treatment, pyrolyzed products were found to be increased. In such conditions, the glucose yield from cellulose I and cellulose II were almost the same as that of starch. With buna wood sample, in addition to glucose, mannose and xylose were also recovered. Based on these results, the potentials of the supercritical treatment of biomass resources were discussed for the future new science and technology.

#### 2: Topochemistry of Wood-Inorganic Composites as Prepared by the Sol-Gel Process

ゾルゲル法による無機質複合化木材のトポ化学

**Shiro Saka**

APAST, 30, 10-14, 1998

Wood has been the most intimate materials with mankind since the ancient time. However, it has some defects due to natural materials such as combustibility, dimensional instability and biodeterioration. To remove such defects and add the value on to woody materials, wood-inorganic composites prepared with metal alkoxides by the sol-gel process have been studied for the property enhancement of wood. Therefore, in this paper, a recent progress in topochemistry of the wood-inorganic composites as prepared by the sol-gel process will be presented on enhancing the properties of wood such as dimensional stability, termite-resistance, fire-retardance, water-repellency, anti-leachability and anti-microbial activity. Throughout the studies, it has been elucidated that the topochemical effects exist for enhancing these properties of wood in wood-inorganic composites.

### 3: Biomass for Clean Energy Sources

クリーンエネルギー源・バイオマス

**Shiro Saka**

Energy Review, 18, No.6, 28-29, 1998

エネルギーレビュー, 18, No.6, 28-29, 1998

For coming century, global problems related with food, energy, natural resources and environments will seem to be serious. In such conditions, biomass resources which are photo-synthetically produced will be important. Therefore, in this review, the potentials of the biomass resources were introduced for its significance as energy sources as well as for its conversions to useful chemicals which have been produced during this century from petroleum.

### 4: Environmental Life Science of NO

一酸化窒素の環境生命科学

**K. Makino**

KAN KYO NOW, Vol.23, pp.2-7 (1999).

環・京・NOW, 23, 2-7 (1999).

### 5: Review on Present State of Human Model Researches in Nuclear Engineering and the Prospect for their Industrial Applications

原子力におけるヒューマンモデル研究の現状と応用領域の展望

Yoshikawa,H., Furuta,K(Univ. of Tokyo), Nakagawa,T.(Nuclear Power Engineering Corp), Yoshimura,S.(Institute of Electric Power Industry), Yoshida,K.(Japan Atomic Energy Research Institute), Naito,N.(Toshiba Corp.)

Journal of Atomic Energy Society of Japan, Vol.41, No.1, pp.2-14 (1999)

日本原子力学会誌, Vol.41, No.1, pp.2-14 (1999)

Reviews have been made on the researches and developments for human models in the field of nuclear engineering. Until now, the related works have been made mainly for the modeling of plant operator and operator crew in the control room, but also there arise new tendencies of extending the modeling works for maintenance field as well as for personnel training purposes. The whole range of human model research is divided into the five areas of (a) modeling for machine system, (b) measurement and analysis of human information behavior, (c) modeling of human internal information process, (d) modeling of human interaction with machine system, and (e) that of between human themselves. The real examples of the human model developments as well as their methods, applications, and the model validations are described, and then, the further subjects and efforts are pointed out which would be needed for the broader industrial application of the human modeling.

## 6: Nuclear Energy Demand in Asia

アジアにおける原子力需要

Teruaki Ohnishi

IES Report (Institute of Environmental Systems, Kyushu University) No.12, PP.43 - 48 (1998)

IES Report No.12, PP.43 - 48 (1998)

Estimation is made on the time evolution of the amount of nuclear generation in Asia during the next one hundred years when the emission right of  $\text{CO}_2$  is controlled in a worldwide scale. Nuclear energy is assumed here to be introduced in any country whenever a certain threshold for economics and public affluence is cleared. Some case studies with model calculation are shown. (in Japanese)

## 7: Constraint of $\text{CO}_2$ Emission Right and Estimation of Nuclear Generation in Asia

$\text{CO}_2$ 排出権制限とアジアの原子力発電量予測

Teruaki Ohnishi

Proc. of the 8th Symposium for the Use of Radiation, pp.1-7 (1999)

第8回放射線利用総合シンポジウム資料集, pp.1 - 7 (1999)

Estimation is made on the time evolution of the amount of nuclear generation in Asia during the next one hundred years when the emission right of  $\text{CO}_2$  is controlled in a worldwide scale.

## II Department of Fundamental Energy Science

(エネルギー基礎科学専攻)

### 8: Surface Modification by Molten Salt Electrochemical Process

熔融塩電気化学プロセスによる表面改質

**Yasuhiko ITO and Toshiyuki NOHIRA**

The Journal of the Surface Finishing Society of Japan, Vol.49, No. 4, p.336-340, 1998

表面技術, Vol.49, No. 4, p.336-340, 1998

Among surface modification methods using molten salt electrochemical process, we describe the electrochemical formation of intermetallic compound films and the surface nitriding by electrochemical implantation and so on, which are expected as new technical seeds.

### 9: New Trends in Molten Salt Technology

熔融塩技術の新しい潮流

**Yasuhiko ITO**

DENKI KAGAKU, Vol.68, No.8, p.795-800, 1998

電気化学および工業物理化学, Vol.68, No.8, p.795-800, 1998

Expectations for molten salt technology have been increasing more and more, which have resulted in making new strong trends of molten salt technology, such as, a new point of view that molten salts can be regarded as condensed plasma. The author describes some selected topics of the new molten salt technology.

### 10: Crystal Chemistry of Novel Complex Vanadium Oxides with Layered Structures

層状構造をもつ新規複合バナジウム酸化物の結晶化学

**Yoshio Oka\*, Takeshi Yao**

**\*Faculty of Integrated Human Studies**

Journal of the Crystallographic Society of Japan, Vol. 40, No. 6, pp. 397-402, 1998

日本結晶学会誌, 40 巻, 6 号, pp. 397-402, 1998

Some of complex vanadium (IV, V) oxides are categorized into bronze compounds that adopt open-frame structures with foreign metals in their interstitial sites. There can be a variety of open-frame structure types depending on sizes and amounts of foreign metals as well as on vanadium-oxygen compositions. Utilizing hydrothermal methods we have succeeded in synthesizing single crystals of new vanadium bronze compounds with layered structures. Here we describe crystal structures of the selected novel layered compounds of  $\delta$ - $A_{0.5}V_2O_5$ ,  $\sigma$ - $A_{0.25}V_2O_5 \cdot H_2O$ ,  $A_xV_3O_8(VO)_y \cdot nH_2O$  and  $Cs_2V_4O_{11}$ . Each

of these compounds exhibits interesting structural features such as interlayer metal distributions, novel layer frameworks and unusual vanadium-oxygen coordinations.

**11: Characterization of Mixed Conducting Fluorite Oxides and Their Application to Electrodes for High Temperature Steam Electrolysis**

混合導電性蛍石型酸化物の特性と高温水蒸気電解用電極への適用

**Yoshiharu Uchimoto, Takeshi Yao**

ソーダと塩素、49 巻, pp. 282-290, 1998

**12: Electronic Structure of Cathode Materials for 5V Lithium Ion Batteries**

リチウム二次電池 5V 級正極活物質の電子状態

**Yoshiharu Uchimoto, Takeshi Yao**

マテリアルインテグレーション, 12 巻, pp. 43-48, 1998

**13: Structural Phase Transition of Metastable A-type Vanadium Dioxide VO<sub>2</sub>(A)**

準安定相二酸化バナジウム A 型 VO<sub>2</sub>(A) の構造相転移

**Yoshio Oka\*, Takeshi Yao, Shoichi Sato\*\***

**\*Faculty of Integrated Human Studies, \*\*Rigaku Corporation**

The Rigaku-Denki Journal, Vol. 30, No. 1, pp. 4-10, 1999

理学電機ジャーナル, 30 巻, 1 号, pp. 4-10, 1999

Vanadium dioxide shows several metastable phases besides the stable rutile-type VO<sub>2</sub>, for example, VO<sub>2</sub>(A) and VO<sub>2</sub>(B). The exact structures of VO<sub>2</sub>(A) for low- and high-temperature phases have remained unclear as well as the transition mechanism. Single-crystal X-ray diffraction studies were performed to provide the detailed structural information from which the transition mechanism has been derived. The transition is due to the formation of V<sup>4+</sup>-V<sup>4+</sup> pairs in the low-temperature phase, which is analogous to that of the rutile-type VO<sub>2</sub>. Surprisingly, twinning is induced in the high-temperature phase but disappears in the low-temperature phase on subsequent cooling. This unusual phenomenon is interpreted by the transition mechanism.

**14: Progress of Plasma Physics**

プラズマ物理の進展

**Masahiro Wakatani**

Parity, Vol.13, No.12 pp.116-117. 1998

パリテイ・13巻・12号・116-117頁・1998年

The progress of plasma physics is briefly summarized for the period of 1997-1998.

**15: Long-range Attractive Interaction between Macroparticles in Solvents**

溶媒中における超長距離性の微粒子間引力相互作用

**Masahiro Kinoshita**

表面, Vol.36, No.6, pp.304-312, 1998

When macroparticles are immersed in a solvent, a layer (surface-induced layer) within which the structure of solvent molecules differs largely from that in the bulk is formed around each macroparticle, with the result that a new interaction is induced between macroparticles. The review in this article is focused on the range-range attractive interaction between macroparticles immersed in a binary fluid mixture. It is suggested that the surface-induced phase transition, sudden growth in the thickness of the surface-induced layer (appearance of a second phase around each macroparticle), causes the long-range interaction. The transition can occur even when the bulk mixture is thermodynamically stable as a single phase.

**16: Theoretical Analysis on Structure of the Metal-Aqueous Electrolyte Solution Interface**

金属-電解質水溶液界面構造の理論解析

**Masahiro Kinoshita**

表面科学, Vol.20, No.4, pp.70-76, 1999

Theoretical studies on the metal-aqueous electrolyte solution interface are critically reviewed with emphasis on the studies using quantum treatments for the metal side and classical approaches, above all, integral equation theories, for the solution side. With the integral equation theories an infinitely large system can be mimicked, and ions can readily be incorporated in the solvent at a finite concentration. The density structure of water molecules and ions, water and ion configurations near the metal surface, and the potential drop across the interface are discussed and some of them are compared with experimental observations. Future subjects to be considered such as how to connect the quantum system with the classical system in a more realistic manner, are also discussed.

**17: The Present Active Status of Domestic Critical Assemblies and the Perspective for Their Future - Thire Role Explored in National Nuclear Power Utilization -**

臨界集合体の現状と将来利用 —今後果たすべき役割の検証と展望—

日本原子力学会誌、VOL 40、NO 4、254-281 (1998)

**18: Visualization and Measurement Technique Using Neutron Radiography**

Journal of the Japan Society of Mechanical Engineers, vol. 101, pp. 885-887, 1998

An outline of visualization and measurement technique using neutron radiography was briefly given.

**19: The Proposal to Evaluate Activation of Protect Pollution by Photocatalysis**

光触媒防汚活性の評価法の提案

**K. Takami, T. Nakasone, K. Hashimoto, A. Fujisima**

Kogyozairyou, Vol.46, No.5

工業材料, 46 (5), 特集 酸化チタン光触媒の新たな展開

**20: TiO<sub>2</sub> Photocatalyst for Water Treatment**

酸化チタン光触媒による水処理

**A. Fujishima, S. Fujita**

J. Adv. Sci., Vol.9, No.3 & 4, pp.192-195 (1998).

**21: Be the Real Active Core of Research Exchange**

真に活発な研究交流の中核たれ

**A. Fujishima**

Hikari Kagaku. Vol.27, No.1 (1998)

光化学, 27, 1 (1998).

**22: Possibility to apply Photocatalyst for Hypersensitivity of Chemical Substances**

化学物質過敏症への光触媒の適用の可能性

**A. Fujishima**

Kino Zairyo, Vol.18, No.9, pp.29-33 (1998)

機能材料, 18 (9), 29-33 (1998).

**23: Photocatalyst-Applied Expansion for the Field of Illumination**

光触媒-照明分野への応用展開

**A. Fujishima**

Shomei Gakkaishi, Vol.80, No.12, pp.925-926 (1998)

照明学会誌, 80 (12), 925-926 (1998).

**24: "Light Cleaning" Learn a Plant**

植物を見習って「光クリーン革命」をすすめる

**A. Fujishima**

Hirogari, Vol.63

ひろがり, 63, いま、化け学が面白い 研究室探訪6

**25: BUKKATENPOU**

物華天宝

**A. Fujishima**

Hitachi Kasei Tech. Rep., Vol.31, pp.5-6 (1998)

日立化成テクニカルレポート, 31, 5-6 (1998).

**26: TiO<sub>2</sub> Photocatalyst build Next Generation of Civilization**

次代の文明を築く酸化チタン光触媒

**A. Fujishima**

Kokumin Kinyukoko Tyosageppo, Vol.447, pp.20-23 (1998)

国民金融公庫調査月報, 447, 20-23, (1998).

**27: The Light Start a Revolution of the Environment**

光が環境を革命する。—酸化チタン光触媒技術

**A. Fujishima**

Bayer in Japan

**28: Related Topics and Future View of the Research of Photocatalyst**

光触媒研究の現状と将来展望

**A. Fujishima**

GA Japan, No.33, pp.162-165 (1998).

**29: Antibacteria and Protect Pollution by TiO<sub>2</sub> Photocatalyst**

酸化チタン光触媒による抗菌と防汚

**A. Fujishima**

Bosabikanri, 1998-8, pp.13-17 (1998)

防錆管理, 1998-8, 13-17 (1998).

**30: Photocatalyst—The Light Clean the Environment**

光触媒—光が環境を浄化する

**A. Fujishima**

Technology Future, 4(1), (1998).

**31: TiO<sub>2</sub> Photocatalyst can Clean the Environment**

酸化チタン光触媒で環境浄化ができる

**A. Fujishima**

Sut Bulletin, No.11, pp.2-7 (1998).

**32: Antibacteria by TiO<sub>2</sub> Photocatalyst Reaction**

酸化チタン光触媒反応による抗菌効果

**A. Fujishima**

J. Antibact. Agents., Vol.26, No.11, pp.611-620 (1998).

**33: Active Species Behavior of TiO<sub>2</sub> Photocatalyst Reaction**

酸化チタン光触媒反応における活性種の挙動

**K. Ishibashi, K. Hashimoto, A. Fujishima**

Hikarikagaku, Vol.29, pp.2-5 (1998).

光化学, 29, 2-5 (1998).

**34: The Photocatalyst of Today and Future**

光触媒の今日と未来像

**A. Fujishima**

JETI, 47(2),65-67 (1998).

### III Department of Energy Conversion Science

(エネルギー変換科学専攻)

#### 35: Engineering Approach for Mitigation of Greenhouse-Effect Gases

温室効果ガス低減に対する工学的アプローチ

**Makoto Ikegami**

Nogyo Gijutsu, 53(4), pp181-185, 1998

農業技術, 53(4), pp181-185, 1998

Considering the mitigation of global warming, it is greatly expected for agriculture and forestry to produce biomass fuels as well as to reduce greenhouse gas emission during the agricultural production. It is important that the carbondioxides emission will be reduced if the biomass fuels are introduced into other industrial sectors consuming great amount of fossil fuels. From this viewpoint, in this paper, the possibility of engineering approach for mitigation of the warming in agriculture was discussed. (in Japanese)

#### 36: Development of Combustion Diagnostics

燃焼計測技術の進展

**Masahiro Shioji**

Transaction of Combustion Society of Japan, Vol. 112, pp.15-24, 1998

燃焼研究, 112号, pp.15-24, 1998

Recent technologies and possible applications are reviewed for the optimal design and control in practical combustion systems. In particular, as the first in a serial articles, laser light-sheet methods are demonstrated to visualize a jet and a jet flame, and soot clouds in the diesel combustion processes. Those applications may afford to fundamentally clarify the complicated structure in unsteady turbulent flames. (in Japanese)

#### 37: Development of Combustion Diagnostics 2 Gas-Flow Measurement using Particle Image Velocimetry

燃焼計測技術の進展 2 - 粒子画像流速測定法 (PIV) によるガス流動計測 -

**Masahiro Shioji, Hiroshi Kawanabe**

Transaction of Combustion Society of Japan, Vol.113, pp.11-20, 1998

燃焼研究, 113号, pp.11-20, 1998

As the second in a serial articles of recent technologies for combustion diagnostics, cross-correlation PIV is explained to exhibit its principle and features. This method has a great possibility of full-field

velocity measurements in practical turbulent flows and flames. At first, procedures of data analysis and error assessments are shown in general cases. Also, an application to obtain instantaneous velocity vectors in a jetting flame is demonstrated based on the change of scattering images of soot particles. (in Japanese)

### 38: Combustion in Hydrogen Engines

水素のエンジン内燃焼

Masahiro Shioji

Journal of Japan Society of Energy and Resources, 19-5, pp.429-433, 1998

エネルギー・資源, 19-5, pp.429-433, 1998

Hydrogen has been regarded as a future secondary fuel for internal combustion engines mainly because of CO<sub>2</sub>- and HC-free combustion. Hydrogen fuel features a very wide range of flammability limits and an extremely high burning velocity. This article surveys the characteristics of various combustion systems in hydrogen engines, and also introduces their problems and the attempts at direct-injection system for avoiding abnormal combustion such as backfire, preignition and knocking of hydrogen mixture, which is usually observed in a hydrogen premixed-charge spark-ignition engine. (in Japanese)

### 39: Technology for Emission Control in Internal Combustion Engines

各種内燃機関における排ガス浄化技術

Masahiro Shioji

Journal of Society of Automotive Engineers of Japan, Vol.52, No.9, pp.4-10, 1998

自動車技術, Vol.52, No.9, pp.4-10, 1998

Although every effort has been made at the great improvement in engine performance and emission control for all kinds of vehicles, a rapid increase in the number of convenient and comfortable automobiles urgently requests further reduction of pollutant emissions. This paper surveys a feature of various types of internal combustion engines and summarizes their strategies for emission control, based on which we can hopefully hit on an idea of the advanced technology. (in Japanese)

### 40: Fuel-Air Turbulence Mixing and It's Effects

燃料-空気の乱流混合とその作用

Masahiro Shioji

Journal of the Marine Engineering Society in Japan, Vol.34, No.2, pp.140-146, 1999

日本船用機関学会誌, 第34巻, 第2号, pp.140-146, 1999

Turbulent mixing model for predicting the combustion in Diesel engines and the NO formation is

introduced to describe the heterogeneous state of mixture concentration and temperature. This model can afford to estimate the change of heterogeneity associated with turbulence intensity and scale and also the turbulence production due to spray-jet energy, swirl and local heat release and their effects. Based on the model, the major process of diesel combustion is theoretically investigated and the strategy for NO<sub>x</sub> reduction may be found. The results shown here, however, are dependent on engine design and operating parameters, so that further clarification are required for a quantitative discussions. (in Japanese)

#### 41: Solid Mechanics under Magnetic Field

**Eiji Matsumoto**

Material Science Research International, Vol.5, No.1, pp.1-12, 1999

This paper reviews the governing equations for deformable electromagnetic materials, their typical behaviors under the magnetic field and applications utilizing magnetic or magnetomechanical phenomena. Electromagnetic field equations and conservation laws for moving deformable materials are laid down, on the basis of continuum theory of electromagnetic materials. Under the magnetic field, the magnetized material is subjected to several kinds of magnetic forces. If the material is electrically conductive and the magnetic field is changing in time, there may exist the eddy current, the induced magnetic field, the Lorentz force, etc. In the case of ferromagnetic materials, can not be neglected magnetic nonlinearity and hysteresis and magnetomechanical effects such as magnetostriction and stress-dependence of magnetization. In many cases, the magnetic field is static, periodically changing in time, or applied to the demagnetized material. In these cases, the equilibrium theory of deformable magnetic materials can be applied to each magnetization process in which the magnetic field is changing in one-direction including the case of rotating magnetic fields. Mechanical properties under such magnetic field and the magnetization properties in the stress are discussed. As related topics to the above physical phenomena, reviewed are magnetoelastic problems, nondestructive evaluation of material properties and the deformation and applications of magnetic forces.

#### 42: Fracture and Probabilistic Models in Advanced Materials — (2) Ceramics, Part 1 Properties of Static Fracture Strength

先進材料の破壊と確率モデル — (2) セラミックス その 1 静的破壊強度特性

**Akiyoshi Sakaida<sup>1)</sup>, Akira Ueno<sup>2)</sup>, Toshihiko Hoshide, Nagatoshi Okabe<sup>3)</sup>, Toshio Sakuma<sup>4)</sup>**

**1) Akashi College of Technology, 2) Toyota Technological Institute, 3) Ehime University, 4) Central Research Institute of Electric Power Industry**

Science of Machine, Vol.50, No.12, pp.1265-1270, 1998

機械の研究, 第 50 卷, 第 12 号, pp.1265-1270, 1998

The first part of this article deals with statistical properties of static strength, which have been observed

experimentally, for reference. Statistical models related to effects of component geometry and loading mode are reviewed in comparison with experimental observations. The effective volume or effective surface based on the Weibull theory is mentioned with respect to the size effect on strength in ceramics. The applicability of fracture criterion to strength under multiaxial stress states is examined by referring to the models proposed by Ichikawa and Matsuo. In these models, the classification and distribution of cracks dominating fracture of ceramics are specified. An approach based on microstructural fracture mechanics is also described for a solution to the crack-size effect on strength. In this approach, the criterion for fracture initiating from a small flaw is modified by the addition of a specific length to the original flaw-size. Some results simulated by this approach are illustrated. The stochastic process in fracture of brittle solids is also discussed compared with aforementioned models. (in Japanese)

**43: Fracture and Probabilistic Models in Advanced Materials — (2) Ceramics, Part 2  
Properties of Static and Cyclic Fatigue**

先進材料の破壊と確率モデル — (2) セラミックス その2 静疲労・繰返し疲労特性

Akira Ueno<sup>1)</sup>, Akiyoshi Sakaida<sup>2)</sup>, Toshihiko Hoshide, Nagatoshi Okabe<sup>3)</sup>, Toshio Sakuma<sup>4)</sup>

1) Toyota Technological Institute, 2) Akashi College of Technology, 3) Ehime University, 4) Central Research Institute of Electric Power Industry

Science of Machine, Vol.51, No.1, pp.76-82, 1999

機械の研究, 第51巻, 第1号, pp.76-82, 1999

In the present article, experimental results on statistical characteristics of fatigue life are indicated in  $P-S-N$  diagrams and Weibull probability papers for investigations of related probabilistic models. Properties of static and cyclic fatigue strength are also compared for reference. The static fatigue life is formulated by using the crack growth law obtained under dead load, and is further converted to the cyclic fatigue life for the discussion on effect of cyclic load. The dispersion of fatigue life is explained by introducing the crack growth formulations for time-dependent and/or time- and cyclic-dependent fracture models. It is shown that the cumulative distribution of life derived using the models is reduced to the distribution function similar to the Weibull type. Another approach using the Markov process is stated with respect to the stable crack growth in static fatigue. By this approach combined with the Griffith criterion, the probability density function is derived for the fracture of arbitrary volume element in a material. The comparison of theoretical analysis with experimental results is also illustrated. (in Japanese)

**44: Fracture and Probabilistic Models in Advanced Materials — (2) Ceramics, Part 3  
Proof Testing**

先進材料の破壊と確率モデル — (2) セラミックス その3 保証試験

Akira Ueno<sup>1)</sup>, Akiyoshi Sakaida<sup>2)</sup>, Toshihiko Hoshide, Nagatoshi Okabe<sup>3)</sup>, Toshio Sakuma<sup>4)</sup>

1) Toyota Technological Institute, 2) Akashi College of Technology, 3) Ehime University, 4) Central Research Institute of Electric Power Industry

Science of Machine, Vol.51, No.2, pp.297-304, 1999

機械の研究, 第51巻, 第2号, pp.297-304, 1999

A large scatter is observed in the static strength, the static and cyclic fatigue strength in ceramic materials. Proof testing for ceramic materials has been proposed as an efficient procedure to exclude such components with a lower strength, which are not permissible in the structural design. In this article, formulations for strength characteristics after proof testing are reviewed by referring to the analysis of stable crack growth from inherent flaws. These formulations are classified according to the strength variation due to the slow crack growth during loading and/or unloading processes in a proof testing. The validity of the formulations is examined in comparison with some examples of proof testing applied to ceramic static and cyclic fatigue strength. The associated problems are also cited. Influences of proof testing conditions, including the prescribed proof stress and stress rates during loading and unloading processes are discussed. It is remarked that the condition of proof testing should be appropriately prescribed for efficient screening in consideration of the fracture mechanism. (in Japanese)

**45: Fracture and Probabilistic Models in Advanced Materials — (2) Ceramics, Part 4  
Evaluation of Scatter in Strength and Fatigue Life**

先進材料の破壊と確率モデル — (2) セラミックス その4 強度・寿命のばらつきの評価法

Akira Ueno<sup>1)</sup>, Akiyoshi Sakaida<sup>2)</sup>, Toshihiko Hoshide, Nagatoshi Okabe<sup>3)</sup>, Toshio Sakuma<sup>4)</sup>

1) Toyota Technological Institute, 2) Akashi College of Technology, 3) Ehime University, 4) Central Research Institute of Electric Power Industry

Science of Machine, Vol.51, No.3, pp.405-411, 1999

機械の研究, 第51巻, 第3号, pp.405-411, 1999

It is important to assess a scatter in ceramic strength properties adequately, because the reliability of ceramic components should be retained in the design for successful applications. Two approaches are mainly reviewed from such an aspect in this article. A fracture mechanics approach correlates a group of S-N curves with the distribution of static strength through the size of inherent flaw. It should be noted that the proof testing is not always efficient for the improvement of the fatigue limit. A unified evaluation of various strength characteristics is cited as another approach. The evaluating procedure is derived by using the crack growth law and parameters in a fitted Weibull distribution function. The results obtained by the procedure shows a good correlation among static, fatigue and creep strength. (in Japanese)

**46: Method for Reducing Noise of a DC-Motor with Constant Current Control**

直流モータの定電流制御による騒音抑制法

**Kosuke Nagaya, Hideto Yuzawa<sup>1)</sup>, Iwanori Murakam<sup>1)</sup>, Masaji Yokota<sup>2)</sup>, Kouichi Takasaki<sup>2)</sup>**

**1) Gunma University, 2) Calsonic Co. Ltd**

Journal of the Japan Society of Applied Electromagnetics and Mechanics, Vol.7, No.1, pp.36-40, 1999

日本 AEM 学会誌、Vol.7, No.1, pp.36-40, 1999

Since a commutator of the DC- motor is divided into a number of segments to have the torque in the same direction, the currents in the coils of the rotor vary and have alternative waves during the rotor rotation even in a constant input voltage. The currents become sharp waves, so that they have high frequency components. This implies that the rotor shaft and the case of motor are excited electromagnetic forces with various frequency components. Since high frequency noises are loud when they are input to human ears, so that when high frequency vibrations are suppressed, noises become small. From this situation, this paper discusses a method of noise reduction of DC-Motor. In the method, the current waves are controlled to be a constant value. The method and the control algorithm are given. In order to validate the method, experimental tests are carried out. It is proven that our method is applicable to the motor noise control. (in Japanese)

**47: On the Electromagnetic Vibration of Rotating Machine**

回転機の電磁振動特集号に寄せて

**Kosuke Nagaya**

Journal of the Japan Society of Applied Electromagnetics and Mechanics, Vol.7, No.1, pp.1-2, 1999

日本 AEM 学会誌, Vol.7, No.1, pp.1-2, 1999

This report is a review paper on the vibration of rotating machines caused by electromagnetic forces. In the report, a survey of the vibrations of various motors is made. The papers concerning noise radiated from the motor and rotating machines are also discussed. The report also introduces a number of methods for controlling vibrations and sound of the machines. (in Japanese)

## IV Department of Energy Science and Technology

(エネルギー応用科学専攻)

### 48: Integrated Circuit

**Keikichi Tamaru\* and Hiroshi Nozawa**

**\*: Graduate School of Information, Kyoto University**

Kyoritu Shuppan, Tokyo March 1999

This book describes basis and its application including solid state physics of semiconductor to introduction of circuits design on CMOS integrated circuits, which is important devices currently. This is a suitable text book for students or graduate students of university or college and fresh engineers to study electric, electronics and information.

### 49: Phase Control of photoabsorption processes

光励起過程の位相制御

**Takashi Nakajima Masahiro Kawasaki\***

**\* Department of Molecular Engineering, Kyoto University**

Bunko-Kenkyu, Vol. 48, pp.5-14 (1999)

分光研究, 48 卷, pp.5-14

***D. Books***

D. 著書

# Chapter 4

## Books

### 1: Pursuit of Happiness

幸福ということ：エネルギー社会工学の視点から

Shingu, P.H. .

新宮秀夫

.: 日本放送出版協会

1998 / 08 / 25 published

### 2: The Encyclopedia of Wood Industry

最新木材工業事典

最新木材工業事典出版委員会編、河本晴雄

.: (社)日本木材加工技術協会

1999 / 02 / 25 published

### 3: Human Interface

ヒューマンインタフェース

Edited by Tamura,H.(Kyoto Institute of Technology), Yoshikawa,H. and otehrs .

田村博編、吉川榮和他

Ohmsha, Japan . : オーム社出版局

1998 / 05 / 30 published

Handbook about overall of Human Interface.

#### 4: Cognitive Systems Engineering in Process Control '96

Edited by Hollnagel,E. & Yoshikawa,H. .

ESSCS, Groningen, The Netherlands . :

1998 / / published

Selected papers from the International Conference held on November 12-15, 1996, Kyoto Japan. "Cognitive Syetems Engineering in Process Control '96"

#### 5: Tomorrow Energy and Environment, Suggestion from Kyoto, Japan

明日のエネルギーと環境

Kasahara,M., Kaya,Y., Saka,S., Sawa,T., Shingu,H., Tezuka,T., Nagasato,Y., Yoshikawa,H.

笠原三紀夫、茅陽一、坂志朗、佐和隆光、新宮秀夫、手塚哲央、永里善彦、吉川榮和

The Japan Industrial Journal . : 日本工業新聞社

1998 / 10 / 12 published

#### 6: Stellarator and Heliotron Devices

Masahiro Wakatani .

Oxford University Press . :

1998 / / published

1 INTRODUCTION 2 DESIGN PRINCIPLES OF COIL SYSTEMS IN THE STELLARATOR AND HELIOTRON 3 A DESCRIPTION OF MAGNETICALLY CONFINED PLASMAS 4 THE MHD EQUILIBRIUM OF A TOROIDAL PLASMA IN THREE-DIMENSIONAL GEOMETRY 5 MHD INSTABILITIES IN HELIOTRONS 6 THE PARTICLE ORBIT IN HELIOTRONS 7 NEOCLASSICAL TRANSPORT IN THE STELLARATOR AND HELIOTRON 8 THE HEATING AND CONFINEMENT OF STELLARATOR AND HELIOTRON PLASMAS 9 THE STDAY-STATE FUSION REACTOR

**7: Modeling and simulation methods for plasma processing**

S. Hamaguchi .

IBM J.Res.Develop., vol.43 No. 1/2 (1999) . :

1999 / 01 / published

**8: Gas-Flow Measurement of Micro-Structure in a Jet Flame by PIV(Innovative Measurements in Thermo-Fluids)**

PIVによる噴流火炎内ガス流動の微細構造計測／熱流体の新しい計測法

Masahiro Shioji .

塩路 昌宏

. : 養賢堂

1998 / / published

**9: Hydrogen Engine (Exergy Engineering)**

水素エンジン／エクセルギー工学

Masahiro Shioji .

塩路 昌宏

. : 共立出版社株式会社

1999 / 02 / published

**10: Fundamentals of Strength Analyses**

基礎強度学

Toshihiko Hoshide .

星出 敏彦

Uchida Rokakuho Publishing Co., Ltd . : 内田老鶴圃

1998 / 11 / 25 published

This book is intended as a text for the initial course in fields of fracture and reliability analyses. In Captor One, a history of failure in components and/or structures is briefly stated, and it is emphasized how important the strength analyses of materials as well as systems are. The relation between strength analyses and materials design is examined in the system design. Chapter Two presents detailed mathematical treatments of cracks in linear elastic solids. The stress intensity factor  $K$  is introduced as one of important parameters in the linear elastic fracture mechanics. Chapter Three deals with the plasticity of crack-tip, and emphasizes the limitation in applications of stress intensity factor. The dependence of size and shape of the plastic zone at crack-tip on the stress-strain state and/or loading mode is cleared, and it is indicated that they are correlated with the stress intensity factor in the situation of small-scale yielding. In Chapter Four, energetic theories on fracture in micro- and macro-scales are discussed with respect to the energy balance for crack growth in a linear or non-linear elastic solid, the relation between the energy release rate and the stress intensity factor, and the crack resistance curve. A path-independent integral  $J$  is introduced as an energy release parameter in non-linear elastic solids. Simple methods of  $J$  evaluation are represented for some typical loading systems. Chapter Five presents actual failure modes, especially static fracture and fatigue, with experimental results which are mainly correlated with fracture mechanics parameters  $K$  and  $J$ . Recent standards in relation to the fracture mechanics approach are included. The importance of short crack is emphasized in practical fracture analyses, and comments on creep and environment-assisted cracking are also mentioned. Chapter Six introduces the reliability of typical systems, and describes typical probabilistic distributions with ranking methods. Particularly, the Weibull distribution with his fundamental idea is explained in detail because of its wide applicability in strength analyses. Basic concepts of reliability in the strength design are also presented as follows; FMECA (failure mode, effects and criticality analysis), safety factor, proof testing, fail safe, damage tolerance design, and leak-before-break.

**11: Handbook of Cryogenic Engineering, Chapter 3 Cryogenic Heat Transfer, 3-3-2 Predicting the Critical Heat Flux for a Horizontal Cylinder in Saturated Liquid He I**

M. Shiotsu .

Taylor &amp; Francis, USA . :

The critical heat flux (CHF) is the heat flux at which boiling changes from nucleate boiling to film boiling. Knowledge of the critical heat flux in liquid He I is important as a basis for designing liquid-helium-cooled superconducting magnets. Experimental CHF data for a horizontal cylinder in liquid He I have been measured by Frederking with very thin 16- and 32- $\mu$  m-diameter wires under pressures ranging from 5.7 to 97 kPa. Shiotsu et al. measured the CHF for 0.3-, 0.5-, and 1.2-mm-diameter horizontal cylinders under saturated conditions at pressures ranging from 24.4 kPa ( $P/P_{cr} = 0.11$ ) to 198.6 kPa ( $P/P_{cr} = 0.87$ ). Shiotsu et al. presented a correlation which can describe the CHF data within  $\pm 15\%$  difference. They showed that the correlation with  $D \rightarrow \infty$  would also be applicable for CHF on horizontal plates in various liquids. Data for He I ( $P/P_{cr} = 0.027 - 0.95$ ) by Lyon, data for ethanol ( $P/P_{cr} = 0.016 - 0.92$ ) by Chichelli and Bonilla, and data for water ( $P/P_{cr} = 0.046 - 0.85$ ) by Kazakova et al. were compared with the predicted values. Almost all the data were within  $\pm 25\%$  of the new correlation throughout the pressure range.

# *List of Academic Staff*

教官名簿

## Chapter 5

# List of Academic Staff

March 31, 1999

### Department of Socio-Environmental Energy Science

#### PROFESSORS:

SHINGU, Hideo	SAWA, Takamitsu	SAKA, Shiro
MAKINO, Keisuke	YOSHIKAWA, Hidekazu	KASAHARA, Mikio
MIYAZAWA, Tatsuo	KANDA, Keiji	

#### ASSOCIATE PROFESSORS:

ISHIHARA, Keiichi	NAGATA, Yutaka	KAWAMOTO, Haruo
OOTUKI, Toru	TEZUKA, Tetsuo	TOHNO, Susumu
OHNISHI, Teruaki	NAKAGOME, Yoshihiro	BESSHO, Yasunori (Visiting AP)

#### INSTRUCTORS:

MORII, Takashi	MIYAFUJI, Hisashi	SHIMODA, Hiroshi
YAMAMOTO, Kouhei	NAGAMATSU, Takashi	ONO, Koichi
FUJINE, Shigenori	TAKEUCHI, Takayuki	HAYASHI, Masatoshi

### Department of Fundamental Energy Science

#### PROFESSORS:

ITO, Yasuhiko	YOSHIDA, Katsukuni	YAO, Takeshi
FUJISHIMA, Akira (Visiting P)	WAKATANI, Masahiro	KONDO, Katsumi
MAEKAWA, Takashi	OBIKI, Tokuhiro	SANO, Fumimichi
OGATA, Yukio	HARADA, Makoto	OHKUBO, Taketoshi
KATAGIRI, Akira	SHIROYA, Seiji	MISHIMA, Kaichiro

**ASSOCIATE PROFESSORS:**

HAGIWARA, Rika	ITOH, Sumiko	TOMII, Yochi
UCHIMOTO, Yoshiharu	YOSHIDA, Zensho (Visiting AP)	HAMAGUCHI, Satoshi
NAKAMURA, Yuji	TANAKA, Hitoshi	MIZUUCHI, Tohru
HANATANI, Kiyoshi	SAKKA, Tetsuo	KINOSHITA, Masahiro
KOTAKI, Tsutomu	MISAWA, Tsuyoshi	HIBIKI, Takashi

**LECTURERS:**

ADACHI, Motonari

**INSTRUCTORS:**

GOTO, Takuya	NOHIRA, Toshiyuki	KAJIHARA, Koichi
NAKASUGA, Masahiko	BESSHOU, Sakae	NAGASAKI, Kazunobu
OKADA, Hiroyuki	SHIOI, Akihisa	HARADA, Toshio
MIZUTANI, Yasuo	KOBAYASHI, Keiji	UNESAKI, Hironobu
SAITO, Yasushi		

**Department of Energy Conversion Science****PROFESSORS:**

IKEGAMI, Makoto	SHIOJI, Masahiro	INOUE, Tatsuo
MATSUMOTO, Eiji	INOUE, Nobuyuki	YOSHIKAWA, Kiyoshi
KIMURA, Akihiko	NAGAYA, Kosuke (Visiting P)	

**ASSOCIATE PROFESSORS:**

ISHIYAMA, Takuji	IMATANI, Shoji	HOSHIDE, Toshihiko
YAMAMOTO, Yasushi	OHNISHI, Masami	MORISHITA, Kazunori

**LECTURERS:**

TAMAGAWA, Masaaki

**INSTRUCTORS:**

KAWANABE, Hiroshi	TSUTSUMI, Mitsuyoshi	MASUDA, Kai
-------------------	----------------------	-------------

**Department of Energy Science and Technology****PROFESSORS:**

NOZAWA, Hiroshi	SHIOTSU, Masahiro	ONO, Katsutoshi
IWASE, Masanori	NISHIYAMA, Takashi	HATTA, Natsuo
ISHII, Ryuji	YAMAZAKI, Tetsuo	KOHYAMA, Akira
MIYAZAKI, Kenzo		

**ASSOCIATE PROFESSORS:**

TANAKA, Isao

FUJIWARA, Hiroyasu

FUKUNAKA, Yasuhiro

NAKAJIMA, Takashi

SHIRAI, Yasuyuki

KUSUDA, Hiromu

CHIBA, Meiro

SUZUKI, Ryosuke

TAKUDA, Hirohiko

KATOH, Yutai

**INSTRUCTORS:**

UEDA, Yukitomi

FUJIMOTO, Hitoshi

JINBO, Kouichi

UCHIDA, Yuichi

KUSAKA, Eishi

HATA, Koichi

CHEN, Youqing

KII, Toshiteru

## エネルギー科学研究科教官名簿

1999/03/31 現在

## エネルギー社会環境専攻

## 教授:

新宮秀夫	佐和隆光	坂 志朗	牧野圭祐
吉川榮和	笠原三紀夫	宮沢龍雄	神田啓治

## 助教授:

石原慶一	永田 豊	河本晴雄	大槻 徹
手塚哲央	東野 達	大西輝明	中込良廣
別所泰典 (客員)			

## 助手:

森井 孝	宮藤久士	下田 宏	山本浩平
長松 隆	小野光一	藤根成勲	武内孝之
林 正俊			

## エネルギー基礎科学専攻

## 教授:

伊藤靖彦	吉田起國	八尾 健	藤島 昭 (客員)
若谷誠宏	近藤克己	前川 孝	大引得弘
佐野史道	尾形幸生	原田 誠	大久保捷敏
片桐 晃	代谷誠治	三島嘉一郎	

## 助教授:

萩原理加	伊藤澄子	富井洋一	内本喜晴
吉田善章 (客員)	浜口智志	中村祐司	田中 仁
水内 亨	花谷 清	作花哲夫	木下正弘
小瀧 努	三澤 毅	日引 俊	

## 講師:

足立基斎

## 助手:

後藤琢也	野平俊之	梶原浩一	中須賀正彦
別生 榮	長崎百伸	岡田浩之	塩井章久
原田敏夫	水谷保男	小林圭二	宇根崎博信
斎藤泰司			

## エネルギー変換科学専攻

## 教授:

池上 詢	塩路昌宏	井上達雄	松本英治
井上信幸	吉川 潔	木村晃彦	長屋幸助 (客員)

## 助教授:

石山拓二	今谷勝次	星出敏彦	山本 靖
大西正視	森下和功		

## 講師:

玉川雅章

## 助手:

川那辺洋	上原 拓也	増田 開
------	-------	------

## エネルギー応用科学専攻

## 教授:

野澤 博	塩津正博	小野勝敏	岩瀬正則
西山 孝	八田夏夫	石井隆次	山寄鉄夫
香山 晃	宮崎健創		

## 助教授:

田中 功	白井康之	鈴木亮輔	藤原弘康
楠田 啓	宅田裕彦	福中康博	千葉明朗
加藤雄大	中嶋 隆		

## 助手:

植田幸富	内田祐一	陳 友晴	藤本 仁
日下英史	紀井俊輝	神保光一	畑 幸一

平成11年11月30日印刷

平成11年12月1日発行

編集兼  
発行者

京都市左京区吉田本町

京都大学エネルギー科学研究科

代表者

伊藤靖彦

印刷所

(株)北斗プリント社  
京都市左京区下鴨高木町38-2